UNIVERSIDAD COMPLUTENSE DE MADRID

FACULTAD DE CIENCIAS FÍSICAS

Departamento de Física de la Tierra, Astronomía y Astrofísica I (Geofísica y Meteorología) (Astronomía y Geodesia)

ESTUDIO DE LOS CALENTAMIENTOS ESTRATOSFÉRICOS EN EL HEMISFERIO NORTE Y SU HUELLA TROPOSFÉRICA :PASADO RECIENTE, PRESENTE Y FUTURO

MEMORIA PARA OPTAR AL GRADO DE DOCTOR
PRESENTADA POR

Blanca Ayarzagüena Porras

Bajo la dirección de los doctores

Encarnación Serrano Mendoza
Ulrike Langematz

Madrid, 2012

ISBN: 978-84-695-3544-8

Universidad Complutense de Madrid

Facultad de Ciencias Físicas

Departamento de Física de la Tierra, Astronomía y Astrofísica I

Estudio de los calentamientos estratosféricos en el hemisferio norte y su huella troposférica: pasado reciente, presente y futuro

(Study of stratospheric warmings in the Northern Hemisphere and their tropospheric fingerprint: recent past, present and future)

Memoria para optar al grado de Doctora presentada por:

Blanca Ayarzagüena Porras

Bajo la dirección de las Doctoras:

Encarnación Serrano Mendoza

Ulrike Langematz

Madrid, 2011

A mis padres

The present study has been funded by the Spanish Ministerio de Ciencia e Innovación project CGL2008-06295, the European Social Funds and “Consejería de Educación de la Comunidad de Madrid” under the contract (CPI/0423/2007).

Agradecimientos

Ésta es la parte más emotiva de toda la tesis y con ello, quizá la más difícil. Muchas han sido las personas que de una manera directa o indirecta han contribuido a que esta tesis viera la luz y no quisiera dejar a nadie sin nombrar. Si así sucede, pido disculpas por adelantado.

En primer lugar, quisiera dar las gracias a las directoras de mi tesis, Encarna Serrano y Ulrike Langematz. Sin ellas, el trabajo de todos estos años no habría sido posible. Encarna, gracias por haberme "acercado" a la estratosfera, aunque esté a más de 10 km, por todo tu cariño, por las horas en el "banquito", pero, sobre todo, gracias por creer en mí. Ulrike, vielen Dank für deine Hilfe. Ich möchte mich bei dir auch bedanken, dass du seit dem ersten Tag mich freundlich aufgenommen hast.

Me gustaría dar las gracias al departamento de Geofísica y Meteorología por brindarme sus instalaciones y por todo su apoyo durante todos estos años. Asimismo, quisiera reconocer toda la ayuda que me han brindado Salvador, Lucía y Pedro. Gracias por hacer todo lo posible por solucionar mis problemas burocráticos e informáticos.

Muchas gracias a mis compañeros "estratosféricos". Álvaro, no hay palabras con las que pueda agradecerte todo tu apoyo, tus ideas, tu ayuda en estos años y… por supuesto, tus bromas en los momentos de "bajón", que me han ayudado a seguir adelante. Marta, gracias por tu ayuda en todo momento, por tu entusiasmo y por reconocer cuándo necesitaba un abrazo (aunque fuera poco frecuente). Bea, aunque ahora estés en tierras más cálidas, siempre recordaré la alegría de tus "Buenos díaaas!" de cada mañana.

Quisiera también agradecer a Belén y Carlos. Belén, gracias por transmitir esa ilusión y por estar dispuesta a escuchar en todo momento. Para mí, las SSTs siempre estarán ligadas a ti (y… el running). Carlos, gracias por ser tan buen "jefe", por tu apoyo, por CIBA 2008, por Portugal y, especialmente, por estar siempre en todo. GRACIAS a los dos!

Gracias a todos los que habéis ido formando parte del laboratorio "Elvira Zurita" (gracias a ti también, Elvira por esa ternura con la que nos tratabas a los "pequeños"). Todos habéis dejado un trocito vuestro en mí, al igual que en el laboratorio: Javi G., Teresa, Irene, Samu, Álvaro y … en una segunda etapa, Marta A., Bea, Nube, Mariano, David, Étor, Esteban, Javi B. Jorge, Marta M., Íñigo, "Cahlo" y Jesús. Gracias por vuestro cariño y vuestro apoyo cuando más lo necesitaba.

Gracias a la "pequeña familia" de las comidas y el café, gracias por vuestro cariño, vuestros consejos, vuestras ingeniosas conversaciones y… por descubrirme el pádel!! Habéis hecho que venir a trabajar sea un verdadero placer. Gracias a Ana, Elsa, Javi P., Sara, Juan, Fátima, Maurizio, Juan Luis, los "Luises", Víctor, Cristina, V. Carlos, Gregg. En definitiva, gracias a todos aquéllos que habéis dado la oportunidad de conocer a esa chica que miraba al suelo.

Gracias a Pablo Z. por siempre estar disponible para escuchar mis dudas de "dinámica". Gracias a Diana por enseñarme las prestaciones ocultas del Corel, pero sobre todo, por ese "agosto" intenso en el 121. Gracias también a María, Bea, Sergio y resto de becarios del dpto. Gracias a Pablo O., por contarnos nuestras penas, nuestras alegrías y… los plazos :-) Gracias a Natalia por las primeras clases de atmósfera media.

Ich möchte auch bei meinen Kollegen von der Arbeitsgruppe „Physik der mittleren Atmosphäre" bedanken. Ihr habt mich mit den plötzlichen Stratosphärenerwärmungen viel, viel geholfen, aber ich habe auch mit euch die deutsche Landeskunde entdeckt (Und die Kuchen, natürlich!). VIELEN DANK: Anne, Markus, Janna, Katja, Sophie, Steffi, Anke, Christian. Ich möchte auch bei Frau Labitzke bedanken. Es ist immer wunderbar mit Ihnen über die Stratosphäre zu sprechen.

Gracias a mis compañeros de la carrera, por haber hecho de esos años los más felices de mi vida: Elena (llevamos casi 25 años juntas y espero que aguantemos mínimo otros 25 más!!!), Vicky (gracias por estar siempre dispuesta a escucharme y por tus consejos, que, aunque no te lo creas, te hago caso), Mario (mi primer amigo en el laboratorio de química), Sergio, Celia (gracias por aportar serenidad), Jarín, Chechu, Willy, Guada… Gracias a mis compañeros atmosféricos, MariCarmen (gracias por tus sabias recomendaciones y por todo lo que te has preocupado por mí), Vanesa (gracias por compartir esas ganas de vivir), Marta, Paul (gracias por todos los años que hemos compartido en la facultad, por escuchar todas mis alegrías y mis penas, por estar ahí cuando te necesitaba), José Miguel,… Gracias a Irene (sólo por ti, el Erasmus mereció la pena), a Ángel (por acompañarme en las clases de radiación y dinámica de las 8.30), a Loreto,… Gracias a Maripili, aunque no seas física :-)

Gracias a mis "Friends" del piso de abajo, Marcos y Joaquín. Gracias por esas horas de largas charlas en "Pinocho". Marcos, creo que es imposible devolverte todo lo que me has aportado en estos años.

Gracias a Ana, por tu apoyo incondicional. Siempre he podido contar contigo y estoy segura de que así será en el futuro, no importa dónde estemos.

Vielen Dank, Maria. Ich möchte dir für viele Sachen danken... z. B: Ich habe Deutsch mit dir gelernt; du hast für mich gesorgt, als ich in Berlin war ....

Y como en todo, los últimos serán los primeros… Abuela, gracias por todo el tiempo que me has dedicado desde hace 29 años. Mamá, Papá, gracias por esas "cenas", por escucharme y por saber que siempre puedo contar con vosotros, estéis donde estéis. Gracias por haberme tranquilizado cuando lo necesitaba, por no hacerme caso cuando decía tajantemente "yo nunca haré …" (sabíais que ése era el primer paso para decidirme a hacerlo), y en definitiva, gracias por haber hecho que sea lo que soy.

Index

I. Introduction

Stratospheric warming is one of the most important stratospheric variability phenomena. This PhD thesis aims to present a comprehensive study of stratospheric warmings. This first chapter is a description of the motivation of this work, followed by an explanation of the main goals and a layout of the PhD thesis.

1. Motivation

Most of the relevant atmospheric phenomena take place in the *troposphere*, which is the atmospheric layer closest to the surface, extending upward to 10 km approximately. It contains about 85% of the total mass of the atmosphere. The vertical distribution of the temperature in the troposphere allows vertical air motions and is completely different from the next upper layer, the *stratosphere*, characterized by a stratified air. Based on this, tropospheric processes have been traditionally considered as the only ones that could influence the weather on surface, with no effects from the upper atmospheric layers. However, in the last 50 years, several studies have given evidence of the existence of a coupling between the troposphere and the stratosphere. First, it was found that the troposphere could influence the stratospheric state by the upward propagation of tropospheric disturbances that reach the upper layer, thus conferring a passive role to the stratosphere [e.g.: Charney and Drazin, 1961]. More recently, some authors [e.g.: Baldwin and Dunkerton, 1999, 2001] have given observational evidence of an active role of the stratosphere on the determination of the surface weather, when strong stratospheric anomalies propagate downward and reach tropospheric levels within some weeks. This has also led to the consideration of the stratosphere as a potential predictive tool for middle range surface weather [e.g.: Baldwin et al., 2003; Jung and Barkmeijer, 2006].

Stratospheric warmings are one of the most abrupt and prominent phenomena that take place in the wintertime polar stratosphere and seem to have important effects on the atmospheric circulation, even beyond this layer. This phenomenon consists of an increase of temperature in the polar stratosphere in wintertime, which leads to an abrupt weakening, and occasionally even the reversal, of the typical wintertime circulation in that region [Andrews et al., 1987]. Different types of stratospheric warmings can be distinguished depending on their intensity and timing. In midwinter, the most important warmings are called *major stratospheric warmings* (MSWs). They are characterized by an abrupt breakdown of the westerly stratospheric circulation (stratospheric polar vortex) and the subsequent recovery of the polar vortex. In late winter, the transition to the summer structure of high temperatures and easterly winds is achieved by the so-called *stratospheric final warmings* (SFWs).

Since the discovery of stratospheric warmings by Scherhag [1952], the scientific community has shown a growing interest in their understanding. In recent years, the amount of work about this topic has remarkably increased. In particular, the main aim is

to obtain a good representation of future climate change by model projections, due to the mentioned feedback of these events on the troposphere.

Nevertheless, there still exits a great uncertainty in the knowledge of stratospheric warmings, particularly in the mechanisms leading to their appearance. Although some studies have proven that a sudden increase in the upward propagation of planetary wave activity is responsible for these events [e.g.: Matsuno, 1971; Polvani and Waugh, 2004; Black and McDaniel, 2007], the trigger mechanisms causing the abrupt amplification of wave activity are under discussion. Some work has related it to the appearance of anomalous tropospheric circulation structures, such as blockings, [e.g., Labitzke, 1965; Martius et al., 2009; Woollings et al., 2010] or to the effects of Eurasian snow cover [Orsolini and Kvamstø, 2009]. However, the precise nature of the link between them and stratospheric warmings is still unclear. Other external factors add to the uncertainty, such as the modulation of the polar stratospheric circulation by the equatorial Quasi-Biennial Oscillation (QBO) [Holton and Tan, 1980], the solar activity [e.g., Labitzke and van Loon, 1988] and the oceans, in particular, of the well-known El Niño-Southern Oscillation (ENSO) events [e.g., Ineson and Scaife, 2008; Cagnazzo and Manzini, 2009].

As a consequence of this uncertainty, climate model projections do not reveal a coherent picture of stratospheric change. There is a wide range from a projected intensification and longer persistence of the winter polar stratospheric circulation in a future climate [e.g., Shindell et al., 2001] to a projected weakening of this circulation due to enhanced tropospheric wave forcing in a future climate [e.g., Schnadt et al., 2002; Huebener et al., 2007].

This PhD thesis explores some of the features of stratospheric warmings that show currently the highest uncertainty. Thus, driving mechanisms, impact on the tropospheric circulation and their possible changes in the future due to the increase in greenhouse gases concentration are examined in detail by using both, reanalysis data and model simulations.

2. Objectives and layout

Objectives

The main aim of this PhD thesis is to improve the knowledge of boreal stratospheric warmings, with a special focus on the associated tropospheric-stratospheric feedbacks. To achieve this goal, different features of these phenomena that have not been investigated yet or that do not show a consensus among previous studies are analyzed in detail. This analysis refers to the two most relevant types of warmings, MSWs and SFWs, in different periods of time: the recent past and present (since 1960), and the future.

Concerning **major stratospheric warmings** (MSWs), the specific questions to be addressed and the methods how they are dealt with are:

Recent past and present

- *Which are the main aspects related to MSWs where chemistry climate models (CCMs) and atmosphere-ocean general circulation models (AOGCMs) show deficiencies?*

  MSWs in three different types of model simulations are studied and compared with reanalysis data. Two of these simulations correspond to transient[1] and constant present-day conditions respectively, both run with a CCM. The third simulation has been run with an AOGCM under present-day conditions. The analysis of possible differences among the simulations in the performance of MSWs can highlight the role of some processes involved in MSWs that are described in a different way in each model.

- *What are the most important trigger mechanisms causing the abrupt amplification of the upward propagating wave activity prior to MSWs? And how can other factors, not directly related in space and time to MSWs, modulate this sudden increase of wave activity?*

  To answer these two questions, two recent MSWs (occurred in 2009 and 2010), are examined. Both MSWs were preceded by nearly the strongest injection of tropospheric wave activity on record and their central date was almost coincident. However, the typical external factors that influence the occurrence of MSWs (the Quasi-Biennial Oscillation, sunspot cycle or El Niño) were dissimilar in the two midwinters: favorable in 2010 but unfavorable in 2009.

Future

- *Will a future increase in greenhouse gas concentrations affect major stratospheric warmings?*

  The comparison of relevant features of future projected MSWs, including the associated tropospheric changes, in two different CCM simulations will give an answer to the question. Both simulations covered the period 1960-2100, but while one includes a prescribed climate change, the other one does not.

[1] A *transient simulation* is an experiment in which the forcing is allowed to evolve gradually according to a prescribed emission scenario, so that the climate of the model represents a mode of possible change according to the variations in the forcing [IPCC, 2007].

In the case of **stratospheric final warmings** (SFWs), this study addresses the following questions:

Recent past and present

- *Does a relationship exist between variations in the timing of SFWs and changes in the troposphere?*

  This question is addressed by the study of changes in monthly fields associated with the interannual variability in the timing of SFWs in observations (from 1960 to 2000).

- *Can CCMs reproduce the interannual variability of the timing of SFWs? If so, can they simulate the same relationship between the dates and circulation anomalies in the troposphere as identified in observations?*

  The validation of a CCM to reproduce the interannual variability of SFW dates and their associated changes in tropospheric circulation is carried out by the comparison of the results derived from observations with those of a transient CCM simulation.

Future

- *Will the persistence of the polar stratospheric vortex show a trend in the future?*

  This question is addressed by comparing selected past and future periods in two CCM simulations, one run under climate change and the second under non-climate change conditions.

Layout

This PhD thesis is composed of nine chapters being this introduction Chapter I. Chapter II contains a state-of-the-art of stratospheric processes and, in particular, stratospheric warmings. Chapter III and IV describe, respectively, the data and methodology used in this work. Next, the main results of this study are explained in two chapters, the first one corresponding to major stratospheric warmings (Chapter V) and the second one to stratospheric final warmings (Chapter VI). Both chapters are divided into two sections: a) the analysis of specific dynamical processes of stratospheric warmings in the recent past and present period and b) impact of a prescribed future increase of greenhouse gases concentrations on each phenomenon. Then, a summary with the main conclusions drawn from this work is presented in Chapter VII and ideas for future research are proposed in Chapter VIII. Finally, Chapter IX includes an extended summary in Spanish of the PhD thesis.

II. Background and state-of-the-art

In this chapter, the most relevant aspects regarding the boreal stratospheric circulation and in particular, stratospheric warmings up to date are summarized. Section II.1 includes basic notions of the stratosphere. Section II.2 describes the climatological features of the stratospheric circulation and Section II.3 is focused on the dynamics that determines large-scale stratospheric circulation. The main concepts of the stratospheric variability are presented in Section II.4. A detailed description of stratospheric warmings is included in Section II.5. Finally, Section II.6 introduces some aspects regarding the influence of the climate change on the stratosphere.

1. Stratosphere: Definition, relevance and history

The atmosphere can be divided into several regions depending on different classifications. One of the most common is based on the vertical structure of the temperature field (Figure II.1) that identifies four layers: troposphere, stratosphere, mesosphere and thermosphere [Andrews et al., 1987].

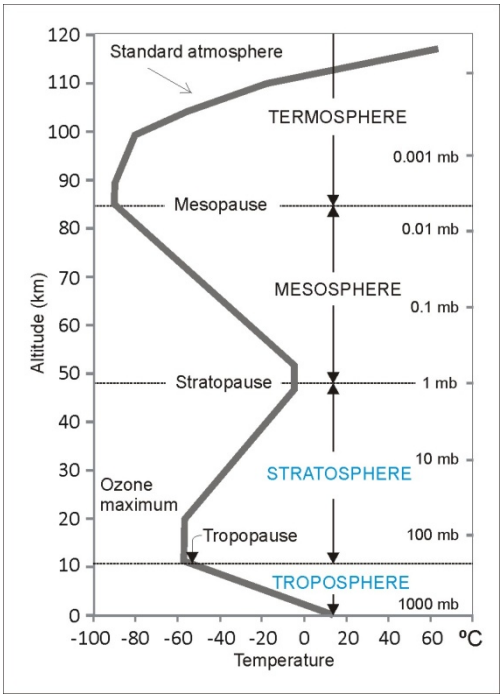

Figure II.1. Atmospheric layers according to the vertical distribution of the air temperature (heavy line). [Adapted from Ahrens [2000]].

The *troposphere* extends from the Earth's surface to the tropopause, that is, the lowest 8-18 km depending on the latitude. It has a negative gradient of temperature, which is mainly determined by the distribution of the water vapor that decreases with height in this region (Figure II.2). It is probably the most relevant atmospheric layer for

human beings, as it contains almost 85% of the total mass of the atmosphere and it is the portion of the atmosphere where most of the meteorological phenomena occur [Holton, 1992].

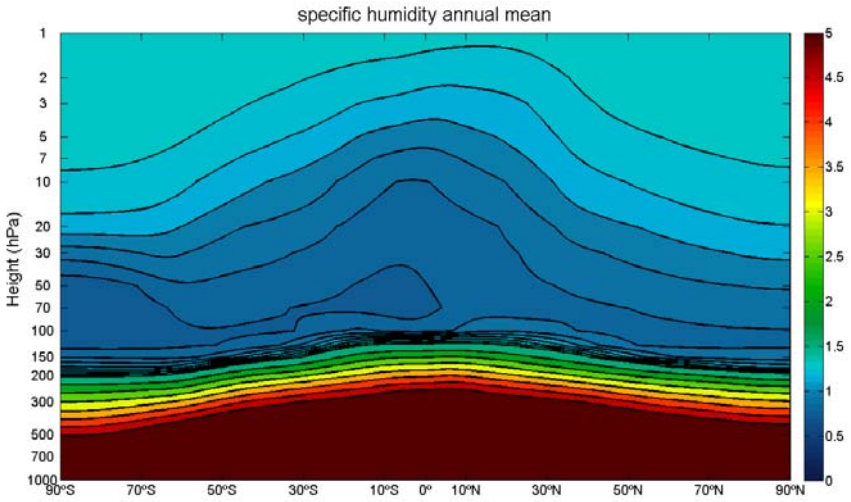

Figure II.2. Annual mean distribution of specific humidity. Dataset: ERA-Interim (1989-2001).

The *stratosphere* is localized just over the tropopause, extending upward to 50 km approximately. It is characterized by a quasi-isothermal behavior in its first few kilometers and a positive vertical gradient of temperature above that, which implies a stratified atmosphere and thus, the practical non-existence of vertical air motions. The sign of the temperature vertical gradient is explained by the distribution of the main chemical trace species of the atmosphere, i.e water vapor, CO_2 and ozone. The minimum shown by the water vapor concentration in the lower stratosphere is the main responsible for the very low temperature at that level (Figure II.2). However, it is the ozone, with its maximum molecular concentration at around 22 km, which determines the positive temperature vertical gradient in this atmospheric layer, due to the energy released in its exothermic photochemistry reactions of formation and destruction. In these numerous and complex reactions, both, solar ultraviolet radiation and the so-called ozone-depleting substances (ODS), such as the chlorofluorocarbons (CFCs), play important roles [Fahey and Hegglin, 2011].

The next higher atmospheric layer is the *mesosphere,* which is localized between the stratopause and the mesopause (at around 95 km). In this layer, the temperature decreases again with height. Finally, the *thermosphere* is the atmospheric shell above the mesosphere with a strong positive vertical temperature gradient due to the absorption by the oxygen and nitrogen molecules of the most energetic solar radiation (wavelengths less than 0.2 μm).

Although the troposphere is the most important region of the atmosphere in the climate system, the stratosphere also plays an important role. The relevance of this layer

is mainly based on two facts. First, it contains most part of the ozone that absorbs harmful ultraviolet radiation, avoiding that it reaches the Earth's surface. Since the first observations of the ozone depletion in the 1980s over the Antarctic, the concern for this atmospheric shell has grown, particularly focusing on the understanding of ozone control. Secondly, in recent decades some studies have given evidence of a stratospheric influence on surface climate, linked to variations of the polar stratospheric circulation in winter [e.g.: Quiroz, 1977; Baldwin and Dunkerton, 1999] or by changes in the radiative forcing. For instance, a large amount of work is recently being done on analyzing the processes involved in the stratosphere-troposphere coupling in order to improve, for example, the seasonal forecasting [e.g.: Marshall et al., 2009; Maycock et al., 2011].

The discovery of the stratosphere is attributed to Teisserenc de Bort at the beginning of the 20th century, who established that above the troposphere there is a region where the temperature becomes approximately isothermal or even slightly increases with height [Teisserenc de Bort, 1902]. In the same year, Assmann also claimed about the existence of a warm layer between 10 and 15 km [Assmann, 1902]. After that, the main information on the atmospheric temperature was obtained based on the refraction of sound waves [Whipple, 1923; Geller, 2010].

After World War II, an important progress in the understanding of the stratosphere was made due to the advent of rockets and radiosondes measurements. These observations gave evidence, for example, of a very important stratospheric phenomenon such as a **stratospheric sudden warming** in 1952 [Scherhag, 1952]. Moreover, systematic observations of the middle atmosphere were done since the International Geophysical Year of 1957-58.

During the 1960s, two different networks (one of meteorological radiosondes and the other of rockets) led to the establishment of the climatology of the lower and middle stratosphere up to 10 hPa in the Northern Hemisphere and to the availability of wind and temperature measurements in the upper stratosphere and lower mesosphere, respectively. However, these measurement techniques provided only in-situ data and, thus, no global information was obtained. Since 1969, this problem began to be resolved with the use of satellite information (Nimbus 3, TIROS-N or NOAA-6) [Andrews et al., 1987].

The availability of a large number of global data in recent decades has allowed the scientific community to improve the understanding of the most important stratospheric phenomena. Moreover, the advances in computer technology have also made possible the development of global, 3-dimensional general circulation models (GCMs) that are able to reproduce the stratosphere and even include interactively coupled chemistry. In the last years, several projects and initiatives have used these climate models to run simulations in order to prove some hypotheses about physical and chemical mechanisms related to the stratospheric circulation. They have also been used to try to determine the possible effects of the increasing greenhouse gas (GHG) concentrations on

the stratospheric state. One of the most important examples is the project called *Stratospheric Processes and their Role in Climate* (SPARC) of the *World Climate Research Programme (WCRP)* of the *World Meteorological Organization (WMO).*

2. Seasonal climatological stratospheric circulation

As already mentioned, some of the chemical constituents of the stratosphere, such as water vapor or ozone, play an important role in the determination of the stratospheric state, as they are radiatively active. However, mechanisms of other kinds have also a very relevant influence on the stratosphere. In this Section, the seasonal climatological characteristics of the longitudinally averaged (usually called zonal mean) distributions of temperature and zonal wind are first described in order to give a short overview of the main aspects of the stratospheric basic flow in each season. Then, the climatological two-dimensional circulation at selected stratospheric levels in each season will be explained. The description will be referred to the Northern Hemisphere, as this PhD thesis is focused on the boreal region.

a. Zonal-mean temperature and zonal wind distributions

Figure II.3 shows the climatology of the zonal-mean temperature for each season. In the lower and middle troposphere, the typical distribution with maximum heating at low latitudes and maximum cooling at high latitudes, particularly at the winter pole, is observed. In the upper troposphere, this structure changes, with a cold equatorial tropopause and polar lower stratosphere.

Focusing on the stratosphere, in the winter season, a maximum heating at the summer pole and a maximum cooling at the winter pole are observed. During the equinoxes, the meridional temperature gradient decreases. This distribution is approximately in agreement with the net radiative heating, which results from the sum of solar heating and infrared heating or cooling [Andrews et al., 1987]. However, there are some features inconsistent with the solar radiative flow. This includes the extremely cold tropical tropopause and the maximum temperature at mid-latitudes in the lower stratosphere of the winter hemisphere. However, the major deviation from radiative equilibrium in the stratosphere is the relatively warm temperatures in the winter pole, which would be much colder if only the solar radiative flow was taken into account. Another relevant aspect is the quantitative asymmetry in polar temperatures between both hemispheres in winter, i. e. the southern pole is much colder than the northern one during the winter season. Thus, dynamical processes must play an essential role as well to determine the basic stratospheric state.

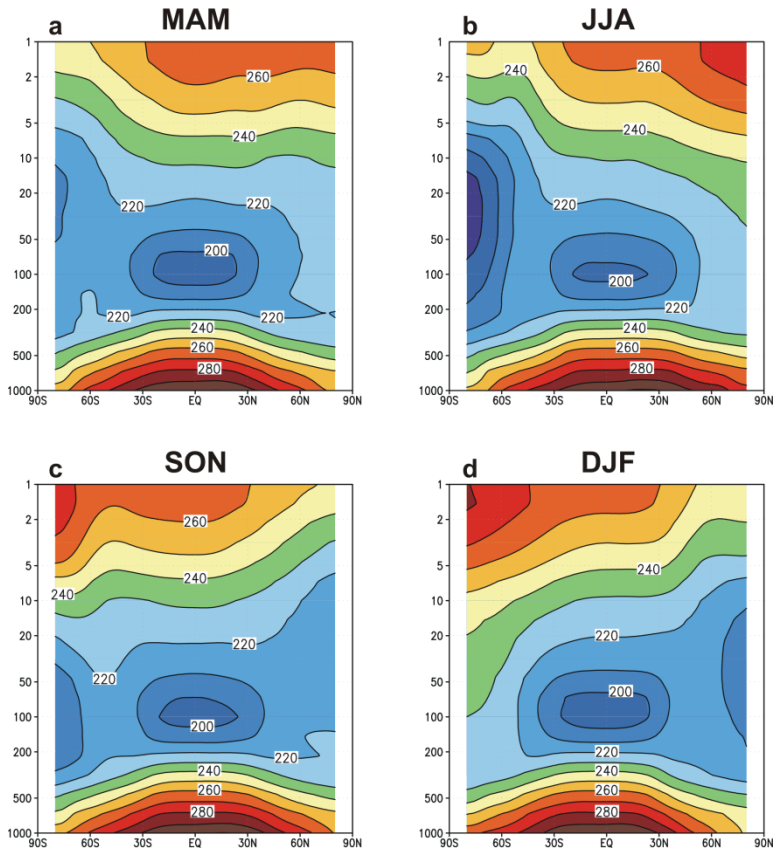

Figure II.3. Seasonal climatology of zonal-mean temperature for March-April-May (MAM), June-July-August (JJA), September-October-November (SON) and December-January-February (DJF). Contour interval: 10 K. (Data from SPARC climatology).

The zonal-mean zonal wind distribution is consistent with that of the zonal-mean temperature, as it follows the thermal wind balance (Figure II.4). So, in the stratosphere, whereas the summer hemisphere shows zonal-mean easterlies, the winter hemisphere is characterized by zonal-mean westerlies with its maximum called *polar night jet* [Holton, 1992]. This stream is localized around 60°-65° at the middle stratosphere and delimits the *stratospheric polar vortex,* a strong cyclonic circulation of great importance not only in the stratosphere but also in the troposphere. At the equinoxes, weak westerlies appear in both hemispheres. As observed in the zonal-mean temperature field, there is also an asymmetry between the Northern and Southern hemisphere with stronger values in the austral one.

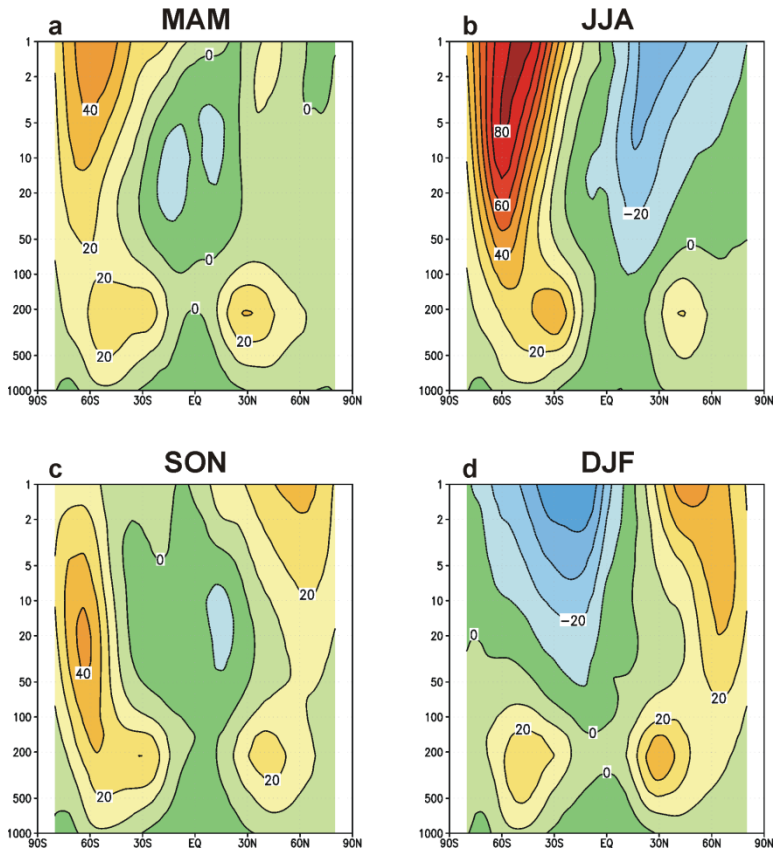

Figure II.4. As Figure II.3 but for zonal wind. Contour interval: 10 m s^{-1}.

b. Longitude-latitude stratospheric mean circulation

Figure II.5 illustrates the mean stratospheric circulation at 10 hPa for each season in the Northern Hemisphere, the region of interest in this study. Whereas the summer season is characterized by an anticyclonic circulation over polar latitudes, consistent with the zonal-mean easterlies; in wintertime the strong cyclonic circulation (the aforementioned *stratospheric polar vortex*) is identified at high latitudes. In the equinoxes, the boreal stratospheric circulation displays weak structures, resulting from the transition from the two opposite structures of solstices: the formation of the polar vortex in autumn (due to the disappearance of the solar heating at polar regions) and the decay of this structure in spring (as a consequence of the returning of the sunlight to high latitudes).

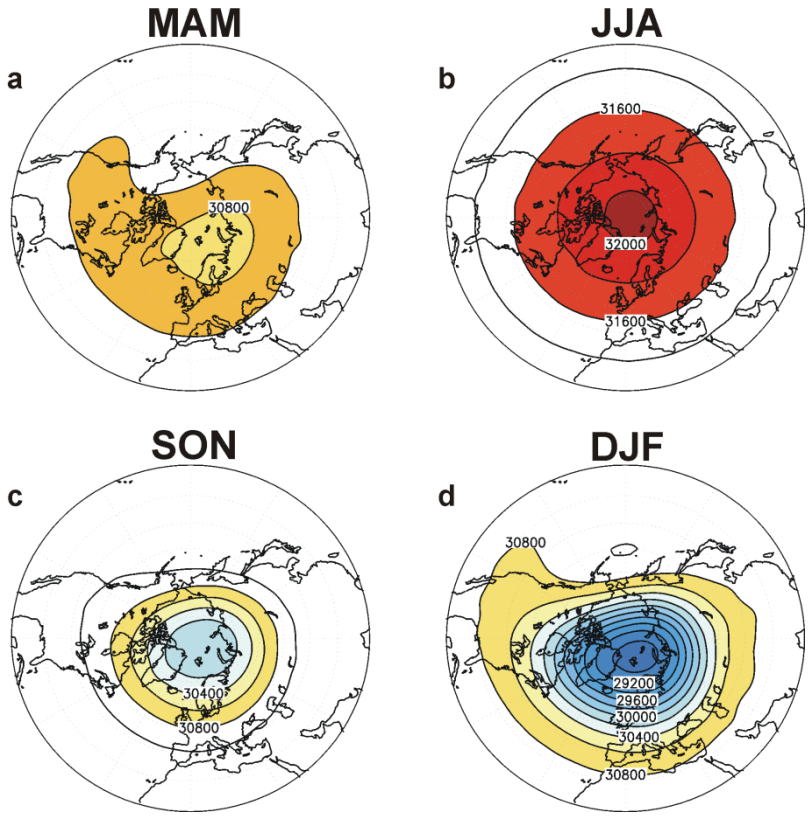

Figure II.5. Seasonal climatology of geopotential height at 10 hPa for March-April-May (MAM), June-July-August (JJA), September-October-November (SON) and December-January-February (DJF). Contour interval: 200 gpm. Dataset: NCEP/NCAR reanalysis (1979-2010).

As mentioned before, the *stratospheric polar vortex* is the most prominent structure of the wintertime stratosphere. Acting like an air-barrier, it prevents the mixing between the air coming from lower latitudes and the polar air. Due to this fact, the Arctic vortex plays a relevant role in the distribution of trace gases and, in particular, of ozone. Additionally, the isolation of the polar air allows the occurrence of extremely low temperatures, which favors the formation of polar stratospheric clouds (PSCs) when temperatures fall below about -78°C. These clouds are the key in the chemical destruction of ozone, since the reactions on liquid and solid PSC particles lead to the formation of the highly reactive chlorine gas (i.e., ClO), which catalytically destroys ozone [Fahey and Hegglin, 2011].

Unlike the Southern Hemisphere, the northern polar vortex is not completely centered over the polar cap, but slightly shifted towards Eurasia due to the weak stratospheric Aleutian high that results from the different distribution of land-sea and orography.

Because of dynamical processes, the polar vortex shows a large variability during winter, with periods of extreme low and high intensity (stratospheric warmings and polar vortex intensifications, respectively) and rapid transitions from one state to the other [Waugh and Polvani, 2010]. As will be explained in Section II.4, the Northern

Annular Mode (NAM) is the variability mode that gives a measure of variations in the intensity of the polar vortex [Thompson and Wallace, 1998, 2000]. This mode is also the dominant variability pattern in the extratropical stratosphere and troposphere [Baldwin and Dunkerton, 1999, 2001].

3. Stratospheric dynamics

As indicated in Section II.2, dynamical processes play a very important role in the determination of the basic stratospheric state. In this Section, the main equations that describe the most important large-scale motions in the stratosphere are explained. (Appendix 1 contains the basic equations from which these equations are derived). Then, a specific description of the main atmospheric waves is included.

a. The Eulerian-mean equations

The stratospheric basic flow traditionally is referred to as the zonal-mean flow. The basic flow is also the background flow upon which disturbances, called "eddies", are superimposed, forming the total stratospheric flow. The interaction between these two components of the flow is done in two ways (the mean-flow state influences the propagation of the disturbances, whereas eddies can in turn cause significant mean-flow changes). This interaction is responsible for important phenomena in the stratosphere such as stratospheric warmings, the issue of this study.

The zonal mean of a variable A is computed as

$$\left[A(\varphi,z,t)\right]=(2\pi)^{-1}\int_0^{2\pi}A(\lambda,\varphi,z,t)d\lambda \qquad \text{(II.1)}$$

and the departures from the zonal mean will be denoted as $A^*(\lambda,\varphi,z,t)=A-[A]$. When the zonal mean is calculated in this way, i.e. over longitude (λ), at fixed latitude, altitude and time values (φ, z and t, respectively), the mean is called *Eulerian mean*. In the case that the mean is computed at a fixed packet of fluid parcels, the mean is called *Lagrangian mean* [Andrews et al., 1987]. As this study is based on the Eulerian mode, the description of motions will be done hereafter according to this formulation.

When applying the decomposition of each variable into the zonal mean and the eddy components to the set of primitive equations of the quasi-geostrophic[1] Eulerian-mean flow (Appendix 1, eq. (A1.5)) and taking the zonal-mean average, the following expressions are obtained:

[1] An explanation of the quasi-geostrophic approximation is found in Appendix 1.

$$\begin{aligned}
&\frac{\partial[u]}{\partial t} - f_0[v_a] - \left[F_{f_\lambda}\right] = -\frac{\partial\left[v^* u^*\right]}{\partial y} \\
&\frac{\partial[\theta]}{\partial t} + [w_a]\frac{\partial \theta_0}{\partial z} - [Q] = -\frac{\partial\left[v^* \theta^*\right]}{\partial y} \\
&\frac{\partial[v_a]}{\partial y} + \frac{1}{\rho_0}\frac{\partial\left(\rho_0[w_a]\right)}{\partial z} = 0 \\
&f_0\frac{\partial[u]}{\partial z} + \frac{R}{H}e^{-Rz/Hc_p}\frac{\partial[\theta]}{\partial y} = 0
\end{aligned} \qquad \text{(II.2)}$$

where (u, v, w) are the velocity components, θ is the potential temperature $\left(\theta = T\left(\frac{p_0}{p}\right)^{R/c_p}\right)$, F_f corresponds to friction or other non-conservative mechanical forcing, f is the Coriolis parameter (=2 Ω sin φ), Q is the diabatic heating, ρ_0 is the air density, R is the specific gas constant for the air, c_p is the specific heat capacity at constant pressure and H is the scale height (7 km for the middle atmosphere). The subscript a denotes the ageostrophic part of a variable and the subscript 0 indicates reference values. Finally, the terms $[v^*u^*]$ and $[v^*\theta^*]$ correspond to eddy fluxes of horizontal momentum and heat, respectively.

From equations (II.2), $[u]$, $[v]$ and $[\theta]$ can be derived. They determine ***the mean meridional circulation*** that consists of a two-cell structure in the winter stratosphere, with rising motion in both the tropics and polar latitudes and sinking in mid-latitudes (Figure II.6) [Dunkerton, 1978]. However, this cell structure is not consistent with the distribution of atmospheric trace species observed by Brewer and Dobson [Brewer, 1949; Dobson, 1956], because it is based on the Eulerian formalism and so, it cannot describe the transport of the air parcels [Kinoshita et al., 2010]. Neither does the Eulerian-mean meridional circulation explain the extratropical temperatures away from their radiatively determined values.

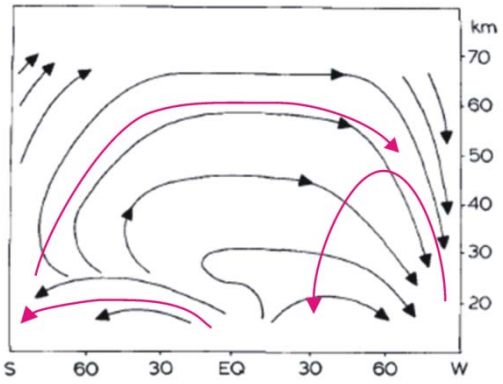

Figure II.6. Eulerian-mean meridional (magenta lines) and Brewer-Dobson (black lines) circulations in the stratosphere at the solstice [Adapted from Dunkerton [1978]]

b. The transformed Eulerian-mean equations

In order to solve the aforementioned problem, other formulations have been suggested, some of them based on the generalized Lagrangian-mean (GLM) theory [Andrews and McIntyre, 1978a]. However, the most widely used formulation is the transformed Eulerian-mean (TEM) equations of Andrews and McIntyre [1976, 1978b], which uses the Eulerian formalism. These equations ((II.3) for the quasi-geostrophic case) are obtained by transforming the Eulerian-mean equations to an alternative form, in which the effects of eddies on the zonal-mean state are highlighted.

$$\begin{aligned}
&\frac{\partial[u]}{\partial t} - f_0[\tilde{v}] - \left[F_{f_x}\right] = \frac{1}{\rho_0}\nabla\cdot\mathbf{F} \\
&\frac{\partial[\theta]}{\partial t} + [\tilde{w}]\frac{\partial[\theta]}{\partial z} - [Q] = 0 \\
&\frac{\partial[\tilde{v}]}{\partial y} + \frac{1}{\rho_0}\frac{\partial}{\partial z}\left(\rho_0[\tilde{w}]\right) = 0 \\
&f_0\frac{\partial[u]}{\partial z} + \frac{R}{H}e^{-Rz/Hc_p}\frac{\partial[\theta]}{\partial y} = 0
\end{aligned} \tag{II.3}$$

where $(0, [\tilde{v}], [\tilde{w}])$ is the *residual mean meridional circulation*, defined by the following equations:

$$[\tilde{v}] \equiv [v] - \frac{1}{\rho_0}\frac{\partial}{\partial z}\left(\frac{\rho_0[v^*\theta^*]}{\frac{\partial[\theta]}{\partial z}}\right) \quad ; \quad [\tilde{w}] \equiv [w] + \frac{\partial}{\partial y}\left(\frac{[v^*\theta^*]}{\frac{\partial[\theta]}{\partial z}}\right) \tag{II.4}$$

and **F** is the Eliassen-Palm flux, given by:

$$\mathbf{F} \equiv \left(0, -\rho_0[v^*u^*], \rho_0 f_0 \frac{[v^*\theta^*]}{\frac{\partial[\theta]}{\partial z}}\right) \tag{II.5}$$

The *residual mean meridional circulation* is a good approximation of the mean meridional mass cell (also called, *Brewer-Dobson cell/circulation,* illustrated in Figure II.6), which explains the stratospheric meridional distributions of tracers. This circulation consists of a rising motion of the tropical air across the tropical tropopause, a drift in the stratosphere towards the extratropical latitudes and finally, the air descends into the troposphere. As observed in equation (II.4) this circulation is driven by the wave-induced force in a steady-state limit [Haynes et al., 1991]. This wave-induced force is expressed as the divergence of the Eliassen-Palm flux ($\nabla\cdot\mathbf{F}$), where the eddy momentum flux and the eddy heat flux ($[v^*u^*]$ and $[v^*\theta^*]$, respectively) act in a combined

way. The divergence of the Eliassen-Palm flux is zero for linear, steady and conservative waves. In this case, the waves do not affect the mean flow (*Charney-Drazin non-acceleration theorem*) [Andrews et al., 1987].

c. Atmospheric waves

As just explained, waves are an essential component of the stratospheric circulation: they transport momentum that generates the *mean meridional circulation* and they also mix the atmospheric constituents. Thus, waves constitute the dominant source of stratospheric variability, being responsible for relevant phenomena such as the Quasi-Biennial Oscillation and stratospheric warmings [e.g: Charney and Drazin, 1961; Lindzen and Holton, 1968; Matsuno, 1971; Polvani and Waugh, 2004].

This section will be devoted to a description of their main properties in tropics and extratropics, separately.

i. Definition and classification of atmospheric waves

The term "*wave*" denotes perturbations with a (quasi-) periodicity in time and/or space that transport momentum and heat, which is fed back into the basic flow as the wave dissipates. In the atmosphere, they result from the competition between the inertia and a restoring force that act on air parcels [Andrews et al., 1987; Holton, 1992].

Atmospheric waves, in particular those that can be linearized, can be described by the *wave motions equations* (eq. (II.6)). They are derived by applying equations (II.2) to small-amplitude disturbances to the zonal mean:

$$\begin{aligned}
&\frac{Du^*}{Dt}+v^*\left(\frac{1}{\cos\varphi}\frac{\partial\left([u]\cos\varphi\right)}{\partial y}-f\right)+w^*\frac{\partial[u]}{\partial z}=-\frac{\partial\Phi^*}{\partial x}\\
&\frac{Dv^*}{Dt}+u^*\left(\frac{2[u]\cos\varphi}{a}+f\right)=-\frac{\partial\Phi^*}{\partial y}\\
&\frac{\partial\Phi^*}{\partial z}=\frac{R}{H}T^*\\
&\frac{\partial u^*}{\partial x}+\frac{1}{\cos\varphi}\frac{\partial\left(v^*\cos\varphi\right)}{\partial y}+\frac{1}{\rho_0}\frac{\partial\left(\rho_0 w^*\right)}{\partial z}=0\\
&\frac{D\theta^*}{Dt}+w^*\frac{\partial\theta^*}{\partial z}=\frac{[\theta]}{[T]}Q^*
\end{aligned} \qquad \text{(II.6)}$$

where Φ is the geopotential and a is the mean Earth's radius.

Solutions in the form $\left(u^*,v^*,w^*,\Phi^*\right)=e^{z/2H}\,\mathrm{Re}\left\{\left[\hat{u},\hat{v},\hat{w},\hat{\Phi}\right]\exp i\left(kx+mz-\omega t\right)\right\}$ are usually sought for the above equations.

Atmospheric waves can be classified according to different physical or geometrical features.

One of the most common classifications of atmospheric waves is based on the restoring force. In this case, waves can be (*internal) gravity waves*, if the responsible mechanism is the internal gravity or *Rossby waves,* when the restoring force is the poleward gradient of the planetary vorticity. When both mechanisms are combined, waves called *inertio-gravity* appear [Andrews et al., 1987].

Waves can be also categorized based on the type of excitation mechanism. If waves are continually maintained by a given mechanism of a certain phase speed and wave number, they are called *forced waves*. In contrast, if this mechanism is not maintained, they are known as *free*.

As the types of waves and the characteristics of their propagation vary latitudinally, principally because of the different latitudinal Coriolis effect on horizontal flow, the most important waves are described next according to the region of interest, i.e., tropics and extratropics.

ii. Equatorial waves

The effect of the Coriolis torque at low latitudes is small, being zero at the equator. This determines the nature of the atmospheric waves that propagate in the equatorial area, as their main restoring force cannot be related to the rotation effects. In fact, equatorial waves propagate vertically and zonally through the middle atmosphere and are trapped within 10°-15° of the equator, as the Coriolis torque reduces their amplitude away from the equator [Lindzen and Holton, 1968]. The generation of these equatorial waves is mainly due to the convection in the tropical troposphere and then, waves propagate vertically from there into the stratosphere [Gray, 2010]. Depending on the scale, different types of waves can be found in the tropics.

In the case of the small horizontal scales, the most important waves are the *internal gravity waves.* They have horizontal wavelengths of up to 100-200 km and vertical ones from 5-15km. According to their small scale, rotation effects and Earth's spherical problems are neglected and thus, internal gravity waves owe their existence to buoyancy restoring force [Andrews et al. 1987].

In the case of large-scale equatorial waves, they have planetary scale in the zonal direction, but they are latitudinally confined as it happens with those of small scale. In this case, the beta-plane approximation is applied, being centered at the equator, so that the Coriolis parameter can be expressed as:

$f = f_0 + \beta y$ with $f_0 = 0$ and $\beta = 2\Omega / a$, being Ω the Earth's rotation rate.

Moreover, the quasi-geostrophic approximation is not valid in this case. There are several types of large-scale equatorial waves that show different characteristics:

- *equatorial Kelvin waves,* with surfaces of constant phase (kx+mz-ωt) that propagates eastward with height and move downward with time;
- *Rossby gravity waves,* that show a westward phase with respect to the basic flow;
- *inertio-gravity waves,* with high frequencies that can propagate both eastward and westward; and
- *equatorial Rossby waves* for low frequencies, that can only propagate westward.

The mentioned equatorial waves have been shown to play an important role in the stratospheric equatorial dynamics, as they are believed to be, at least in part, responsible for the two most important phenomena of the stratospheric equatorial variability: the Quasi-Biennial Oscillation (QBO) and the Semi-Annual Oscillation (SAO) that are explained in Section II.4 [Andrews et al. 1987].

iii. Extratropical waves (Planetary-scale Rossby waves)

Although stratospheric extratropical variability is affected by small-scale waves (internal gravity waves) and large-scale waves (planetary Rossby waves), the latter dominate the dynamics at these latitudes, particularly in the wintertime boreal hemisphere [Plumb, 2010].

As their name indicates, planetary Rossby waves have horizontal wavelengths of the same order as the earth's radius. Concerning their time-scale, they have an important quasi-stationary component that leads to consider them as forced. Besides the in-situ generation in the winter stratosphere due to barotropic instability, their sources are principally located in the troposphere and they are responsible for variations of the potential vorticity in the mean flow, such as large-scale topography, asymmetric heating (e.g.: ocean-continent contrast) or averaged interactions on the mean flow from synoptic-scale eddies [Charney and Drazin, 1961; Plumb, 2010]. These variations are the origin of Rossby waves, since they are based on the conservation of the potential vorticity, being the restoring force the beta-effect (i.e., the variation with latitude of the Coriolis force) [Holton, 1992].

The linear wave theory that describes these waves is expressed by the linearized equation of the quasi-geostrophic potential vorticity (q) (eq. (II.7)). As these waves are typical of extratropics, the quasi-geostrophic approximation can be applied. Moreover, it is assumed that they are propagating in a basic constant zonal flow, whose properties vary only with height. For simplicity, non-conservative terms are not considered [Andrews et al., 1987].

$$\left(\frac{\partial}{\partial t}+[u]\frac{\partial}{\partial x}\right)q'+\frac{\partial \overline{q}}{\partial y}\frac{\partial \psi'}{\partial x}=0$$

$$\text{being } q'=\nabla^2\psi'+\frac{1}{\rho_0}\frac{\partial}{\partial z}\left(\frac{\rho_0 f^2}{N^2}\frac{\partial \psi'}{\partial z}\right) \text{ and} \qquad \text{(II.7)}$$

$$\frac{\partial \overline{q}}{\partial y}=\beta-\frac{1}{\rho_0}\frac{\partial}{\partial z}\left(\frac{\rho_0 f^2}{N^2}\frac{\partial \overline{u}}{\partial z}\right)$$

where ψ is the streamfunction and N is the log-pressure buoyancy frequency.

This equation can be transformed into the canonical wave equation $\frac{d^2\hat{\psi}}{dz^2}+n^2\hat{\psi}=0$, where n is a dimensional refractive index. Solutions of the form $\psi'=\hat{\psi}(z)\sqrt{\rho_0}\exp\left[i\left(kx+ly+mz-\omega t\right)\right]$ are sought, where the vertical wave number m is expressed as $m^2=\frac{N^2}{f^2}\left(\frac{\beta k}{k[u]-\omega}-k^2-l^2\right)-\frac{1}{4H^2}$. According to this, the dispersion relation is given by:

$$\left(\omega-k[u]\right)=-\frac{k\beta}{k^2+l^2+\frac{f^2}{N^2}\left(m^2+\frac{1}{4H^2}\right)} \qquad \text{(II.8)}$$

In the above expression, m should be real in the case of internal waves, i.e., vertically propagating. Under this condition, surfaces of constant phase show a westward tilt with height $\left(kx+mz=const.\rightarrow z=-\frac{k}{m}x, \text{ as k and m >0}\right)$.

Moreover, the positive m condition leads to the well-known *criterion of Charney-Drazin [1961]* (eq.(II.9)) that expresses the conditions required for the vertical propagation of Rossby waves.

$$0<\ [u]-c\ <\frac{\beta}{\left(k^2+l^2+\frac{f^2}{N^2}\frac{1}{4H^2}\right)} \qquad \text{(II.9)}$$

According to eq.(II.9), the stationary Rossby waves, which satisfy that c = 0, can only propagate if these two conditions are satisfied:

1) The background flow is westerly.

2) Westerlies should be weaker than a critical value that depends inversely on the horizontal wave number. Thus, only waves with very low horizontal wave numbers propagate vertically into the stratosphere.

From applying the *Charney-Drazin criterion* to the climatology of the zonal wind in the stratosphere, it can be inferred that Rossby waves will not be detected in the extratropics in summer or in the tropics, where easterlies prevail.

In the case of the winter extratropical stratosphere, there is an asymmetry between both hemispheres. Westerlies in the austral stratosphere are much stronger than in the boreal one and thus, the Rossby wave activity entering into the stratosphere is lower in the former. Moreover, due to the lower abrupt topography and land-sea contrasts, the generation of planetary waves in the Southern Hemisphere is clearly reduced with respect to the Northern Hemisphere [Andrews et al., 1987].

Thus, Rossby waves play a more relevant role in the northern extratropical stratosphere than in the southern one. In fact, as will be indicated on the next pages, quasi-stationary Rossby waves strongly influence the extratropical stratospheric circulation in the Northern Hemisphere, being responsible for the most important variability phenomena such as stratospheric warmings, the issue of this PhD thesis.

4. Stratospheric variability

Once the main source of stratospheric variability, atmospheric waves, has been presented, the most relevant phenomena of the equatorial and extratropical regions are described next.

a. Stratospheric equatorial variability

Quasi-Biennial Oscillation (QBO) and Semi-Annual Oscillation (SAO) are the dominant phenomena of stratospheric equatorial variability. As their name indicates, they are alternative series of easterly and westerly zonal wind regimes at equatorial latitudes, which propagate downward with time [Pascoe et al., 2005].

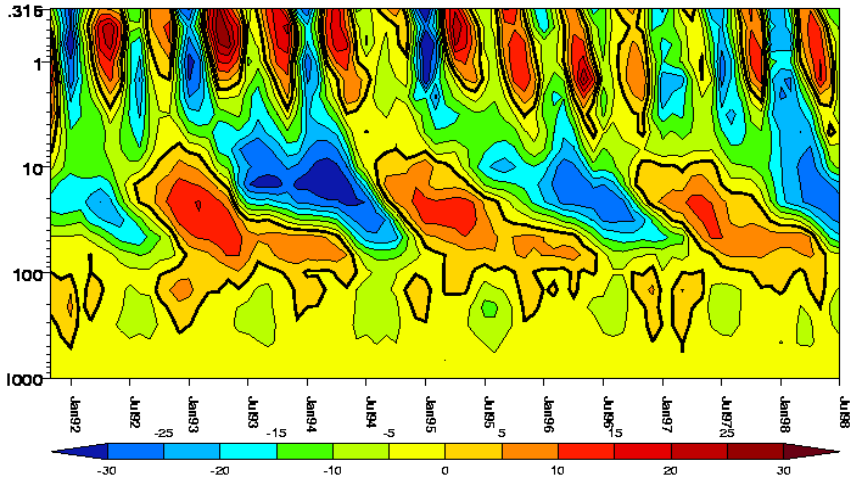

Figure II.7. Monthly mean zonal-mean zonal wind (m s^{-1}) at 1.25°N from the UKMO assimilated dataset. [Taken from http://ugamp.nerc.ac.uk/hot/ajh/qbo.htm].

In the case of the *QBO*, the oscillatory pattern extends from 100 hPa to 5 hPa (Figure II.7), showing a symmetric latitudinal structure about the equator with a half meridional width of 12° approximately and an average downward rate of 1 km $month^{-1}$ [Baldwin et al., 2001]. Concerning altitude, the maximum QBO amplitude is found at around 20 hPa [Naujokat, 1986]. However, the phases of QBO are classified by several authors according to the mean equatorial zonal-mean zonal wind at lower altitudes (40 hPa) [Pascoe et al., 2005]. The reason for selecting the 40-hPa level is that it is with respect to this level where the QBO signal in the extratropical Northern Hemisphere was found to be the greatest [Baldwin and Dunkerton, 1998]. The period of the QBO is approximately of 28 months and it is determined by the amplitude of equatorial waves involved in this oscillation (i.e., Kelvin, Rossby-gravity, inertio-gravity and gravity waves) [Plumb, 1984; Scaife et al., 2000].

The mechanisms responsible for the QBO involve momentum transport associated with equatorial waves that propagate upward and interact with the basic flow in an internal two-way feedback process. A further description of these mechanisms can be found, among others, in Plumb [1984] and Gray [2010].

Above 5 hPa, it is the SAO that dominates the equatorial variability (Figure II.7) [Gray, 2010]. It shows the maximum amplitude at the equator and a latitudinal half-width of about 25° latitude. Its period is of approximately 6 months and it is strongly influenced by the annual cycle [Andrews et al., 1987]. In this case, the involved equatorial waves are those that can propagate through the QBO winds and reach the area affected by the SAO. For instance, planetary waves propagating towards the equator from the winter hemisphere seem to have an important contribution and advection of summer easterlies by the Brewer-Dobson circulation as well. These contributions from Rossby waves and the Brewer-Dobson circulation would explain the semiannual period of the SAO as they are also strongly influenced by the annual cycle [Gray, 2010].

Although the QBO and SAO are restricted to the equator, they have relevant impacts on the extratropical flow. In particular, the QBO has been proven to modulate the propagation of planetary waves in the stratosphere and thus, the mid- to high latitudes stratospheric circulation. As explained next in Section II.5, this modulation plays an important role in the occurrence of stratospheric warmings in the Northern Hemisphere.

b. Stratospheric extratropical variability

The dominant low-frequency variability mode in the NH extratropical stratosphere is the Northern Annular Mode (NAM), which is also the leading mode in the wintertime troposphere [Baldwin and Dunkerton, 1999, 2001]. The NAM has usually been identified as the first empirical orthogonal function of monthly-mean, hemispheric geopotential height anomalies poleward of 20°. However, taking into account that the NAM is a

representation of a zonally symmetric mode [Wallace, 2000], Baldwin and Thompson recently proposed a new methodology based on daily zonally averaged geopotential [Baldwin and Thompson, 2009]. This formulation has been proven to detect more clearly the evolution of stratosphere-troposphere coupling events than the previous ones.

The anomaly structure that defines the NAM in the stratosphere is composed of two centers of action of opposite sign, one over the polar cap and a second one, much weaker, located at mid-latitudes, primarily over the Pacific [Baldwin and Dunkerton, 1999] (Figure II.8 upper row). Based on this, the stratospheric NAM index gives a measure of the strength of the polar vortex. In the lowermost troposphere, the NAM pattern also shows strong anomalies at high latitudes, but the mid-latitudes center is in this case divided into two parts, one over the Atlantic and the other one over the Pacific region (Figure II.8 lower row). This near-surface NAM is usually called Arctic Oscillation (AO) [Thompson and Wallace, 1998; Baldwin and Dunkerton, 1999]. At this level, the NAM explains a modulation of the climatological circulation features in the Euro-Atlantic sector, with a deepening of the Icelandic low and a strengthening of the Azores high in the positive phase.

The regional expression of the NAM over the Atlantic region is usually known as the North Atlantic Oscillation (NAO) [Walker and Bliss, 1932]. In the case of the Pacific basin, the physical interpretation of the AO is not as meaningful as in the Atlantic one. This, together with the observed independence between the two subpolar centers of action, has led some authors to disagree with the recognition of the AO as the hemispheric expression of the regional NAO. Thus, there is still much controversy in this correspondence [e.g.: Wallace, 2000; Ambaum et al., 2001; Rogers and McHuge, 2002].

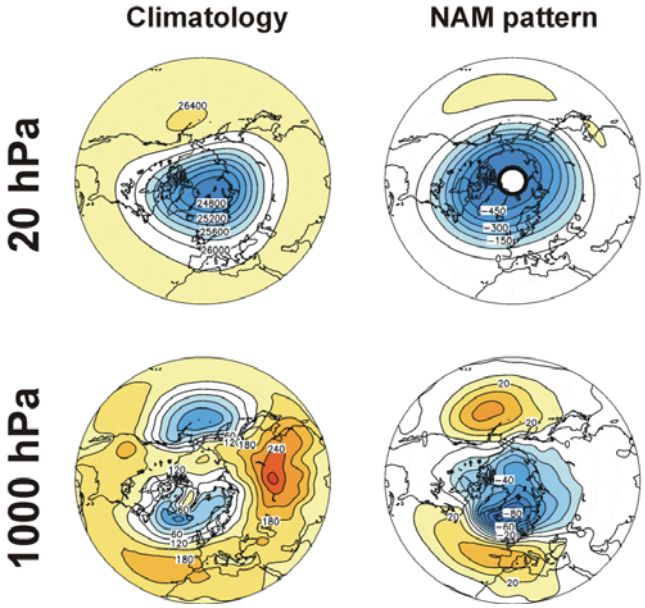

Figure II.8. (Left) Seasonal climatology of geopotential height (gpm) for December-January-February at 20 and 1000 hPa. **(Right)** Northern Annular Mode pattern at the same levels (positive phase). Dataset: NCEP/NCAR reanalysis.

The mechanisms responsible for the NAM are related to the internal dynamics of the atmosphere. In particular, variations in the quasi-stationary planetary waves and their interaction with the zonal flow have been shown to determine the northern annular variability, in such a way that changes in the planetary wave sources and propagation modify the polar vortex state [Hartmann et al., 2000].

Concerning the processes involved in the downward influence of the stratospheric NAM, some possible mechanisms have been proposed since the first identification of the association between the NAM pattern in the troposphere and changes in the strength of the polar vortex by Thompson and Wallace [1998]. Possible physical mechanisms are related to a direct potential vorticity inversion [Ambaum and Hoskins, 2002; Black, 2002], changes in the Rossby wave propagation [Hartmann et al., 2000] or in the wave reflection [Perlwitz and Harnick, 2003]. However, the exact dynamical procedure is still unclear.

Despite this uncertainty in the understanding of the exact dynamical process involved in the downward influence of the stratospheric NAM, some concepts concerning the impact of stratospheric anomalies on the troposphere have been developed in the last years. For instance, Baldwin and Dunkerton [1999 and 2001] showed that strong stratospheric NAM-like anomalies preceded tropospheric AO anomalies with a delay of weeks and even of months, what confers a predictive ability to the stratosphere. These strong stratospheric anomalies are associated with extreme regimes of the polar vortex. One of these regimes is related to an undisturbed, strong and anomalously cold polar vortex. It corresponds to a positive NAM index and is known as *stratospheric vortex intensification* [Limpasuvan et al., 2005]. In contrast, a negative NAM is associated with a disturbed, weak and anomalously warm polar vortex. These events are known as *stratospheric sudden warmings* (SSWs). They will be explained in more detail in the following section.

5. Stratospheric warmings

According to the last explanation, one of the most important extreme events of the wintertime boreal stratosphere are *stratospheric warmings.* In this Section, a detailed description of these phenomena, including their main features and life cycle, the driving mechanisms and their impact on the tropospheric circulation, is contained.

a. Definition and classification

As explained in Section II.2, the wintertime stratospheric circulation is characterized by zonal westerly wind, peaking in the polar night jet which is located approximately between 60° and 65°. This distribution of winds is consistent with a zonal-mean

temperature gradient decreasing towards the winter pole, due to the absence of sunlight in the polar region.

However, the mentioned wintertime configuration is disrupted in occasions by an increase in the polar stratospheric temperature that leads to the weakness of the polar vortex [Andrews et al., 1987]. This phenomenon is called stratospheric warming and takes place every year by the end of winter and in some years in midwinter as well. In 1952 Scherhag observed for the first time a phenomenon of this kind in midwinter. Based on its intensity and timing, the stratospheric warmings are classified into different types in the literature [Labitzke, 1981b]:

- Major stratospheric warmings (MSWs): This type of stratospheric warmings usually happens in January-February and in the NH, as only one MSW (in 2002) has been observed in the SH since Antarctic records began in the late 1950s [Roscoe et al., 2005]. They consist in a reversal of the meridional temperature gradient poleward of 60°N and a change of the polar stratospheric circulation, i. e. the breakdown of the polar vortex, which is reestablished after the occurrence of these events. As a result of the MSW, the polar vortex is either displaced from the polar cap (*vortex displacement*) or split into two parts of approximately the same size (*vortex splitting*) (Figure II.9a and b, respectively) [Labitzke and Naujokat, 2000]. These two types of vortex breakups are associated with large amplitudes of longitudinal wave number 1 and 2 preceding the warming, respectively. Consequently, MSWs have been traditionally classified as wave 1 (WN-1) and wave 2 (WN-2) events. However, the classification based on the shape of the polar vortex has been shown to be more accurate than that based on the wave amplitude due to the nonlinearity of the flow [Waugh, 1997; Charlton and Polvani, 2007].

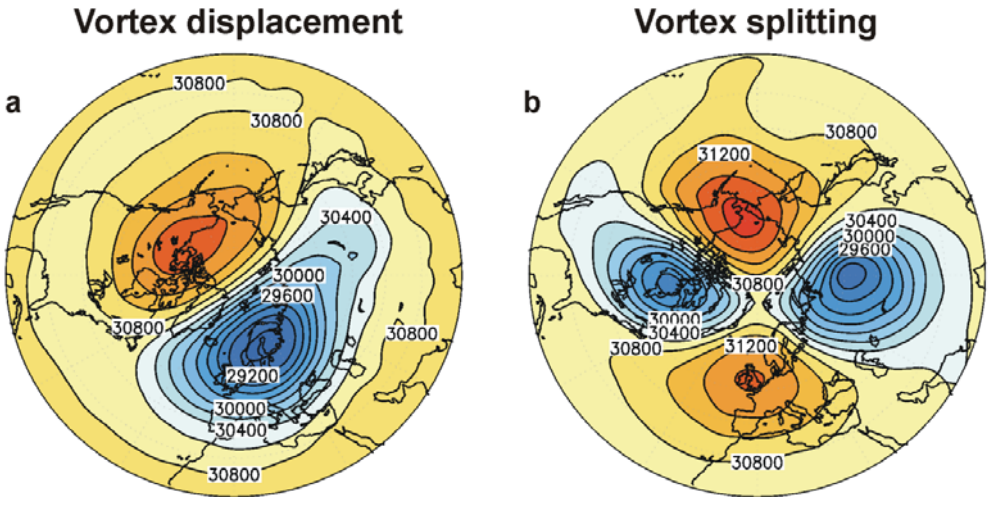

Figure II.9. Geopotential height at 10 hPa corresponding to **(a)** a vortex displacement type MSW that happened on 23 January 1987 and **(b)** a vortex splitting type MSW that happened on 24 January 2009. Contour interval: 200 gpm.

- Minor stratospheric warmings: This type of events can take place during the whole winter season and in both hemispheres. They consist of an abrupt increase of the polar stratosphere temperature, which can be very intense too, but it does not result in a reversal of the westerly circulation.

- Canadian warmings (CWs) usually happen in November-December. They originate through an anomalous strengthening of the stratospheric Aleutian anticyclone. CWs may reverse the meridional temperature gradient north of 60°N and on some occasions, CWs can even briefly change the zonal wind direction over the polar cap, but they do not lead to a breakdown of the cyclonic polar vortex. Some authors have shown that CWs can be a stratospheric response to the establishment and variations of the climatological east Asian low in the troposphere [Juckes and O'Neill, 1988].

- Stratospheric final warmings (SFWs) take place every spring in both hemispheres. They mark the final transition of zonal winds from wintertime westerlies to summertime easterlies at high latitudes in the stratosphere. As shown by Black and McDaniel [2007], SFWs are typically associated with a shift of the polar vortex off the polar cap. Two types of SFWs can be identified. One of them corresponds to the rapid transition to summer conditions driven by dynamical processes. The other one refers to the radiatively induced slow transition [Labitzke and Naujokat, 2000]. Another important aspect of SFWs in the NH is the high interannual variability in their timing [Waugh and Rong, 2002].

b. Life cycle of warmings

Several authors have pointed out that stratospheric warmings are usually preceded by an anomalously high injection of planetary wave into the stratosphere [e.g: Matsuno, 1971; Labitzke, 1977; McIntyre, 1982; Polvani and Waugh, 2004]. As a result, planetary waves interact with the mean flow and decelerate it, weakening the polar vortex. However, different evolutions of the polar vortex are identified depending on the type of the warming.

In the case of *MSWs*, in the literature the process has been traditionally divided into three phases: the *prewarming*, the *warming* and the *postwarming* stage [Kodera and Chiba, 1995]. Other authors such as Limpasuvan et al. [2004] have identified more steps in the life cycle of MSWs, but they can be embraced in the aforementioned three phases. The *prewarming* stage corresponds to a previous state of the polar vortex, when it is cold and well developed. In this stage, the upward propagating wave activity is deflected equatorward. Then, in the *warming stage*, this wave activity gets stronger and switches poleward, converging in the upper polar stratosphere. As a result, the temperature rises and the zonal flow decelerates, weakening and moving the polar vortex off the pole cap

[Kodera and Chiba, 1995; Limpasuvan et al., 2004]. The perturbation signal (weakening of the zonal flow and warming of the polar cap) propagates downward, even reaching tropospheric levels [Labitzke, 1977, Limpasuvan et al., 2004]. The anomalous upward propagation of the wave activity decreases due to the existence of easterly winds in the polar stratosphere and the polar vortex begins to recover from upper levels. The last period is the *postwarming stage* and is also called the *late winter cooling*, when the temperatures of the upper stratosphere depend only on radiative processes, as no wave energy is transported to those levels [Labitzke, 1981b].

Other observational aspects about the time evolution of MSWs can be found. For instance, some authors have suggested the existence of a preconditioned polar night jet, i.e., anomalously shifted towards the pole [Labitzke 1981a; McIntyre, 1982; Kodera and Chiba, 1995; Limpasuvan et al., 2004]. The responsible for the displacement of the PNJ would be a pulse of wavenumber-1 geopotential amplitude concurrent with a minimum of wavenumber-2 some time before the wind reversal [Labitzke, 1981a]. However, later, Charlton and Polvani [2007] have observed the preconditioned state of the PNJ only preceding the vortex splitting MSWs.

The *minor stratospheric warmings* show a very similar evolution to that of MSWs in many respects [Labitzke, 1977]. In fact, several studies have suggested that major and minor warmings are different manifestations of a continuum of midwinter stratospheric warmings [Yoden et al., 1999; Coughlin and Gray, 2009]. However, some studies have shown that there are some differences in the ratio of the amplitudes of geopotential height waves 1 and 2 between major and minor warmings [Labitzke, 1977].

Concerning the *CWs*, important differences are found with respect to MSWs. As indicated before, they originate from an intensification of the stratospheric Aleutian high due to an enhancement of wavenumber-1 wave activity. The intensified anticyclonic circulation moves eastward and displaces the cold stratospheric polar vortex center from the pole towards Siberia, being the net zonal-mean zonal wind north of 60°N consequently from the east [Labitzke, 1977]. However, despite this displacement of the vortex and the easterly flow, the cyclonic vortex remains strong and thus, a breakdown of the vortex does not exist. Another important aspect of CWs is that the intensity of the disturbance decreases with height and so, the flow is affected mainly in the middle and lower stratosphere. In contrast, the rest of winter warmings peak in the upper stratosphere and then, propagate downward.

In the case of the *SFWs*, Black et al. [2006] and Black and McDaniel [2007] found a similar evolution to that observed for the MSWs, with the largest deceleration of the mean flow at stratospheric levels that descends reaching the troposphere. Moreover, these events were also preceded by anomalous wave driving associated with upward propagating tropospheric waves as in the other warmings. However, some differences were found with respect to MSWs, in particular, after the events. Whereas after SFWs the stratospheric circulation relaxes toward climatology and easterly winds remain until

the subsequent autumn, MSWs are followed by an intense and cold polar vortex (the aforementioned *late winter cooling*). Additionally, radiative processes are also very important in the onset of SFWs, even though some studies have shown that SFWs are substantially wave driven [Yamazaki, 1987; Black and McDaniel, 2007]

c. Precursors

As discussed in the previous subsection, most stratospheric warmings are initiated by an anomalous upward propagating wave activity. Different dynamical models have been proposed to explain these phenomena and how the internal variability is modulated by external factors, but uncertainties still exist related to this topic, as will be seen next.

The first dynamical model of stratospheric warmings was proposed by Matsuno in 1971, based on the baroclinic instability of the polar night jet in the zonally averaged winter stratospheric flow. Although other models have been suggested after Matsuno's, all are generalizations of it [Andrews et al., 1987].

Matsuno's model explains stratospheric warmings by the interaction of upward propagating planetary waves with the zonal-mean flow. As indicated in Section II.4, most planetary waves are generated in the troposphere and propagate into the stratosphere. They establish a meridional circulation, where upward displaced air parcels move towards the equator and downward displaced ones move towards higher latitudes. Thus, the mean upward motion is induced by the convergence of heat flux at higher latitudes and downward motion at lower latitudes. Vertical motions accelerate the mean flow. In particular, warmings are usually associated with easterly accelerations on the higher latitude side at the leading edge of waves or on a critical surface, if waves are incident on it. This transport of eddy heat and momentum flux by planetary waves is responsible for the warming of the polar air and the deceleration of the westerly mean flow [Matsuno, 1971].

In winter, forced stationary waves of moderate intensity are the most predominant disturbances in the boreal polar stratosphere, controlling the atmospheric circulation in that region. Due to their low intensity, they are refracted towards the equator, as the polar night jet acts as a barrier for planetary wave propagation. As a result, waves accelerate tropical stratospheric mean flow, by depositing easterly momentum, but as their intensity is weak, there is not a significant result [Matsuno, 1971]. However, in some cases, an anomalously high upward propagation of planetary wave activity is injected into the stratosphere. Under these conditions, the polar night jet weakens, what allows planetary waves to propagate upward at higher latitudes. The zonal flow at those levels where waves deposit the momentum flux decelerates and even reverses from westerlies to easterlies. Due to the appearance of easterly values in the upper stratosphere, planetary waves will not be able to propagate up there and will deposit the easterly momentum at lower levels, propagating polar easterly winds downward.

This is the most accepted dynamical model that explains the generation of winter stratospheric warmings. Some generalizations of it have been made later, but the essential idea has not been changed. Nevertheless, some important questions remain to be answered. For instance, the mechanisms causing the anomalous increase in the tropospheric wave activity are still unknown. Some authors have identified, prior to some MSWs, the existence of free external Rossby waves that show westward travelling components between stratosphere and troposphere and an amplitude increase with height [Naujokat et al., 2002; Nishii et al., 2009]. These free waves cannot influence directly the mean flow, but they can interact with quasi-stationary waves, resulting in an amplification of the latter that, in turn, will impact on the mean flow. Actually, in a recent study, Garfinkel et al. [2010] have shown that the best and most effective way of enhancing the planetary wave pattern is obtained when regional tropospheric anomalies are collocated in phase with the climatological planetary wave pattern. Different phenomena seem to be related to this enhancement of planetary waves, but the detailed trigger processes of these free Rossby waves are still unclear.

One of these structures that have been proven to be associated with an abrupt increase in the upward wave activity prior to MSWs are the *blocking events*. These phenomena describe anticyclonic anomalies in the tropospheric pressure field that are persistent for several days to weeks and may block the usually prevailing westerlies and midlatitude storms [e.g., Tyrlis and Hoskins, 2008]. While some early work revealed single examples of MSWs that were preceded by tropospheric blockings [e.g., Julian and Labitzke, 1965; Quiroz, 1986], some authors have confirmed more recently that the presence of blockings modifies tropospheric planetary waves in a way that it can influence the onset and even the type of MSWs [Nishii and Nakamura, 2004; Martius et al., 2009; Woollings et al., 2010; Castanheira and Barriopedro, 2010]. However, the precise nature of the link between tropospheric blockings and stratospheric warmings is still unclear, as blockings, depending on their geographical location, may both enhance or weaken the stratospheric polar vortex [e.g.: Nishii et al., 2010; Garfinkel et al., 2010]. Figure II.10 illustrates an example of a blocking over the east Pacific coast some days before the MSW of 24 January 2009.

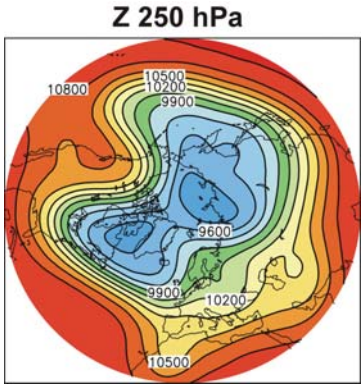

Figure II.10. Geopotential height at 250 hPa for the period 15-19 January 2009 (some days prior to a MSW). Contour interval: 150 gpm.

Other studies have identified another tropospheric structure linked to an increased upward propagation of stationary wave fluxes. This structure consists of a geopotential height anomaly dipole across the northern part of the Eurasian continent, which is seen as a signature of the effect of the eastern *Eurasian snow cover* [e.g.: Cohen et al, 2007; Orsolini and Kvamstø, 2009; Kolstad and Charlton-Perez, 2010; Garfinkel et al., 2010].

Another potential driving mechanism for MSWs is related to the *El Niño-Southern Oscillation* (ENSO). Some work has linked El Niño events to warm polar stratosphere in midwinter and thus, to the occurrence of MSWs [e.g.: van Loon and Labitzke, 1987; Manzini et al., 2006; García-Herrera et al., 2006]. This relationship is based on the excitation of the Pacific North American pattern (PNA) by ENSO events [e.g.: Garfinkel and Hartmann, 2008]. In the positive phase of this pattern, associated with El Niño events, a strengthening of the tropospheric Aleutian low is observed that leads to an amplification of the mid- to high latitude tropospheric geopotential stationary wavenumber-1 (one example of this is shown in Figure II.11) [Taguchi and Hartmann, 2006; Garfinkel and Hartmann, 2008]. The enhanced wavenumber-1 wave activity propagates into the stratosphere causing the weakening of the polar vortex, and, in some cases, a MSW during the warm winters of ENSO [Shiogama and Mukougawa, 2005].

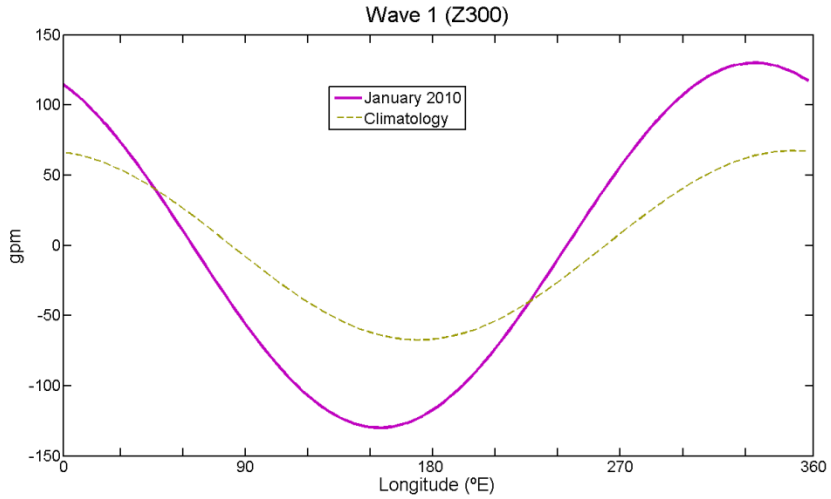

Figure II.11. 300-hPa geopotential height wavenumber-1 (gpm) averaged over 50°N-80°N as function of longitude for January 2010, a warm winter of ENSO, (solid line) and the climatology of January (period 1979/80-2009/10) (dashed line).

Finally, other external factors such as the *11-yr sunspot cycle* and the *QBO phase* seem to modulate the injection of the tropospheric wave activity into the polar stratosphere. In the case of the QBO phase, Holton and Tan [1980, 1982] showed that the east phase of the QBO is associated with a warm and weak polar stratospheric circulation at high latitudes in the NH, while the QBO west phase often comes along with cold and stable

polar winters (the so-called *Holton-Tan relationship*). This relation is explained by variations in planetary waves, which propagate vertically through the mean winter westerly flow at mid- and high latitudes and perturb the polar stratospheric circulation. As this kind of waves can only propagate through background westerly flow, when the QBO shows an east phase, planetary waves cannot propagate into the tropics and they are refracted towards high latitudes, disturbing the polar circulation and leading to the occurrence of a higher number of MSWs. The opposite happens in a westerly QBO phase.

Later and using longer datasets than the previous authors, Labitzke and van Loon [1988] and van Loon and Labitzke [2000] concluded that the solar cycle modifies the QBO influence in the NH stratospheric extratropics in winter, with warmer polar temperatures being more likely to occur under solar minimum conditions during the QBO east phase and under solar maximum conditions during the QBO west phase. The mechanisms related to this possible interaction are not clear and two main routes have been proposed: the "polar" one, consisting of a change in polar stratospheric temperatures that would modify the propagation of planetary waves and as a result the subtropical upper stratosphere [Kodera and Kuroda, 2002]; and a direct "equatorial" route, based on temperature and wind changes associated with the solar cycle in the upper stratosphere that would affect the descent rate of the QBO [Pascoe et al., 2005]. Additionally, Pascoe et al. [2006] found that the variability in the equatorial stratosphere (QBO and SAO) also has influence on the timing of midwinter stratospheric warmings. Nevertheless, there is still much uncertainty in this topic, as exceptions have been observed to the mentioned pattern of QBO-solar cycle modulation of polar stratospheric variability, particularly in recent years, e.g. in the 2008/09 winter.

In the case of SFWs, several studies have shown that changes in the upward propagating wave activity also play an important role in these phenomena. Apart from being a precursor of SFWs [Black and McDaniel, 2007], Salby and Callaghan [2007] have pointed out that variations in the vertical component of Eliassen-Palm flux can alter the timing of SFWs by as much as 1-2 months. Just as MSWs, SFWs are also sensitive to the QBO, as it modulates the propagation of planetary waves in the stratosphere.

d. Downward propagation of stratospheric warming signal

The influence of the tropospheric circulation on stratospheric warmings has been just described, as it acts in some cases as a precursor of these phenomena. However, in the last decades, evidence of a possible impact of stratospheric warmings on the tropospheric circulation has also been given. As anticipated some pages before, Baldwin and Dunkerton [1999, 2001] showed that stratospheric anomalies associated with extreme polar vortex events (extreme AO events) progress downward in the stratosphere over periods of several weeks. These anomalies reach the lower stratosphere and at that level they favor tropospheric anomalies of the same sign, lasting until two months after the central date of the extreme vortex event.

Based on Baldwin and Dunkerton's theory, MSWs are followed by a negative phase of AO pattern at surface with the strongest centers of action over the Euro-Atlantic sector and the associated changes in the near-surface temperature (Figure II.12 corresponding to MSWs in ERA-40 reanalysis data).

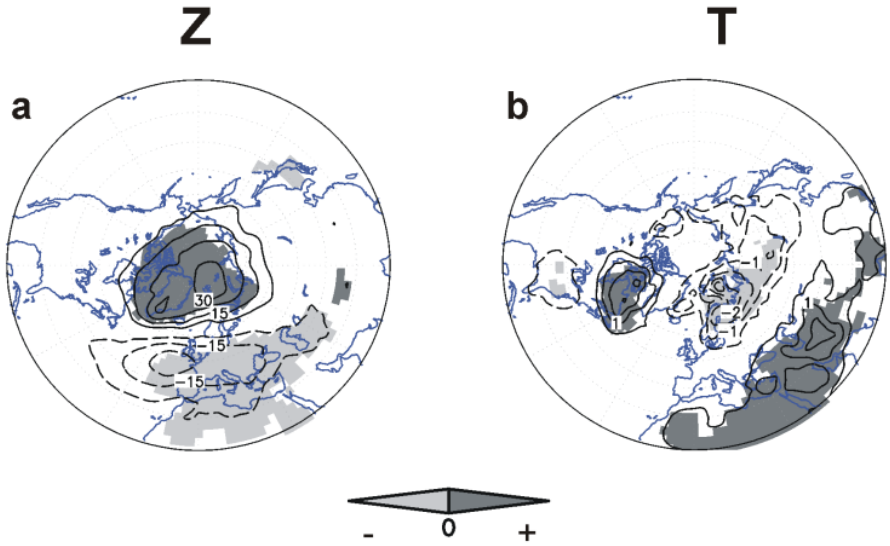

Figure II.12. Composite anomalies of 1000-hPa geopotential height (**left**, contour interval: 7.5 gpm) and temperature (**right**, contour interval: 0.5 K) averaged over 0-60 days following the occurrence of MSWs in ERA-40 (1960/61-1999/2000). Shadings correspond to statistically significant values at a 95% confidence level (Student's t-test).

In recent years, a high number of publications has been devoted to the analysis of the influence of MSWs on tropospheric climate [e.g.: Thompson et al., 2002; Limpasuvan et al., 2004; Nakagawa and Yamazaki, 2006; Charlton and Polvani, 2007; Kuroda, 2008; Gerber et al., 2009]. For instance, Thompson et al. [2002] found a connection between weak vortex events and surface weather, characterized by cold air flow over North America and Northern Europe. Latter, Nakagawa and Yamazaki [2006] identified that only the signal of midwinter stratospheric warmings preceded by an enhanced upward flux of wavenumber-2 wave propagates into the troposphere. However, Charlton and Polvani [2007] found a very similar tropospheric signature of both, vortex displacement and vortex split MSWs, but with the latter showing a center of positive anomalies over the Pacific that is inexistent in the case of displacement MSWs. The possible difference between the results of these two studies can be at least partially explained by the criterion used to identify the occurrence of a winter stratospheric warming. Whereas Nakagawa and Yamazaki used a criterion based on the increase of the polar stratospheric temperature, Charlton and Polvani imposed the reversal of the circumpolar circulation, which is only related to MSWs. In addition, Kuroda [2008] extended the study of the tropospheric fingerprint of MSWs to the tropical region and found the connection of these phenomena with a reduced convection in the tropical NH.

The amplitude of the tropospheric response to MSWs was assessed by Gerber et al. [2009], who pointed out that it is very sensitive to the depth of MSWs, conferring an active role to the stratosphere in the troposphere-stratosphere coupling, even though the initial signal (i.e. the upward propagating planetary wave that triggers MSWs) is forced from below.

Based on the mentioned connection between MSWs and surface weather, some authors have taken advantage of the analysis of NAM anomalies in the lower stratosphere to improve the skill of medium term weather forecast [e.g.: Baldwin et al., 2003; Christiansen, 2005; Jung and Barkmeijer, 2006]

On the other hand, a downward influence of MSWs has also been seen on the phenomena that have been identified as precursors of stratospheric warmings. Labitzke [1965] and Woollings et al. [2010] have found some indications of stratospheric warmings leading blocking events over certain regions, but the mechanism of which remains still unclear. Concerning ENSO, the tropospheric teleconnection between ENSO and the North Atlantic and European region in late winter is only fully observed when a MSW has previously occurred [Ineson and Scaife, 2009; Cagnazzo and Manzini, 2009].

In the case of SFWs, Black et al. [2006] and Black and McDaniel [2007] obtained similar tropospheric patterns after these events to those found following MSWs. However, some structural discrepancies between each other were found. In particular, the pattern associated with SFW is retracted northward in comparison with canonical NAM patterns. These differences led the authors to think that some discrepancies also exist in the involved processes in the troposphere-stratosphere coupling during SFWs and MSWs. In a later study, Black and McDaniel [2009] found that whereas the development and onset of MSWs are dominated by the stratospheric NAM variability, SFWs are controlled by two variability modes: the stratospheric NAM and the so-called polar annular mode. The latter mode was first defined by Black and McDaniel [2009] and represents the submonthly variability in the latitudinal position of the polar vortex. Additionally, it possesses a poleward-retracted dipole anomaly structure.

6. Influence of the climate change on the stratosphere

Another important aspect of the stratospheric circulation that nowadays deserves the attention of climate researchers is the analysis of the stratospheric climatic response to increasing greenhouse gas (GHG) concentrations.

In the last decades, a possible relationship has been found between an increase in GHG concentrations and a raise in tropospheric temperatures (Figure II.13) [IPCC, 2007]. This relationship is explained by the fact that high levels of GHG concentrations, in particular of CO_2, lead to increased absorption and emission of thermal infrared radiation in the atmosphere. As a result, part of this additional radiation turns back to

the surface and so, energy is again transferred to that level and the lower atmosphere, causing a raise-up of the air temperature there.

However, the effects of increasing GHG concentrations are not limited to the troposphere, but they also have an impact on the stratosphere [Fels et al., 1980]. As the absorption of IR radiation is greater in the lower atmosphere, most of the outgoing infrared radiation is trapped there. Hence, only a small amount of the IR radiation reaches upper levels. Moreover, CO_2 of those higher levels emits heat radiation, which is larger than the energy received from below and so, there is a net energy loss from the stratosphere, which leads to the stratospheric cooling. On the other hand, the anthropogenic emission of ozone-depleting substances (such as CFCs) along with this stratospheric cooling reinforces the cooling at this atmospheric layer, as the extremely low temperatures favor the creation of polar stratospheric clouds, on the surfaces of which photochemical reactions result in ozone depletion [Newman, 2010]. Due to the cooling of winter polar stratosphere, the meridional temperature gradient would intensify and according to the thermal wind balance, the zonal wind as well. Finally, as a result, the polar vortex would strengthen. Another consequence of the winter stratospheric cooling would be a longer persistence of the polar vortex in spring [e.g.: Waugh et al., 1999].

As a proof of the existence of the mentioned stratospheric cooling in the last decades, some studies have given evidence of negative trends in Arctic stratospheric temperature in the satellite era [e.g.: Labitzke and Kunze, 2005; Langematz and Kunze, 2006; Randel et al., 2009]. A tendency of the polar vortex towards a longer persistence in the last decades has also been detected [e.g.: Offermann et al., 2003 and 2004; Langematz and Kunze, 2006]. However, in most cases these trends are not statistically significantly different from zero, particularly in winter and spring, due to the high interannual dynamical variability in these seasons [Langematz and Kunze, 2006; Randel et al., 2009].

As already explained in this chapter, not only do radiative processes determine the stratospheric circulation, but also dynamical mechanisms play a relevant role. Concerning these mechanisms, several studies have already shown an increase in the upward propagating wave activity due to climate change [e.g.: Sigmond et al., 2004; Haklander et al., 2008; Garcia and Randel, 2008; Winter and Bourqui, 2010]. The enhanced wave activity would imply a more perturbed and thus, warmer polar vortex in the wintertime boreal stratosphere. Different suggestions have been proposed to explain this enhancement of wave activity. Whereas Sigmond et al. [2004] linked it to a higher transparency of the NH midlatitude tropopause for tropospheric wave activity or to more generation of wave activity near the tropopause, Haklander et al. [2008] related it to an increase in the longitudinal temperature variability at the lower stratosphere.

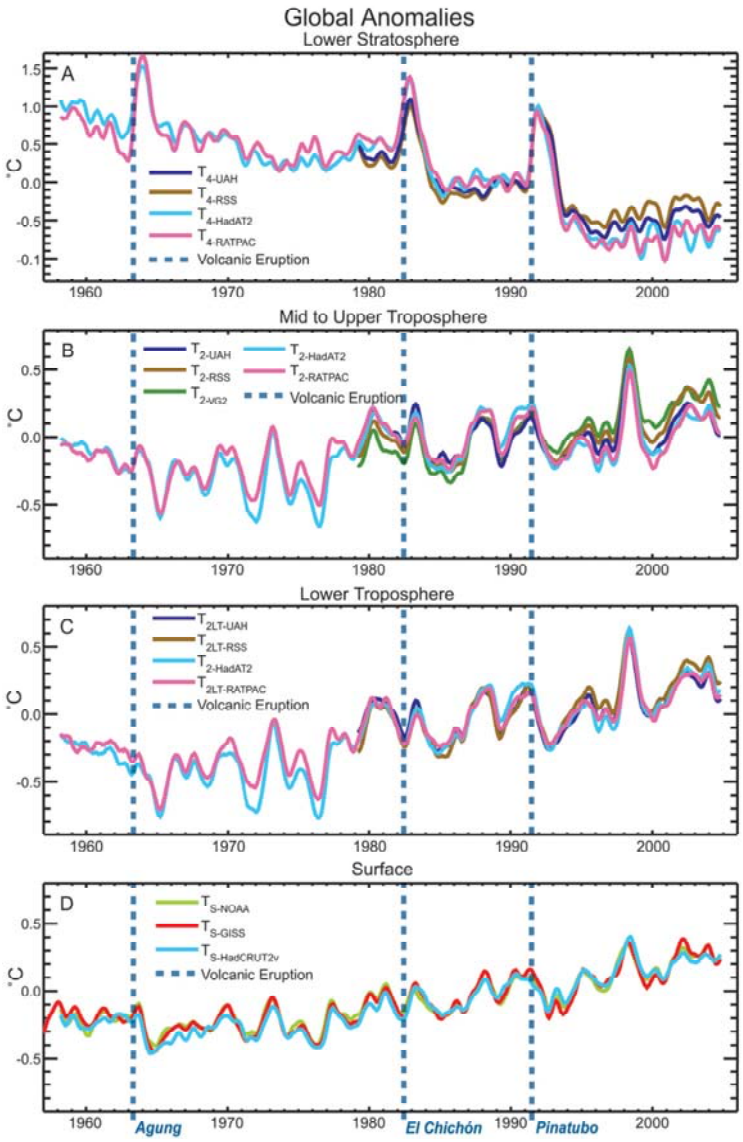

Figure II.13. Observed temperature anomalies (°C) at different atmospheric regions from different datasets. All time series are monthly mean anomalies relative to the period 1979-1997 smoothed with a seven-month running mean filter [From IPCC [2007]].

To sum up, climate change impacts on the NH polar stratosphere in two different ways with opposite effect: infrared radiative cooling and dynamical warming. However, there is still a large uncertainty about the net response of the stratospheric circulation to the joint concurrence of these two effects. Due to this, projections made by stratosphere-resolving models do not show a coherent picture of stratospheric change. This uncertainty also affects the projections of possible changes in stratospheric warmings. Thus, since the earliest study of these potential future changes by Rind et al. [1990], a wide range of conclusions have been drawn from different analyses performed with GCMs, AOGCMs and more recently, CCMs. Rind et al. found an increase of stratospheric warmings in early winter under doubled atmospheric CO_2 with a GCM. More recent analyses have found different predictions ranging from an increase in MSWs frequency

[e.g.: Huebener et al., 2007; Charlton-Perez et al., 2008; Bell et al., 2010; Butchart et al., 2010] to a reduced frequency [Shindell et al., 1998] and even others have identified no change [e.g: Butchart et al., 2000; McLandress and Shepherd, 2009b]. The mentioned lack of consensus points out the necessity of further analyses of future stratospheric circulation and stratospheric warmings.

Finally, an improvement in the knowledge of future changes in the stratosphere may also help to a better determination of possible future variations in the troposphere due to climate change. Based on the troposphere-stratosphere coupling, several studies have already shown that the introduction of a well-resolved stratosphere allows for a better simulation of surface climate variations in the last decades, in particular, in the North Atlantic sector [e.g.: Scaife et al., 2005]. In this sense, Scaife et al. [2011] have found very recently that changes in stratospheric circulation could play a relevant role in future climate change in the extratropical troposphere.

III. Data

In this PhD thesis, two types of data have been used: reanalysis data and model simulation output. Their main characteristics are described in this Chapter.

1. Reanalysis data

Atmospheric reanalyses constitute a useful tool in climate variability research. Their main purpose is to provide a dataset that is generated by using a "frozen" single model in data assimilation, so that changes observed in time are mostly due to variations in the atmospheric state and not in the data processing model [Kalnay et al., 1996]. Thus, the use of reanalysis datasets guarantees the quality of homogeneity in the data required in climatological studies. The longer this dataset is, the more robustness in the results is obtained. However, the computational cost associated with their production determines strongly the number of years reanalyzed in this type of datasets.

The atmospheric reanalyses consist of simulation outputs that take into account observations and background information. Observations comprise different types of variables and measurements (e.g., from aircrafts, ships, ocean-buoys, radiosonde ascents or satellite-borne instruments) and they are usually assimilated every 6 hours. The background information comes from a short-range forecast. In each time step, both, observations and background information, are combined to provide an accurate representation of the atmosphere at that particular time (e.g.: 00, 06, 12 or 18 UTC). This atmospheric representation is called analysis or rather "reanalysis" when the model used is not the operational one but that established to generate the reanalysis dataset. Then, this model output is used as the initial condition for the next time step of the short-range forecast [Uppala et al., 2005]. Hence, the reanalysis is imposed to follow the observed atmospheric variability.

Different reanalyses are currently available for the scientific community, such as the European ERA-40 and ERA-Interim, the American NCEP/NCAR reanalysis or the Japanese JRA-25. In this study, data from ERA-40 and NCEP/NCAR reanalysis have been used, since they cover the longest periods, from September 1957 to August 2002 and from 1948 until present, respectively. Both reanalyses use a three-dimensional variational system (3D-Var) in the data assimilation process and they produce reanalyzed data for the main synoptic hours, i.e., 00, 06, 12 and 18 UTC.

Despite the mentioned advantages that reanalyses have, some disadvantages and problems have been also documented in literature [e.g.: Trenberth et al., 2001]. These are related to deficiencies in technical choices and the observing system, and constitute a source of small inhomogeneities in the output [Santer et al., 2004]. The first ones correspond to problems in the physics and resolution of numerical model, the techniques employed to adjust for biases in the observational data and the properties of the data assimilation system. The problems in the assimilated data regard

inhomogeneities due to temporal differences in their availability, distribution and quality. In particular, the most important concern refers to the introduction of information derived from satellites in the second half of the reanalyzed period, i.e. in November 1978 in the case of NCEP/NCAR reanalysis and in 1979 in ERA-40 [Kalnay et al., 1996 and Uppala et al., 2005, respectively]. The enumerated deficiencies affect reanalysis products, leading, in some cases, to some fictitious results derived from studies that used these datasets. In particular, some significant problems have been found in climate change research, when estimating trends [Bengtsson et al., 2004; Santer et al., 2004]. Nonetheless, except for the mentioned specific purposes where reanalysis data have to be critically used, they constitute appropriate datasets in climate variability research [e.g.: Bengtsson et al., 2004].

On the other hand, NCEP/NCAR reanalysis and ERA-40 also show differences between them in the observational data and in the data assimilation that lead to some discrepancies in their output. For instance, some differences have been found by Labitzke and Kunze [2005] in their comparison of stratospheric temperatures over the Arctic among the two reanalyses and the Freie Universität Berlin (FUB) stratospheric analyses. FUB analyses can be considered as observations as they are closely linked to radiosonde measurements. However, in the case of the wintertime, even though NCEP/NCAR reanalysis and ERA-40 are not strictly identical, no relevant discrepancies in their output have been found in the polar stratosphere [e.g.: Labitzke and Kunze, 2005; Rico et al. 2008]. Concerning the phenomenon issue of this work, stratospheric warmings, certain studies have shown that both reanalyses can reproduce these events quite well and show very similar results [e.g.: Charlton and Polvani, 2007; Martineau and Son, 2010].

Specific basic features of these two reanalyses will be presented below.

a. ERA-40

The ERA-40 reanalysis was produced by the *European Center for Medium-Range Weather Forecasts* (Reading, UK). Its data assimilation model has a T159 horizontal resolution in spectral space (i.e. around 1.125° x 1.125° in lat-lon) and 60 vertical levels spanning from 1000 hPa to 0.1 hPa as Figure III.1.a shows [Uppala et al., 2005]. As indicated above, this reanalysis covers the period from September 1957 to August 2002. More information about ERA-40 can be found in Uppala et al. [2005] and is also available from http://www.ecmwf.int/research/era/do/get/era-40.

In this study, monthly and daily mean ERA-40 data of different atmospheric fields, such as geopotential, temperature or winds have been used. They have been retrieved from the webpage http://data-portal.ecmwf.int/data/d/era40_daily/. This webpage offers monthly mean and 6-hourly data. Daily mean data have been computed in this study as an average of the 4 times daily data. The data available in this webpage are

already displayed in a horizontal regular grid of 2.5°x2.5° and 23 levels from 1000 hPa to 1 hPa, covering the troposphere and stratosphere.

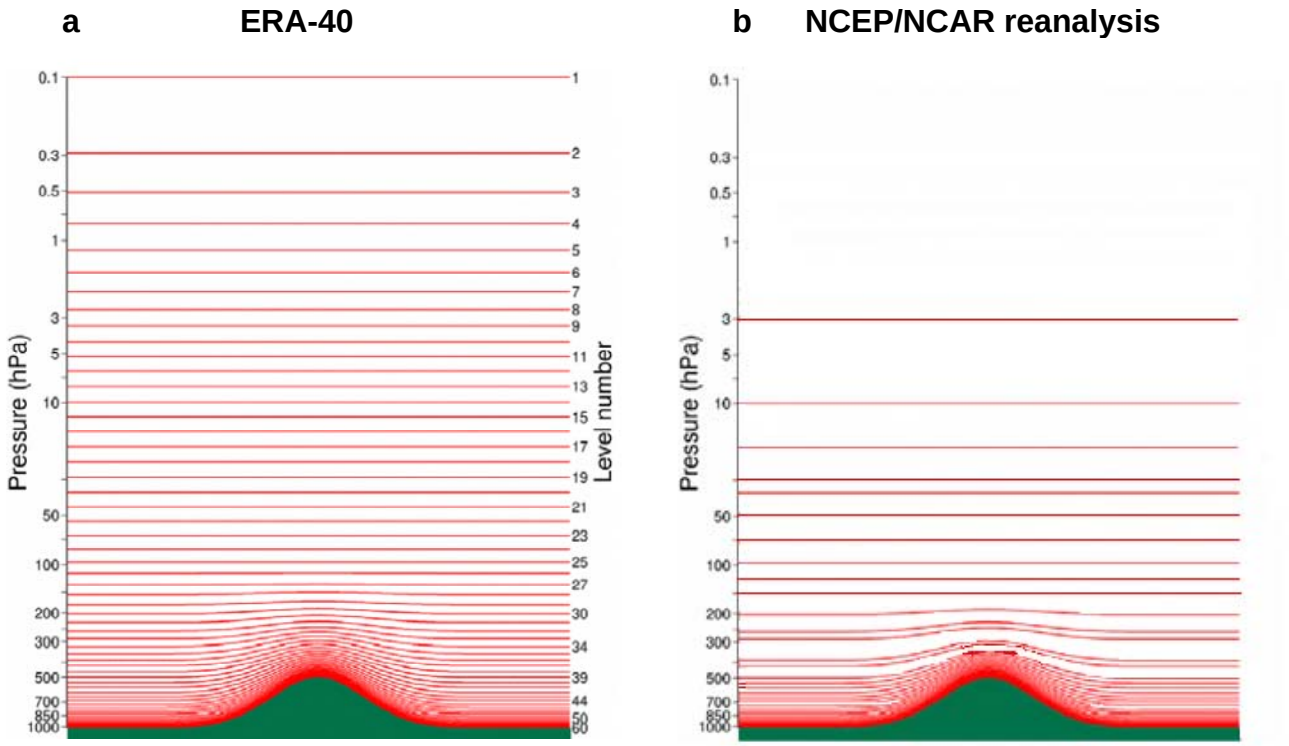

Figure III.1 Distribution of model levels for: ERA-40 [from Simmons [2004]] and NCEP/NCAR reanalysis.

b. NCEP/NCAR reanalysis

As denoted by its acronym, the NCEP/NCAR reanalysis was developed by the *National Centers for Environmental Prediction/National Center for Atmospheric Research* from United States of America [Kalnay et al., 1996]. It initially covered the period 1957-96 and then it has been completed until present. Moreover, data from 1948-57 were also assimilated later. The data of this early period are however a little bit different from the rest, as the available inputs correspond to data at 03, 09, 15, and 21 UTC, and not to the main synoptic hours (00, 06, 12, and 18 UTC), as it happens with the rest of the data. To solve this problem, the data corresponding to the first period were forecasted for the synoptic times and then, the assimilation process took only these forecasted values, which also were used to compute the daily time series and monthly means.

Concerning the spatial resolution, the data assimilation model has a T62 horizontal resolution (around 2° x 2° in lat-lon), thus a lower horizontal resolution than the ERA-40 one (T62 vs T159). In the vertical, the model extends only up to 3 hPa, showing fewer levels than the European reanalysis (28 vs 60 levels), especially in the stratosphere

(Figure III.1.b). More information about NCEP/NCAR reanalysis can be found in Kalnay et al. [1996].

Monthly and daily mean NCEP/NCAR data of different atmospheric fields have been used in this study, which have been retrieved from the webpage http://www.esrl.noaa.gov/psd/data/gridded/data.ncep.reanalysis.html. The available reanalyzed data are already provided in a horizontal regular grid of 2.5°x2.5° and 17 levels from 1000 hPa to 10 hPa. In contrast to ERA-40, the NCEP/NCAR webpage offers directly both monthly and daily mean data.

Thus, concerning time coverage or vertical resolution, the NCEP/NCAR reanalysis and ERA-40 have some advantages and disadvantages in comparison with the other. For instance, the former has a longer dataset in time that reaches until present, but it does not cover the whole stratosphere.

2. Model simulation output

The study of different aspects of stratospheric warmings in model simulations and its comparison with observations is one of the most important contributions of this work. This analysis covers the period from the second half of 20th century until 2100 by using different types of models that, in all cases, can realistically simulate the climate in the troposphere and stratosphere.

It is important to highlight that most of these model simulations correspond to experiments that have been carried out according to the specifications made by the *Chemistry Climate Model Validation* (CCMVal) initiative of the WMO *Stratospheric Processes and their Role in Climate* (SPARC) project [Eyring et al., 2008]. CCMVal simulations have been performed in support of ozone and climate assessments and they have been also useful to evaluate different coupled Chemistry-Climate Models (CCM). In this study, the CCM used is the EMAC model (described below). The CCMVal initiative proposed different simulations to allow the scientific community to achieve the aforementioned aims. One of these proposed simulations is a time-slice experiment performed under constant present-day conditions and designed to evaluate the models against observations (known as *CCMVal REF-B0*). The *CCMVal REF-B1* is a "past" transient simulation, forced by observations and designed to determine how well the models can reproduce the recent past climate from 1960. Additionally, a group of scenario experiments has been performed to determine the future evolution of stratospheric ozone and climate due to an increase of GHG concentrations (*SCN-B2c* and *SCN-B2d*).

Next, the model simulation output used in this study is described according to the period of the simulation, i.e., recent past to present or future.

a. Recent past and present

In the case of the recent past and present period, two types of simulation have been used: one, a *transient simulation* run with a CCM and the other one, under *constant present-day conditions* run with two different models. The details of these simulations are described next.

i. Transient simulation (EMAC CCMVal REF-B1)

The output of a transient simulation for the recent past used in this study were obtained with the state-of-art modular ECHAM Atmospheric Chemistry (hereafter EMAC) model developed at Max-Planck-Institute for Chemistry [Jöckel et al., 2006]. EMAC is composed of the ECHAM5 (version 5.3.01) general circulation model [Röckner et al., 2006] and coupled to an interactive chemistry module (MECCA) [Sander et al., 2005] and other submodels by the MESSy (version 1.6) interface structure. EMAC has a T42 horizontal resolution in spectral space, which corresponds approximately to 2.8° x 2.8° in grid point space, and 90 layers, resolving the full stratosphere and most of the mesosphere from the Earth surface up to 0.01 hPa (about 80 km).

The CCMVal REF-B1 simulation (hereafter *REF-B1*) is a 41-year transient simulation of the recent past (1960-2000) with 2 years of spin-up prior to 1960 following the specifications for natural and anthropogenic forcings given by the CCMVal initiative of the SPARC project [Eyring et al., 2008]. The simulation was performed by the Max-Planck-Institute for Chemistry and the model output kindly provided for this study. The natural forcings are based on changes in the ocean surface, solar variability, QBO, trace gases and volcanic eruptions. In particular, sea surface temperatures (SSTs) and sea ice concentrations (SICs) are prescribed as monthly mean boundary conditions following the HadISST1 data set provided by the UK Met Office Hadley Centre. Daily spectrally resolved solar irradiance data are prescribed with the method described in Lean et al. [2005].

The data of greenhouse gas (GHG) concentrations between 1958 and 1996 are taken from the *Intergovernmental Panel on Climate Change* Third Assessment Report [IPCC, 2001] and from NOAA observations for the period 1997-2000. Surface mixing ratios of ozone depletion substances (ODS) are taken from Table 8-5 of WMO [2007]. Data of emissions of ozone and aerosol precursors come from the extended dataset of the RETRO project [Schultz et al., 2007].

Finally, an important advantage of this model simulation to highlight is that the model is able to simulate the Quasi-Biennial Oscillation (QBO) [Giorgetta et al., 2006], even if it is very weakly guided to synchronize the simulated phenomenon in the model with the observed QBO time series.

ii. Present-day conditions

The output of two models of different characteristics has been analyzed to evaluate the stratospheric warmings in the recent past and present period by a simulation under constant present-day conditions. One of these models is a chemistry-climate model (EMAC in EMAC-FUB configuration) and the other one is a coupled atmosphere-ocean general circulation model (EGMAM). In both cases, the simulations were performed at the Institut für Meteorologie of Freie Universität Berlin.

Chemistry-climate model simulation (EMAC-FUB CCMVal REF-B0)

EMAC-FUB is a configuration of the EMAC model that is used at the Freie Universität Berlin (FUB). This configuration is run at a L39 resolution (i.e., with 39 layers, from the surface to 80 km) and using the improved shortwave radiation parameterization of Nissen et al. [2007].

In this case, the constant present-day conditions simulation corresponds to the CCMVal REF-B0 simulation (hereafter *REF-B0)* mentioned before. Following the recommendations for natural and anthropogenic forcings by the CCMVal initiative of SPARC project, REF-B0 simulation is a 55-year time-slice experiment that has been run for constant values corresponding to the year 2000 [Eyring et al., 2008]. This experiment is composed of three simulations of similar size (two of them integrated over 20 annual cycles and the third one over 15) that have separate starts and 2 years of spin-up. In this PhD thesis, the three simulations are considered together as one experiment of 55 years, given that the only difference among the three runs is related to a diagnostics and does not affect atmospheric fields used in this thesis.

Concerning the natural forcings, SSTs and SICs are prescribed with modeled values obtained from the Max-Planck-Institute Ocean Model (MPI-OM) and averaged over the period from 1995 to 2004. Solar irradiance data derived from the model of Lean et al. [2005] is averaged over the period 1950-2007 to provide a mean solar flux. The QBO is not included in these simulations.

As for the trace species concentrations and precursors, concentrations of GHGs and ODS are characteristic of levels in the year 2000 and based on IPCC Third Assessment Report [2001]. Background aerosol is prescribed from the extended SPARC surface area densities (SAD) data set for the year 2000 [SPARC, 2006]. Finally, data of emissions of ozone and aerosol precursors come from the same dataset as in the REF-B1 simulation (RETRO project dataset) and they are averaged over the years 1998 to 2000.

Simulation from a coupled atmosphere-ocean general circulation model (EGMAM)

The second model used to analyze stratospheric warmings in a simulation under constant present-day conditions is a coupled atmosphere-ocean general circulation model (AOGCM), in particular, the ECHO-G with Middle Atmosphere Model (hereafter, EGMAM) [Huebener et al., 2007]. As EGMAM is an AOGCM model, it is composed of an atmospheric component and an ocean model that are interactively coupled, including a dynamic sea-ice module [Legutke and Voss, 1999]. EGMAM is one of the models used in the IPCC Fourth Assessment Report [2007].

The atmospheric component of EGMAM is the ECHAM4 general circulation model [Röckner et al., 1996] that has been extended up to 0.01 hPa (~ 80 km altitude) and its number of levels has been increased from 19 to 39 in order to be able to study the stratosphere [Manzini and McFarlane, 1998]. Moreover, it includes the processes in the full stratosphere, which allows for studying the dynamical coupling between the stratosphere and troposphere. The EGMAM horizontal resolution is T30.

In the present study, a 300-yr control simulation performed under constant present day conditions with EGMAM has been used. Values of total solar irradiance as well as concentrations of well-mixed greenhouse gases have been set to values for the year 1990. A zonal-mean climatological ozone distribution has been prescribed. The initial conditions for the simulation were taken from a long control simulation that was performed with ECHO-G under constant present-day conditions. After a spin-up of 250 years, which was necessary to reach a quasi-equilibrium with respect to the ocean circulation and near surface temperature, the model was integrated for another 300 years [Spangehl et al., 2010].

It is important to remark that, due to the huge size of the datasets required for the analyses, the subset of years 2200-2299 (denoted as 2200's) was analyzed in detail first and defined as the reference period. Then, the same analyses have been repeated for the periods 2300-2399 (2300's) and 2400-2499 (2400's) to assess the robustness of the results identified in the reference period.

b. Future

Possible future changes of stratospheric warmings have been analyzed in a transient simulation of the period 1960 to 2100 using the EMAC-FUB configuration.

The transient simulation has been performed for a future scenario, known as "scenario 2d" (*SCN-B2d*, but denoted as SCN2d in this PhD thesis), following the specifications by the CCMVal initiative for forcings by halogens, greenhouse gases (scenario A1b, Figure III.2) and volcanic aerosols as well as natural, solar and QBO variability [Eyring et al., 2008; Eyring et al., 2010]. Transient SSTs and sea-ice

distributions are taken from a coupled AOGCM (ECHAM5-MPIOM) integration and prescribed to EMAC-FUB.

In order to isolate the effect of climate change on stratospheric warmings from other factors, the same analyses have been carried out with a "Non-Climate Change" (*NCC*) scenario simulation CCMVal. This scenario simulation is known as *SCN-B2c* (hereafter NCC), being identical to *SCN-B2d* except for the GHG concentrations, which are kept constant at levels corresponding to the year 1960, and the SSTs/SICs that are prescribed with an average of the values used in the SCN-B2d simulation for the period from 1955 to 1964 [Eyring et al., 2010].

These two simulations were performed at the Institut für Meteorologie of Freie Universität Berlin.

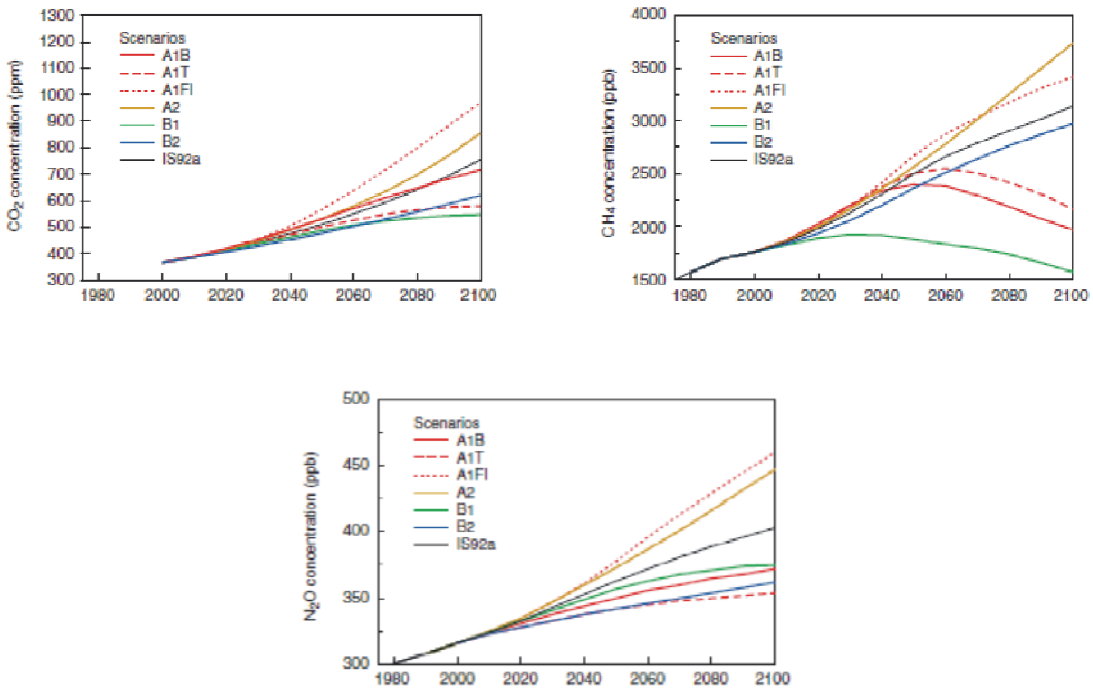

Figure III.2. Atmospheric concentrations of some greenhouse gases (CO_2, N_2O and CH_4) resulting from different SRES scenarios [IPCC, 2000] [Adapted from IPCC [2001]].

A summary of all model simulations used in this study is included in Table III.1 (next page).

Table III.1. Summary of the main properties of all model simulations used in this study.

Model simulation	Period	Resol.	SSTs/SICs	QBO	GHGs	ODS	O_3 and aerosol precursors
CCMVal REF-B1 EMAC	Transient simulation 1960-2000	T42L90	OBS HadISST1	Internally generated (nudged)	OBS [IPCC, 2001]	OBS Table 8-5 WMO [2007]	OBS extended RETRO data set
CCMVal REF-B0 EMAC (EMAC-FUB config.)	Time slice 2000	T42L39	OBS 1995-2004 MPI-OM	None	OBS fixed at 2000 conc. [IPCC, 2001]	OBS Fixed at 2000 conc. [IPCC, 2001] repeating each year	OBS RETRO 1998-2000 mean
Constant 1990 conditions EGMAM (AOGCM)	Time slice 1990	T30L39	Coupled ocean	None	OBS fixed at 1990 conc.	---	Zonal-mean climatology
CCMVal SCN-B2d (SCN2d) EMAC (EMAC-FUB config.)	Transient simulation 1960-2100	T42L39	Modeled (MPI-OM)	OBS/ repeating in future	A1B [IPCC, 2000]	OBS+ adjusted A1 scenario (WMO 2007, Table 8-5)	Same as REF-B1 until 2000 + adjusted IIASA scenario through 2100
CCMVal SCN-B2c (NCC) EMAC (EMAC-FUB config.)	Transient simulation 1960-2100	T42L39	1955-1964 average of values used in SCN2d, repeating each year	OBS/ repeating in future	Fixed at 1960 conc.	Same as SCN2d	Same as SCN2d

IV. Methodology

Several tools have been used in this work to carry out the different analyses and to interpret the results. As this study is focused on climate variability research, most of these tools handle with anomalies and climatological fields. Hence, a definition of both concepts is needed before starting with the description of each tool. Actually, any atmospheric field can be decomposed into two components: *anomalies* and *climatology*. While the climatology is defined as the time mean of the field in a certain period, anomalies are computed as the deviation of the real field from the mentioned time mean.

This Chapter is devoted to the description of all the techniques and methods used to accomplish the main goal: a detailed analysis of stratospheric warmings. Hence, the first Section, Section IV.1, includes the criteria applied to identify the different stratospheric warmings and their central date. In Section IV.2, dynamics tools are described and techniques to filter data are explained in Section IV.3. Section IV.4 focuses on the description of statistics tests that provide statistical significance to the results. Finally, the used graphic tools are indicated in Section IV.5.

1. Criteria for the identification of stratospheric warmings

One of the first steps of this study has been to determine the occurrence and the central date of stratospheric warmings. There are several criteria to accomplish this goal, given that since their discovery different and arbitrary criteria have been proposed involving stratospheric winds, temperatures or even measures of the vortex shape [Coughlin and Gray, 2009]. In this section, the most important ones for each type of warming are enumerated, focusing on those applied in this PhD thesis.

a. Stratospheric midwinter warmings

As indicated in Chapter II, stratospheric midwinter warmings can be generally divided into major and minor warmings.

Minor warmings, according to the World Meteorological Organization (WMO), are identified "*when polar temperatures between 60ºN and 85ºN increase by 25 K or more within a week at any stratospheric level*". However, many other authors identify a minor warming if the 10-hPa zonal-mean temperature difference between 90ºN and 60ºN becomes positive [Andrews et al. 1987, p. 259]. The simplicity of this last criterion, supported by the large literature using it, has led to apply it in this PhD Thesis.

As regards **major stratospheric warmings (MSWs)**, according to the classical definition, as formulated by Labitzke [1981b] and adopted for the STRATALERT warnings by WMO [Andrews et al., 1987, p. 259], a stratospheric warming is defined as

major if the zonal-mean temperature at 10 hPa or below increases poleward of 60°N and an associated circulation reversal is observed at this level. Later, Labitzke and Naujokat [2000] specify the nature of the circulation reversal: *"In addition to warming of the North Polar region and reversal of the meridional temperature gradient, they* (i.e. major stratospheric warmings*) are also associated with a breakdown of the polar vortex, which is replaced by a high. That is, the definition of a Major Midwinter Warming requires not only the warming but also a total change of circulation. The definition of a breakdown of the polar vortex is that the usual westerlies in the Arctic at 10 hPa are replaced by easterlies so that the centre of the vortex moves south of 60°-65°N*." Other definitions of major stratospheric warming only refer to the circulation change, either using a zonal index at 50 hPa [Limpasuvan et al., 2004] or the condition of zonal-mean easterlies at 60°N and 10 hPa at a day during northern winter (November to March) [Charlton and Polvani, 2007]. In the present study, a MSW is identified when the 10-hPa zonal-mean temperature difference between 90ºN and 60ºN becomes positive (thermal criterion) and the zonal-mean zonal wind at the same level and 60ºN (denoted by $[u10]_{60N}$ in this manuscript) becomes easterly (dynamical criterion).

b. Stratospheric final warmings (SFW)

Two types of criteria are mainly found in the literature to determine the annual breakup of the polar vortex [Wei et al. 2007]. One is known as the Nash et al. [1996] criterion and it is based on the potential vorticity and the other one, by Black et al. [2006], is based on the zonal wind. The former defines the SFW date as the day when the average wind speed along the vortex edge falls below a critical value (15.2 m s^{-1}), corresponding the vortex edge to the location of the maximum potential vorticity gradients at 475K [Waugh and Rong, 2002]. On the other hand, Black et al. [2006] define the SFW date as the final day on which the running 5-day average of the zonal-mean of zonal wind at 50 hPa and 70ºN (represented by $[u50]_{70N}$) becomes negative and does not return to a value higher than 5 m s^{-1} until the subsequent late August. The choice of the latitude 70ºN is due to the usual location of the polar vortex core at 50 hPa.

As Wei et al. [2007] point out, the second criterion shows important advantages, particularly in the study of the stratosphere-troposphere coupling related to SFWs. Whereas the typical wintertime westerlies are still present in the date identified according to Nash et al., the criterion by Black et al. determines the date in a later stage of the breakup of the polar vortex, when the typical wintertime stratospheric westerlies have been already replaced by the summertime easterlies. This difference in the state of the polar stratospheric mean flow is particularly relevant for the implications in the upward propagation of planetary waves, i.e. enhanced under the conditions of the Nash et al. criterion and prevented under the conditions of the Black et al. criterion, and thus, for the dynamical coupling between the stratosphere and troposphere.

Because of the advantages of the Black et al. criterion described above, this has been the one applied in this study. Figure IV.1 illustrates the identification of the SFW date in 1964, according to this criterion.

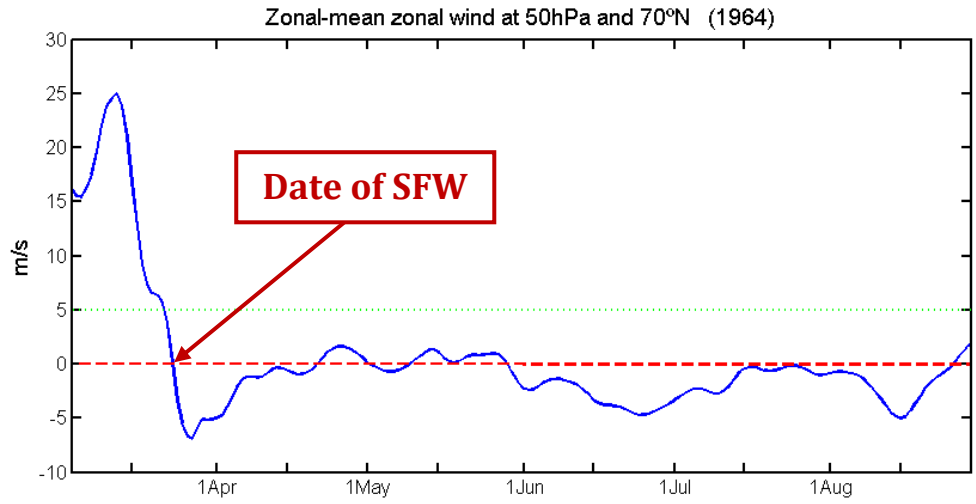

Figure IV.1. 5-day running mean of zonal-mean zonal wind at 50 hPa and 70ºN from March until August 1964 in m s^{-1}.

2. Dynamics tools

Analyses of the dynamical processes involved in the stratospheric warmings and related atmospheric phenomena constitute an extensive part of this work. In this Section, the principal dynamics tools used in this study are presented according to two relevant analyzed topics: the wave activity propagation and the storm track activity.

a. Wave activity propagation

Stratospheric warmings have been shown to be related to an enhancement of tropospheric wave activity that propagates into the stratosphere, interacts with the mean flow and decelerates it [e.g., Charney and Drazin, 1961; Matsuno, 1971; McIntyre, 1982; Limpasuvan et al., 2004; Black and McDaniel, 2007]. Hence, a special focus on the study of the wave activity propagation, in particular from the troposphere to the stratosphere, is done in this PhD thesis. Next, tools applied to quantify and represent the wave activity propagation in one, two and three dimensions are described.

i. One-dimensional wave activity propagation: 100-hPa heat flux and its decomposition

The zonal-mean poleward eddy heat flux at 100 hPa averaged over mid- and high latitudes has been proven to provide a good measure of the injection of tropospheric

wave activity into the stratosphere in midwinter [Hu and Tung, 2003]. Thus, it constitutes an important tool for the study of the processes related to MSWs.

Based on this, in this study the meridional eddy heat flux (*HF*) averaged, in most of cases, over 50ºN-80ºN has been computed according to equation (IV.2.1) to quantify the net upward flux of tropospheric wave activity into the stratosphere.

$$HF = \left[v^* T^* \right] \qquad \text{(IV.2.1)}$$

where brackets and asterisks indicate zonal mean and deviation from it, respectively, v is the meridional wind and T is the temperature.

The planetary wave field shows intraseasonal modulations, such as amplifications and associated enhancement of upward wave-activity injection. The analysis of these modulations is particularly important in the study of MSWs and, in particular, of the tropospheric forcing mechanisms in their occurrence as is done in Section V.1.b.

In this work, the intraseasonal modulations of the planetary wave field are analyzed through a diagnostic tool recently proposed by Nishii et al. [2009]. This method allows for identifying zonally confined *Rossby wave packets* and their interaction with the climatological planetary waves. Rossby wave packets are defined as local departures from the 3-dimensional climatological-mean flow and originate from high-amplitude quasi-stationary circulation anomalies in the troposphere that decay after their mature stage by releasing accumulated wave activity as a stationary Rossby wave train [Takaya and Nakamura, 1997]. As related to quasi-stationary circulation anomalies, this type of unusual wave packets has a larger scale than other disturbances like synoptic-scale transient eddies, making them possible to influence the polar stratospheric circulation.

The methodology by Nishii et al. consists of decomposing the heat flux at 100 hPa into different terms, which correspond to:

- the climatological planetary waves (first right-hand term in equation (IV.2.2)),
- the anomalies associated with Rossby wave packets (second right-hand term in equation (IV.2.2)) and
- the interaction between the climatological planetary waves and anomalies associated with Rossby wave packets (third plus fourth term in the same expression eq. (IV.2.2)).

The climatological daily-mean is considered the basic state and it is calculated in this part of the work as the mean of smoothed daily data by a 31-day running mean for the period 1979/80-2009/10. This filter is applied because of the short period of study (i.e. 31 years, corresponding to the period when the satellite information was implemented in the data assimilation process of the reanalysis). In this case, the anomalies are defined

as the subtraction of the filtered daily climatology from the daily fields. Then, they are smoothed by a 5-day running mean in order to eliminate fluctuations associated with migratory transient eddies [Nishii and Nakamura, 2004] and these 5-day averaged anomalies are associated with quasi-stationary Rossby wave packets.

$$\left[v^{*}T^{*}\right]=\left[v_c^{*}T_c^{*}\right]+\left[v_a^{*}T_a^{*}\right]+\left[v_c^{*}T_a^{*}\right]+\left[v_a^{*}T_c^{*}\right] \qquad \text{(IV.2.2)}$$

where the *a* and *c* subscripts denote anomalies and climatological values, respectively. The analysis has been restricted to the first three zonal wavenumbers, as they account for approximately 90% of the total eddy heat flux, in agreement with Haklander et al. [2007], and because the study is focused only on planetary waves, the main waves being able to penetrate into the stratosphere and perturb the mean flow at high latitudes.

Figure IV.2 illustrates an example of the time evolution of the total eddy heat flux at 100 hPa averaged over 50ºN-80ºN for the 2008/09 winter and its different contributions.

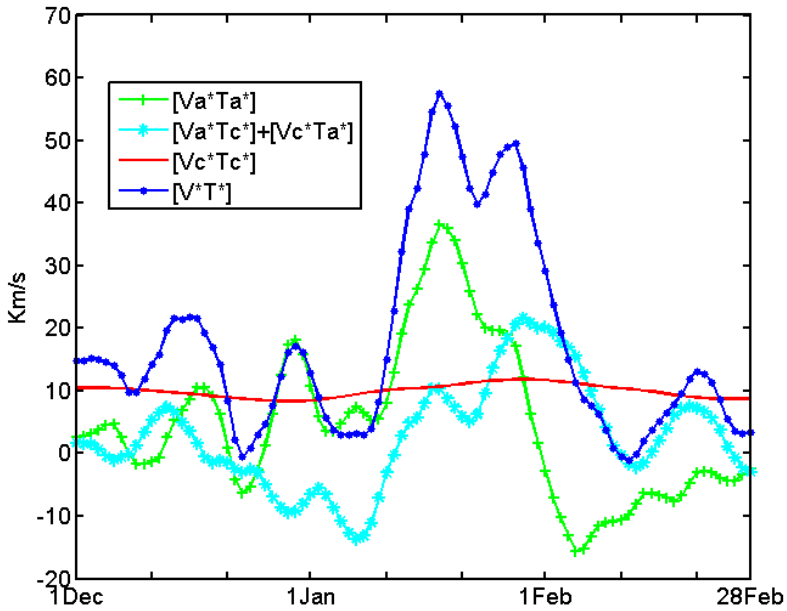

Figure IV.2. Time evolution of zonal-mean meridional eddy heat flux averaged over 50ºN-80ºN (K m s^{-1}) at 100 hPa from 1 December 2008 to 28 February 2009. The different lines indicate total flux (blue line) and its contributions: the climatological-mean planetary waves (red line), the anomalies associated with Rossby wave packets (green line), and the interaction between these anomalies and the climatological planetary waves (cyan line).

ii. Two-dimensional wave activity propagation: Meridional-vertical propagation (EP flux)

The analysis of Rossby wave propagation in the meridional plane and their associated forcing of the mean flow has been performed by using the Eliassen-Palm flux (hereafter,

EP flux) [Andrews et al., 1987]. This flux is based on the transformed Eulerian mean (TEM) formulation. EP flux and its divergence are defined as equations (IV.2.3) and (IV.2.4), respectively[Baldwin et al., 1985]:

$$\mathbf{F} = \left(\mathrm{F}_{\phi}, \mathrm{F}_{z}\right) = a\cos\varphi e^{-z/H}\left(\left[-u^{*}v^{*}\right], \frac{f\left[v^{*}\theta^{*}\right]}{\frac{\partial[\theta]}{\partial z}}\right) \qquad \text{(IV.2.3)}$$

$$\nabla\cdot\mathbf{F} = \frac{1}{a\cos\varphi}\frac{\partial}{\partial\varphi}\left(\mathrm{F}_{\varphi}\cos\varphi\right) + \frac{\partial}{\partial z}\left(\mathrm{F}_{z}\right) \qquad \text{(IV.2.4)}$$

where a is the radius of the earth, φ is the latitude, u is the zonal wind, θ is the potential temperature, f is the Coriolis parameter and z is a log-pressure coordinate with scale height H, namely: $z = -H\ln\left(p/1000\,\mathrm{hPa}\right)$. Moreover, when scaling the divergence of the EP flux by $(a\cos\varphi)^{-1}\exp(z/H)$, this quantity provides a measure of the net driving force by eddies on the mean flow as it can be derived from equation (6) of Baldwin et al. [1985].

When plotting directly cross sections of **F** and $\nabla\cdot\mathbf{F}$ in a (φ, logp) plane, some problems arise, such as the wave propagation at upper levels cannot be properly observed because the arrows are very small. To avoid those problems, several conventions have been proposed in the literature. In this study, EP flux diagrams have been plotted following recommendations by Hartmann et al. [1984]. It consists of multiplying **F** by 10 at 100 hPa and above, so that the arrows in the stratosphere can be more easily seen.

Additional scaling techniques have been applied because the two axes of the diagrams have different scales. Thus, the horizontal and vertical arrow components of **F** as measured on the diagram have been calculated by multiplying their values by the distances occupied by 1 'unit' in the corresponding axis on the diagram (i.e., F_{φ} by a radian of latitude and F_{z} by 1).

An example of an EP flux diagram is included in Figure IV.3 in order to help to understand **F** and $\nabla\cdot\mathbf{F}$. As shown by Edmon et al. [1980], arrows give a measure of net wave propagation from one height and latitude to another. Hence, the arrows pointing upward between 40ºN and 60ºN approximately indicate upward propagating wave activity due to a predominance of poleward heat flux in the EP flux [Peixoto and Oort, 1992]. Then, at the middle and, particularly, upper troposphere the wave activity between 30º and 45º N deflects towards the equator, denoted by the arrows in that region with an equatorward orientation. This indicates an important momentum convergence near the jet stream region. Concerning the shadings of Figure IV.3, they correspond to the divergence of EP flux. Hence, the regions where the arrows converge

(the extratropical middle troposphere or the stratosphere at mid-latitudes) show negative values of $\nabla\cdot\mathbf{F}$. In contrast, in the extratropical lower troposphere and at the tropospheric subtropics, the divergence of EP flux is positive, as the arrows diverge. The convergence and divergence of EP flux gives a measure of the driving of the mean flow by eddies, which transport easterly momentum in the case of Rossby waves [Hartmann et al., 1984]. In basis of this, a convergence of EP flux implies a deceleration of the mean flow by the eddies and just the opposite in the case of the divergence of EP flux.

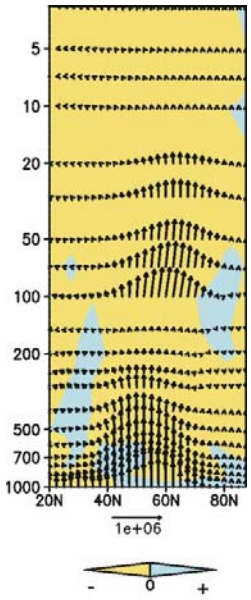

Figure IV.3. Climatology of EP flux (arrows) with its divergence (shading) in March (1960-2000). Arrow scale ($m^3\ s^{-2}$) is indicated at the bottom. The meridional component of EP flux is multiplied by 0.0023 to account for the plot aspect radio. Scaling arrow at 100 hPa and higher is divided by a factor of 10 so that EP flux may be easily seen. Yellow (blue) shading shows negative (positive) values of EP flux divergence. Dataset: ERA-40.

In order to determine the effect of each contribution of the wave activity on the stratospheric mean flow, the scaled $\nabla\cdot\mathbf{F}$ at a stratospheric level (namely, 30 hPa) has been computed. Then, it is decomposed into its different contributors, as done for the heat flux, namely, corresponding to the climatological waves, the anomalies associated with Rossby wave packets and the interaction between the former and the latter.

iii. Three-dimensional wave propagation

As indicated in the previous Subsection, the EP flux is a very powerful tool to analyze the propagation of wave activity and the interaction between waves and mean flow. However, it only provides information about the zonally-averaged latitudinal and vertical wave propagation. To solve this limitation, different expressions of three-dimensional wave activity fluxes have been derived by Plumb [1985] or Takaya and Nakamura [2001], among others.

- Wave activity Plumb flux [1985]

This three-dimensional wave activity flux is, up to now, the most popular expression and it supplies additional features of the propagation of quasi-stationary Rossby waves under quasi-geostrophic approximation, such as the identification of their potential regional sources and sinks along with the diagnostic of other propagation characteristics [McDaniel and Black, 2005].

The Plumb flux is parallel to the group velocity of quasi-stationary Rossby waves and its divergence is clearly related to non-conservative effects, i.e., to generation (sources) or dissipation (sinks) of wave activity [Plumb, 1985]. The three-dimensional wave activity flux (F_s) in pressure (p) coordinates is given by equation (IV.2.5):

$$\mathbf{F}_s = \frac{1}{2}\frac{p}{10^5}\begin{pmatrix} \left(\frac{\partial \psi^*}{\partial x}\right)^2 - \psi^* \frac{\partial^2 \psi^*}{\partial x^2} \\ \frac{\partial \psi^*}{\partial x}\frac{\partial \psi^*}{\partial y} - \psi^* \frac{\partial^2 \psi^*}{\partial x \partial y} \\ \frac{f^2}{S^2}\left(\frac{\partial \psi^*}{\partial x}\frac{\partial \psi^*}{\partial p} - \psi^* \frac{\partial \psi^*}{\partial x \partial p}\right) \end{pmatrix} \qquad \text{(IV.2.5)}$$

where p is the pressure, ψ is the stream function, f is the Coriolis parameter and S^2 is the static stability parameter, defined as:

$$S^2 = -\alpha\left(\frac{\partial \ln\theta}{\partial p}\right) \qquad \text{(IV.2.6)}$$

where θ is the potential temperature and α is the specific volume.

To reduce the successive differentiation that can constitute a source of amplification of noise, in this study, equation (IV.2.5) has been rewritten by using the geostrophic and thermal wind relations. The new expression of this equation in spherical geometry is as follows:

$$\mathbf{F}_s = \frac{p}{10^5}\cos\varphi\begin{pmatrix} v^{*2} - \frac{1}{2\Omega a \sin 2\varphi}\frac{\partial\left(v^{*2}\Phi^*\right)}{\partial\lambda} \\ -u^* v^* + \frac{1}{2\Omega a \sin 2\varphi}\frac{\partial\left(u^*\Phi^*\right)}{\partial\lambda} \\ \frac{f}{\left(\frac{\partial \hat{T}}{\partial p} - \frac{\kappa \hat{T}}{p}\right)}\left(v^* T^* - \frac{1}{2\Omega a \sin 2\varphi}\frac{\partial}{\partial\lambda}\left(T^*\Phi^*\right)\right) \end{pmatrix} \qquad \text{(IV.2.7)}$$

where λ is the longitude, Ω is the Earth's rotation rate, Φ is the geopotential, κ is the Poisson constant (= R/c_p) and T with caret indicates the average over the area north of 20°N of the temperature. The other variables in equation (IV.2.7) represent the same magnitudes expressed in previous ones.

- Wave activity flux by Takaya and Nakamura [2001]

In spite of the advantages indicated previously for the Plumb flux, this flux is restricted to quasi-geostrophic disturbances embedded on a zonal flow. Hence, it is not suitable to determine the sources and to characterize the three-dimensional propagation of Rossby wave packets, that is, the local departures from time-mean flow. To assess the before mentioned characteristics, a particular form of wave activity flux derived by Takaya and Nakamura [2001] has been used.

The wave activity flux by Takaya and Nakamura [2001] is parallel to the local three-dimensional group velocity and independent of wave phase. It constitutes a generalization of the Plumb flux explained above, since it is defined for a zonally varying basic flow, which is particularly useful for the study of the NH troposphere in winter, when the basic state shows inhomogeneities that can modulate the propagation of Rossby wave packets. This particular flux only takes into account the wave activity associated with Rossby wave packets, as the wavy anomalies are considered to be embedded in the basic flow that includes the climatological planetary waves [Nakamura and Honda, 2002].

The wave activity flux (**W**) for quasi-stationary eddies in pressure coordinates is given by equation (IV.2.8):

$$\mathbf{W} = \frac{1}{2\left|\mathbf{U}_c\right|}\begin{Bmatrix} u_c\left(\psi'^2_x - \psi'\psi'_{xx}\right) + v_c\left(\psi'_x\psi'_y - \psi'\psi'_{xy}\right) \\ u_c\left(\psi'_x\psi'_y - \psi'\psi'_{xy}\right) + v_c\left(\psi'^2_y - \psi'\psi'_{yy}\right) \\ \frac{f^2}{S^2}\left[u_c\left(\psi'_x\psi'_p - \psi'\psi'_{xp}\right) + v_c\left(\psi'_y\psi'_p - \psi'\psi'_{yp}\right)\right] \end{Bmatrix} \qquad \text{(IV.2.8)}$$

where primes indicate the wave-associated fluctuation (defined as 5-day averaged anomalies), $\mathbf{U_c}$ denotes the climatological-mean horizontal wind vector (u_c, v_c)

Equation (IV.2.8) can be rewritten as equation (IV.2.9), in spherical geometry and by using the geostrophic and thermal wind relations, in the same way as was done with equation (IV.2.5):

$$\mathbf{W}=\frac{\cos\varphi}{|\mathbf{U}_c|}\begin{Bmatrix} u_c\left(v'^2-\frac{1}{2a\Omega\sin 2\varphi}\frac{\partial}{\partial\lambda}(v'\Phi')\right)+v_c\left(-u'v'+\frac{1}{2a\Omega\sin 2\varphi}\frac{\partial}{\partial\lambda}(u'\Phi')\right) \\ u_c\left(-u'v'+\frac{1}{2a\Omega\sin 2\varphi}\frac{\partial}{\partial\lambda}(u'\Phi')\right)+v_c\left(u'^2+\frac{1}{4a\Omega}\frac{\partial}{\partial\varphi}\left(\frac{u'\Phi'}{\sin\varphi}\right)\right) \\ \frac{2\Omega\sin\varphi}{\frac{\kappa\hat{T}_c}{p}-\frac{\partial\hat{T}_c}{\partial p}}\left[u_c\left(-v'T'+\frac{1}{2a\Omega\sin 2\varphi}\frac{\partial}{\partial\lambda}(T'\Phi')\right)+v_c\left(u'T'+\frac{\sin\varphi}{4a\Omega}\frac{\partial}{\partial\varphi}\left(\frac{T'\Phi'}{\sin^2\varphi}\right)\right)\right] \end{Bmatrix} \quad \text{(IV.2.9)}$$

Note that W_p, the vertical component of **W**, is represented in all plots of this PhD thesis as $-W_p$, so that positive values indicate upward propagation of wave activity.

b. Storm track activity

Storm track activity has been calculated as the standard deviation of the bandpass (2-6 days) filtered variability of geopotential at 500 hPa [Ulbrich et al., 2008]. The data were filtered using a second order bandpass Butterworth filter (described in Section IV.3.a). This variable informs about the regions with the strongest baroclinic wave activity and so, it gives a measure of the synoptic activity [Pinto et al., 2007]. In this PhD thesis, changes in this variable related to the timing of stratospheric final warmings are analyzed in Section VI.1, which appears to be an adequate way of exploring the stratosphere-troposphere connection.

3. Filtering techniques

The variability of data is usually caused by diverse processes that have different spatial and/or time scales. Therefore, in order to isolate the variability associated only with some specific phenomena, it is very common in climate research to decompose data series (based on the frequency or wavelengths) of its different components. In that case, it is said that the series is represented in the frequency or wavelength domain.

In this Section, the filtering techniques used in this PhD thesis with this aim are described, and they are:

- Fast Fourier Transform (applied in the spatial domain)

- Running mean (applied in the time domain)

- Butterworth filter (applied in the time domain)

a. Fast Fourier transform

The Fourier transform is one of the most common methodologies to decompose data series into a spectrum of cycles of different length, and is based on the idea that any waveform can be rewritten as a sum of sinusoids or complex exponentials of different frequencies [Brigham, 1974]. The mathematical relationship between an arbitrary waveform and frequency sinusoids is given by equation (IV.3.1):

$$S(\omega) = \int_{-\infty}^{\infty} s(t)\, e^{-i\omega t} dt \qquad \text{(IV.3.1)}$$

where *s(t)* is the wave to be decomposed into a sum of sinusoids, *S(ω)* corresponds to the Fourier transform of *s(t)*, i is the imaginary unit and ω denotes angular frequency ($\omega = 2 \cdot \pi \cdot freq$).

When the input function is discrete and its non-zero values have a limited duration, the discrete Fourier transform (DFT) is used in Fourier analysis. In that case, equation (IV.3.1) is replaced by equation (IV.3.2):

$$X(k) = \sum_{n=0}^{N-1} x_0(n) e^{-i 2 n \pi k / N} \quad k = 0,1,...,N-1 \qquad \text{(IV.3.2)}$$

where N is the number of samples, $x_0(n)$ are the input data that are assumed to be complex. *X(k)* can be also written in polar form in terms of its sinusoid amplitude (denoted A_k/N) and its phase α_k, calculated from the complex modulus and argument of *X(k)*, respectively. Thus, the original signal could be rewritten as a sum of sinusoidal components with frequency k/N cycles per sample:

$$x(n) = \frac{1}{N} \sum_{k=0}^{N-1} X(k)\, e^{i 2 \pi n k / N} \quad n = 0,1,...,N-1 \qquad \text{(IV.3.3)}$$

In order to calculate this DFT, a particular algorithm is applied, called Fast Fourier Transform (FFT), which computes the DFT much faster than other available methods [Brigham, 1974].

In this work the Fourier transform is not applied in the time domain but in the spatial one, in order to identify the different zonal wavenumber components of some atmospheric fields. In this case, expressions (IV.3.2) and (IV.3.3) are still valid but replacing the frequencies ($\omega/(2\pi) = k/N$) by wavelengths (λ). In this way, a certain

atmospheric field, e.g. the geopotential field Φ at a given time, could be expressed according to its different zonal wavenumber k as equation (IV.3.4) [Andrews et al., 1987]:

$$\Phi = A_0(\varphi,z) + \sum_{k=1}^{N-1} A_k(\varphi,z)\cos\left(k\lambda + \alpha_k(\varphi,z)\right) \qquad \text{(IV.3.4)}$$

where A_k and α_k are the amplitude and the phase of each zonal Fourier harmonic.

b. Running mean

Another type of filter used in this work, but applied in the time domain, is the *running mean* (also called *moving average* or consecutive mean). This time filter is one of the simplest and is typically used to smooth time series, so that fast variations are eliminated. Thus, it is said that it is a *low-pass filter.*

The running mean consists in replacing each observed value X_t with a mean value computed over a selected interval with a 2J+1 length, according to expression (IV.3.5) [von Storch and Zwiers, 2001]:

$$\mathbf{Y}_t = \sum_{j=-J}^{J} \frac{1}{2J+1}\mathbf{X}_{t+j} \qquad \text{(IV.3.5)}$$

In this study, this technique has been used to flatten time series, such as the eddy heat flux or zonal-mean zonal wind.

c. Butterworth filter

In this PhD thesis, apart from the running mean, the other time filter used has been the Butterworth one. This is the simplest electronic filters and it was described for the first time by Butterworth [1930]. This filter, more complicated than the running mean, presents versatility and advantages for filtering different time scales.

As other time digital filters (as elliptic or Chebyshev ones), a Butterworth filter is characterized by a transfer function H(s) that describes the relation between the input x(t) and the output y(t) signals through the Laplace transform (for continuous-time signals) or Z transform (for discrete-time signals). Particularly, the transfer function is defined as:

$$H(s) = \frac{Y(s)}{X(s)} \qquad \text{(IV.3.6)}$$

where *X(s)* and *Y(s)* are the Laplace transforms (or Z transforms) of x(t) and y(t) signals, respectively. The absolute value of *H(s)*, also called *gain*, describes the change in the amplitude of the signal by the filter and its argument is related to the phase shift due to the filter [Proakis and Manolakis, 2003].

Digital filters are designed to retain only the signal in a range of frequencies, also called *passband*. If the passband corresponds to long, short or intermediate time scales, filters are known as low-, high- and band-pass filters, respectively, and their magnitude response is illustrated in Figure IV.4. The *stopband* refers to the band of frequencies that the filter does not allow to pass or attenuates.

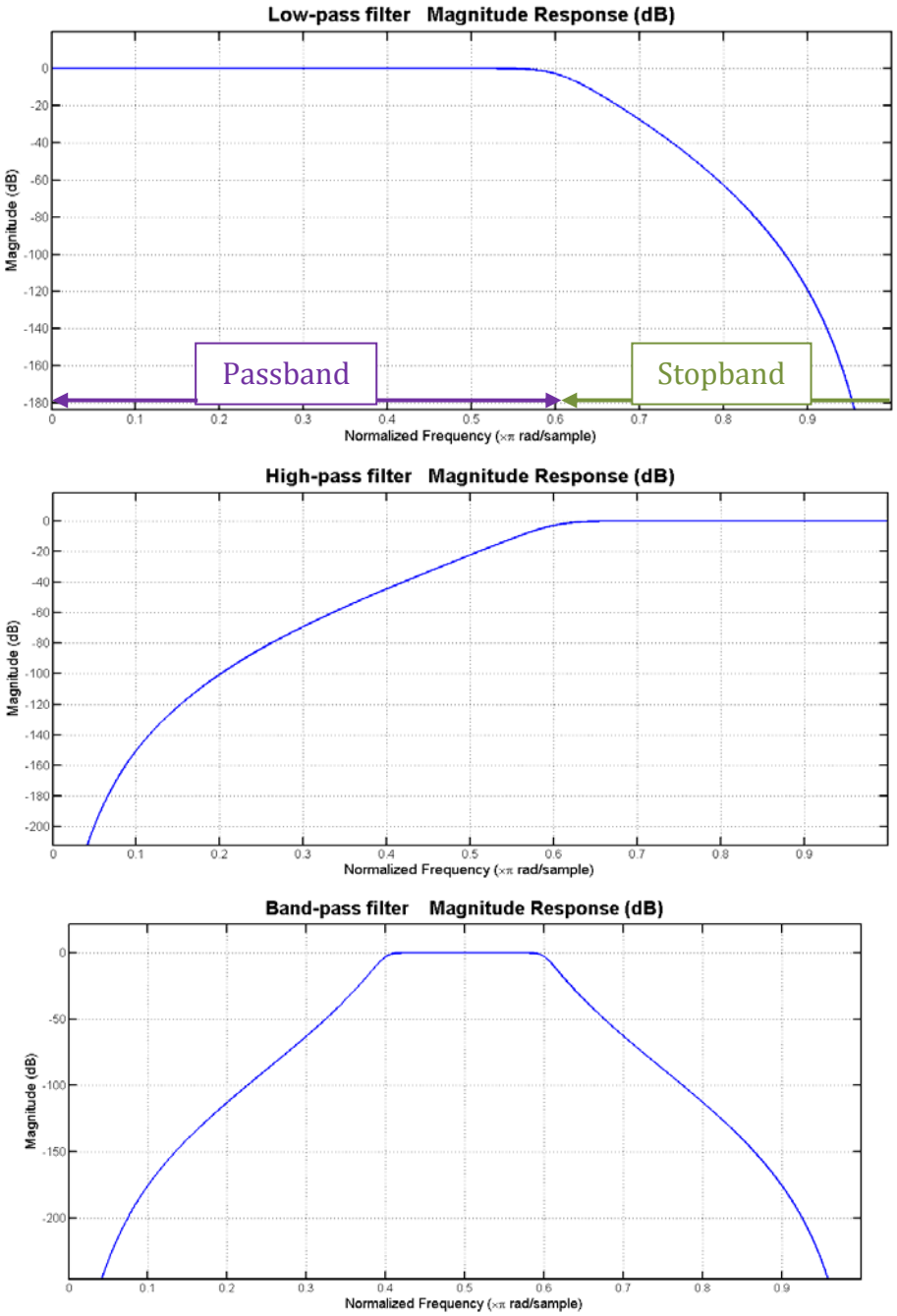

Figure IV.4. Bode plot of: low-pass, high-pass and band-pass filters.

Next, the main characteristics of a Butterworth low-pass filter are briefly explained. This type of Butterworth filter is characterized by the following expression (IV.3.7) of the squared frequency response, $|H(\Omega)|^2$:

$$|H(\Omega)|^2 = \frac{1}{1+(\Omega/\Omega_c)^{2N}} \tag{IV.3.7}$$

where N is the order of filter, Ω_c is the cut-off frequency (approximately -3 dB frequency) and Ω is the analogical frequency. From the previous equation, it can be deduced that as N rises, $|H(\Omega)|^2$ tends to a rectangle function and so the slope of the cut-off becomes sharper, as observed in Figure IV.5. However, although this slope changes depending on the order of the filter, the shape of the filter response is the same, i.e. without ripples, unlike other filters [Proakis and Manolakis, 2003].

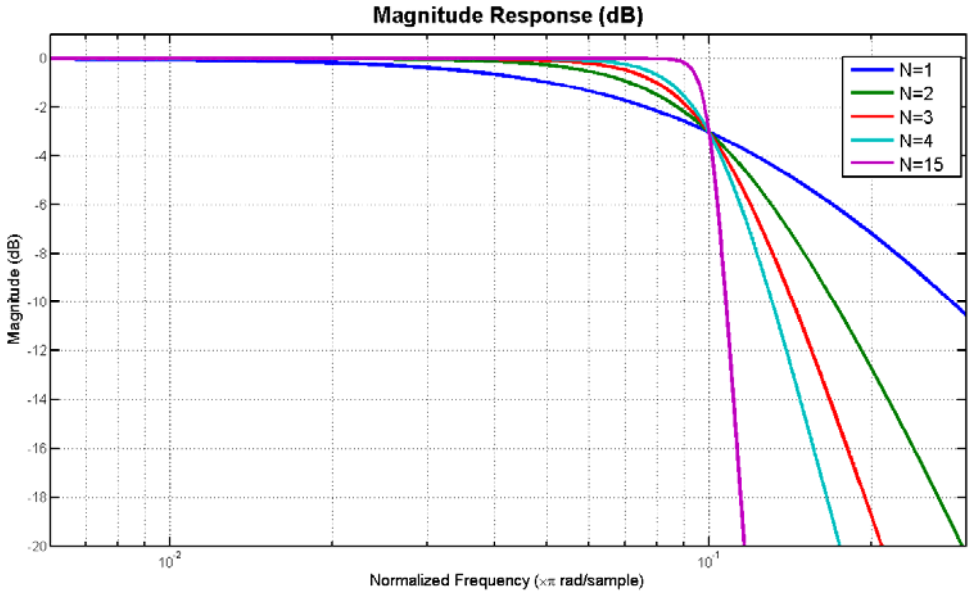

Figure IV.5. Plots of the gain of Butterworth low-pass filters of different orders N.

Moreover, the Butterworth filter has another important advantage over other typical filters, in that its frequency response is as flat as possible in the passband [Butterworth, 1930]. This characteristic can be observed in the logarithmic Bode plot of Figure IV.6 for low-pass filters. In the same figure, it can be seen that the response slopes off linearly towards minus infinity outside the passband.

All these characteristics described above can be also applied to high-pass and band-pass Butterworth filters.

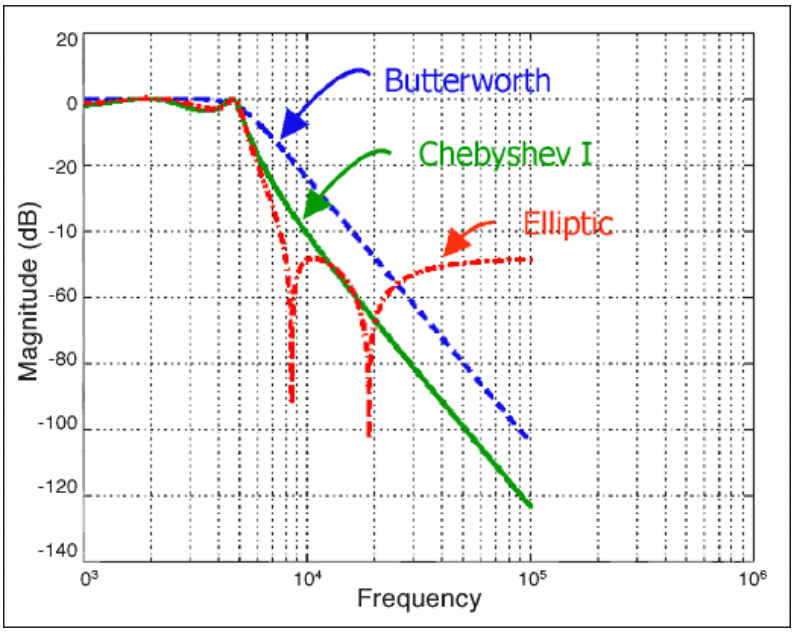

Figure IV.6. Comparison plot of different filter approximations: Butterworth, elliptic and Chebyshev I [adapted from http://www.maxim-ic.com/app-notes/index.mvp/id/3494].

Because of the advantages above mentioned, Butterworth filter has been used in different analyses in this work: some cases as a *low-pass filter* (e.g.: to identify a long varying trend of a time series due to climate change conditions) and others as a *band-pass filter* (e.g.: to isolate the variability of a certain range of frequency, as in the case of the storm tracks activity).

4. Statistical tests

In climate variability research, results should be accompanied by statistical significance, i.e., some kind of information about the probability of having obtained them only by chance. This is due to the fact that results in climate research are derived from a finite number of observations (i.e. limited *samples*), but they are expected to be applicable to the *population*. The use of the so-called *statistical tests* allows us to infer general conclusions from results obtained from samples by the statistical procedure called *hypothesis testing* [von Storch and Zwiers, 2001].

The *hypothesis testing* uses the information from a random sample of the population to decide whether an initial hypothesis (*null hypothesis*, H_0) is rejected, or not, with a certain *significance level* (namely, probability of rejecting H_0 being true). In contrast, the *alternative hypothesis* (H_1) describes the possibilities that may be true when H_0 is rejected.

In basis of the probability distribution for the population of the variable under study (in most of cases, Gaussian distribution) and the null hypothesis, a specific *test statistic*

is used, which in turn follows a certain probability distribution when H_0 is true (e.g. Student's t, F-Fisher, χ^2, ...). This probability distribution, known as the *null distribution*, along with the *significance level* (α) establish the called *non-rejection region* of H_0 (i.e. values of the test statistics for which the null hypothesis cannot be rejected with a *confidence level* of 1-α, see Figure IV.7). If the test statistic computed from the sample is included in the non-rejection region of H_0, this is not rejected with the chosen confidence level. In contrast, if the computed test statistic is not included in the non-rejection region of H_0, the null hypothesis should be rejected with the probability α of being wrong. It should be highlighted the relevance of the value of *α* in this statistical procedure, since it determines the width of the rejection region of H_0 and thus, the resolution made from the statistical test.

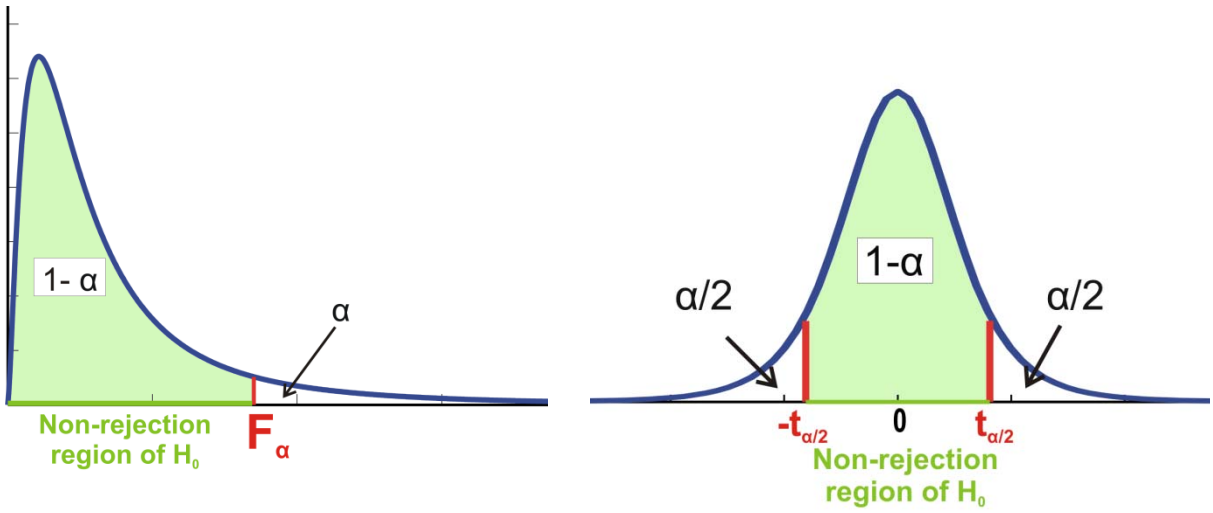

Figure IV.7. Examples of *non-rejection region of* null hypothesis H_0 (green line in the X-axis) in statistical tests: one-tailed test (**left**) and two-tailed test (**right**). The blue line represents the probability density function (pdf) of the test statistic when H_0 is true and the shaded area accounts for the (1-α) probability of non-rejection H_0 being true.

There are two types of statistical tests: parametric and non-parametric ones. The former correspond to those when a theoretical probability distribution is an appropriate representation of the data and/or the test statistic. In contrast, the tests not requiring such assumptions are called non-parametric [Wilks, 1995]. In this case, a discrete approximation to the null distribution is usually built up by resampling the data set (e.g., using Monte-Carlo technique).

Next, the parametric and non-parametric tests used in this work are briefly described.

a. Parametric tests

i. Tests of the mean

One-sample t Test

It determines if an observed sample containing *n* data and with a $\overline{x}$ as mean value has been drawn from a Gaussian population with a specified mean, μ_0. The null and alternative hypotheses are respectively:

H_0: $\mu = \mu_0$

H_1: $\mu \neq \mu_0$

The corresponding test statistic *t,* under unknown population variance, is:

$$t = \frac{\overline{x} - \mu_0}{s / \sqrt{n}} \qquad \text{(IV.4.1)}$$

where *s* is the standard deviation of the sample. If H_0 is true, *t* follows a Student's t-distribution of n-1 degrees of freedom (t_{n-1}). When the sample is large (namely, n > 30), t_{n-1} coincides with the typified Normal distribution (mean = 0, standard deviation = 1).

H_0 is rejected with a significance level of α when the computed *t* does not fall in the non-rejection region defined as $[-t_{n-1,\alpha/2}, t_{n-1,\alpha/2}]$.

This type of test has been widely used in this PhD thesis to check if the anomalies in composite maps of a given variable are statistically significant, namely, different from zero (i.e., $\mu_0 = 0$ in H_0).

Two-sample t Test

In this case, the means of two samples, $\overline{x_1}$ and $\overline{x_2}$, are compared in order to determine if their respective Gaussian population means, μ_1 and μ_2, can be considered equal. The null and alternative hypotheses are:

H_0: $\mu_1 = \mu_2$

H_1: $\mu_1 \neq \mu_2$

The *t* test statistic used in this case, when the population variances, σ_1^2 and σ_2^2, are unknown and different, is given by equation (IV.4.2):

$$t = \frac{\overline{x_1} - \overline{x_2}}{\sqrt{\frac{s_1^2}{n_1} + \frac{s_2^2}{n_2}}} \quad \text{(IV.4.2)}$$

where s_1 and s_2, n_1 and n_2 are the standard deviations and size, respectively, of the two samples [von Storch and Zwiers, 2001]. In this case, the non-rejection region of H_0, with a significance level of α, is given by $[-t_{df,\alpha/2}, t_{df,\alpha/2}]$, where

$$df = \frac{\left(s_1^2/n_1 + s_2^2/n_2\right)^2}{\frac{\left(s_1^2/n_1\right)^2}{n_1 - 1} + \frac{\left(s_2^2/n_2\right)^2}{n_2 - 1}} \quad \text{(IV.4.3)}$$

If $n_1 + n_2 > 30$, the null distribution of Student's t-distribution with *df* degrees of freedom is equivalent to the typified Normal distribution.

This type of parametric test has been widely used as well in this PhD thesis, when comparing results derived from model simulations with those from observations or when comparing two different sets of years that are under different phases of a specific phenomenon like the ENSO or NAM,…

ii. Test of variances

In some cases, not only is it important to determine if *two samples* come from populations with the same mean, but it is also necessary to decide whether these populations share the same variance (σ^2). The statistical test is defined as:

H_0: $\sigma_1^2 = \sigma_2^2$

H_1: $\sigma_1^2 \neq \sigma_2^2$

The test statistic is given by equation (IV.4.4):

$$\mathbf{F} = \frac{s_1^2}{s_2^2} \quad \text{(IV.4.4)}$$

This statistic follows the *F*-Fisher distribution with (n_1-1) and (n_2-1) degrees of freedom under the null hypothesis. Thus, the null hypothesis is rejected with a α significance level when

$$\frac{s_1^2}{s_2^2} \notin \left[F_{1-\alpha/2, n_1-1, n_2-1}, F_{\alpha/2, n_1-1, n_2-1} \right] \quad \text{(IV.4.5)}$$

This test is applied in this work to compare the variability of two climatic phenomena, such as the interannual variability in the timing of SFW in reanalysis data and model simulations.

iii. Tests of independence of characters (χ^2 test)

Along this PhD thesis, it has been necessary to determine whether there is any statistical dependence between two characters (variables X and Y) on the elements of a population, such as, for example, the frequency of MSWs and the period of study. To solve this question, a χ^2 test of independence has been applied, where the null and alternative hypotheses are:

H_0: X and Y are independent

H_1: X and Y are dependent

To apply this test, a n-size sample provides the observed frequencies o_{ij}, corresponding to the simultaneous occurrence of the values x_i and y_j of X and Y, respectively. Assuming the null hypothesis to be true, the expected frequencies, e_{ij}, are determined by (IV.4.6),

$$e_{ij} = \frac{o_{xi} o_{yj}}{n} \tag{IV.4.6}$$

where o_{xi} and o_{yj} are the marginal frequencies of X and Y, respectively. For instance, o_{xi} represents the number of elements of the sample that have the value of x_i regardless of the variable Y [Gorgas et al., 2009].

The test statistic is computed using the equation (IV.4.7),

$$\chi^2 = \sum_{i=1}^{k} \sum_{j=1}^{m} \frac{\left(o_{ij} - e_{ij}\right)^2}{e_{ij}} \tag{IV.4.7}$$

where k and m are the number of possible values of X and Y, respectively.

The statistic χ^2 follows the χ^2 distribution with (k-1) (m-1) degrees of freedom, when the null hypothesis is true. Thus, the null hypothesis is rejected with a α significance level when

$$\chi^2 > \chi^2_{\alpha,(k-1)(m-1)} \tag{IV.4.8}$$

The results from this statistical one-tailed test are reliable only if the expected frequencies are large enough, (i.e., $e_{ij} > 5$, $\forall$ i and j). When this condition is not

accomplished, other tests should be applied. One of these alternative tests, used in this work, will be described in the Subsection "non-parametric Tests".

iv. Tests of the slope in a simple linear regression

Regression is a technique widely used in climate research to estimate parameters that describe the empirical relationship among related random variables, or between a random variable and one or more non-random external factors, when they are measured on a continuous scale [von Storch and Zwiers, 2001].

In this PhD thesis, *simple linear regressions* have been used in order to estimate a relationship between two scalar variables X and Y, such as the heat flux at the upper troposphere and anomalies of polar stratosphere temperature or to determine the trend with time in any characteristic of major stratospheric warmings. This relationship is mathematically defined as: $Y = \gamma + \beta X$

To the purpose of this PhD thesis, the most interesting simple linear regression parameter is the slope β, as it gives the information related to the existence of a linear relationship between X and Y.

<u>One-sample test</u>

In several cases, it is desirable to know whether the linear relationship between two variables, derived from a sample of n pairs (x_i, y_i) is statistically significant or not. In that case, it should be statistically tested if the sample slope (b)[1] has been drawn from a population with a slope β different from zero [von Storch and Zwiers, 2001]. The statistical test is:

H_0: $\beta = 0$

H_1: $\beta \neq 0$

The corresponding test statistic *t* is:

[1] The simple linear regression model Y=f(X) derived from a sample of *n* (x_i, y_i) pairs is estimated as follows $y_i^* = a + bx_i$, where *a* and *b* are the sample regression parameters that are computed by $b = \frac{n\sum_{i=1}^{n} x_i y_i - \sum_{i=1}^{n} x_i \sum_{i=1}^{n} y_i}{n\sum_{i=1}^{n} (x_i)^2 - \left(\sum_{i=1}^{n} x_i\right)^2}$; $a = \frac{\sum_{i=1}^{n} y_i}{n} - b\frac{\sum_{i=1}^{n} x_i}{n}$ [Wilks, 1995].

$$t = \frac{b}{s_r / \left(\sqrt{n-1}\, s_x\right)} \tag{IV.4.9}$$

where s_x is the standard deviation of the abscise points (x_i) and s_r is the standard deviation of residuals, defined as $s_r = \sqrt{\frac{\sum_{i=1}^{n}\left(y_i - a - b x_i\right)^2}{n-2}}$.

H_0 is rejected (i.e., there is a linear relationship between X and Y) with a significance level of α when the computed t value does not fall in the non-rejection region defined as $[-t_{n-2,\alpha/2}, t_{n-2,\alpha/2}]$.

Two-sample test

When comparing the slope of a simple linear regression from two samples to verify if the sample slopes, b_1 and b_2, belong to populations with the same regression parameter, the statistical test would be:

H_0: $\beta_1 = \beta_2$

H_1: $\beta_1 \neq \beta_2$

The corresponding test statistic is:

$$t = \frac{b_1 - b_2}{\left[\frac{s_{r_1}^2}{(n_1-1)s_{x_1}^2} + \frac{s_{r_2}^2}{(n_2-1)s_{x_2}^2}\right]^{1/2}} \tag{IV.4.10}$$

The non-rejection region of H_0 is defined by $[-t_{df,\alpha/2}, t_{df,\alpha/2}]$, where

$$df = \frac{\left(\frac{s_{r_1}^2}{(n_1-1)s_{x_1}^2} + \frac{s_{r_2}^2}{(n_2-1)s_{x_2}^2}\right)^2}{\left(\frac{s_{r_1}^2}{(n_1-1)s_{x_1}^2}\right)^2 (n_1-1)^{-1} + \left(\frac{s_{r_2}^2}{(n_2-1)s_{x_2}^2}\right)^2 (n_2-1)^{-1}} \tag{IV.4.11}$$

[Charlton et al., 2007]

b. Non-parametric tests

When evaluating the statistical significance of data fields defined over large spatial networks for small samples, the *normality* and *independence* of the data values cannot safely be assumed. Thus, the use of classical parametric tests to make significance statements such as those described above is not adequate [Preisendorfer and Barnett, 1983]. To avoid this type of problem, permutation procedures (e.g. Monte Carlo

techniques) are frequently used in order to generate the probability density function (pdf) on which the statistical test of significance is based [Pitman, 1937; von Storch and Zwiers, 2001].

Next, two non-parametric tests used in this PhD thesis are described.

i. Tests of the mean

In Section VI.1 of this work, an adaptation of the so-called "Pool Permutation Procedure" designed by Preisendorfer and Barnett [1983] has been used. This adaptation has been developed by Ayarzagüena and Serrano [2009] to construct the associated pdf of the test statistic that measures the difference between a pair of datasets to be compared. In particular, in that section different atmospheric fields for years with a very early SFW ("early years") and years with a very late SFW ("late years") are compared. The main aspects of this methodology are described next.

E and **L** denote the two datasets of a certain variable (e.g., monthly geopotential at 500 hPa in April) — n_E and n_L years for each "early years" and "late years" sets, respectively—over s grid points. **E** and **L** are considered as two sets of n_E and n_L points in a Euclidean space (ε_s) of dimension s:

$$\mathbf{E} = \left\{ \mathbf{e}(t) : \quad t = 1,2,.....,n_E \right\} \tag{IV.4.12}$$

$$\mathbf{L} = \left\{ \mathbf{l}(t) : \quad t = 1,2,.....,n_L \right\} \tag{IV.4.13}$$

where $\mathbf{e}(t)$ and $\mathbf{l}(t)$ represent vectors of s components for the time t. Consequently, the centroids of the two sets of points, **E** and **L**, are defined by the vectors:

$$\overline{\mathbf{e}} \equiv \frac{1}{n_E} \sum_{t=1}^{n_E} \mathbf{e}(t) \quad ; \quad \overline{\mathbf{l}} \equiv \frac{1}{n_L} \sum_{t=1}^{n_L} \mathbf{l}(t) \tag{IV.4.14}$$

whose graphical representations in geographical coordinates are the composites maps that will be explained below. In this way, the measure of discrepancy for each x grid-point between **E** and **L** used in this work is:

$$\mathrm{DIF}(x) \equiv \left(\frac{1}{n_E} \sum_{t=1}^{n_E} e(t,x) \right) - \left(\frac{1}{n_L} \sum_{t=1}^{n_L} l(t,x) \right) \quad ; \quad x = 1,...,s \tag{IV.4.15}$$

that is, the difference of the corresponding time-means. Overall, DIF(x) is the x–component of the vector **DIF** = $\{\mathrm{DIF(x)}\}_{x=1,..,s}$, which is illustrated by an "early"-minus-"late" difference composite map.

The key aspect of the method to establish the statistical significance of differences between "early" and "late" years is the generation of the pdf of the statistic DIF (for each grid-point of a given atmospheric field). The steps to do this are the following:

1. To construct the union (**U**) of the two data sets **E** and **L** in ε_s, thereby forming a single batch of n_E+n_L elements.

2. The batch **U** is then repeatedly partitioned randomly (5000 times in this work) into two batches $\mathbf{U_1}$ and $\mathbf{U_2}$, with n_E and n_L elements respectively.

3. The statistic **DIF** vector of the pair [$\mathbf{U_1}$, $\mathbf{U_2}$] is computed for each permutation of 1, 2,..., n_E+n_L. The resultant set of values of grid-point DIF formed by all generated partitions provides a number of elements huge enough to construct the pdf of the statistic DIF for each x point.

Once each grid-point DIF(x) of the two original sets E and L (denoted by DIF*) is computed, its location in the associated pdf can be determined. From this, it can be decided for each grid-point whether its DIF* is large by chance or not. In other words, the statistical significance level of the DIF* for each grid-point can be established or it can be determined whether this value is statistically significant at a given significance level (e.g. α=0.05, value used in this work).

ii. Test of independence of characters (Fisher-Irwin exact test)

As mentioned previously, the classical parametric χ^2 test to determine the independence of characters is not accurate when the expected frequencies are small (typically smaller than 5). Under this circumstance, the non-parametric test, named as *Fisher-Irwin exact test,* is often used [Hodges and Lehmann, 2004], being applied in this PhD thesis as well.

The null hypothesis H_0 in the Fisher-Irwin exact test is the same as in the χ^2 test, i.e., the independence between the characters X and Y. However, this test is based on calculating directly the probability of getting the observed results (or more extreme), if H_0 is true, using all possible tables that could have been observed for the same marginal frequencies as the observed data.

The Table IV.1 summarizes the observed frequencies of the characters X and Y derived from a n-size sample, considering two possible values for each character, which is the particular case resolved in this work. The notation used here is the same as in the Subsection of the analogous parametric test.

Table IV.1. 2 x 2 contingence table of the observed frequencies of the possible values of the variables X and Y.

	y_1	y_2	
x_1	o_{11}	o_{12}	$\mathbf{o_{x1}}$
x_2	o_{21}	o_{22}	$\mathbf{o_{x2}}$
	$\mathbf{o_{y1}}$	$\mathbf{o_{y2}}$	**n**

Next, the Fisher-Irwin exact test particularized for a 2 x 2 table problem is described. The steps to be accomplished are the following:

- To create all tables with values more extreme than the observed ones by reducing the value in the cell with the lowest count by 1 in steps.

  For example, this statistical test has been used in Section VI.1 to decide whether there is any statistical dependence between the Arctic Oscillation phase (positive or negative AO) in some months and the late or early occurrence of the SFW. This test applied to the month of April is enclosed here as an example in order to clarify the statistical methodology. In this example, Table IV.2 (left) is the observed table, where the cell with the lowest value corresponds to the number of "late years" that show a negative phase of AO in April (more exactly, 1 year). Table IV.2 (right) is the new-created table with a value in the aforementioned cell more extreme than that in the observed table.

Tables IV.2. (Left) Contingence table displaying the observed number of "early years" and "late years" (in the period 1960-2000) with positive or negative AO phase in April. **(Right)** New contingence table created by reducing the observed frequency o_{22} (cell with a pink shading) by 1.

Observed table	AO $^+$	AO $^-$	Total
Early years	3	5	8
Late years	7	**1**	8
Total	10	6	16

New-created table	AO $^+$	AO $^-$	Total
Early years	2	6	8
Late years	8	0	8
Total	10	6	16

- To calculate separately the probability of obtaining the given results and the probability of getting even more extreme values than the observed ones by computing the expression (IV.4.16) for each table.

$$p = \frac{o_{x1}!\,o_{x2}!\,o_{y1}!\,o_{y2}!}{n!\,o_{11}!\,o_{12}!\,o_{21}!\,o_{22}!} \qquad \text{(IV.4.16)}$$

In this example, the probabilities of obtaining the observed results (denoted by p_{obs}) and the values shown in the second table (p_{ext1}), respectively are given by:

$$p_{obs} = \frac{8!\,8!\,10!\,6!}{16!\,3!\,5!\,7!\,1!} = 0.0559 \quad p_{ext1} = \frac{8!\,8!\,10!\,6!}{16!\,2!\,6!\,8!\,0!} = 0.0035$$

- To sum the separate *p*'s to get the total probability of a table as extreme as or more extreme than the observed. The total *p* represents the exact value of the significance level α of this *hypothesis testing* [Hodges and Lehmann, 2004].

  Applying this to this example, the total probability (p_{tot}) of obtaining Table IV.2 (left) or a more extreme one (Table IV.2, right) is:

$$p_{tot} = p_{obs} + p_{ext1} = 0.0559 + 0.0035 = 0.0594$$

  Thus, as p_{tot} is higher than 0.05, it can be concluded that the hypothesis about the independence of the two analyzed characters (Arctic Oscillation phase and late-early occurrence of the SFW) cannot be rejected at a 5% significance level, i.e. 95% confidence level.

5. Graphical tools

Finally, this Chapter, devoted to the Methodology, concludes by enumerating the different graphical tools used through this report. The results derived from this PhD thesis have been presented by means of the following graphics:

- **Histograms,** to show the frequency distribution of data, such as the occurrence of MSWs in wintertime months or SFW dates.
- **Contingence tables**, already described in Section IV.4.
- **Composite maps**, calculated as the average of a variable under a certain requisite (e.g., years with "early" SFW).
- **Vertical sections**, which show the vertical distribution of a quantity with respect to either time or space [AMS Glossary][2].
- **Hovmöller diagrams**, defined as a two-dimensional plot that shows the variation of some quantity in space-time. One axis corresponds to time and the other to a spatial dimension. This product is very useful to observe the progression of large-scale atmospheric features over a long period of time [AMS Glossary].

[2] Definition from the American Meteorological Society Glossary, that is available online: http://amsglossary.allenpress.com/glossary.

V. Major Stratospheric Warmings

As has been already indicated in Section II.5, major stratospheric warmings (MSWs) are a very prominent phenomenon in the boreal wintertime polar stratosphere that has relevant effects even on the tropospheric circulation. They consist in a reversal of the meridional temperature gradient poleward of 60°N and a change of the polar stratospheric circulation, i. e. the breakdown of the polar vortex, which is reestablished after the occurrence of these events [Labitzke, 1981b]. They happen more often in January and February than in the previous winter months.

Since their discovery by Scherhag in 1952 a large amount of work has been done in order to understand these events. However, there still exists a great uncertainty in MSWs, particularly, in the understanding of the mechanisms leading to their appearance and the stratosphere-troposphere feedback associated with these events. This uncertainty is, at least in part, responsible for the errors in the reproduction of these events by the models [Charlton et al., 2007], the problems of predicting single MSWs (i.e. some month before occurrence) [e.g.: Mukougawa et al., 2005; Hirooka et al., 2007] or the big discrepancies in possible changes in future MSWs projected by different model simulations [e.g.: Shindell et al., 1998; McLandress and Shepherd, 2009b; Butchart et al., 2010].

This part of the study tries to contribute to a better understanding of some of these problematic aspects of MSWs. First, in Section V.1 the analysis is focused on the recent past and present period, when the observed MSWs are used to validate the models and to study in detail some specific aspects of MSWs that show controversy or a lack of consensus among previous studies. Then, in Section V.2 the impact of the future increase in GHG (greenhouse gases) concentration in MSWs is examined in detail by means of two model simulations run with a CCM, one of them under climate change conditions and the other one with no climate change features.

1. Recent past and present

Specific aspects of MSWs in the Northern Hemisphere (NH) are analyzed in this Section, in order to improve the understanding of the involved processes. First, the reproduction of MSWs by stratospheric resolving models and the signatures of these events on the tropospheric circulation are analyzed. Next, two very recent MSWs that occurred under very different external factors are studied in detail, focusing, in particular, on the driving mechanisms that lead to the occurrence of both events.

a. Reproduction of MSWs in different types of model simulations

The ability of three different types of model runs to simulate MSWs is assessed in this Section. The main properties of these events and the tropospheric changes following MSWs in each simulation are examined and compared with those of MSWs in ERA-40[1]. The comparison of results among them and with ERA-40 may help to determine possible deficiencies of each type of simulation. The three analyzed runs are the following:

- EMAC CCMVal REF-B1 (hereafter EMAC REF-B1): A 41-yr transient simulation for the period 1960-2000, run with the chemistry climate model EMAC.
- EMAC-FUB CCMVal REF-B0 (hereafter EMAC-FUB REF-B0): A 55-yr simulation under constant present-day conditions corresponding to the year 2000, run with the chemistry climate model EMAC with EMAC-FUB configuration.
- Present-day EGMAM: A 300-yr simulation under constant present-day conditions corresponding to the year 1990, run with the coupled atmosphere-ocean general circulation model EGMAM. To assess the ability of the model to reproduce the observed major stratospheric warmings, the occurrence of these events in the first 100-yr reference period of the model simulation (denoted as 2200/01-2298/99) is analyzed. A comparison of the most important properties of MSWs in the other two 100-year subsets of the complete model time series (referred to as 2300/01-2398/99 and 2400/01-2498/99) is included to provide confidence in the obtained results for the first subset.

More details about these simulations and models used are found in *Data* chapter, Section III.2.

i. Main features

Main average properties of MSWs in each simulation are analyzed and compared with those corresponding to ERA-40 and the other simulations. In particular, the frequency and timing of MSWs and dynamical features are examined.

[1] ERA-40: ECMWF reanalysis dataset covering the period 1957-2002 (more details in *Data* chapter, Section III.1.a). This study is restricted to the period 1960/61-1999/2000, so that at least the analysis of MSWs with reanalysis and the transient EMAC REF-B1 simulation has a common period.

Frequency and timing of Major Stratospheric Warmings

The extended winter (November-March) has been analyzed to identify major stratospheric warmings in each model simulation, according to the "standard criterion" described in *Methodology* Chapter, Section IV.1. The frequency of these events is indicated in Table V.1.

Table V.1. Mean frequency of MSWs per winter and the associated *standard error*[2] in the analyzed simulations (EMAC REF-B1, EMAC-FUB REF-B0 and EGMAM) and observations (ERA-40 data from 1960/61-1999/2000).

Dataset	Mean frequency (MSWs/winter)	Standard error
EMAC REF-B1 (40 winters)	0.55	0.13
EMAC-FUB REF-B0 (55 winters)	0.58	0.10
EGMAM (99 winters)	0.12	0.09
ERA-40 (40 winters)	0.55	0.10

When comparing the simulated MSWs to those in observations for the period 1960/61 to 1999/2000 (derived from ERA-40 data), the CCM (EMAC) reproduces realistically the frequency of MSWs occurrence with very similar values (0.55±0.13 and 0.58±0.10 MSWs/winter compared to 0.55±0.10 MSWs/winter in ERA-40). This is in good agreement with the results found for most of the CCMs analyzed in the SPARC CCMVal initiative which shows that they can produce the correct number of MSWs in the period 1960/61-1999/2000 [Butchart et al., 2010]. In contrast, the AOGCM (EGMAM) tends to underestimate the occurrence frequency of MSWs with 0.12±0.09 MSWs/winter, consistent with a stronger modeled polar vortex than that identified in observations (Figure V.1). This also agrees well with a previous study by Charlton et al. [2007], where they show that three of the six stratosphere-resolving GCMs significantly underestimated the frequency of MSWs, whereas only one had a higher frequency of MSWs than the reanalysis.

[2] Standard error of mean frequency of MSW: $std\ error = \frac{\sqrt{\sum_x (o-\overline{o})^2 \Pr\{O=o\}}}{\sqrt{N}}$, where o represents an observed frequency of MSW per winter, $\overline{o}$ is the mean frequency of MSWs per winter, N is the number of winters in the dataset and Pr{O=o} is the probability with which that frequency is observed [Charlton et al., 2007].

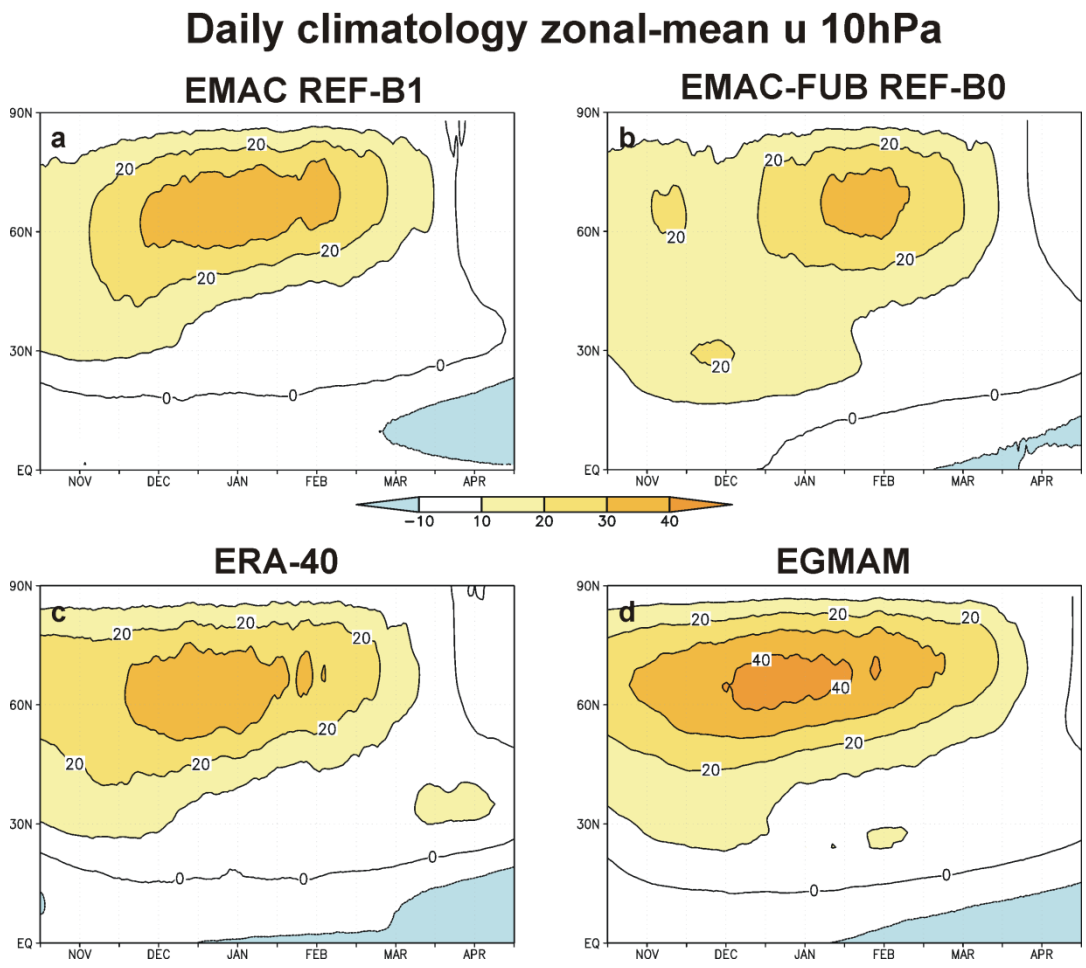

Figure V.1. Zonal-mean zonal wind climatology at 10 hPa for wintertime (from November to April) for ERA-40 (period: 1960/61-1999/2000) and for the model simulations used in Chapter V of this study.

As indicated by Butchart et al. [2010], the above results do not mean that, in general, CCMs can reproduce the stratospheric dynamical variability better than GCMs, but that EMAC and EMAC-FUB produce an improved simulation of the frequency of MSWs than the EGMAM AOGCM. In EGMAM, apart from the lack of an interactive chemistry component, other differences with the CCMs used in this study might be possibly responsible for the misrepresentation of MSWs. Some of these discrepancies can be the lower horizontal resolution (T30 in EGMAM, i.e., 3.75° x 3.75°) and the non-inclusion of the solar cycle in EGMAM. These differences could result in a worse simulation of tropospheric processes that act as MSWs precursors. These deficiencies in EGMAM do not seem to be compensated by the coupled interactive ocean model.

In order to analyze the variability of the MSWs in the models, the intra-seasonal distribution of MSWs in each model is plotted in Figure V.2. In EGMAM, even though the average frequency is not well simulated, a higher frequency of MSWs in midwinter (January and February) than in early-winter (November and December) is reproduced, as in observations.

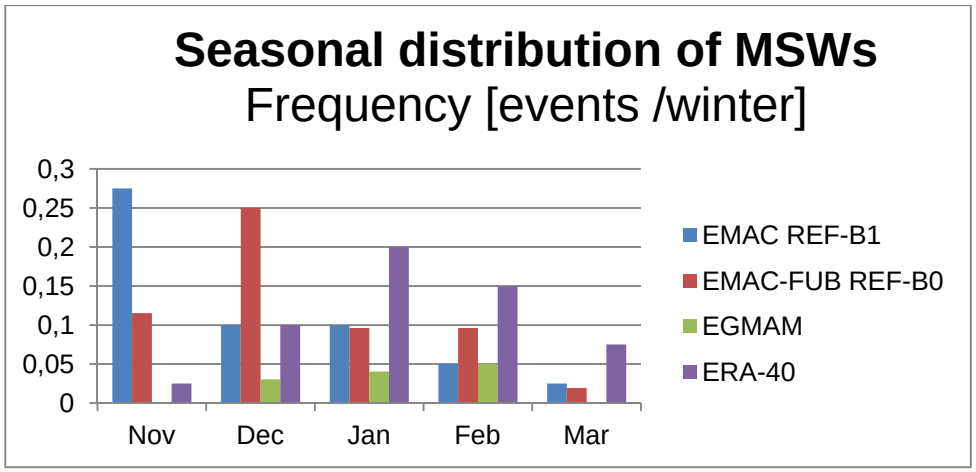

Figure V.2. Frequency of MSWs per winter in given month for EMAC REF-B1, EMAC-FUB REF-B0, EGMAM and ERA-40 reanalysis.

On the contrary, despite the well reproduced frequency of MSWs per winter in the CCM runs (EMAC-FUB REF-B0 and EMAC REF-B1), the distribution per month of these modeled MSWs shows two main discrepancies with respect to ERA-40. The first one corresponds to the low number of MSWs found in midwinter (January and February), which is consistent with the strong modeled vortex in these months (Figure V.1). The second and the most important difference between these CCM simulations and ERA-40 corresponds to the high number of MSWs computed in early winter (November and December), which agrees well with the weak modeled polar night jet seen in these months in both runs, EMAC-FUB REF-B0 and EMAC REF-B1 (Figure V.1). The same problem was also observed by Charlton et al. [2007], when doing a similar analysis for another model (MPI MAECHAM) that includes the same atmospheric GCM (ECHAM5). This could indicate that the overestimation of the frequency of MSWs in early winter is a common problem of the ECHAM5 model version. Cagnazzo and Manzini [2009] suggested that this problem could be only due to the low number of years considered by Charlton et al. [2007], because when they extended the analysis to more cases (180 yrs instead of 29 yrs considered in Charlton's work), they observed a reduction in the frequency of MSWs in November and an increase in March. However, the recurrent appearance of the same problem in EMAC-FUB REF-B0 and EMAC REF-B1 and the MAECHAM5 simulations leads to the assumption that a deficiency in ECHAM5 in early winter might exist. This deficiency is probably related to an artificial tropospheric forcing that would result in anomalous upward wave propagation. As a result, an extraordinary high number of MSWs is observed in early winter, which in some cases show "special" characteristics.

One possibility that explains the appearance of modeled "special" MSWs is that the model simulates some "unrealistic" MSWs in these winter months, i.e. MSWs with features that have not been identified up to date in observations. An example of one of these "unrealistic" MSWs in the EMAC REF-B1 is illustrated in Figure V.3 (upper panel). In this case, although the warming satisfies the dynamical and thermal criteria for MSWs, the vertical propagation of the perturbation signal does not correspond to the

typical one for a warming of this kind (upward instead of downward). For instance, the peak in the zonal-mean temperature gradient between 60°N and 90°N ($\Delta[T]_{90\text{-}60N}$) appears first at low levels (200-50 hPa) and the deceleration of the zonal-mean zonal wind at 60°N ($[u]_{60N}$) takes place first in 50 hPa and then in higher levels too (Figure V.3, left upper panel). Hence, these aspects would indicate that the event is basically a Canadian Warming (CW) [Juckes and O'Neill, 1988]. However, unlike the CWs in observations, the time evolution of the geopotential height field at 10 hPa is not the typical of a CW, as the anticyclonic center should move eastward as the time goes by, instead of westward like it does (Figure V.3, right and upper panel). Thus, the stratospheric warming shown in Figure V.3 (upper panel) would not be realistic, because it does not display characteristics of any specific type of stratospheric warmings. However, as the generation mechanism of CWs is still not understood and the "special" warming satisfies the dynamical and thermal criteria for MSWs, stratospheric warmings of this kind are considered in this study.

Another possible explanation for the extraordinary high number of early winter MSWs performed in both CCM runs is that very strong CWs are found. In fact, they are so intense that they satisfy the criteria for MSWs (in particular, the reversal of the cyclonic polar circulation). However, as indicated by Labitzke [1977], they are not strictly MSWs because the appearance of easterly winds at high latitudes is not associated with a real breakdown of the polar vortex, but only with a poleward displacement of the Aleutian high. Figure V.3 (lower panel) shows an example of a strong CW, where the typical features of this kind of warmings mentioned in the previous paragraph can be detected.

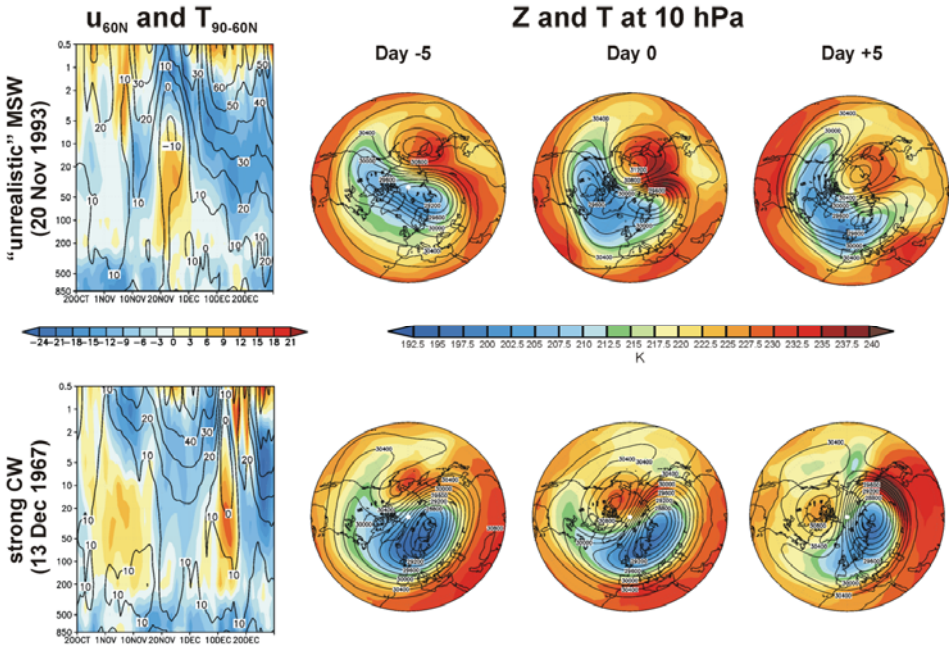

Figure V.3. (Left) Time evolution of the vertical section of zonal-mean zonal wind at 60°N (contours, interval: 10 m s^{-1}) and zonal-mean temperature difference between the pole and 60°N (shadings) from 20 October to 31 December for two years with a "special" MSW in the EMAC REF-B1 simulation. **(Right)** Geopotential height (contours, interval: 200 gpm) and temperature (shadings) at 10 hPa for the central day of the MSW and 5 days before and after the event (day -5 and day +5, respectively).

Other Major Stratospheric Warmings features

Other characteristics of MSWs in the model simulations have been compared with those corresponding to ERA-40. First, the type of these events, i.e vortex displacement or split, has been analyzed. Then, process-based diagnostics defined by Charlton and Polvani [2007] have been calculated.

Table V.2. Number of MSWs for each type in the analyzed simulations and observations (ERA-40 data from 1960/61-1999/2000). Bold numbers indicate that the modeled distribution of vortex displacement and vortex split MSWs is statistically significantly different from that of ERA-40 (at a 95% confidence level according to a χ^2 test).

Dataset	Vortex displacement MSW	Vortex split MSW	Displacement/split
EMAC REF-B1	19	3	**6.3**
EMAC-FUB REF-B0	22	8	2.8
EGMAM	10	2	5.0
ERA-40	11	11	1.0

Concerning the type of MSWs, Table V.2 shows that in the observations about 50% of the MSWs are associated with a split of the polar vortex into two centers of similar size, which is usually linked to an amplification of wavenumber-2 geopotential height. The other 50% is related to a displacement of the polar vortex off the polar cap, which, in turn, is often associated with the intensification of wavenumber-1. All the analyzed simulations show a relevant bias towards vortex displacement MSW, which may indicate that the models simulate a very weak wavenumber-2 planetary wave energy entering the stratosphere. In the case of EMAC REF-B1, the ratio of vortex displacement versus vortex split is statistically significantly different from that shown by ERA-40 (19/3 vs 11/11, respectively) and can be linked to the unrealistic number of modeled MSWs in early winter and thus, to the aforementioned higher occurrence of CWs associated with an intensification of wavenumber-1 tropospheric forcing [Labitzke, 1977]. However, even though the relationship of the wavenumber-1 to wavenumber-2 eddy heat flux can partially explain the ratio of vortex splits to displacements, the reasons for the MSW-type biases in the models can be more complex [Charlton et al., 2007]. For instance, the non-linearity of the flow prevents from the establishment of a direct match between the shape of the polar vortex during a MSW and the amplitudes of longitudinal wavenumber-1 and -2 wave activity [Waugh, 1997].

Table V.3 shows the values of MSW diagnostics benchmarks that allow for the assessment of relevant processes associated with the occurrence and development of MSWs [Charlton and Polvani, 2007]. The computation of the 100-hPa meridional eddy heat flux is explained in *Methodology* Chapter, Section IV.2.

Table V.3. Mean values of MSW diagnostics in ERA-40 (for 1960/61-1999/2000) and the analyzed simulations. In parenthesis, the corresponding standard deviation is included. Bold numbers indicate that the modeled values are statistically significantly different from the observations (at a 95% confidence level after a Student's t-test).

	Deceleration of the polar night jet	Intensity	Wave activity prior to MSW	Heat flux-temperature relationship
Criterion	Difference in 10-hPa zonal-mean zonal wind at 60°N, 15-5 days prior to the onset date minus 0-5 days after the onset date	Area-weighted mean 10-hPa polar cap temperature anomaly (90-50°N) averaged ± 5 days around the onset date	Area-weighted mean 100-hPa meridional eddy heat flux anomaly (45-75°N), 20-0 days before the onset date	Linear regression of the area-weighted mean 10-hPa polar cap temperature anomalies (90-50°N) ±5 days around the MSW onset versus the area weighted (45-75°N) 100-hPa meridional eddy heat flux anomalies
EMAC REF-B1	**17.8 m s^{-1} (std:7.6 m s^{-1})**	6.5 K (std: 5.2 K)	**6.8 K m s^{-1} (std: 3.6 K m s^{-1})**	0.97 s m^{-1} (std error[3]: 0.11 s m^{-1})
EMAC-FUB REF-B0	23.3 m s^{-1} (std: 10.5 m s^{-1})	7.9 K (std: 4.1 K)	8.2 K m s^{-1} (std: 4.3 K m s^{-1})	0.89 s m^{-1} (std error: 0.07 s m^{-1})
EGMAM	29.0 m s^{-1} (std: 12.8 m s^{-1})	10.4 K (std: 3.1 K)	10.6 K m s^{-1} (std: 4.6 K m s^{-1})	0.84 s m^{-1} (std error: 0.11 s m^{-1})
ERA-40	29.2 m s^{-1} (std: 11.5 m s^{-1})	8.6 K (std: 5.0 K)	9.9 K m s^{-1} (std: 5.7 K m s^{-1})	0.82 s m^{-1} (std error: 0.06 s m^{-1})

According to the values of Table V.3, the *EMAC REF-B1* simulation does not compare favorably with some of the MSW features found for ERA-40 data, as most of them are statistically significantly lower values than in the observations. These discrepancies can be probably related to the aforementioned higher number of early winter MSWs. This is verified by the higher values of the MSWs features computed without considering the MSWs that take place in November and December (Table V.3 vs Table V.4). Nevertheless, all of the quantities in the model are included within the observational interval defined by the mean value plus/minus one standard deviation. In addition, an accord is also found in the stratospheric response to the tropospheric wave activity (Figure V.4a), which is consistent with other studies that show this kind of relationship between the stratospheric polar cap temperature and the meridional heat flux at 100 hPa [Hu and Tung, 2002].

[3] Standard error of the slope parameter (b) of a linear regression: $std\ error = \frac{\sqrt{\sum_{i=1}^{N}(y_i - bx_i)^2}}{\sqrt{N-1}\sqrt{\sum_{i=1}^{N}x_i^2}}$, where N is the number of pairs (x_i, y_i) [Charlton et al., 2007].

Table V.4. Same as Table V.3 but only for the EMAC REF-B1, the EMAC-FUB REF-B0 and ERA-40 without considering the MSWs that take place in early winter (November and December).

	Deceleration of the polar night jet	Intensity	Wave activity prior to MSW	Heat flux-temperature relationship	Ratio displacement /split MSWs
EMAC REF-B1	23.6 m s^{-1} (std: 8.4 m s^{-1})	10.7 K (std: 5.9 K)	10.6 K m s^{-1} (std: 3.1 K m s^{-1})	1.03 s m^{-1} (std error: 0.16 s m^{-1})	1.3
EMAC-FUB REF-B0	31.1 m s^{-1} (std: 9.7 m s^{-1})	11.7 K (std: 3.1 K)	11.1 K m s^{-1} (std: 4.8 K m s^{-1})	0.96 s m^{-1} (std error: 0.10 s m^{-1})	1.8
ERA-40	31.2 m s^{-1} (std: 11.7 m s^{-1})	8.6 K (std: 4.7 K)	10.4 K m s^{-1} (std: 5.9 K m s^{-1})	0.78 s m^{-1} (std error: 0.06 s m^{-1})	0.7

In the case of the *EMAC-FUB REF-B0*, similar problems to those observed in the EMAC REF-B1 are found, i. e., the values for MSWs in Table V.3 are weaker than those corresponding to the reanalysis. The reason for these differences could be the same to that in the EMAC REF-B1, as it is clearly seen in Table V.4 (values after removing the early winter MSWs in the computation). However, the differences between the model results and those corresponding to ERA-40 are not as large as in EMAC REF-B1 and in this case, they are not statistically significantly different from those of ERA-40. This is probably, because the EMAC REF-B1 shows a bias towards an earlier occurrence of MSWs in early winter than that of the EMAC-FUB REF-B0 simulation (Figure V.2).

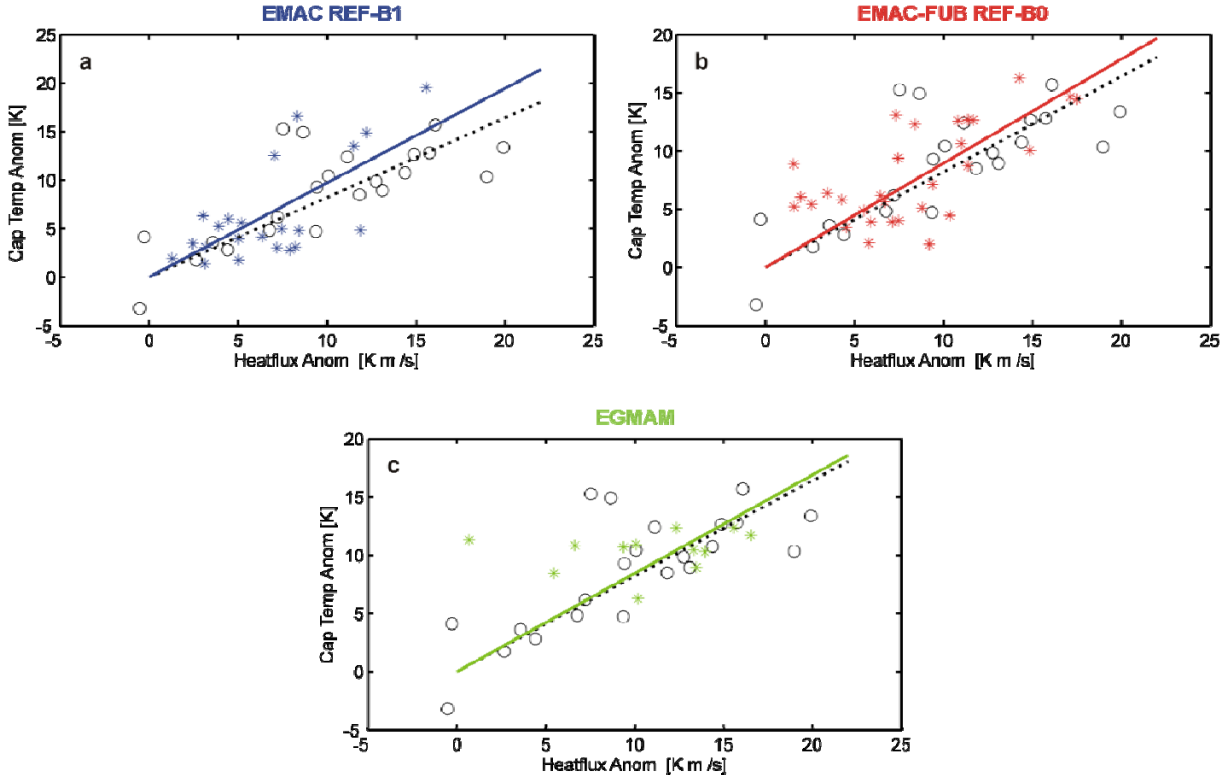

Figure V.4. Scatter plot of the area-weighted mean 10-hPa polar cap temperature anomalies (90-50°N) (in K) during ±5 days around the MSW onset versus the area-weighted mean 100-hPa meridional heat flux anomalies (45-75°N) (in K m s^{-1}) during 20-0 days before the MSW onset for ERA-40 between 1960/61 and 1999/2000 (black circles) and the analyzed simulations (colored asterisks). Solid line shows the linear regression for each simulation and the dotted line for ERA-40.

As for *EGMAM*, it can be seen that despite its problems to realistically simulate the frequency of MSWs, it captures quite well the mechanism of the development of a MSW and its intensity in the stratosphere, once the tropospheric forcing has been sufficient to initiate the process. When comparing with ERA-40, this model can also reproduce a linear-like relationship between the anomalous mid-latitude meridional heat flux at 100 hPa in the previous 20 days and the mid-stratosphere polar cap warming around the central date of the MSW (Figure V.4c). When comparing the results for this simulation with those for the other present-day simulation (EMAC-FUB REF-B0), the values of magnitudes in Table V.3 are more similar to the observations in the former than in the latter.

Finally, a comparative analysis of the most important properties of MSWs in the three 99-year subsets of the complete EGMAM time series has been carried out to provide confidence to the results derived from the EGMAM simulation (Table IV.5). All dynamical features of MSWs of the additional two 100-year subsets of the complete model simulation compare favorably with those of the observations, but the model still underestimates the average occurrence of MSWs. However, although the frequency of MSW occurrence is very low in the additional 200 years too (0.21 and 0.18, respectively), it is remarkably higher than in the first period. This difference could be related to multidecadal changes in tropospheric processes or in the ocean variability. For instance, Pinto et al. [2011] found for the same long present-day simulation multi-decadal periods with an enhanced or a weakened coupling between the two most important atmospheric teleconnection patterns of the NH, the Pacific/North American (PNA) and the North Atlantic Oscillation (NAO). Whereas the first 100-yr reference subset of the present-day EGMAM simulation is completely included in the period of enhanced coupling, most of the years of the third subset correspond to a period of weakened coupling. This could be responsible for the different values in the wave activity prior to MSWs and intensity of the warmings between the two subsets, being the latter even statistically significant weaker at a 95% confidence level.

Table V.5. Mean values of main features of MSWs for the three 100-yr periods of the present-day EGMAM simulation.

Dataset	Frequency of MSWs per winter	Deceleration of the polar night jet	Intensity	Wave activity prior to MSW	Heat flux-temperature relationship
2200s (Reference)	0.12	29.0 m s^{-1} (std: 12.8 m s^{-1})	10.4 K (std: 3.1 K)	10.6 K m s^{-1} (std: 4.6 K ms^{-1})	0.84 s m^{-1} (std error: 0.11 s m^{-1})
2300s	0.21	26.4 m s^{-1} (std: 13.0 m s^{-1})	9.0 K (std: 4.0 K)	9.3 K m s^{-1} (std: 6.5 K ms^{-1})	0.81 s m^{-1} (std error: 0.07 s m^{-1})
2400s	0.18	28.7 m s^{-1} (std: 15.37 m s^{-1})	7.8 K (std: 3.2 K)	8.7 K m s^{-1} (std: 5.6 K m s^{-1})	0.76 s m^{-1} (std error: 0.07 s m^{-1})
ERA-40	0.55	29.2 ms^{-1} (std: 11.5 ms^{-1})	8.6 K (std: 5.0 K)	9.9 K m s^{-1} (std: 5.7 K m s^{-1})	0.82 s m^{-1} (std error: 0.06 s m^{-1})

ii. Tropospheric changes after Major Stratospheric Warmings

Some studies, most of them based on reanalysis-observational data, have given evidence of a link between extreme vortex events, in particular MSWs, and changes in tropospheric fields some weeks after these stratospheric phenomena [e.g.: Baldwin and Dunkerton, 2001; Thompson et al., 2002; Limpasuvan et al., 2004; Charlton and Polvani, 2007]. Based on this, in this part of the study it has been evaluated if these tropospheric changes associated with MSWs are performed in the different model simulations examined in the previous Subsection. Discrepancies among the models in the reproduction of the MSW signal in the troposphere have been also examined.

Based on the definition of extreme vortex "regimes" as the 60-day periods after the occurrence of the stratospheric events [Baldwin and Dunkerton, 2001], composite maps of 1000-hPa geopotential height (Z) and temperature (T) anomalies have been plotted for the 60 days following the MSWs (Figure V.5). It should be noted that, in this part of the study, only MSWs that take place in December, January and February have been considered to improve the comparison of results among the different model simulations, since no MSWs happened in this November in the EGMAM run. Additionally, unrealistic MSWs of this month in the EMAC REF-B1 and EMAC-FUB REF-B0 simulations (particularly in the former) are avoided.

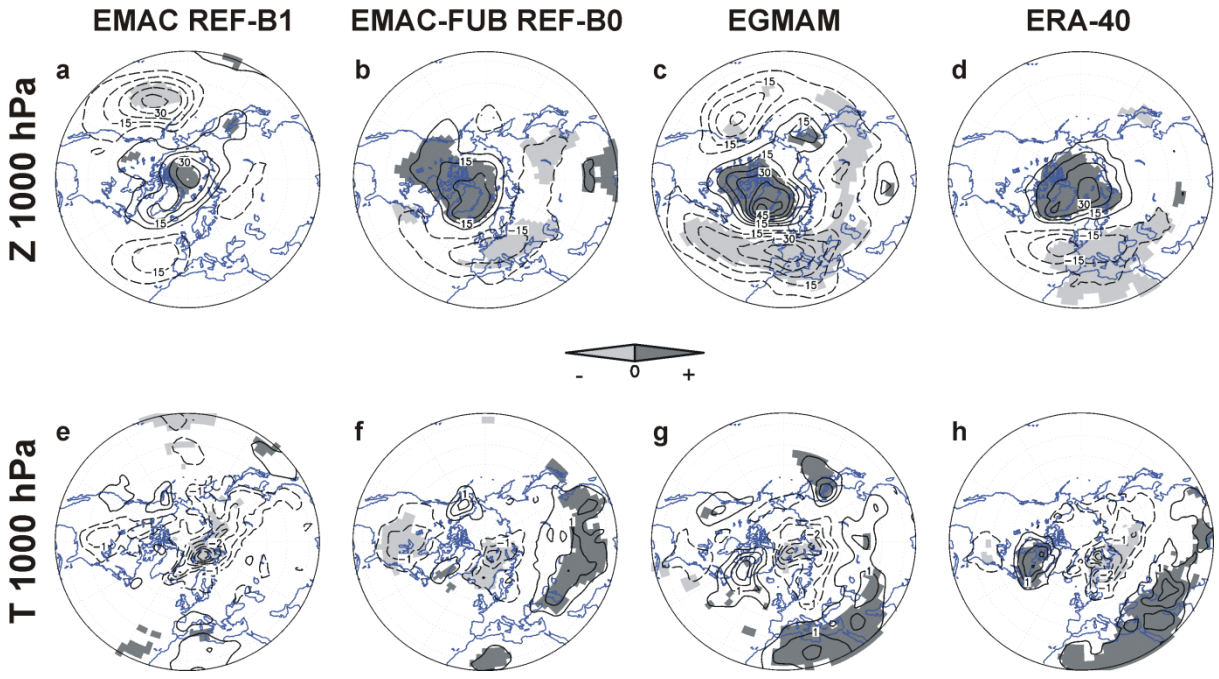

Figure V.5. Composite anomalies of 1000-hPa geopotential height (**upper panel**, contour interval: 7.5 gpm) and temperature (**bottom panel**, contour interval: 0.5 K) averaged over 0-60 days following the occurrence of the MSWs that took place in December, January and February in the different simulations and in ERA-40. Shadings show statistically significant anomalies at a 95% confidence level (Student's t-test).

In general, in all the simulations, the composite anomalies of 1000-hPa Z averaged over days 0-60 following the central date of MSWs show positive anomalies at high latitudes surrounded by negative anomalies at mid-latitudes, particularly in the Euro-Atlantic sector (Figure V.5, upper panel). This near-surface Z response to MSWs agrees well with that found by Charlton and Polvani [2007] for displacement-type MSWs in NCEP/NCAR reanalysis, except for the negative anomalies over the Pacific in some of the runs. This is consistent with the bias towards vortex displacement MSWs found in all the simulations. The 1000-hPa Z pattern observed in Figure V.5 also projects strongly onto a negative phase of the AO and NAO. In fact, it closely resembles the anomaly pattern derived for weak vortex regimes by Baldwin and Dunkerton [2001], which indicates the clear correspondence between MSWs and extreme polar events that lead to changes in the tropospheric circulation.

Consistent with the geopotential pattern, all the simulations and ERA-40 show, in general, a near-surface T pattern, consisting of a cooling of the Eurasian continent, associated with the weakening of the polar low (positive anomalies in Z at high latitudes); a warming over Northern Africa, Greenland to Eastern Canada, Northeastern America and Eastern Siberia and a weaker cooling over Eastern America (Figure V.5, lower panel). This pattern shows very good agreement with the temperature change patterns between weak and strong stratospheric vortex events derived from NCEP/NCAR reanalysis by Thompson et al. [2002] and is also consistent with the temperature patterns associated with the near-surface signature of the Northern Annular Mode [Hurrell, 1995; Thompson and Wallace, 2001].

Despite the overall agreement in the Z and T anomalies structure, there are also remarkable differences among the results for the models and the observations. *EMAC REF-B1* shows the most dissimilar patterns to ERA-40, with a low statistical significance of the centers of action and stronger negative Z anomalies over the Pacific than over Europe (Figure V.5, first column). These discrepancies can be probably related to the fact that some of the unrealistic MSWs happened in December, and so they are included in the computation of the anomalies plot.

In the case of the other *EMAC-FUB REF-B0* simulation, a very good agreement is found with the observations, indicating that the processes involved in the downward propagation of the stratospheric signal are well simulated and that the problem observed in the previous CCM run is not related to an intrinsic deficiency in CCMs (Figure V.5, second column).

Concerning the *AOGCM* run (Figure V.5, third column), the Z pattern presents a very similar structure to that of the observations, but with stronger values and with negative but not statistically significant anomalies over the Pacific that are not present in the ERA-40 plot. The availability of two other 100-yr subsets of the EGMAM run has allowed to provide robustness to the main results obtained for the 100-yr reference subset of the EGMAM run (Figure V.6). On the other hand, the discrepancies among the three long

subsets of the EGMAM simulation also give another additional result. In particular, the negative Z anomalies over the Pacific (which are only statistically significant in the second subset and do not even appear in the third one) could be probably associated with multi-decadal variability and with the periods of anticorrelation and correlation between the PNA and NAO modes described by Pinto et al. [2011]. This multi-decadal aspect would explain that the center of anomalies over the Pacific is not present in other datasets with a shorter length, such as the ERA-40 or the EMAC-FUB REF-B0. Moreover, due to the time-scale of this variability, it would be more probably to be captured by models with a coupled interactive ocean (AOGCM) than in other kind of models, as it can be related to ocean variability given that the ocean response is usually slower than the atmospheric one [Peixoto and Oort, 1992].

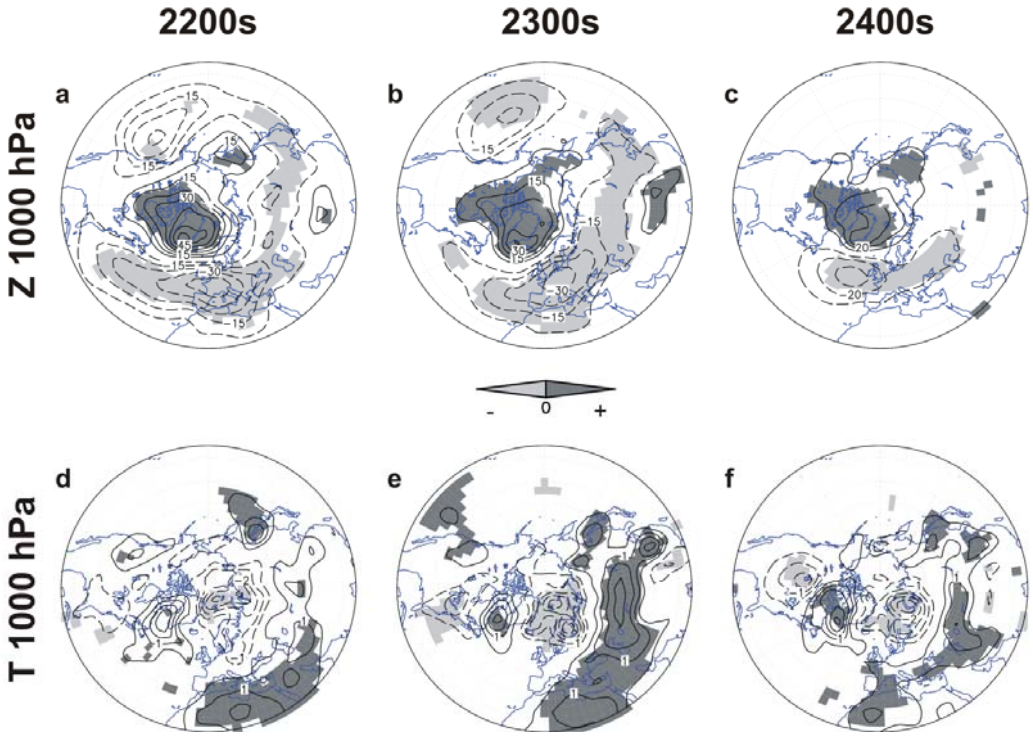

Figure V.6. Same as Figure V.5 but for the three subsets of the long EGMAM present-day simulation (2200s, 2300s and 2400s).

Final remarks

In summary, it can be concluded that the analyzed model simulations reproduce satisfactorily well the MSWs, as well as the tropospheric response to this kind of events. Thus, they can be used in further studies on stratosphere-troposphere coupling. However, it is important to previously take into account some specific problems in each model, such as the anomalous stratospheric variability in early winter in models with the ECHAM5 component (as in EMAC) or the reduced interannual stratospheric variability in the AOGCM EGMAM. Apart from these individual aspects, it can be also derived that large differences in the reproduction of MSWs under present-day conditions have not been found between the AOGCM and the CCM models analyzed in this study.

b. Tropospheric forcing of the stratosphere: 2009 and 2010 MSWs[4]

The study of the driving mechanisms of MSWs is currently a hot topic for scientific inquiry. As explained in Chapter II, these phenomena have been shown to be triggered by an enhancement of tropospheric wave activity that propagates into the stratosphere, interacts with the mean flow and decelerates it [e.g., Charney and Drazin, 1961; Matsuno, 1971; McIntyre, 1982; Limpasuvan et al., 2004]. However, some external factors, such as the 11-year sunspot cycle, the phase of the Quasi-Biennial Oscillation (QBO) or El Niño-Southern Oscillation (ENSO) events, have been proven to influence the mentioned enhancement of tropospheric wave activity. For instance, Labitzke and van Loon [1988] and van Loon and Labitzke [2000] concluded that MSWs are more likely to occur under solar minimum conditions during the QBO east phase and under solar maximum conditions during the QBO west phase. Concerning ENSO, van Loon and Labitzke [1987] suggested a relationship between El Niño events and a warm polar stratosphere in mid-winter and the occurrence of MSWs. However, in spite of these past achievements in understanding the basic tropospheric driving mechanisms of MSWs and their modulation by QBO, solar and ENSO effects, there is still uncertainty in the details of the tropospheric forcing of MSWs as well as in the interaction between the different internal and external influence factors.

The aim of this part of the study is to improve the understanding of the tropospheric forcing mechanisms in the occurrence of MSWs. To do that, two recent MSWs are analyzed in depth, in particular their driving mechanisms. These MSWs happened in the 2008/09 and 2009/10 winters as can be seen in the evolution of the zonal-mean zonal wind averaged over 60°N-65°N and at 10 hPa, shown in Figure V.7a. In both winters, the polar night jet weakened abruptly on approximately the same days (mid-January), and the MSW took place by the end of January. Both MSWs were exceptional for different reasons. As shown in Figure 13 of Gray et al. [2010], extraordinarily high values of North Pole 30-hPa geopotential height were observed in the subsequent February of both events. Moreover, they were characterized by a high 100-hPa eddy heat flux, with values among the three strongest recorded since 1958 (Figure V.7e). However, the conditions of external factors in these winters were different. While in the case of 2010, all of them were favorable to the occurrence of a MSW, that is, a minimum of the sunspot cycle during the east phase of the QBO and an El Niño event, the external factors did not support the onset of a MSW in 2009 (i.e., a minimum of the sunspot cycle during the west phase of the QBO and neutral conditions of ENSO) [Labitzke and Kunze, 2009] (Figure V.7b-d). Hence, these MSWs are specifically suited for a detailed examination of their driving mechanisms.

[4] Most of the results shown in this section are included in Ayarzagüena et al. [2011].

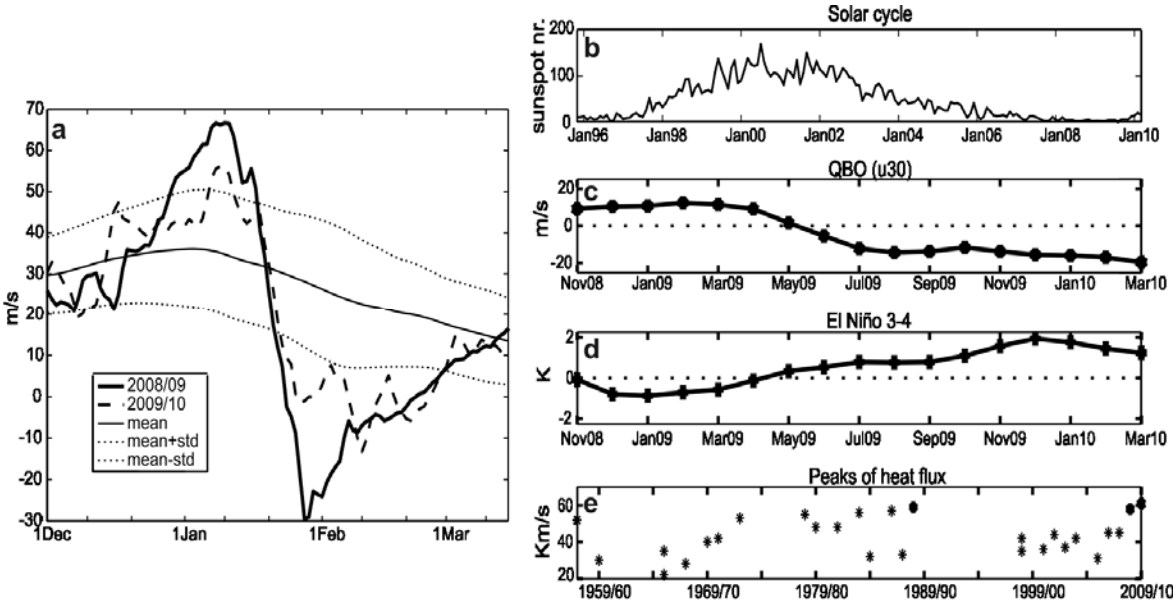

Figure V.7. a) Time series of 10-hPa zonal-mean zonal wind averaged over 60°N-65°N from 1 December to 15 March 2008/09 (thick solid line) and 2009/10 (dashed line). The thin solid line corresponds to the climatology for the period 1979/80-2009/10 and the dotted lines to the climatology plus or minus one standard deviation. Time series of: **b)** the solar cycle (sunspot number), **c)** Quasi-Biennial Oscillation (i.e., zonal-mean zonal wind at 30 hPa over the equator in m s^{-1}), **d)** El Niño 3-4 index (i.e., sea surface temperature anomalies in K) and **e)** the strongest values of 100-hPa eddy heat flux averaged over 50°N-80°N observed prior to a MSW (K m s^{-1}). The three highest values stand out in bold and the dates of MSWs for the period 1958-2002 were taken from Charlton and Polvani [2007]. (This figure has been taken from Ayarzagüena et al. [2011])

The detailed analysis of 2009 and 2010 MSWs also includes the description of the evolution of the polar vortex in both winters and a study of the tropospheric changes after each MSW, apart from the evaluation of the driving mechanisms. This complete analysis will be carried out by using NCEP/NCAR reanalysis data, as it is the longest reanalysis with available data that extends until present (more details about this dataset in *Data* chapter, Section III.1.b). Another important aspect to remind concerns the way of computing the climatological mean in Subsections V.1.b.i and V.1.b.ii, which has been calculated as the mean of smoothed daily data by a 31-day running mean for the period 1979/80-2009/10 (as indicated in *Methodology* chapter, Section IV.2.a).

i. Time evolution of the polar vortex in 2008/09 and 2009/10 winters

In this Subsection, the time evolution of the polar vortex associated with the 2009 and 2010 MSWs, as well as other aspects related to these events are described to provide an overview of them.

Figure V.7a shows the evolution of the zonal-mean zonal wind at 10 hPa averaged over 60°N-65°N ($[u10]_{60\text{-}65N}$) from 1 December to 15 March in the 2008/09 and

2009/10 winters, along with the climatology. In both winters, the polar night jet (PNJ) is slightly weaker than the climatology during the first half of December, consistent with an elongated and equatorward shifted polar vortex (e.g., Figures V.8a and b). After this period, the polar vortex becomes very strong (e.g., Figures V.8c and d), more intense in the 2008/09 winter than in the 2009/10 one, with $[u10]_{60\text{-}65N}$ values higher than the climatological mean plus one standard deviation during approximately 30 days in the former case and 6 days in the latter, both with a peak around 10 January.

In the second half of January 2009, the difference of the 10-hPa temperature between the North Pole and the zonal mean at 60°N, $\Delta_\varphi[T10]$, becomes positive, rising 32 K in 5 days, coinciding with an abrupt weakening of the PNJ (Figure V.9a) and satisfying the thermal requisite for a MSW. On 24 January 2009, $[u10]_{60\text{-}65N}$ furthermore becomes negative. This indicates the fulfillment of the dynamical criterion for a MSW, as the usual winter westerlies in the Arctic at 10 hPa are replaced by easterlies so that the centre of the vortex moves south of 60°N-65°N [Labitzke and Naujokat, 2000]. Thus, both criteria for a MSW[5], the thermal and the dynamical one, are satisfied on that date. Figure V.9e shows that, just after 24 January 2009, the polar vortex is clearly broken into two parts of approximately the same intensity, typical of a wavenumber-2 MSW in agreement with Manney et al. [2009].

In 2010, $\Delta_\varphi[T10]$ changes the sign in the same midwinter period as the 2009 MSW, and even though the zonal wind does not show as strong easterly values as in the latter, the typical stratospheric cyclonic circulation is not present any longer over the pole but displaced towards Eurasia by the end of January 2010 (Figure V.8f). Thus, the concurrent thermal and dynamical requisites for a MSW are fulfilled in 2010. Based on $[u10]_{60\text{-}65N}$, this MSW is dated on 27 January 2010, when $\Delta_\varphi[T10]$ became positive and the polar easterlies at 10 hPa appeared simultaneously over the Arctic.

It is important to remark that a dynamical criterion based on the value of $[u10]_{60\text{-}65N}$ instead of the typical one that uses $[u10]_{60N}$ has been applied in order to define the central date consistently for the two MSWs. In the case of the 2009 MSW, this criterion is fulfilled on the same day as if $[u10]_{60\text{-}65N}$ were used. In 2010, the MSW also fulfills the typical dynamical criterion, but later and not concurrently with the thermal one because of the very specific synoptic evolution in this year.

[5] Criteria for the identification of MSWs are described in Section IV.1.a (*Methodology* chapter).

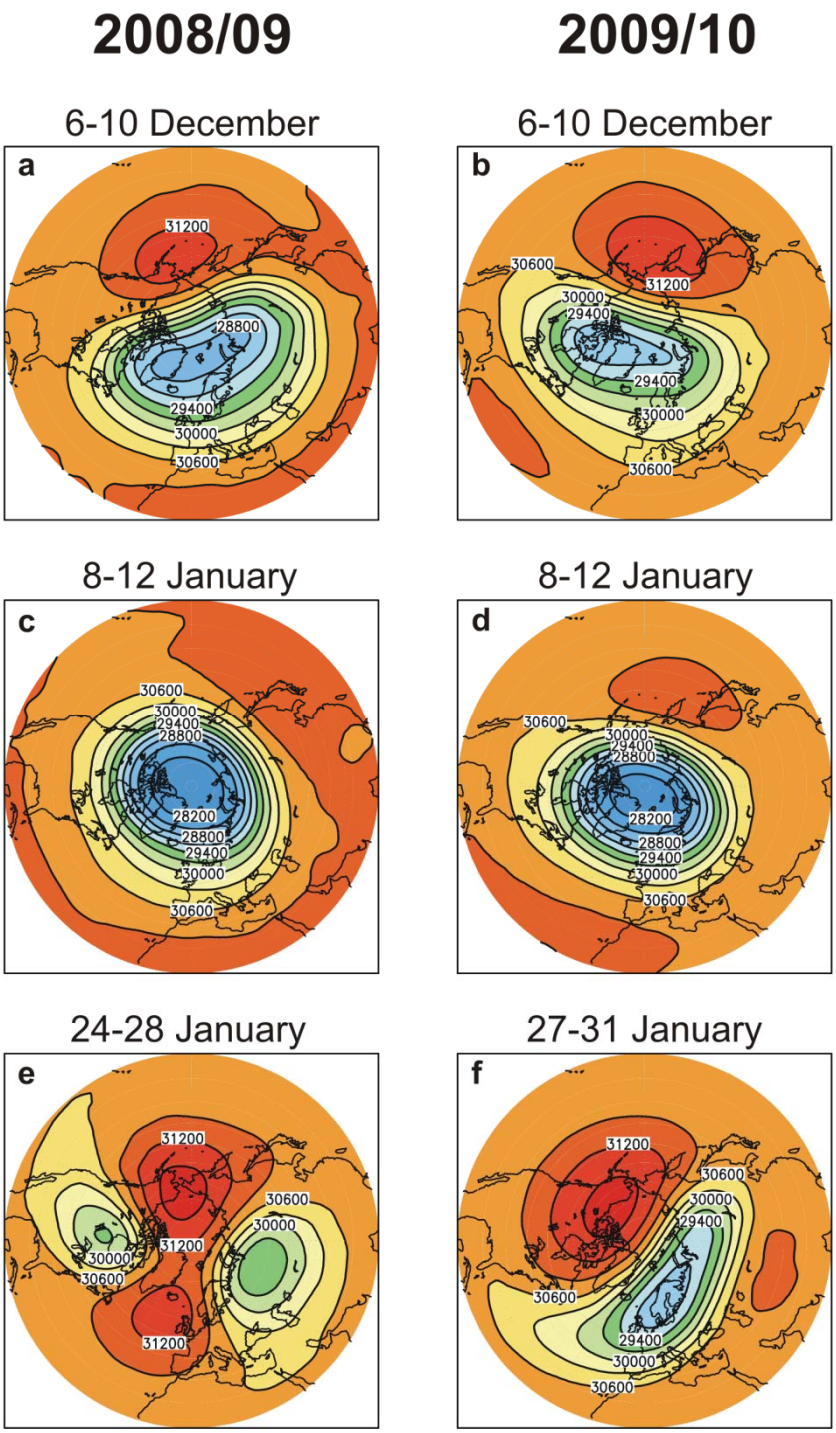

Figure V.8. Composite maps of 10-hPa geopotential height for three 5-day periods of the 2008/09 winter (**left column**) and 2009/10 winter (**right column**). Contour interval: 300 gpm [From Ayarzagüena et al. [2011]].

Hence, according to these results, both MSWs were not preceded by a weak vortex, particularly the 2009 MSW, in contrast to other cases in which the polar vortex was shown to be in a preconditioned state prior to a MSW, particularly a wavenumber-2 MSW [Charlton and Polvani, 2007].

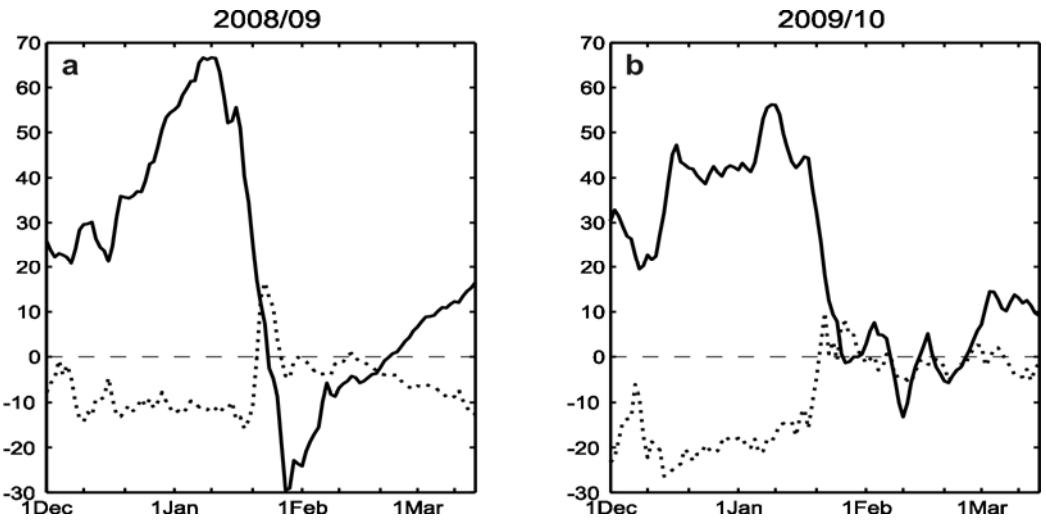

Figure V.9. a) Meridional zonal-mean temperature gradient between the North Pole and 60°N (K, dashed line) and zonal-mean zonal wind averaged over 60°N-65°N (m s^{-1}, solid line) at 10 hPa from 1 December 2008 to 15 March 2009. **b)** Same as **a)** but for 2009/10 [From Ayarzagüena et al. [2011]].

ii. Tropospheric forcing

In this Subsection the role of tropospheric forcing mechanisms in the occurrence of the MSWs in 2009 and 2010 is analyzed. In particular, as explained in detail in the *Methodology* chapter (Section IV.2.a), the injection of tropospheric wave activity into the stratosphere associated with these two events is studied by computing the time evolution of total eddy heat flux at 100 hPa, area-weighted averaged over 50°N-80°N. Moreover, by applying the methodology of Nishii et al. [2009] (hereafter N09) the modulation of the climatological planetary waves by intraseasonal and zonally confined *Rossby wave packets*[6] in the individual 2008/09 and 2009/10 winters is quantified, as well as their contribution to the resulting deceleration of the polar night jet associated with the MSWs. The sources for these Rossby wave packets in the two observed MSW cases are compared by computing the specific expression of the wave activity flux by Takaya and Nakamura [2001].

2009 MSW

A period of exceptionally strong *100-hPa eddy heat flux*[7] is identified from mid-January until the beginning of February 2009 (solid line in Figure V.10a). In these days, the total heat flux [v^*T^*] reaches values of almost 60 K m s^{-1}, the third strongest values prior to MSWs on record since 1958 and higher than the 90th percentile of this distribution (Figure V.7e).

[6] *Rossby wave packets:* defined in *Methodology* chapter, Section IV.2.a.
[7] The computation of *100-hPa eddy heat flux* and its contributors is explained in *Methodology* chapter, Section IV.2.a.

Two peaks are identified during this episode of extremely high 100-hPa eddy heat flux. The first and highest one (16-20 January, prior to the central date of the 2009 MSW) is characterized by the predominance of the wave activity associated exclusively with Rossby wave packets, whereas the second peak (26-30 January, after the 2009 MSW) mainly arises from the sum of similar contributions from the anomalies associated with Rossby wave packets and the interaction between these anomalies and the climatological planetary waves (Figure V.10a).

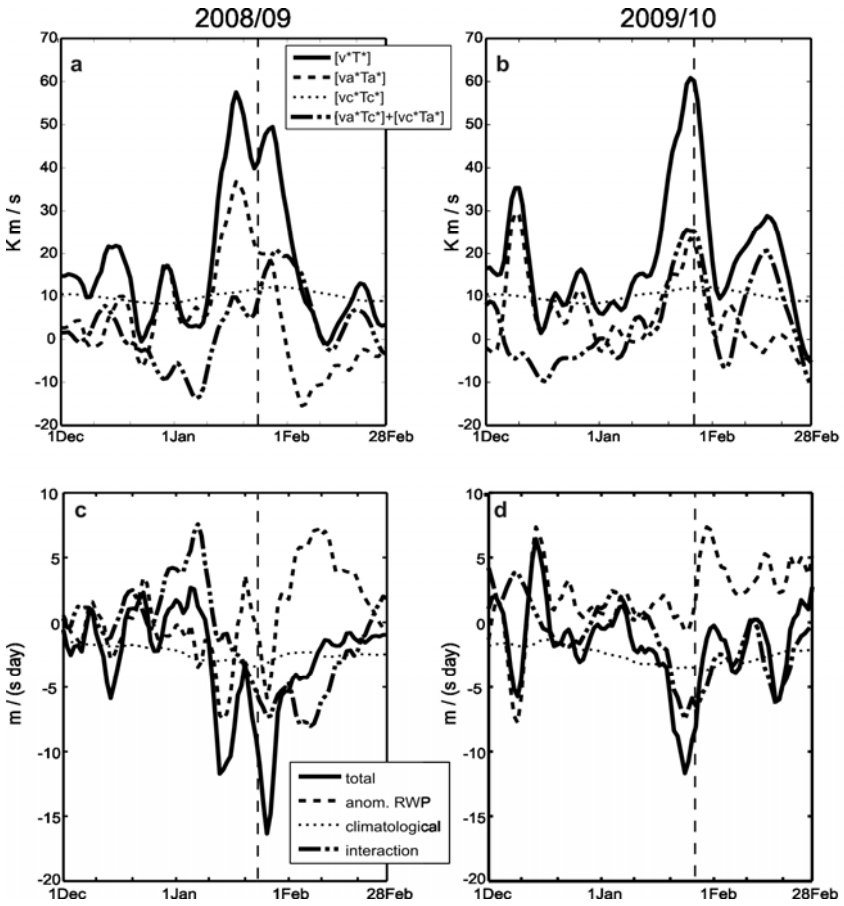

Figure V.10. a) Time evolution of zonal-mean meridional eddy heat flux averaged over 50°N-80°N (K m s^{-1}) at 100 hPa from 1 December 2008 to 28 February 2009. The different lines indicate total flux (solid line) and its contributions: the climatological-mean planetary waves (dotted line), the anomalies associated with Rossby wave packets (RWP) (dashed line), and the interaction between these anomalies and the climatological planetary waves (dash-solid line). The vertical line indicates the central date of the MSW. **b)** Same as a) but for 2009/10. **c)** and **d)** Same as a) and b), respectively, but for the divergence of Eliassen-Palm flux (m $s^{-1}$$(day)^{-1}$) at 10 hPa and 60°N [From Ayarzagüena et al. [2011]].

When analyzing the time evolution of the total divergence of *Eliassen-Palm flux*[8] (hereafter, divEP) at 60°N and 30 hPa, a period of strong convergence can be seen from approximately 10 January until the end of this month (solid line in Figure V.10c), being consistent with the strong deceleration of the polar night jet (Figure V.7a). It also agrees

[8] The computation of the *Eliassen-Palm flux* and its divergence is explained in *Methodology* chapter, Section IV.2.a.

well with the period of high values of 100-hPa eddy heat flux (Figure V.10a). Moreover, the principal contributors of the two negative peaks of 30-hPa $divEP_{60N}$ are the same as those identified as being mainly responsible for the peaks observed in the 100-hPa heat flux. This agreement highlights the link between the deceleration of the stratospheric mean flow and the injection of tropospheric planetary waves into the stratosphere.

It should be noted that a delay is observed between the central dates of the peaks of 30-hPa $divEP_{60N}$ and the 100-hPa eddy heat flux. In particular, in the first peak the eddy heat flux reaches its highest value a few days after the divergence, whereas, in theory, it should be the opposite, as the wave activity responsible for the deceleration of the stratospheric flow comes from the troposphere. However, both variables begin simultaneously to show values higher than those exclusively due to climatological planetary waves and so, it is possible that a positive feedback process occurs: initially the wave activity probably decelerates the polar stratospheric flow, and then, the latter is weak enough to allow a strong upward propagation of tropospheric wave activity into the stratosphere according to the theory on upward propagation of wave activity by Charney and Drazin [1961].

Hereafter in this Subsection, the analysis of the 2009 MSW will mainly focus on the first peak of $[v^*T^*]$, since the interest of this part of the study concerns the precursors of the MSW. By calculating the contributions of the first three zonal harmonics to the 100-hPa heat flux it can be shown that wavenumber-2 activity is predominant in the pre-MSW peak (Table V.6) providing 54 K m s^{-1} of the 58 K m s^{-1} of total heat flux. This is consistent with the 2009 MSW being a wavenumber-2 MSW, as indicated in the previous Subsection. The main reason for the peak of $[v^*T^*]$ observed prior to the 2009 MSW is the southerlies over the Pacific and the northerlies over Canada collocated with high and low temperatures, respectively, as shown in Figure V.11a. These spatial structures are related to the strong ridge over North America illustrated in Figure V.12a, associated with a blocking over this region [e.g., Newman and Nash, 2009]. Additional minor contributions to the first peak of $[v^*T^*]$ come from other zonal wavenumbers (see Table V.6); in particular, k=1 contributes 10% to the total $[v^*T^*]$. This feature implies that the four regions displayed in Figure V.11a do not contribute equally to the peak of $[v^*T^*]$, with the regions over the Pacific and Canada being more predominant than those over the Atlantic and Siberia.

Table V.6. Zonal-mean poleward heat flux at 100 hPa, area-weighted averaged over 50°N-80°N, corresponding to the period 16-20 January 2009 calculated from the first three zonal harmonics (k=1, 2 and 3, and their sum). The total value of heat flux, $[v^*T^*]$, is shown in the left column and its contributors in the others. The *a* and *c* subscripts denote anomalies and climatological, respectively. Units: K m s^{-1} (Values are rounded to the nearest integer).

	$[v^*T^*]$	$[v_a^*T_a^*]$	$[v_c^*T_a^*]$	$[v_a^*T_c^*]$	$[v_c^*T_c^*]$
k=1	**6**	3	-4	1	7
k=2	**54**	34	3	12	4
k=3	**-2**	0	0	-3	0
k=1-3	**58**	**37**	**0**	**10**	**11**

The contribution of the climatological planetary waves term during 16-20 January 2009 to the [v^*T^*] at 100 hPa accounts only for 19% (Table V.6). The meridional wind shows a wavenumber-2 (k=2) pattern, whereas the temperature has a wavenumber-1 (k=1) pattern. The correlation of both fields results in a predominance of the k=1 pattern with the main center over the Pacific area (southerlies collocated with high temperatures) (Figure V.11b). The interaction term [$v_a^*T_c^*$] plays a similar role for the total [v^*T^*] as the one due to climatological waves (Table V.6 and Figure V.11d). However, the contribution of [$v_c^*T_a^*$] is negligible, since the positive correlation between v_c^* and T_a^* over Canada is counterbalanced by the negative one over Europe (Figure V.11e). This situation changes during the time evolution of the MSW and [$v_c^*T_a^*$] represents the highest contributor to the total 100-hPa heat flux for the peak after the MSW, due to the overlap of the v_c^* and T_a^* structures, both of them showing a clear k=2 wave pattern (not shown).

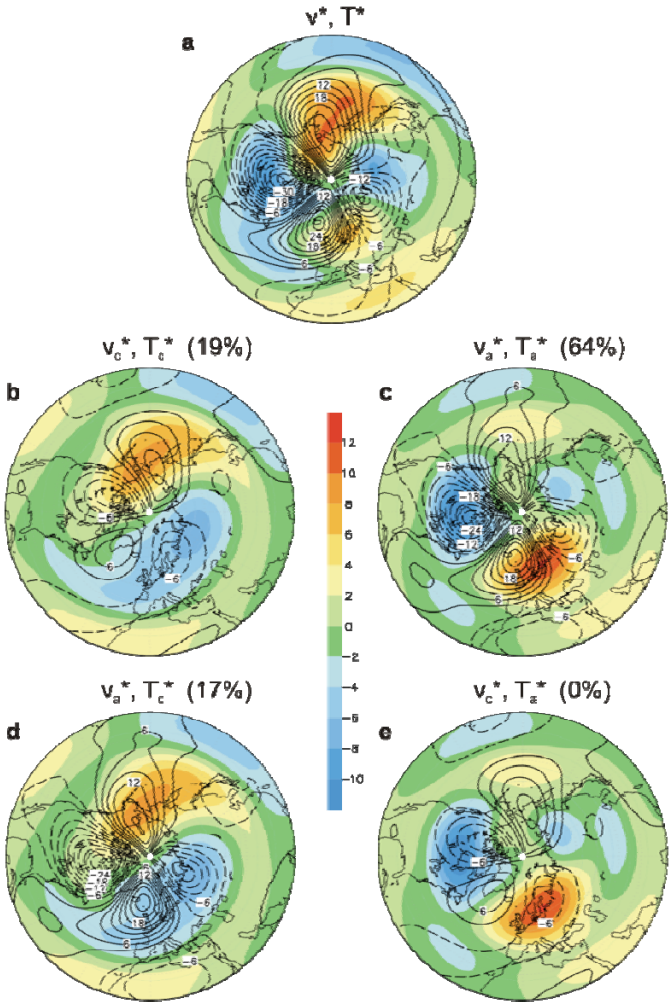

Figure V.11. a) 100-hPa meridional wind (contours, interval: 3 m s^{-1}) and temperature (shading in K) considering the first three zonal wavenumbers for 16-20 January 2009. **b)** and **c)** Same as a) but for the climatological-mean and anomalies of both fields, respectively. **d)** Same as a) but for anomalies of meridional wind and the climatological-mean of temperature. **e)** Same as a) but for anomalies of temperature and the climatological-mean of meridional wind. Zero contours are omitted for clarity. The contributions (in percentages) of [$v_c^*T_c^*$], [$v_a^*T_a^*$], [$v_a^*T_c^*$] and [$v_c^*T_a^*$] to the total [v^*T^*] are shown in brackets. [From Ayarzagüena et al. [2011]]

From Table V.6, it can be further concluded that the dominant contributor to the total 100-hPa eddy heat flux (i.e. $[v^*T^*]$) during the pre-MSW heat flux peak in 2009 is the term associated with Rossby wave packets (64% of the total), which is consistent with results from Harada et al. [2010] derived by using another methodology. This result mainly arises from the southward wind and cold anomalies over Canada along with the warm anomalies over Europe collocated with northward wind anomalies (Figure V.11c). The decrease in importance of the $[v_a^*T_a^*]$ term in the total eddy heat flux after the 2009 MSW, displayed in Figure V.10a, can be explained by the decrease of the v_a^* and T_a^* values at 100 hPa along with a reduction in the overlap of the respective patterns (not shown).

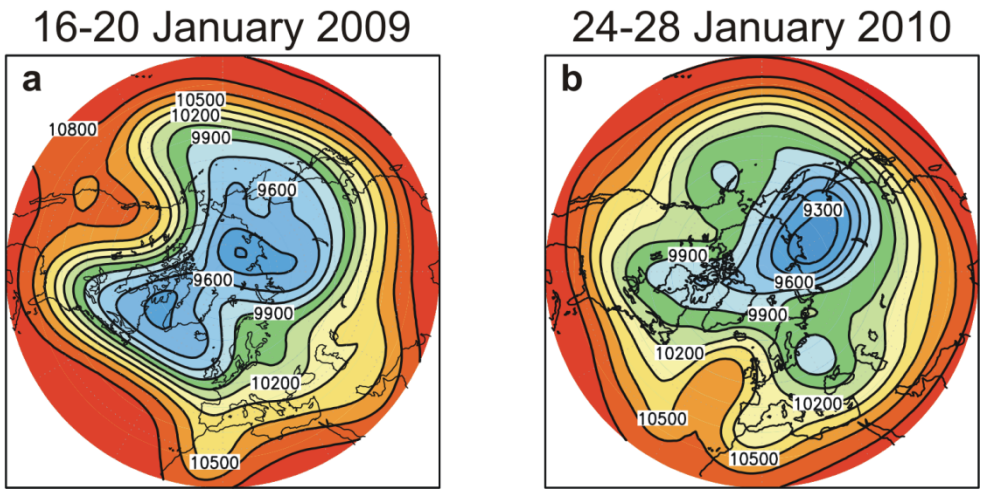

Figure V.12. Composite maps of 250-hPa geopotential height for 16-20 January 2009 and 24-28 January 2010. Contour intervals: 150 gpm. [Adapted from Ayarzagüena et al. [2011]]

In order to complete the analysis of Rossby wave packets and determine their sources and 3-dimensional propagation, their associated *wave activity flux*[9] at different levels, calculated from equation (IV.2.9) is shown in Figure V.13. At the tropopause level, a region of very strong upward wave-activity injection into the stratosphere is identified on the east side of a center of strong anticyclonic anomalies over Canada (Figure V.13a), which belongs to a tripole structure (with weaker cyclonic anomalies over the Pacific and the east coast of North America) related to a blocking. In the same area, the horizontal component of the wave activity flux (W_h, computed from equation (IV.2.9)) is clearly eastward and perpendicular to the geopotential anomaly contours (see arrows in Figure V.13a). All this indicates that this anomalous circulation over Canada acts as a source of Rossby wave packets that propagate upward into the stratosphere, in good agreement with the results of Harada et al. [2010]. Figure V.13a shows another source of upward propagating Rossby wave packets, which is however much weaker than the one over Canada and is located over the Atlantic. It corresponds to a high-latitude cyclonic center showing a westward phase tilt with height (Figure V.13c) and located upstream of a second region of upward propagation of wave activity. The two aforementioned sources of upward-propagating Rossbv wave packets spatially coincide with the areas of

[9] The computation of the *wave activity flux* is explained in *Methodology* chapter, Section IV.2.a.

highest correlation of v_a^* and T_a^* in Figure V.11c, which highlights the relevant role that plays this correlation in the determination of the vertical component of the wave activity flux for quasi-stationary eddies of equation (IV.2.9).

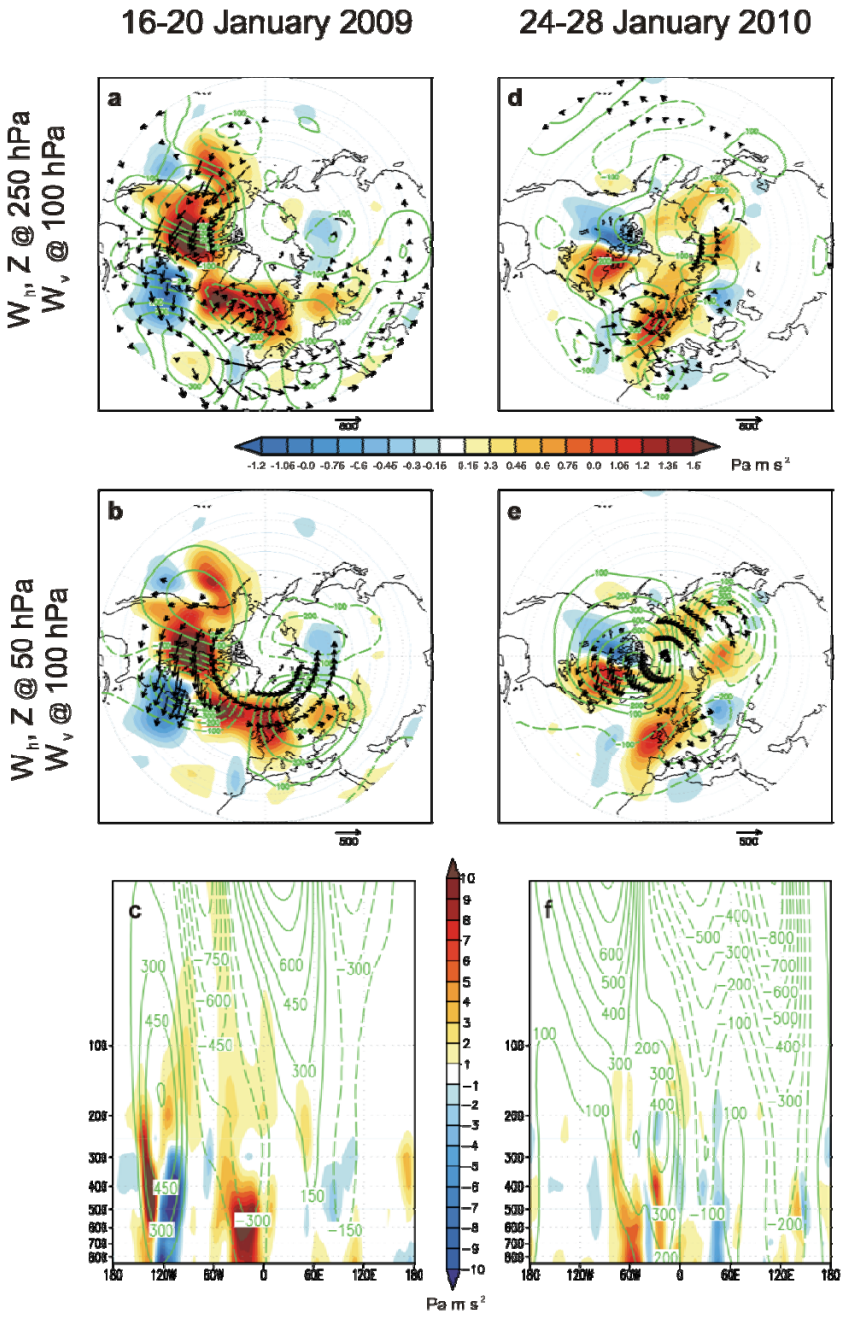

Figure V.13. a) Vertical component of wave-activity flux associated with Rossby wave packets at 100 hPa (Pa m s^{-2}, shading), horizontal component of this flux (m^2 s^{-2}, arrows) and geopotential anomalies at 250 hPa (gpm, contours) for 16-20 January 2009. **b)** Same as a), but the horizontal component and the geopotential anomalies are shown at 50 hPa. **c)** Zonal cross section at 55°N of geopotential anomalies (contours) and vertical component of wave activity flux (shading) for 16-20 January 2009. **d), e)** and **f)** Same as a), b) and c), respectively, but for 24-28 January 2010. The geopotential anomalies are multiplied by sin(43°N)/sin(latitude). Arrows smaller than 100 m^2 s^{-2} are omitted for clarity and their scale (m^2 s^{-2}) is indicated at the bottom of plots [From Ayarzagüena et al. [2011]].

In the lower stratosphere, two anomalous anticyclonic and cyclonic centers are observed (Figure V.13b, contours). The anticyclonic center over western America is clearly connected with the tropospheric deep ridge over Canada. As regards the two strongest centers, namely, the cyclonic one over the western Atlantic and the anticyclonic one over western Europe, they seem to have been amplified by the injection of wave activity from the troposphere, traveling along the zonal-mean flow, since horizontal wave activity around them (arrows) and regions of upward wave activity (shading) on their upstream sides are observed.

2010 MSW

As in the 2008/09 winter, a strong peak of total eddy heat flux at 100 hPa was observed in January 2010 just preceding the MSW, even higher than the former (61 vs. 58 K m s^{-1}, solid line in Figure V.10b) and the strongest one prior to a MSWs since 1958. However, in contrast to the 2009 MSW, not only the anomalies associated with Rossby wave packets contributed to this peak of $[v^*T^*]$ at 100 hPa prior to the 2010 MSW, but also, and with a similar weight, the interaction between these anomalies and the climatological planetary waves. From Table V.7, it can be identified that it is the interaction term $[v_a^*T_c^*]$ that contributes the most to the total wave activity injection into the stratosphere during 24-28 January 2010, namely, the interaction between the meridional wind anomalies and the climatological temperature.

Table V.7. As Table V.6, but for the period 24-28 January 2010.

	$[v^*T^*]$	$[v_a^*T_a^*]$	$[v_c^*T_a^*]$	$[v_a^*T_c^*]$	$[v_c^*T_c^*]$
k=1	**55**	21	0	26	7
k=2	**0**	-2	-5	2	4
k=3	**6**	4	-1	2	0
k=1-3	**61**	**24**	**-5**	**30**	**12**

Another outstanding difference in the peak of total 100-hPa eddy heat flux between both MSWs is a clear predominance of the zonal wavenumber-1 wave activity in the 2010 MSW, whereas the zonal wavenumber-2 wave activity (i.e., the most important in the 2009 MSW) does not play any role in January 2010 (Table V.7). Figure V.14a illustrates the atmospheric conditions that lead to this result: northerlies and low temperatures over Eurasia, along with southerlies and high temperatures over the Pacific. Moreover, the position of the meridional wind pattern relative to the temperature one in Figure V.14b-14e for each term contributing to $[v^*T^*]$ at 100 hPa explains the degree and sign of the correlation between both variables, v^* and T^*, and thus, the relevance of each term in the peak of total 100-hPa eddy heat flux in January 2010. The main contributor, $[v_a^*T_c^*]$, comes from the overlap between the v_a^* and T_c^*,

both of them showing a k=1 wave pattern with a coincident phase (Figure V.14d). The second important contributor, $[v_a^* T_a^*]$, arises from the southward wind and cold anomalies over Eurasia and secondarily from the northward wind and high temperature anomalies over North America (Figure V.14c). Notice that T^* and v^* anomalies in Figure V.14c and the overlap of their patterns are weaker than in Figure V.11c, which could explain the reduction in the importance of the $[v_a^* T_a^*]$ term in the 2010 MSW with regard to the 2009 MSW. This mentioned lower relevance of Rossby wave packets in the peak of $[v^* T^*]$ at 100 hPa (i.e., 24-28 January 2010) compared with the 2009 MSW is also clearly observed in the much lower values of their associated wave activity flux (Figure V.13d, e and f). In fact, in contrast to the 2009 MSW, a single tropospheric source of upward-propagating Rossby wave packets is identified during the peak of $[v^* T^*]$: a center of anticyclonic anomalies over the Atlantic (Figure V.13d), which is related to a strong ridge (Figure V.12b). This finding is supported by the westward phase tilt with height of this anomalous circulation (Figure V.13f) and its location upstream of a center of upward wave-activity propagation, emitting horizontal wave activity downstream. Moreover, there is not a so clear coincidence of areas with the highest overlap of v_a^* and T_a^* patterns and the strongest upward fluxes of wave activity in 2010 as in 2009. This is probably due to the fact that there are other terms in the third component of equation IV.2.9 that also represent important contributions to the vertical propagation of Rossby wave packets.

In the lower stratosphere, a strong anomalous anticyclonic center is identified over Canada and a region of a two-centre anomalous cyclonic system is observed over Eurasia (Figure V.13e), which results from the displacement of the polar vortex towards Eurasia (displayed in Figure V.8f). However, in this case, only a weak center of anomalies, i.e the one over Eastern Europe, seems to be amplified by the Rossby wave packets.

The other interaction term, $[v_c^* T_a^*]$, represents a slight negative contribution to the total heat flux. Whereas v_c^* shows a predominant k=2 wave pattern, T_a^* has a k=1 one (Figure V.14e). This difference in the structure explains the negative correlation between each other.

The climatological planetary wave term, $[v_c^* T_c^*]$, in the 2010 MSW plays a very similar role to that of the 2009 MSW (20% and 19% of the total value $[v^* T^*]$, respectively), as Tables V.6 and V.7 indicate.

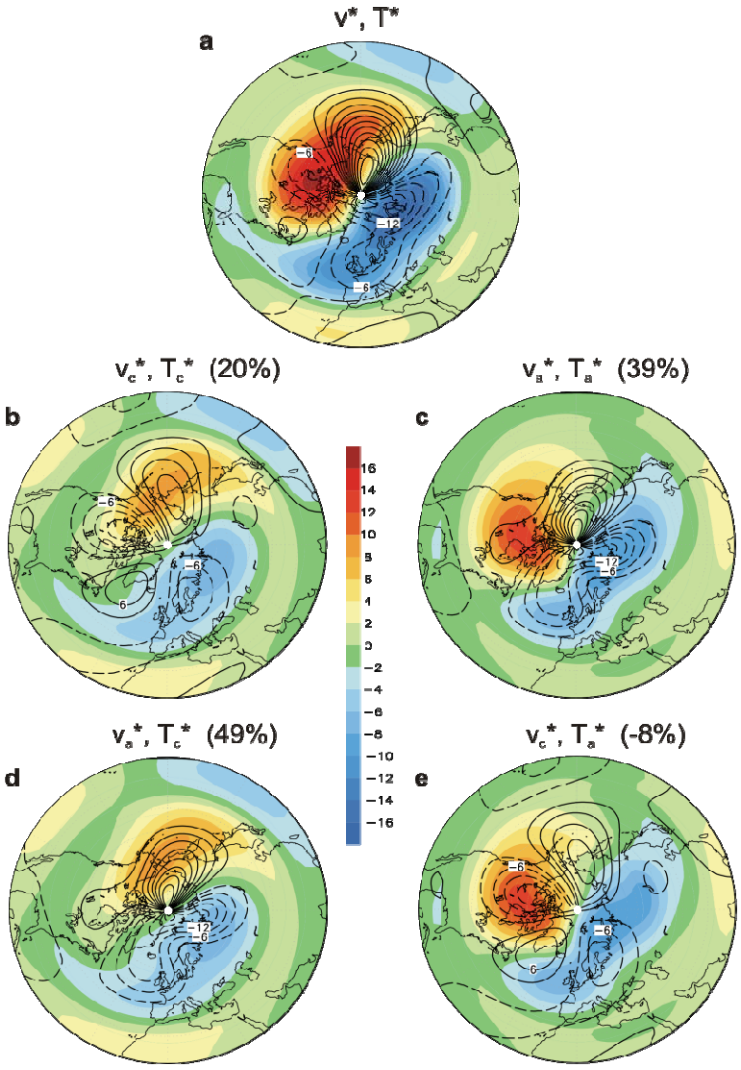

Figure V.14. Same as Figure V.11 but for 24-28 January 2010 [From Ayarzagüena et al. [2011]].

The clear predominance of zonal wavenumber-1 wave activity in the 2010 MSW is consistent with previous results from Shiogama and Mukougawa [2005], who concluded that an amplification of stationary stratospheric wavenumber-1 waves is important for the onset of MSWs during ENSO warm events. In fact, a link between the 2009/10 El Niño event and the 2010 MSW is further supported by our analyses.

ENSO events are known to be able to generate extratropical teleconnections, with El Niño exciting the positive phase of the Pacific-North American (PNA) pattern [e.g., Garfinkel and Hartmann, 2008]. Figure V.15a resembles a clear positive PNA pattern for January 2010 with negative anomalies in the 500-hPa geopotential height field over the northern Pacific and southeastern North America, and positive anomalies over Canada, resulting in a positive PNA index of 1.25 (http://www.cpc.ncep.noaa.gov/data/teledoc/telecontents.shtml). As shown by Itoh and Harada [2003], Taguchi and Hartmann [2006] and Garfinkel and Hartmann [2008], this is equivalent to an enhancement of the mid- to high latitude tropospheric geopotential

height wavenumber-1 which then propagates into the stratosphere leading to a weakening of the polar vortex and MSWs. Similarly, the 2010 MSW was associated with an enhanced amplitude of the geopotential height wavenumber-1 in January at mid- to high latitudes (Figure V.15b), in very good agreement with the model results of Taguchi and Hartmann [2006], shown in their Figure 7b. Hence based on these results, a contribution of the 2009/10 El Niño event to the enhanced tropospheric forcing and the MSW in January 2010 seems probable. This is supported by Figure V.16 that shows the evolution of each term of equation IV.2.2 associated with composite anomalies with respect to El Niño or La Niña events from December to February. When comparing both plots, a clear and statistically significant enhancement of the interaction terms of eddy heat flux, in particular $[v_a^* T_c^*]$, by the end of January is observed under El Niño conditions, which is also coincident in time with the peak of heat flux related to the 2010 MSW. Moreover, the synoptic evolution of the lower stratospheric circulation in this winter is similar to that found by van Loon and Labitzke [1987] following the El Niño phenomenon (not shown). Finally, the analysis of the EP flux divergence at stratospheric levels also confirms the high relevance of the amplification of stationary waves for the occurrence of the 2010 MSW, very likely related to the El Niño event. Figure V.10d shows that an outstanding negative peak in the 30-hPa divEP_{60N} occurs at the same time as the amplification of the upward wave propagation prior to the 2010 MSW. This negative divEP_{60N} is dominated by the interaction between the anomalies associated with Rossby wave-packets and the climatological planetary waves. It is thus the main contributor decelerating the polar stratospheric flow. Although the anomalies associated with Rossby wave packets are an additional important contributor to the peak of $[v^* T^*]$ at 100 hPa prior to the 2010 MSW, the Rossby wave packets identified in the troposphere have only a slight influence on the lower stratosphere circulation in this case, as seen before.

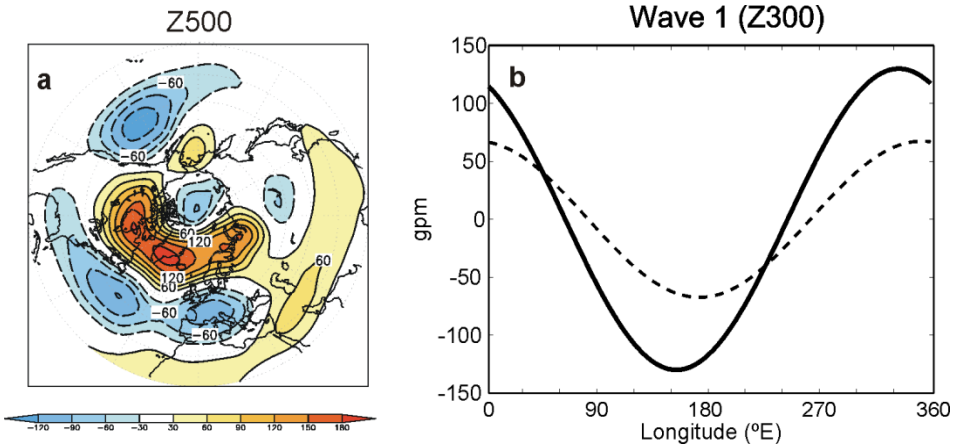

Figure V.15. a) 500-hPa geopotential height anomalies for January 2010 (contour interval: 30 gpm). **b)** 300-hPa geopotential height wavenumber-1 (gpm) averaged over 50°N-80°N as function of longitude for January 2010 (solid line) and the climatology of January (dashed line). [Adapted from Ayarzagüena et al. [2011]]

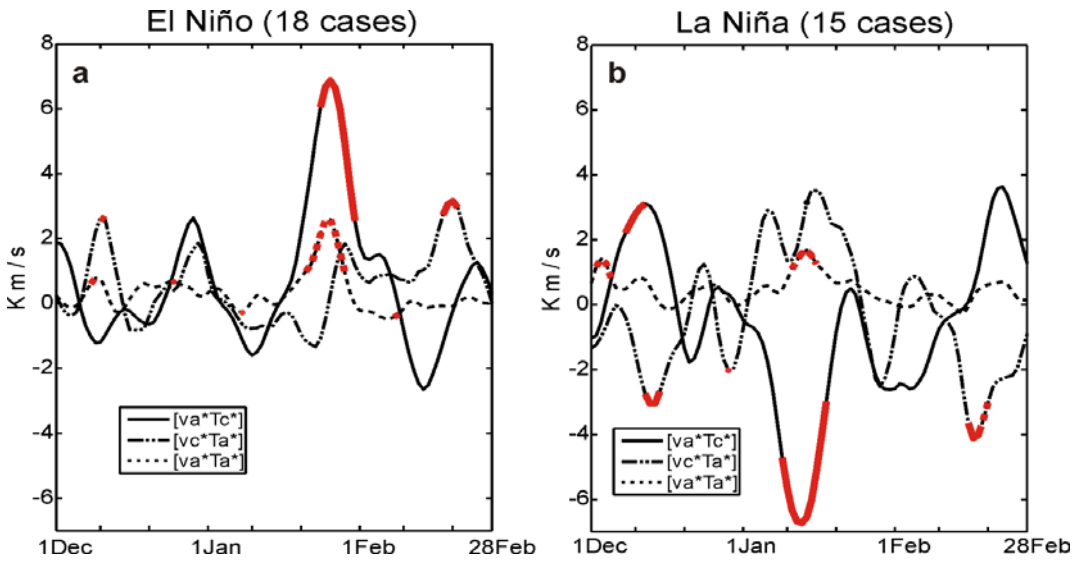

Figure V.16. Time evolution of contributing terms to zonal-mean eddy heat flux averaged over 50°N-80°N (K m s^{-1}) at 100 hPa associated with composite anomalies with respect to El Niño and La Niña winters for the period 1957/58-2009/10. Red lines indicate statistically significant values of each term at a 95% confidence level from a one-tailed Monte Carlo test using 500 permutations (i.e.: those values with an absolute value exceeding the 95-percentil of the pdf generated from 500 random permutations) [From Ayarzagüena et al. [2011]].

iii. Tropospheric changes after each MSW

Another aspect worthy of analysis in 2009 and 2010 MSW is the possible changes in the tropospheric circulation following these events and related to the downward propagation of their signal.

Figure V.17 shows the anomalies of 1000-hPa geopotential height (Z) and temperature (T) averaged over 0-60 days after the onset of each MSW. In the case of the 2010 MSW, the Z and T patterns are analogous to the averaged near-surface response to MSWs described in the previous section for ERA-40 (Section V.1.a; compare Figure V.5 d and h with Figure V.17b and d). The NAO signature is clearly identified in the Z pattern, showing positive anomalies at high latitudes and negative anomalies at mid-latitudes centered over the eastern Pacific and more intense over the Atlantic (Figure V.17b). This pattern agrees well with the composite map of 1000-hPa Z anomalies found by Charlton and Polvani [2007] for vortex displacement MSWs in the NCEP/NCAR reanalysis, except for the center of negative anomalies over the eastern Pacific that is not present in their plot. However, this center can be understood as a fingerprint of the influence of the El Niño event, as it is related to the above mentioned intensification of the Aleutian low. In addition, Figure V.17b shows a very similar pattern to the surface climate response to El Niño identified by Ineson and Scaife [2009] for years with MSWs.

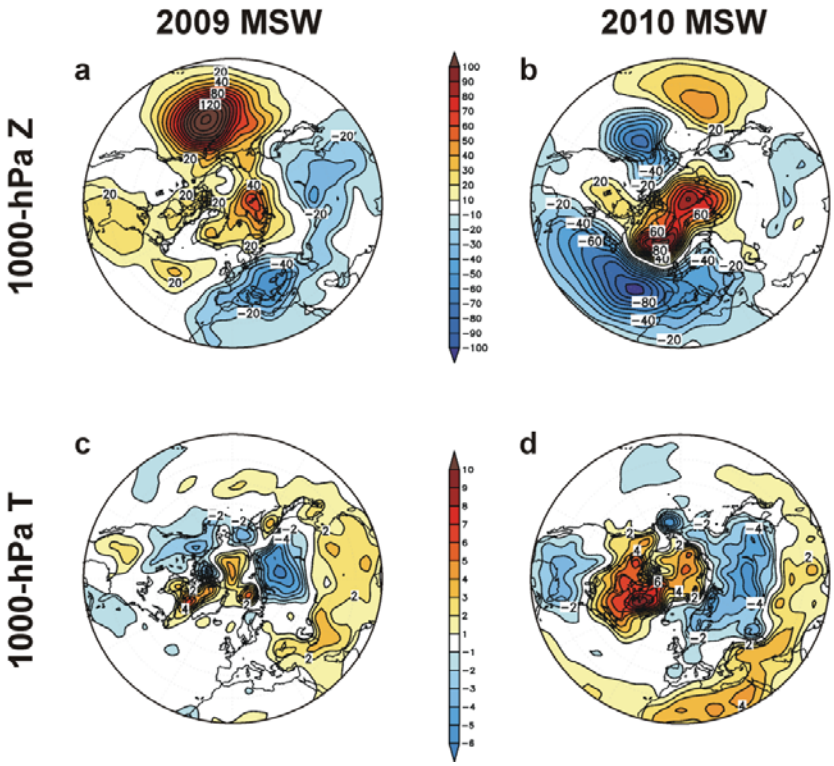

Figure V.17. Composite anomalies of 1000-hPa geopotential height (upper panel, contour interval: 10 gpm) and temperature (lower panel, contour interval: 1 K) averaged over 0-60 days following the onset of the 2009 MSW (**left**) and 2010 MSW (**right**).

In the case of the 2009 MSW, given that it was a very strong event, it should be expected to observe a tropospheric response characterized by a very strong negative phase of the NAO, but it was not so (Figure V.17a). The 1000-hPa Z anomaly structure after the 2009 MSW is determined by weak negative anomalies over Europe and positive anomalies over northern Siberia, the east coast of North America and the central Pacific, the latter being the strongest center (Figure V.17a). In this structure, no well-known teleconnection pattern is clearly identified and so, the observed one can be a result of a combination of different processes. For instance, the strong anomalies over the Pacific can be related to two different phenomena. One of them could be a tropospheric blocking, in agreement with Woollings et al. [2010] that showed an increased number of blockings in this region after splitting type MSWs. A second phenomenon that would explain the center of anomalies over the Pacific might be a weak La Niña event and its associated negative phase of the PNA. Consistent with the 1000-hPa geopotential results, the near-surface temperature pattern is also different from that of 2010 MSW (Figure V.17c vs d).

As a further analysis of the absence of a clear MSW fingerprint on the troposphere in 2009, the time-height evolution of the zonal-mean zonal wind at 60°N around both MSWs has been plotted. The plots in Figure V.18 show that while the anomalies associated with the 2010 MSW extend to the surface, those related to the 2009 MSW are restricted to the stratosphere and they do not reach tropospheric levels (Figure V.18b).

According to these results, the signal of the 2009 MSW does not propagate downwards in the usual way, consistent with results of Figure V.17.a and Newman and Nash [2009]. Thus, in this case, it seems that tropospheric processes play a more important role than the MSW in perturbing the near-surface conditions.

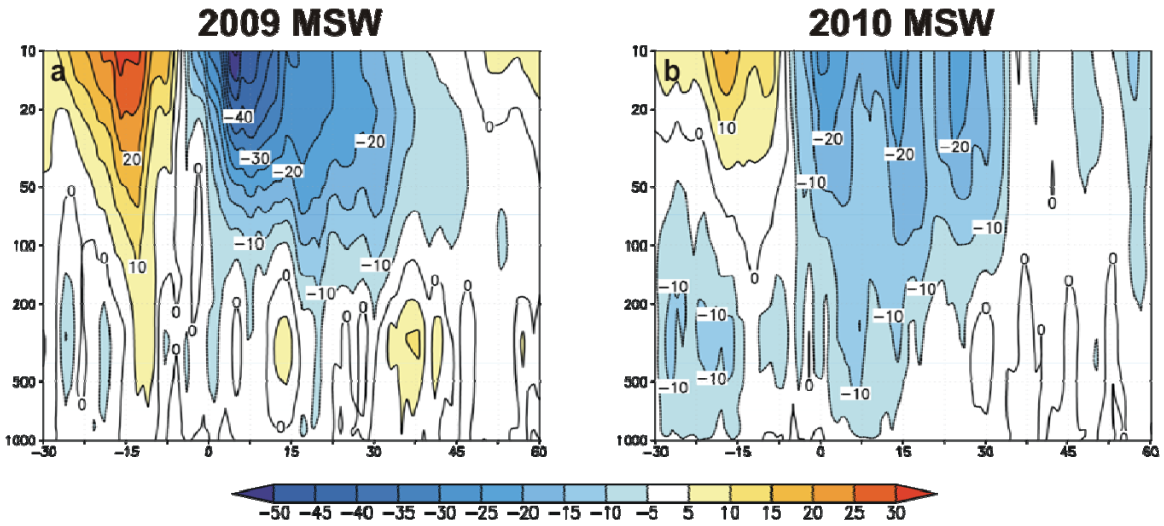

Figure V.18. Time-height evolution of zonal-mean zonal wind anomalies at 60°N for the 2009 MSW **(left)** and 2010 MSW **(right)**. The x-axis labels indicate the lag in days referred to the onset of the event. Contour and shading interval: 5 m s^{-1}.

Final remarks

In short, in this part of the study, it has been shown that polar stratospheric circulation anomalies associated with certain combinations of phases of the solar cycle, the QBO and the ENSO may facilitate or hinder the vertical propagation of planetary waves into the stratosphere. This was the case for the 2010 MSW that happened under minimum solar activity, an easterly QBO phase and with a clear influence of the El Niño event of 2009/10 winter. However, the occurrence of the 2009 MSW clearly demonstrated that a strong enough forcing from tropospheric planetary waves is able to generate a MSW, even if an exceptionally intense stratospheric polar vortex preceded the event (as in early January 2009) and there was an unfavorable configuration of the typical external factors that influence the occurrence of these phenomena.

Results from this comparative study between the 2009 and 2010 MSWs give further evidence of the important role of tropospheric wave forcing for the generation of MSWs in NH winters beyond other influences like solar cycle, QBO and ENSO, when these influences do not play any relevant role. Consequently, this relevant role of tropospheric waves in the generation of MSWs should be taken into account in the study of future MSWs as it might be that the tropospheric wave forcing would enhance in the future due to increased greenhouse gas concentrations, regardless of the solar and QBO phases. The latter might, in turn, result in a break-down of the well established correlations between MSWs and the solar/QBO forcing.

2. Possible future changes in Major Stratospheric Warmings

The study of effects of increasing GHG concentrations in the future on climate are currently a topic of special interest in climate research. This is due to the possible dramatic consequences to the whole climate system. Thus, this Section is focused on the study of the possible impact of a prescribed climate change on MSWs.

Several recent studies have already reported the existence of a possible relationship between changes in atmospheric constituents and changes in the dynamics of the stratosphere [McLandress and Shepherd, 2009a and b; Winter and Bourqui, 2010]. Hence, an analysis of the possible impact of climate change on major stratospheric warmings (MSWs) is highly important. In fact, some authors have already examined a possible impact of climate change on MSWs by analyzing GCMs [e.g.: Shindell et al., 1998; Butchart et al., 2000], AOGCMs [e. g.: Huebener et al., 2007] and more recently, CCMs [Charlton-Perez et al., 2008; McLandress and Shepherd, 2009b; Butchart et al., 2010], mainly focusing on the frequency and intensity of these events. However, whereas some of them have predicted a small increase in MSWs frequency [e.g.: Huebener et al., 2007; Charlton-Perez et al., 2008; Butchart et al., 2010], others have identified no change [e.g: Butchart et al., 2000; McLandress and Shepherd, 2009b] and some others have even projected a reduced frequency [Shindell et al., 1998]. Since a clear consensus in the effects of the climate change on the MSWs has not been reached yet, more work about this topic is still demanded.

In this Section V.2, possible future changes in MSWs are examined with the EMAC model using the EMAC-FUB configuration in two transient simulations, SCN-B2d and SCN-B2c (hereafter referred as SCN2d and NCC, respectively; see Section III.2 for more details). Both simulations are identical, except that GHG concentrations are kept constant at levels corresponding to the year 1960 in NCC run, but they increase following the A1B scenario in the case of SCN2d. In this study, two different comparative studies are presented from the output of both runs:

- a comparison of the MSWs in the first 40 winters (1960/61-1999/2000, hereafter denoted *past*) with those of the last 40 ones (2060/61-2099/2100, hereafter *future*) in each experiment, and

- a comparison of the MSWs between the two experiments for the same period (*past* or *future*).

In a preliminary step, changes in the wintertime boreal climatology are evaluated in the *past* and the *future* periods in order to understand the variations found in MSWs.

a. Changes in the boreal wintertime basic state

Changes in the wintertime basic state between past and future are analyzed in both transient SCN2d and NCC simulations to find a connection between the possible future changes identified in MSWs and the variations in the atmospheric state. Two specific aspects are analyzed: the atmospheric state in the middle stratosphere and the wave activity propagation. The first one was chosen given that MSWs are typically identified in that region, in particular at 10hPa. Additionally, the wave activity propagation is really interesting in this study because it has been clearly demonstrated in the extensive literature that a sudden increase in planetary wave activity initiates a MSW [e.g., Charney and Drazin, 1961; Matsuno, 1971; McIntyre, 1982; Limpasuvan et al., 2004; Black and McDaniel, 2007]. The statistical significance in the changes found has been established by using a Student's t-test.

i. Middle stratosphere (10 hPa)

Possible changes in the basic state of the middle stratosphere are explored. The focus is made on the daily evolution of the zonal-mean temperature and zonal wind from November until March to determine possible variations in the seasonal cycle of the boreal stratosphere and in the main features of the development and latitudinal extent of the polar night jet (PNJ). The basic state is defined here as the 40-year daily means of each period of study.

Daily zonal-mean temperature

The polar stratosphere becomes, in general, significantly colder in the *SCN2d* experiment in the future (Figures V.19a-c). However, this cooling is not clear from late-January to late-February. In fact, while a statistically significant cooling is identified in the stratosphere in November and December (Figure V.20a), a slight and not significant warming is observed in the polar stratosphere in January and February (Figure V.20c). The last result agrees well with Figure 2a of Sigmond et al. [2004], where they plot the zonally averaged temperature difference between a uniformly doubled CO_2 run and a control run for December, January and February. This warming is also observed in a similar study by Winter and Bourqui [2010]. Moreover, as a result of this high-latitude warming, the meridional temperature gradient decreases and it results in a possible weakening of the polar vortex based on the thermal wind relationship (as seen below).

As expected, relevant changes in time are not found in the stratospheric temperature under non-climate change conditions (Figures V.19d-f and V.20b and d).

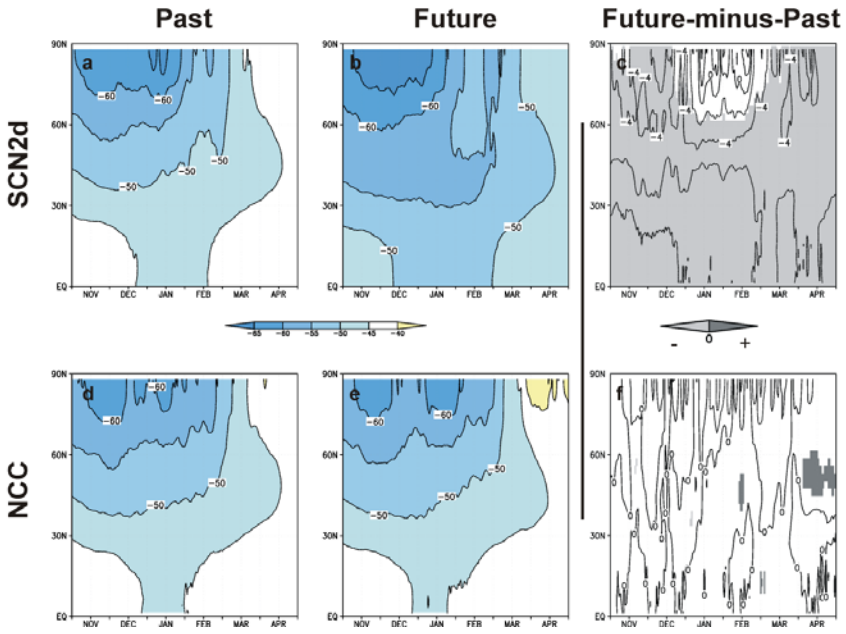

Figure V.19. Zonal-mean temperature climatology at 10 hPa in the Northern Hemisphere for the SCN2d run and for the NCC run: in the past (**left** column), in the future (**central** column) and future-minus-past difference (**right** column). Contour interval: 5K (a, b, d and e) and 2K (c and f). Shadings in c and f show statistically significant values at a 95% confidence level (Student's t-test).

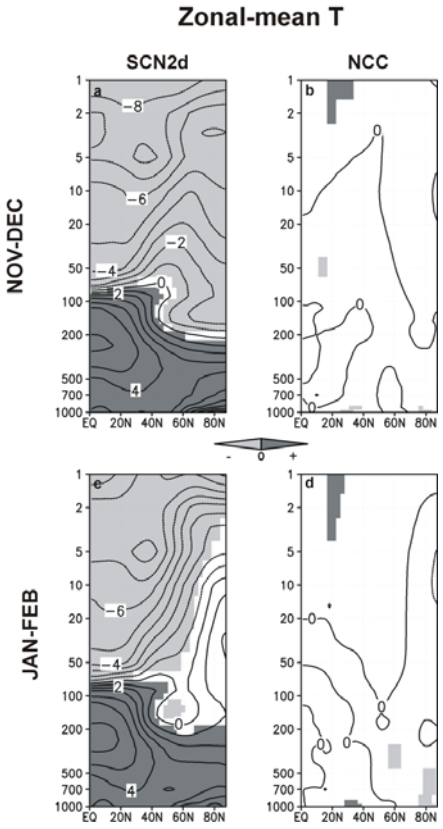

Figure V.20. Future-minus-past difference of zonal-mean temperature climatology in the SCN2d and NCC runs for November-December (**upper panel**) and for January-February (**bottom panel**). Shadings correspond to statistically significant values at a 95% confidence level (Student's t-test). Contour interval: 1 K.

Daily zonal-mean zonal wind

The zonal-mean zonal wind jet shows spatial and temporal changes in the future comparing with the past in the *SCN2d* experiment (Figures V.21 a-c). It is shifted equatorward in agreement with previous studies [e.g.: Sigmond et al., 2004 or Charlton-Perez et al., 2008] and consistent with the change in the meridional temperature gradients (Figure V.19 a-c). Moreover, a strengthening of the PNJ is observed in early winter (particularly in December) and a weakening is seen from mid-January (Figures V.21 a and b). These changes in the intensity of the PNJ are statistically significant at a 95% confidence level from a Student's t-test (Figure V.21c) and can be also seen in the cross section of differences of zonal-mean zonal wind for November-December and January-February (Figure V.22 a and c, respectively). Figure V.22c also shows good agreement with the results of Sigmond et al. [2004] for a uniform CO_2 doubling.

Concerning the *NCC* experiment, the PNJ does not show almost any change in its spatial extension (Figures V.21 d-e). Although for the last period the PNJ becomes slightly weaker in early winter and stronger from mid-January till March, these changes are not statistically significant at a 95% confidence level (Figures V.21f and V.22 b and d). These non-statistically significant changes can be possibly explained by the high internal variability of the polar stratospheric flow in winter [Erlebach et al., 1996; Butchart et al., 2000], given that the model is able to reproduce some typical features of this variability in both simulations such as the clustering of MSWs in some decades (not shown).

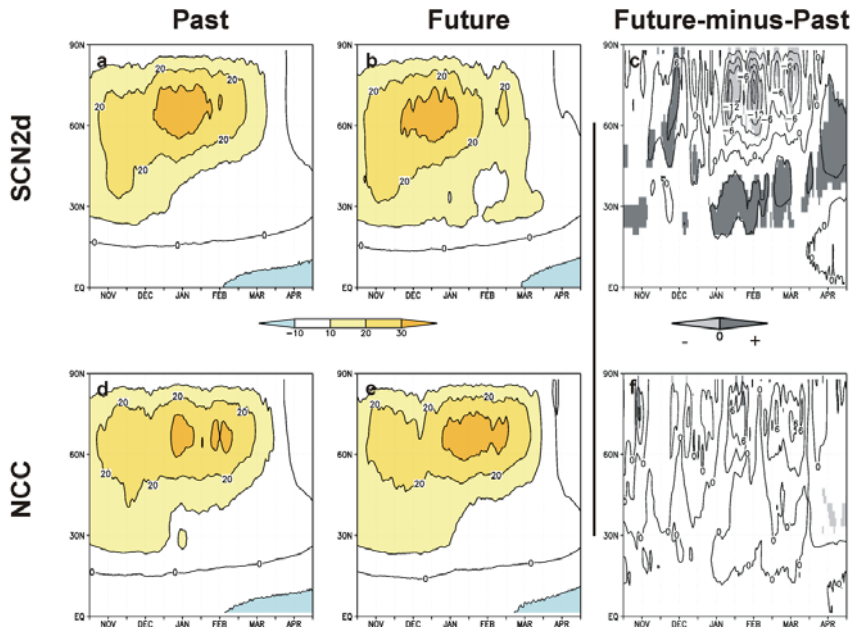

Figure V.21. As Figure V.19 but for the 10-hPa zonal-mean zonal wind. Contour interval: 10 m s^{-1} (a, b, d and e) and 3 m s^{-1} (c, f).

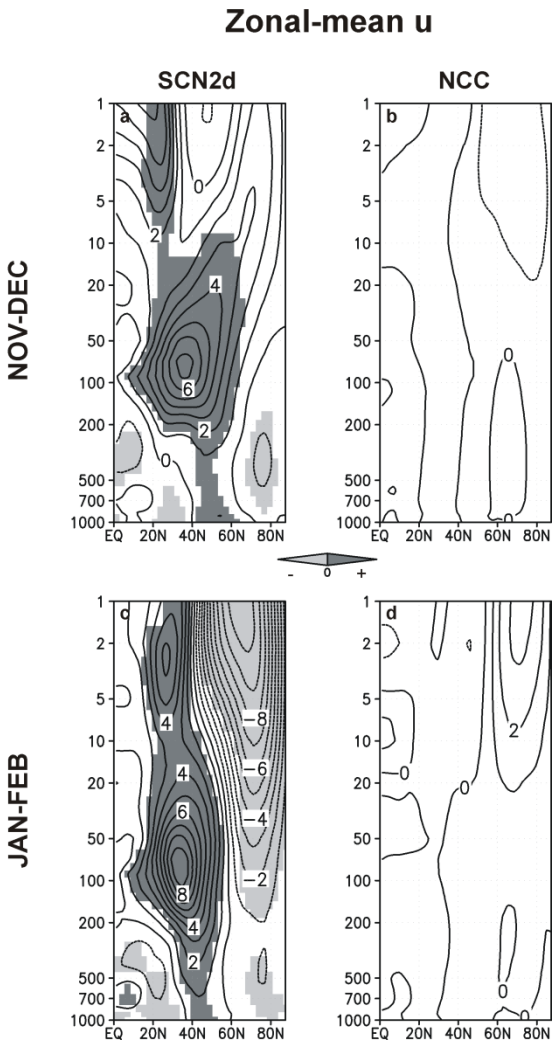

Figure V.22. As Figure V.20 but for zonal-mean zonal wind. Contour interval: 1 m s^{-1}.

ii. Wave activity propagation

Because of the causal relationship between the occurrence of MSWs and the planetary wave propagation, a special attention deserves the variations in the climatology of the latter. The different expressions to evaluate the wave activity propagation were described in the *Methodology* chapter (Section IV.2.a).

Daily meridional eddy heat flux at 100 hPa

The daily climatology of the meridional eddy heat flux at 100 hPa in the extended winter has been analyzed for each period and simulation, as it is known that this variable represents a proxy for Rossby wave flux entering the stratosphere [Austin et al., 2003; Hu and Tung, 2003]. As explained in the *Methodology* chapter, the eddy heat flux is computed as [v^*T^*], i.e., the zonal average of the product of the deviation of the meridional wind and the temperature respect to their zonal mean values. Note that v

and *T* have been smoothed by a 5-day running mean in order to get a clearer drawing of the seasonal evolution of the heat flux. However, some oscillations of higher period can be identified in the evolution of meridional eddy heat flux such as the *16-day component* [Hirooka and Hirota, 1985].

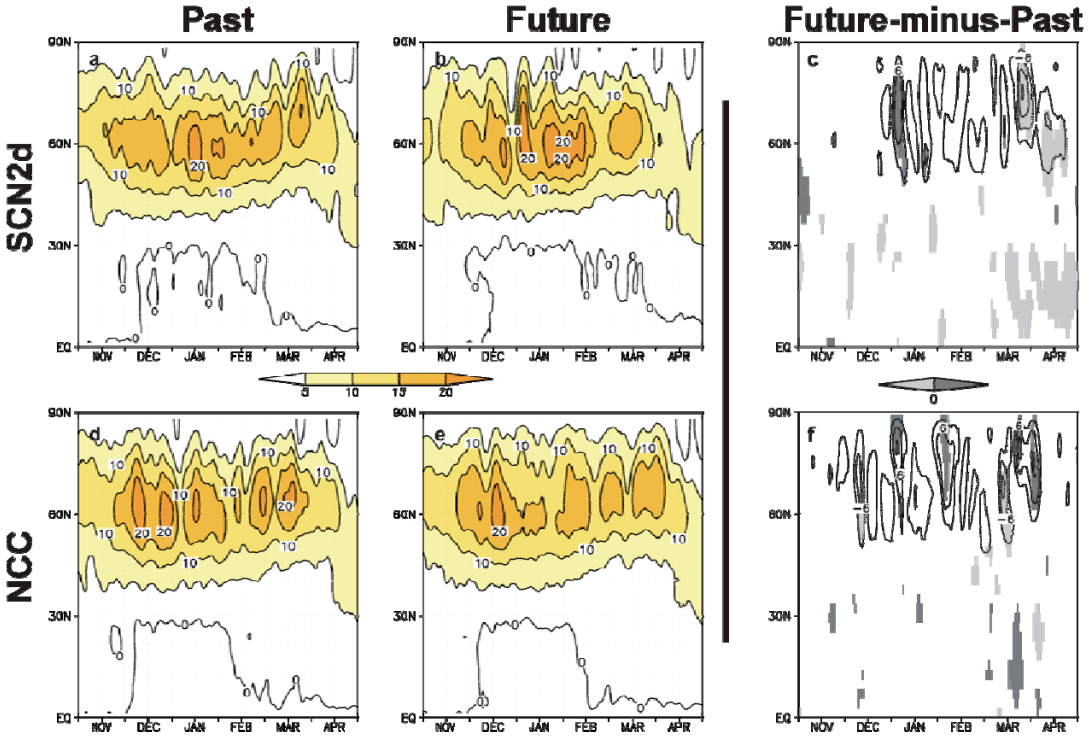

Figure V.23. As Figure V.19 but for the meridional eddy heat flux at 100 hPa. Contour interval: 5 K·m·s^{-1} (a, b, d and e) and 3 K·m·s^{-1} (c, f).

In the *SCN2d* run, while no important changes in [*v*T**] between the future and the past are found concerning the latitudinal extent of the highest values, a time shift of about one month is observed in the maximum, i.e, from mid-January until March in the past to mid-December until mid-February in the future (Figure V.23 a-c). In consequence, an increase in the 100-hPa heat flux at 50°-70°N is observed from January until mid-February in the late 21st century (Figure V.23a and b), but it is only statistically significant at the beginning of January (Figure V.23c). These results are also in good agreement with other studies such as that by Winter and Bourqui [2010] that evaluates the change in the wave forcing of the stratosphere but, in that case, under doubled-CO_2 conditions.

The stronger future wave activity observed in January is consistent with the weakening of climatological polar night jet that extends from mid-January till March previously mentioned. The delay between the statistically significant changes in the 100-hPa heat flux and 10-hPa zonal wind is explained by the fact that the former has been proven to be a precursor of changes in zonal wind at stratospheric levels. In late winter (from mid-March until April), a statistically significant decrease in the future heat flux is observed, which is also in good agreement with the polar vortex recovery in the aftermath of the high number of future MSWs in February (as shown in next pages).

In the case of the *NCC* experiment, a decrease in the future wave activity is identified in mid-winter, which agrees well with higher values in the zonal-mean zonal wind in the future (see Figure V.23d vs Figure V.23e). Moreover, small statistically significant differences in the heat flux between the future and past are also observed. However, they are localized in the 80°-90°N band (Figures V.23f), out of the area of the high wave activity propagation from the troposphere to the stratosphere [Hu and Tung, 2003].

Monthly climatology of daily Eliassen-Palm flux

Changes in the 2-D wave activity propagation are analyzed by means of the monthly climatologies of daily Eliassen-Palm flux (EP-flux). For brevity, only the statistically significant differences between the two runs for each period and those between the two periods for each run are shown in this Section.

In the case of the *NCC* run, no important changes have been found between the two periods of study, as expected.

Concerning the *SCN2d* experiment, in early winter (November and December) the wave activity at tropospheric high latitudes in the future is statistically significantly stronger than in the past (Figures V.24a and e). However, this anomalous wave activity is deflected towards the equator at the upper troposphere and so it does not enter into the stratosphere, in agreement with Figure V.23.b. This is also consistent with a stronger polar vortex in these two months (Figure V.21c) that would favor the reflection of tropospheric wave activity towards the subtropics [Perlwitz and Harnik, 2003; Kodera et al., 2008]. This equatorward deflection of wave activity has been recently shown to be more typical in early winter than in the next stages of the winter season [Shaw et al., 2010]. In contrast, in January, the increase in the future upward tropospheric wave activity at mid-latitudes does propagate into the stratosphere, decelerating the polar night jet (Figures V.25a), in agreement with results shown by McLandress and Shepherd [2009a] in transient simulations from the Canadian Middle Atmosphere CCM. In February, significant differences are not observed in the stratosphere (Figure V.25e), as expected from results obtained for the meridional 100-hPa eddy heat flux.

When comparing SCN2d and NCC runs for the future, results are similar to those found in the comparison between the two periods of SCN2d, particularly in the troposphere (Figures V.24-25, d and h plots). This is understandable, given that GHG concentrations are kept constant at 1960 levels in the NCC run. In the stratosphere, the statistically significant differences are more extensive in this case than in the comparison between the two periods of SCN2d. A possible explanation for this could be the differences in the SSTs between the SCN2d and NCC runs, i.e. interannually varying ones in the first case and with a fixed annual cycle in the second. Bearing in mind that important interannual variability SST phenomena, such as El Niño, are associated with variations in the intensity of planetary waves [e.g.: Taguchi and Hartmann, 2006;

Manzini et al., 2006], the absence of this variability in one of the two compared runs would enhance the features of the wave activity propagation in the other run when compared both of them. This explanation is supported by previous studies that showed lower climate change response in experiments using prescribed SSTs with a fixed annual cycle than in simulations forced with interannually varying SSTs [Braesicke and Pyle, 2004; Winter and Bourqui, 2010].

The same argument can be applied for the statistically significant differences found between both experiments in the past (Figures V.24-25, b and f plots). However, they are not very extensive.

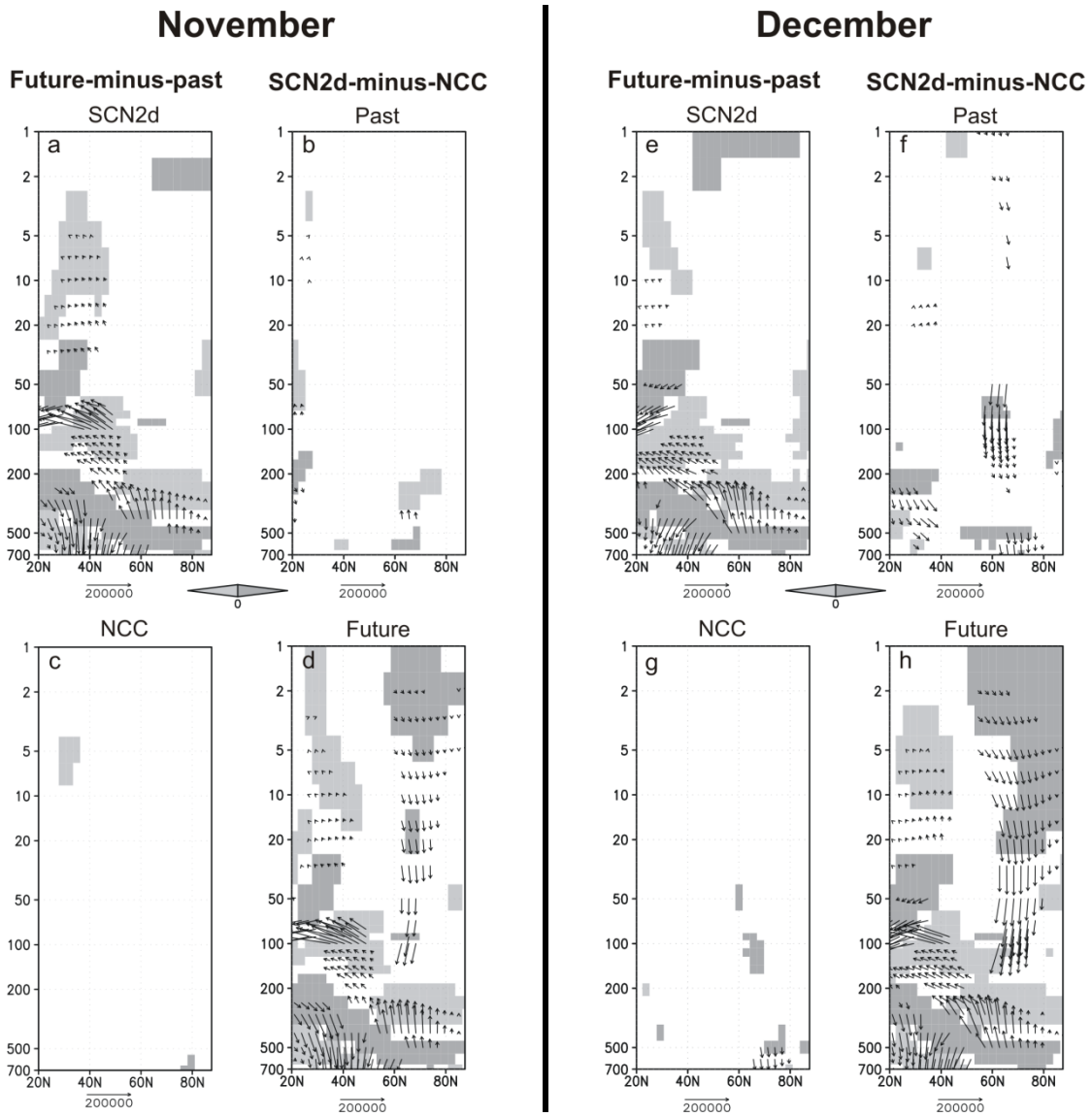

Figure V.24. Difference composite maps of monthly Eliassen-Palm flux (arrows) and its divergence (shadings) for November and December. Scaling arrow at 100 hPa and higher is divided by a factor of 10 so that EP flux may be easily seen. Arrows are drawn when the vertical component of the EP flux is statistically significant at a 95% confidence level. Shadings indicate statistically significant differences of EP flux divergence at 95%. (Student's t-test is used to establish the statistical significance).

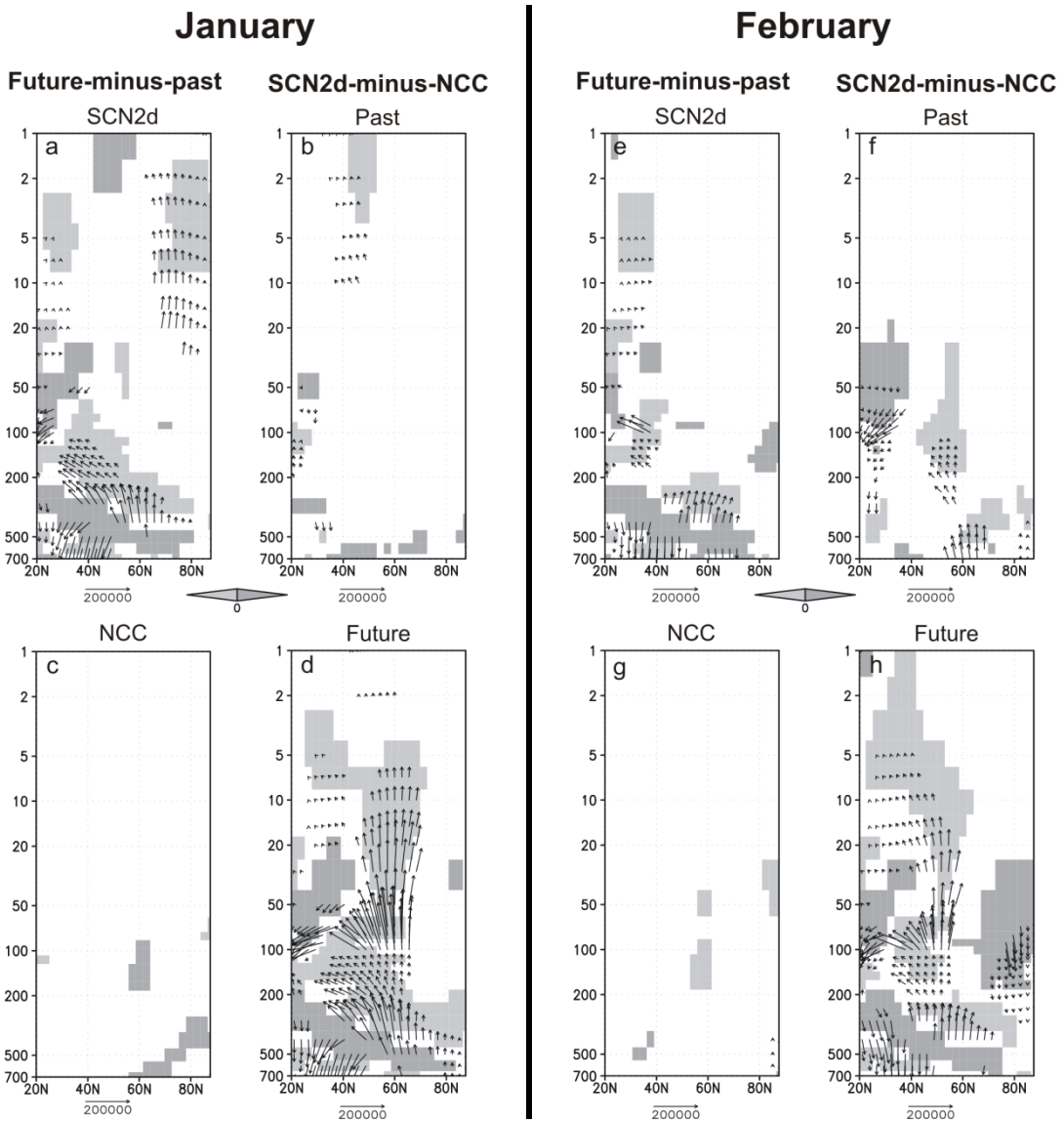

Figure V.25. As Figure V.24 but for January and February.

Monthly climatology of daily Plumb flux

The last step in the analysis of changes in the climatological wave activity is the study of its 3-D propagation by means of the Plumb flux at the upper troposphere (in particular, at 300 hPa). As explained in the *Methodology* chapter, this would allow us to determine the sources of the future changes found in the zonally averaged wave propagation under climate change conditions (more details in Section IV.2.a).

In November, a general decrease with time in intensity of the climatological wavetrains over western Pacific and Asia is observed in the SCN2d run (Figures V.26a). The other important wavetrain, the one over western Atlantic, shows a northeastward shift. In December, both wavetrains, in particular the Atlantic one, present a northeastward shift in the future with respect to their position in the past (Figure

V.26b). A shift of the same sign of the Atlantic wavetrain was found by McDaniel and Black [2005] associated with a positive NAM phase, and thus, with a strong polar vortex. Hence, the change in the position of the Atlantic wavetrain would agree with a strengthening of the polar vortex in the future in early winter and might also explain the changes observed in the zonally averaged wave propagation in these two months. In January, an increase with time in the upward wave propagation in the SCN2d run is clearly seen over the Pacific-Asian region (Figure V.27a). This increase seems to be the main responsible for the future stronger upward wave activity that enters into the stratosphere. In February, as observed in the 2-D wave activity propagation, significant differences are not observed in the Plumb flux

Similar results are found when comparing the two runs, SCN2d and NCC, in the future (Figure V.26-27, d and h plots).

Finally, it is worthy to highlight the relevant differences found when comparing the two runs in the past (Figures V.26-27, b and f plots). These differences are almost restricted to the Pacific and they could be related to discrepancies in SSTs between both runs just mentioned, when analyzing the differences in the EP flux.

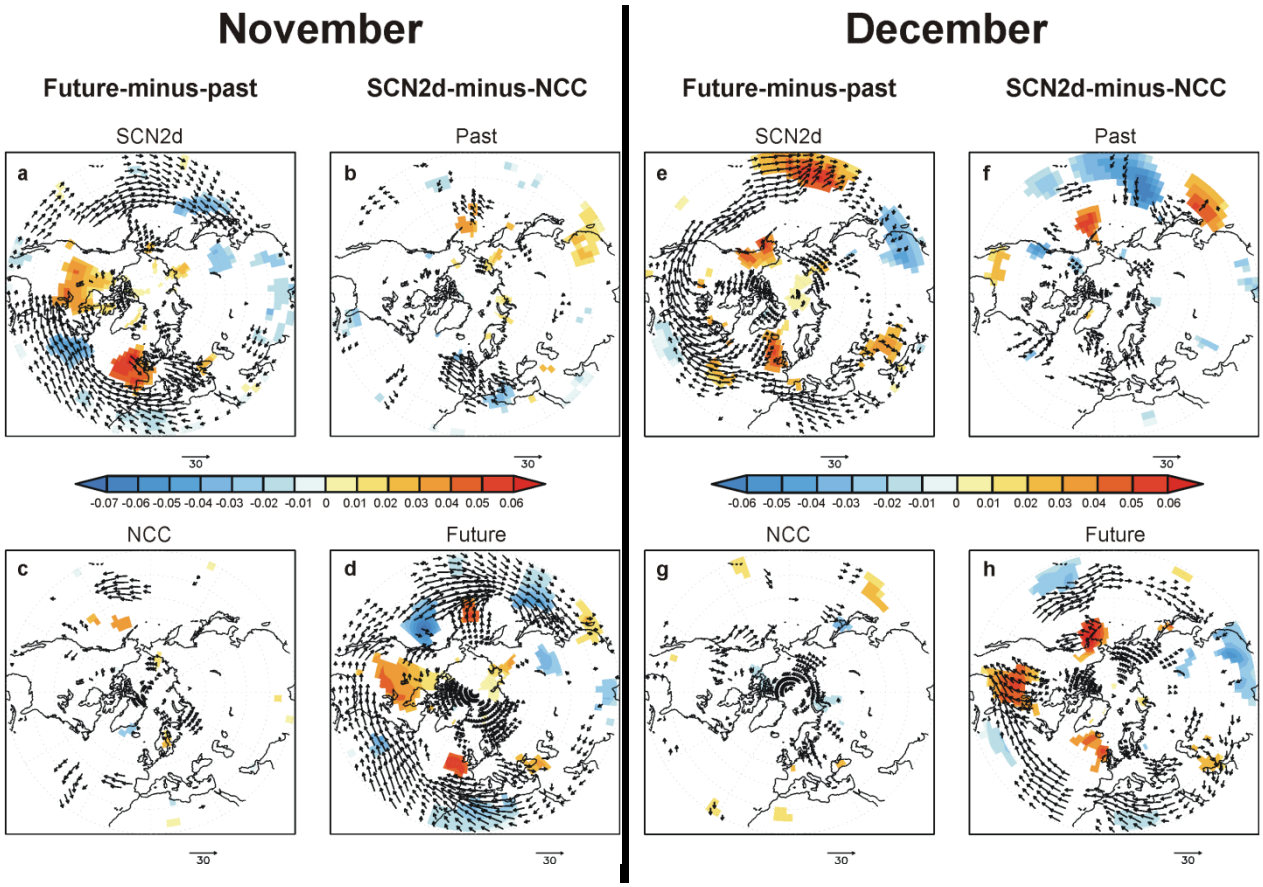

Figure V.26. Difference composite maps of monthly 300-hPa Plumb flux (horizontal components in arrows and vertical one in shadings (m^2 s^2)) for November and December. Arrows are drawn when one of the horizontal components of Plumb flux is statistically significant at a 95% confidence level. Colour shadings indicate statistically significant differences of Plumb flux at 95%. (Student 's t-test is used to establish the statistical significance).

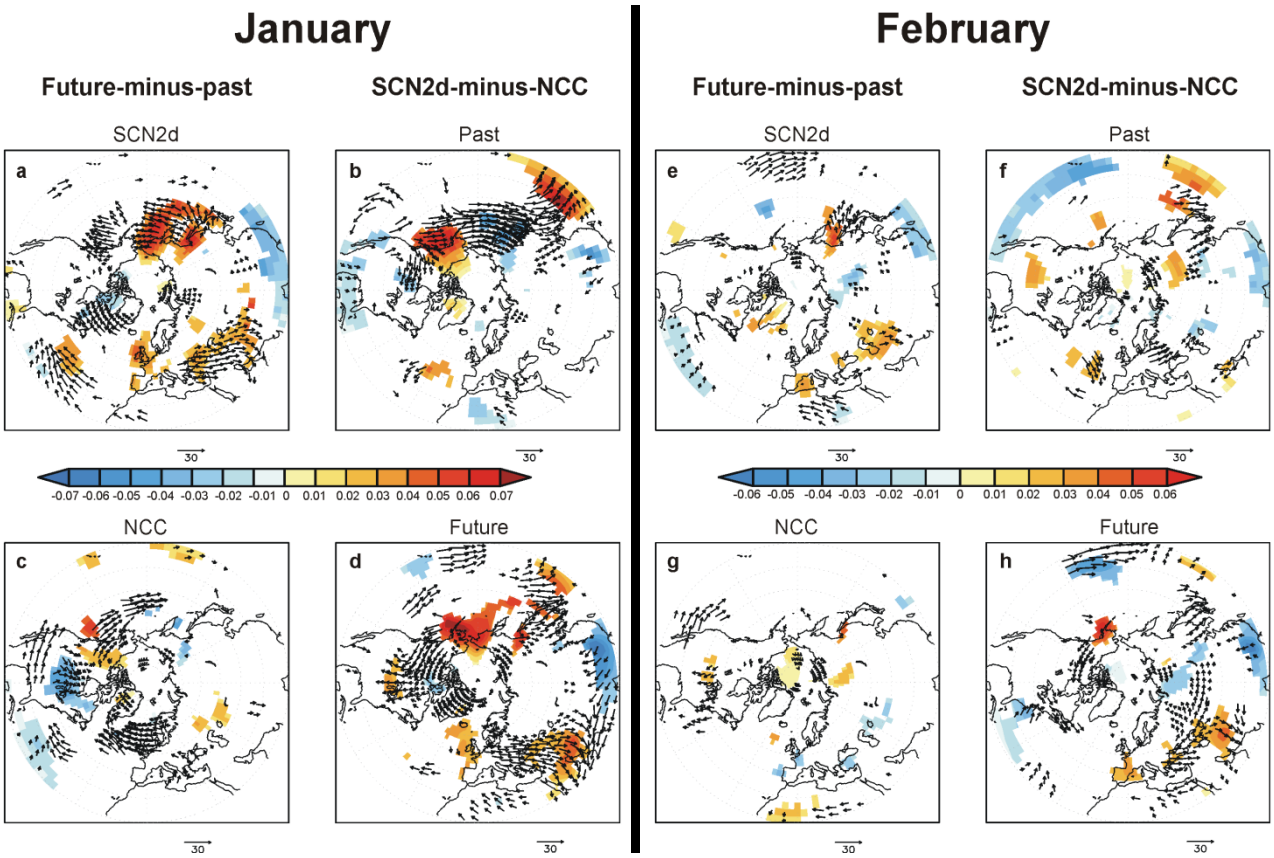

Figure V.27. As Figure V.26 but for January and February.

b. Changes in major stratospheric warmings

After having analyzed the main changes in the boreal wintertime climatology due to climate change, it has been explored if these differences are connected to changes in major stratospheric warmings. To achieve this study, major stratospheric warmings (MSWs) were identified during the extended winter (November-March) according to the "standard criterion", described in the *Methodology* chapter (more details in Section IV.1.a). As done in the previous part of this report of results, in order to determine possible changes in MSWs due to the increase of GHG concentrations in the SCN2d simulation, different aspects of these phenomena are explored in the two periods and runs with the EMAC-FUB (e.g., past and future in the SCN2d and NCC simulations). First, the main features that characterize these events and the time evolution of the atmospheric circulation during the development of MSWs are studied. Then, a special focus is made on the performance of the stratosphere-troposphere coupling during this type of events.

i. Main features

This part of the study is devoted to the analysis of important features of MSWs reproduced by the EMAC using the EMAC-FUB configuration, such as the frequency, the

seasonal distribution and some dynamical benchmarks proposed by Charlton and Polvani [2007] to assess the variations in the main characteristics of MSWs in the future. First, in order to verify if the model can realistically reproduce the MSWs, a comparison of the results from the two experiments in the past with those from ERA-40 in the same period (1960/61-1999/2000) is carried out. Then, a similar comparison is done among the different periods and experiments to account for the possible influence of the climate change on this relevant stratospheric phenomenon.

Comparison reanalysis vs model simulations (1960/61-1999/2000)

Although it has been demonstrated in Section V.1.a that the EMAC can quite realistically reproduce the main characteristics of MSWs for the recent past period, an additional verification has been made in the present Section considering the SCN2d and NCC experiments.

Table V.8 shows the values of the main characteristics of MSWs for each experiment and period versus ERA-40 dataset. Additionally, Table V.9 summarizes the pairs of cases (dataset and/or period) whose differences in the MSW diagnostics are statistically significant. From both Tables, it can be seen that MSWs in the recent past of both experiments are, in general, well reproduced, even though they show lower values than in ERA-40. An exception is, however, found in the SCN2d run related to the deceleration of the PNJ associated with the occurrence of a MSW. In that case, a statistically significant low value is obtained with respect to that of ERA-40. This difference can be at least partially explained by the extraordinarily high number of MSWs performed in this run for early winter (November and December), as will be seen next in this Section. As explained in the previous Section, the occurrence of these early winter MSWs is probably due to artificial forcings and as a result, they can show unrealistic properties. In fact, when computing the deceleration of the PNJ without considering the MSWs of these two months, the value rises up (23.2 m s^{-1} with a standard deviation of 8.5 m s^{-1}) and the resulting difference between the mean values of ERA-40 and SCN2d is not statistically significant at a 90% confidence level.

Despite the aforementioned difference, an overall agreement in the most important features of MSWs exists between both experiments (SCN2d and NCC) and the reanalysis for the past period. Hence, the analysis of possible trends and changes in the future in MSWs by using these runs can be said to be reliable, as the main mechanisms related to them seem to be well simulated.

Comparison among the different periods and model experiments

Once it has been verified that MSWs are realistically reproduced in the recent past by SCN2d and NCC simulations, future changes in their main features are explored. In

general, statistically significant differences have not been found among the different periods and runs, except for the deceleration of the PNJ (Table V.9). Moreover, the non-significant changes observed in time have the same sign for both runs and so, they cannot be attributed to the prescribed increase in GHG concentrations, but they could be explained by the large multi-decadal variability of these phenomena [Butchart et al., 2000; Schimanke et al. 2011].

Table V.8. Mean values of MSW diagnostics in the SCN2d and NCC simulations for the *past* (1960/61-1999/2000) and *future* (2060/61-2099/2100) periods and in ERA-40 data. In parenthesis, the same statistical parameter of variability as in Tables V.1 and V.3. Anomalies have been computed based on the respective climatology of each period and each simulation.

	Dataset	Past	Future
Frequency [MSWs per winter]	SCN2d	0.6 (std error: 0.1)	0.6 (std error: 0.1)
	NCC	0.7 (std error: 0.13)	0.6 (std error: 0.1)
	ERA-40	0.6 (std error: 0.1)	--------
Deceleration of PNJ [m s^{-1}]: Difference in zonal-mean zonal wind at 60°N, at 10 hPa, 15-5 days prior to the onset date minus 0-5 days after the onset date	SCN2d	21.3 (std: 7.4)	25.6 (std: 8.8)
	NCC	24.0 (std: 11.7)	20.6 (std: 9.3)
	ERA-40	29.2 (std: 11.5)	--------
Intensity of MSW [K]: Area-weighted polar cap (90°-50°N) 10-hPa mean temperature anomaly, averaged ± 5days around the onset date	SCN2d	7.7 (std: 3.9)	7.0 (std: 3.1)
	NCC	8.2 (std: 3.5)	7.5 (std: 3.1)
	ERA-40	8.6 (std:5.0)	--------
Wave activity prior to MSW [K m s^{-1}]: Area-weighted (45°-75°N) 100-hPa meridional eddy heat flux anomaly from climatology, 20-0 days before the onset date	SCN2d	7.3 (std: 5.0)	8.6 (std: 4.8)
	NCC	8.1 (std: 4.1)	9.7 (std: 4.7)
	ERA-40	9.9 (std: 5.7)	--------
10-hPa temperature and 100-hPa heat flux relation [s m^{-1}]: Regression between the anomalies of area weighted (50-90°N) polar cap temperature at 10 hPa ±5 days around the MSW onset and the area weighted (45-75°N) meridional eddy heat flux at 100 hPa	SCN2d	0.86 (std error: 0.10)	0.70 (std error: 0.07)
	NCC	0.89 (std error: 0.08)	0.66 (std error: 0.08)
	ERA-40	0.82 (std error: 0.06)	--------

Table V.9. Pairs (dataset or period) showing statistically significant differences in MSW diagnostics at a 90% confidence level.

Magnitude	Pairs (dataset/period) with statistically significant differences
Deceleration of PNJ	SCN2d past vs future
	ERA-40 vs SCN2d (past)
	SCN2d (future) vs NCC run (future)
10-hPa temperature and 100-hPa heat flux relation	NCC past vs future

As for the deceleration of the PNJ associated with MSWs, the future shows a significant higher mean value than the past in the SCN2d run. Different causes might explain this result:

1. As indicated before, the SCN2d run in the past shows a bias towards the occurrence of a high number of MSWs in early winter, when the climatology of [u] is weaker in the past than in the future (Figure V.21).

2. The easterlies at high latitudes in the aftermath of the MSW are stronger in the future, as the wave activity prior to the MSW is higher as well (but not statistically significant) and waves would deposit higher easterly momentum in the polar stratosphere.

3. In general, the basic state of the PNJ in the future may be stronger than in the past, but because of the high number of MSWs in January and February, the climatology would show weaker values. Figure V.28 indicates that this is the most valid explanation to the obtained result of the three stated causes. The deceleration of the PNJ in the future is more abrupt than in the past: it starts from a stronger value of [u] in the future, but it reaches maximum easterlies values in the days after the MSWs similar to those observed in the past.

In the following Subsection, it will be verified that the last option is the best explanation of the changes in the deceleration of the PNJ associated with MSWs due to the prescribed increasing GHG concentrations in the future.

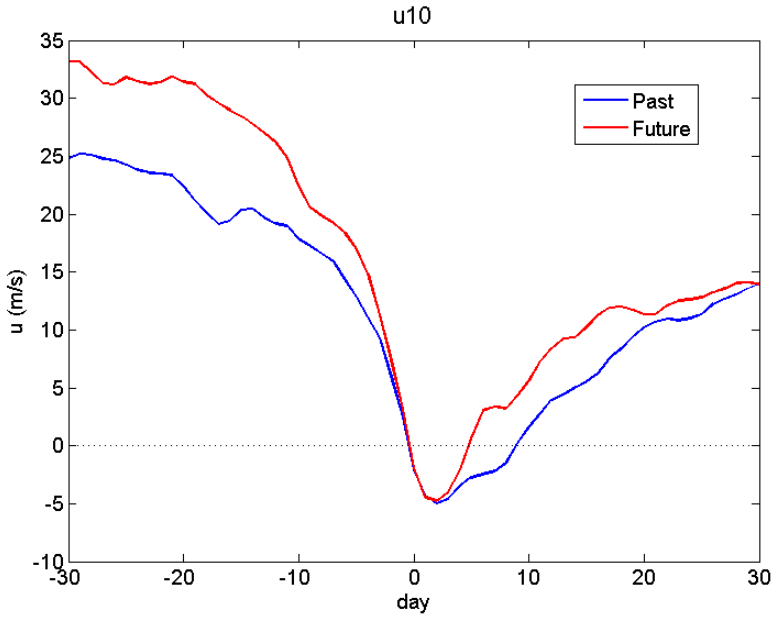

Figure V.28. Composite time evolution of 10-hPa zonal-mean zonal wind (m s^{-1}) at 60°N, surrounding the MSWs in the past (blue line) and the future (red line) for the SCN2d experiment.

When comparing the results relative to the deceleration of the PNJ in SCN2d and NCC runs in the future, a statistically significant difference between them at a 90% confidence level is also found. The explanation of this result can be the same as the proposed above.

On the other hand, no statistically significant trends in any of the magnitudes of Table V.8, averaged over 10-yr intervals, have been found from 1960 till 2100 (not shown). This result is in line with the findings of McLandress and Shepherd [2009b], although these authors identified MSWs with another criterion (one based on the Northern Annular Mode index).

Seasonal distribution

Another interesting feature of MSWs to analyze is their timing during the wintertime, which has been shown to have influence on important phenomena such as, for example, Arctic ozone depletion when associated with climate change effects [Austin and Butchart, 1994].

In the case of the *SCN2d* experiment, a decrease in MSWs in November and December and an increase in January and February are observed in the future (Figure V.29, left). A statistical χ^2 test has been carried out in order to determine if this change was statistically significant. The null hypothesis (H_0) is the independence between the period

of time (past and future) and the seasonal distribution of MSW (early winter and mid-winter) (Table V.10). MSWs that take place in March have not been taken into account in this calculation to avoid identifying any possible stratospheric final warming (SFW) in this month as a MSW. The result of this test indicates that the H_0 can be rejected at a 95% confidence level. Thus, the different seasonal distribution of MSWs above indicated between past and future in SCN2d simulation can be said to be statistically significant (at a 95% confidence level). More details about the statistical χ^2 test is described in the *Methodology* chapter (Section IV.4.b)

This change in the seasonality of MSWs is consistent with the differences found in the climatology of zonal-mean zonal wind between the past and the future in this run. It is also in agreement with the changes in time observed in the meridional heat flux.

Table V.10. Number of MSWs in early and mid-winter in each period of study (*past* and *future*) in the SCN2d run.

	Early winter (Nov-Dec)	**Mid-winter (Jan-Feb)**	**Total**
Past	9	11	20
Future	3	17	20
Total	12	28	40

Concerning the *NCC* experiment, future changes in the seasonal distribution of MSWs are also observed in this simulation. They consist of an increase in MSW in early winter (Nov-Dec) and a decrease from January until March (Figure V.29, right), which are the opposite of those seen in SCN2d experiment. These differences in the seasonal distribution are also consistent with the changes in the climatology of the zonal-mean zonal wind between the late 20th and the late 21st century. However, they are not statistically significant according to the χ^2 test of independence (Table V.11).

Table V.11. As Table V.10 but for the NCC run.

	Early winter (Nov-Dec)	**Mid-winter (Jan-Feb)**	**Total**
Past	9	16	25
Future	13	10	23
Total	22	26	48

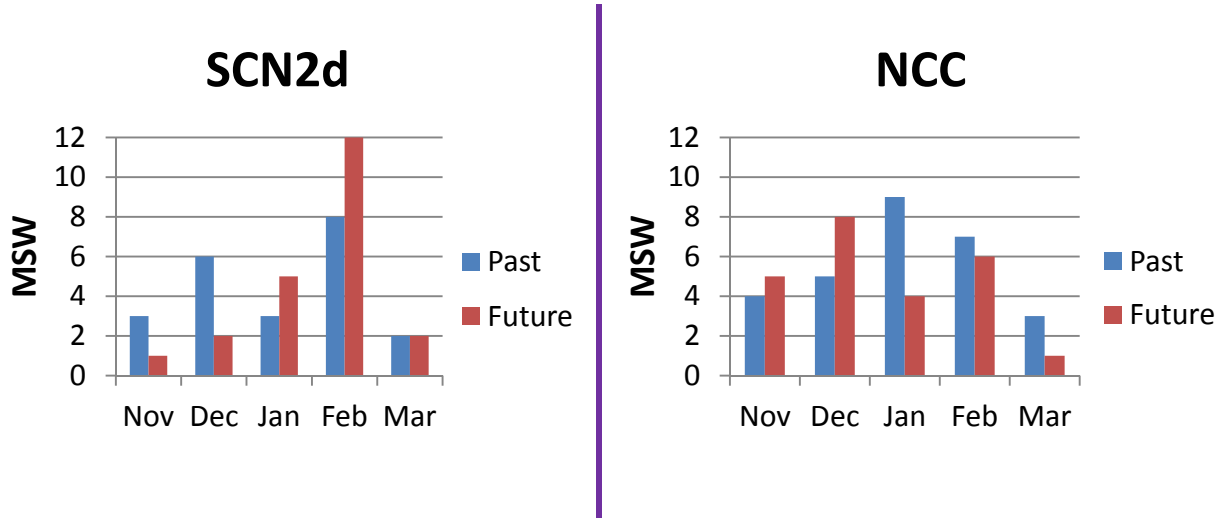

Figure V.29. Seasonal distribution of MSWs by month in the past and future performed by the SCN2d and NCC runs.

Finally, possible differences in the seasonal distribution of MSWs between the two runs for each period of study (past and future) are explored. In this case, the null hypothesis (H_0) is the independence between the runs (*SCN2d* and *NCC*) and the seasonal distribution of MSWs (early winter and mid-winter).

As expected, any statistically significant difference in the timing of MSWs between the two runs was found in the past. In contrast, in the future, whereas the occurrence of MSWs in the SCN2d run is clearly biased towards mid-winter, MSWs in the NCC are equally distributed during the whole winter with a slight bias towards early winter. This bias could be probably due to the problem of ECHAM5 already mentioned, which does not appear in the SCN2d run, because the signal of the climate change would be stronger than a possible anomalously strong tropospheric forcing. Moreover this difference in the future is statistically significant even at a 90% confidence level.

Briefly, according to the above results, no changes in time in the frequency of MSWs or in other characteristics of these phenomena have been identified due to the prescribed increasing GHG concentrations. However, climate change might affect the occurrence of MSW in the future, given that a statistically significant change in the seasonality of MSWs is observed, showing a bias towards more MSWs in mid-winter (January-February). A possible explanation to this change in the seasonal distribution of MSWs is the following:

- It is known that December is the quietest winter month from a dynamical point of view. So, climate change might have the strongest radiative impact on the polar stratosphere in early winter and so, the polar night jet in that season would be also stronger than normal. This would lead to the equatorward deflection of the increased

tropospheric wave activity, not entering into the stratosphere. In contrast, in mid-winter (January and February) when the tropospheric wave activity is even stronger due to climate change effects, there is an increase in the frequency of MSWs in these two months.

ii. Development of MSWs

As a second step of the analysis of future changes in MSWs, the evolution of the atmospheric circulation prior to and after their occurrence is studied.

Firstly, **the time evolution of the zonal-mean middle stratospheric circulation surrounding the onset of MSW** is analyzed for the total field and anomalies [10]. As it has been shown in this Section that the climatology of the zonal-mean zonal wind changes from the late 20th century to the late 21st century and that the seasonal distribution of MSWs changes in time too, the seasonal cycle was removed from the data before averaged in order to eliminate any implicit bias. However, the features observed in both analyses, total field and anomalies, agree well and so, for brevity, only results corresponding to the latter are shown in this report (Figures V.30 and 31).

Focusing on the results from the *SCN2d* run, Figures V.30 a-c show that the PNJ in the days prior to MSWs is statistically significantly stronger in the future, particularly prior to day -10, even showing positive anomalies. Moreover, the negative anomalies associated with MSWs stand shorter after these events in the future than in the past, which can be an indication that the polar vortex recovers more quickly (from day +5 onwards). Thus, the future MSWs tend to happen in a more abrupt way and the recovery of the polar vortex after them is also quicker. This preliminary conclusion is confirmed by the values corresponding to the duration of MSWs of Table V.12, which show a bias of MSWs to be shorter in the future under climate change conditions, and it is also supported by the results concerning the deceleration of the PNJ of Table V.8. However, the abruptness and duration of the future MSWs are not in agreement with Tomikawa [2010] results that relate short (long) duration of MSWs to a preconditioned (non-preconditioned) PNJ prior to these events. This mismatch between Tomikawa's and the present results can be justified by the fact that the relation found by the former between the duration of MSWs and the initial state of the PNJ is not reproduced by the model in the past period (not shown).

[10] Except for cases when indicating something different in this Section, the climatological mean always corresponds to the mean field for each period (past and future) and experiment. The anomalies are defined as the departures from this mean.

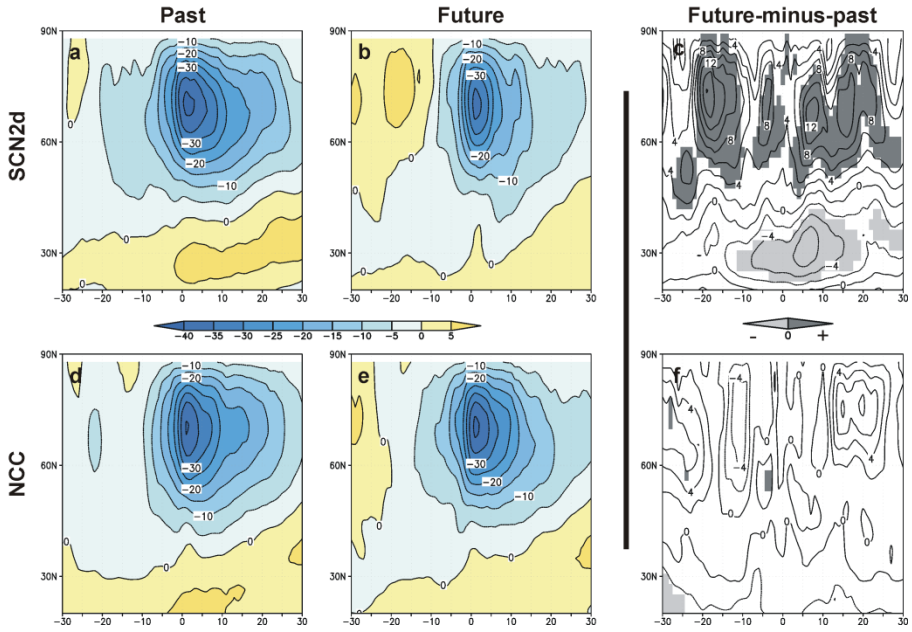

Figure V.30. Zonal-mean zonal wind anomalies at 10 hPa from 30 days before until 30 days after the central date of MSW for the SCN2d and NCC runs: in the past and in the future. **Right column**: the difference future-minus-past values. Contour interval: 5 m s^{-1} (a, b, d and e) and 2 m s^{-1} (c and f). Grey shadings in c and f show statistically significant differences at a 95% confidence level (Student's t-test).

When comparing the results for the future under the two different climate conditions (SCN2d vs. NCC), variations in the zonal-mean stratospheric circulation appear, in general, similar to those found between the two periods in the SCN2d run, but with a reduction in the statistical significance (Figure V.31b). Thus, the abruptness of future MSWs can be attributed to the increase in GHG concentrations. A possible explanation could be found in the concurrence of two opposite mechanisms. On one side, there is a strong upward propagation of tropospheric wave activity enhanced by the climate change effects on the troposphere, which triggers the MSW. On the other side, the increase in GHG concentrations causes a radiative cooling in the stratosphere, which tries to restore the low temperatures over the polar cap as soon as possible.

Table V.12. Duration of the MSWs, i.e. number of days with zonal-mean easterly wind at 10 hPa and 60°N after the onset of each MSW for each simulation and period of study [Tomikawa, 2010]. (*) indicates that the mean values are statistically different between each other at a 90% confidence level. (Student's t-test). In parenthesis, the standard deviation associated with the mean value.

	Past	Future
SCN2d	10.6 days (*) (std: 6.9 days)	5.8 days (*) (std: 4.3 days)
NCC	7.6 days (std: 5.4 days)	7.8 days (std: 6.1 days)

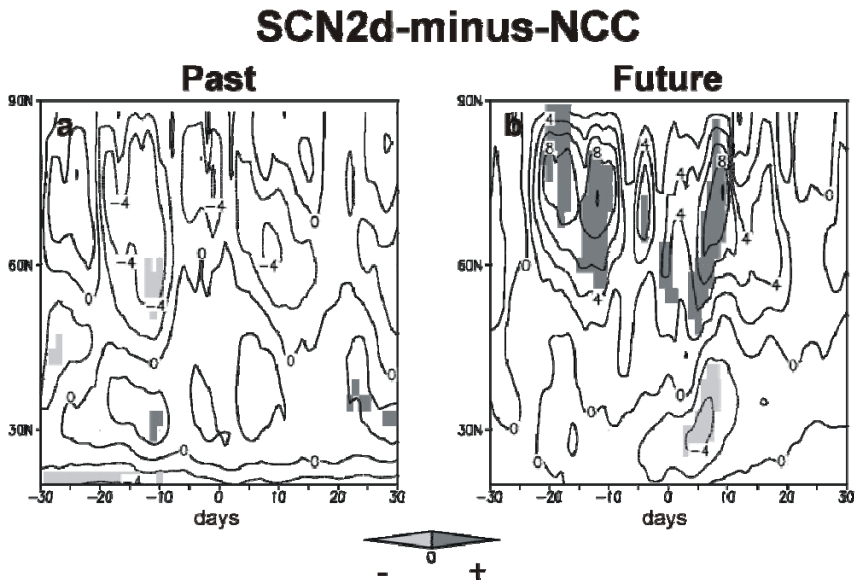

Figure V.31. SCN2d-minus-NCC difference composite maps of 10-hPa zonal-mean zonal wind from 30 days before until 30 days after the central date of MSW in the past and the future. Shadings show statistically significant differences at a 95% confidence level (Student's t-test).

The next step is to analyze the synoptic evolution of the atmospheric circulation at stratospheric and tropospheric levels prior to and after the onset of the MSW. Composite maps of geopotential height anomalies at tropospheric and stratospheric levels have been plotted for different phases of the time evolution of the MSW. Following the method of Limpasuvan et al. [2004], five phases with respect to the central date of the MSW have been considered: the onset phase (average of days -37 to -23), the growth phase (average of days -22 to -8), the mature phase (average of days -7 to +7), the decline phase (average of days +8 to +22) and the decay phase (average of days +24 to +37).

In the middle stratosphere (10 hPa), the stratospheric polar vortex shows approximately the same time evolution in the two periods and experiments (Figure V.32). Prior to the occurrence of the MSW, positive geopotential height (Z) anomalies over western America get stronger with time, being an indication of the intensification of the stratospheric Aleutian high. As this anticyclonic structure intensifies and moves towards the polar cap, the polar vortex weakens and is shifted towards Eurasia, indicated by the displacement of the negative Z10 anomalies towards that area (Figure V.32, first and second rows). Then, at the mature phase, the polar vortex is significantly weakened, denoted by the positive Z10 anomalies over the polar cap, while the mid-latitudes show negative anomalies, particularly over the Atlantic and Europe (Figure V.32, third row). During the following phases, decline and decay, the positive Z10 anomalies over the polar cap weaken progressively and the negative ones over the North Pacific intensify, which implies a recovery of the polar vortex and a weakening of the Aleutian high (Figures V.32, fourth and fifth rows). Despite of the common synoptic

evolution of the polar vortex during the life cycle of the MSW in all periods and experiments, it is important to highlight some differences observed among them. First, during the onset phase, the NCC run in the future does not show positive anomalies over western America. Moreover, the center of positive Z10 anomalies in the SCN2d run is stronger in the past than in the future, what could be related to the longer duration of MSWs observed in the past.

In the lower stratosphere (50hPa), the evolution of the stratospheric polar vortex is very similar to that seen at 10 hPa, but with some delay due to the downward propagation of the anomalies associated with MSWs (Figure V.33). This delay would explain the absence of relevant anomalies in the onset phase.

In the upper and middle troposphere, the study in the stages preceding the MSWs is clearly important to identify possible circulation structures that could act as tropospheric precursors. Actually, during the growth phase, strong and statistically significant negative anomalies of Z200 and Z500 are observed over the Aleutian Islands, indicating an intensification of the tropospheric Aleutian low (Figure V.34 and 35, second row). As shown in the previous Section V.1.b, the strengthening of this structure is related to the enhancement of the mid to high latitude tropospheric Z wavenumber-1 that leads to the weakening of the polar vortex. Moreover, as shown by Taguchi and Hartmann [2006], the origin of this wave activity enhancement can be associated with SST anomalies over the Pacific and, in particular, with El Niño event. In fact, during the growth phase, significant positive Z200 and Z500 anomalies are observed over the subtropical Pacific in the past and future periods for each run, being this a fingerprint of tropical ocean heating. After the occurrence of the MSW, the Pacific negative Z anomalies weaken and significant positive geopotential anomalies over the polar cap in the mature phase are observed at 200 hPa in all cases, particularly in the NCC simulation (Figure V.34, third row). After that phase, the statistical significance of the Z200 and Z500 anomalies decreases considerably from the past to the future, particularly in the SCN2d experiment (Figures V.34 and 35, fourth and fifth row). Moreover, the typical AO-like pattern associated with a weak stratospheric polar vortex appears in both experiments in the past. The AO-like pattern is observed in the future as well, but only in the NCC experiment and much weaker.

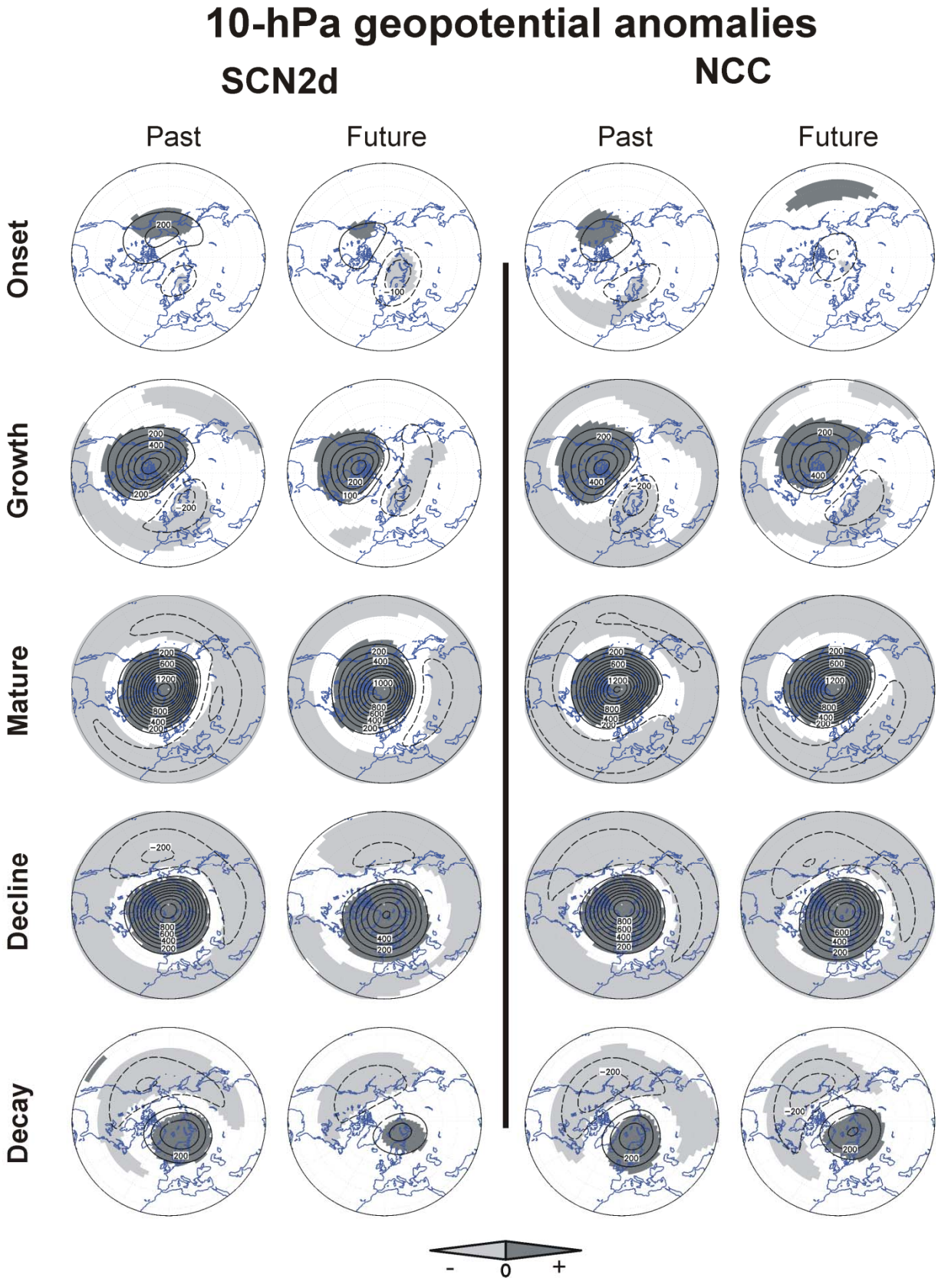

Figure V.32. Geopotential height anomalies at 10 hPa (in gpm) during the onset, growth, mature, decline and decay phases of MSWs in the SCN2d and NCC runs for two periods: past and future. Shaded areas indicate significances at a 95% confidence level (Student's t-test). Contour interval: 100 gpm.

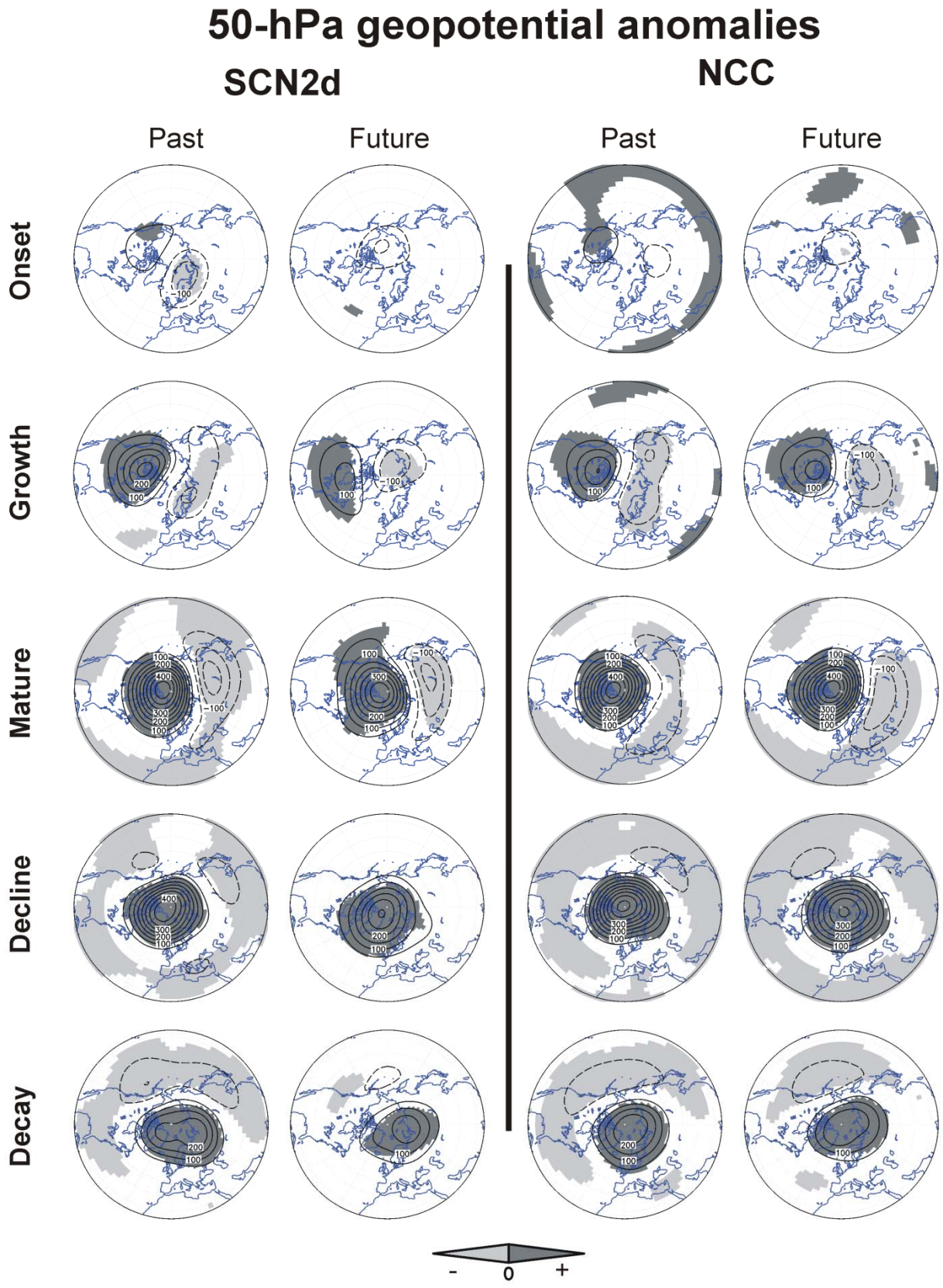

Figure V.33. As Figure V.32 but at 50 hPa.

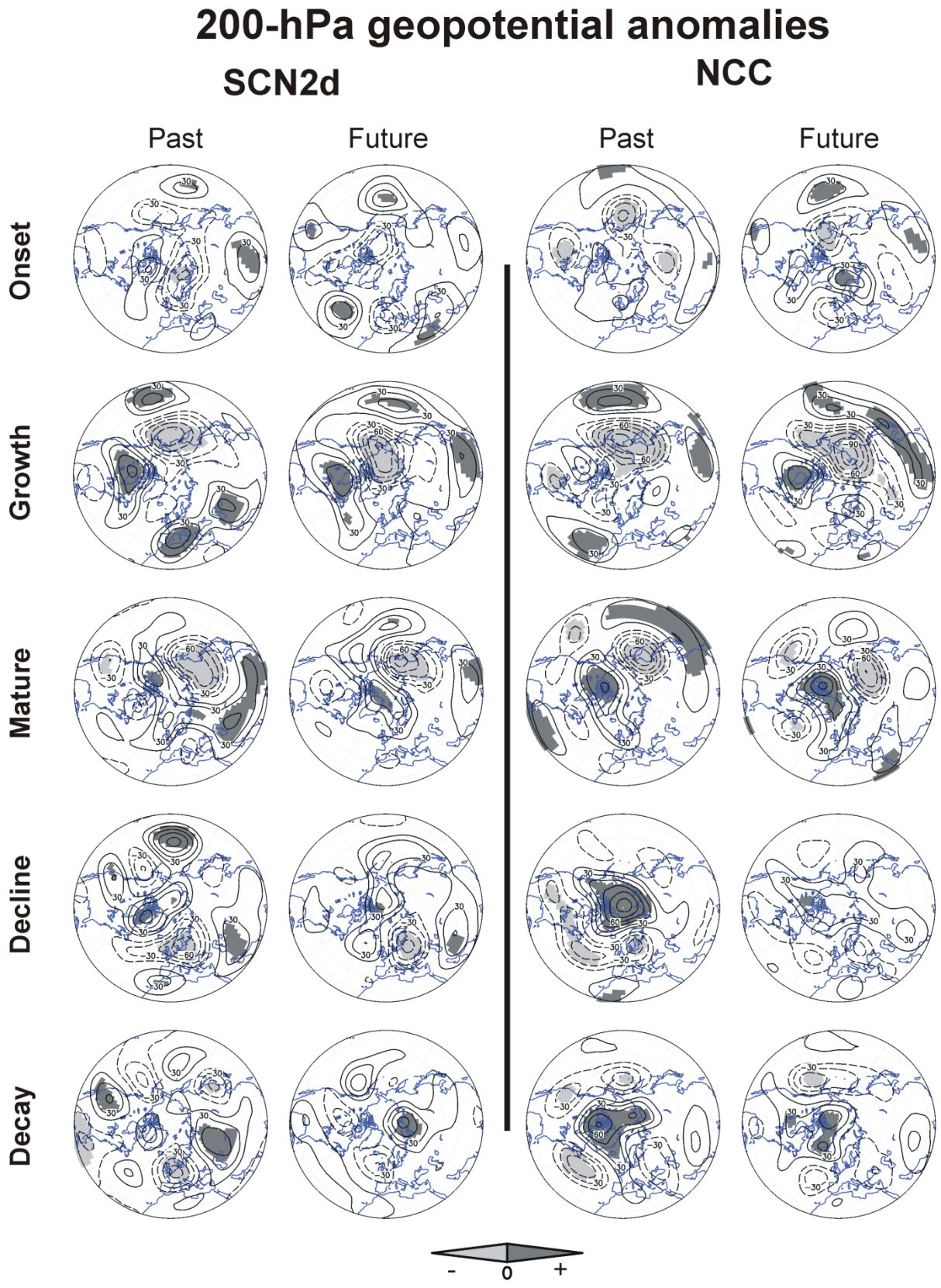

Figure V.34. As Figure V.32 but at 200 hPa.

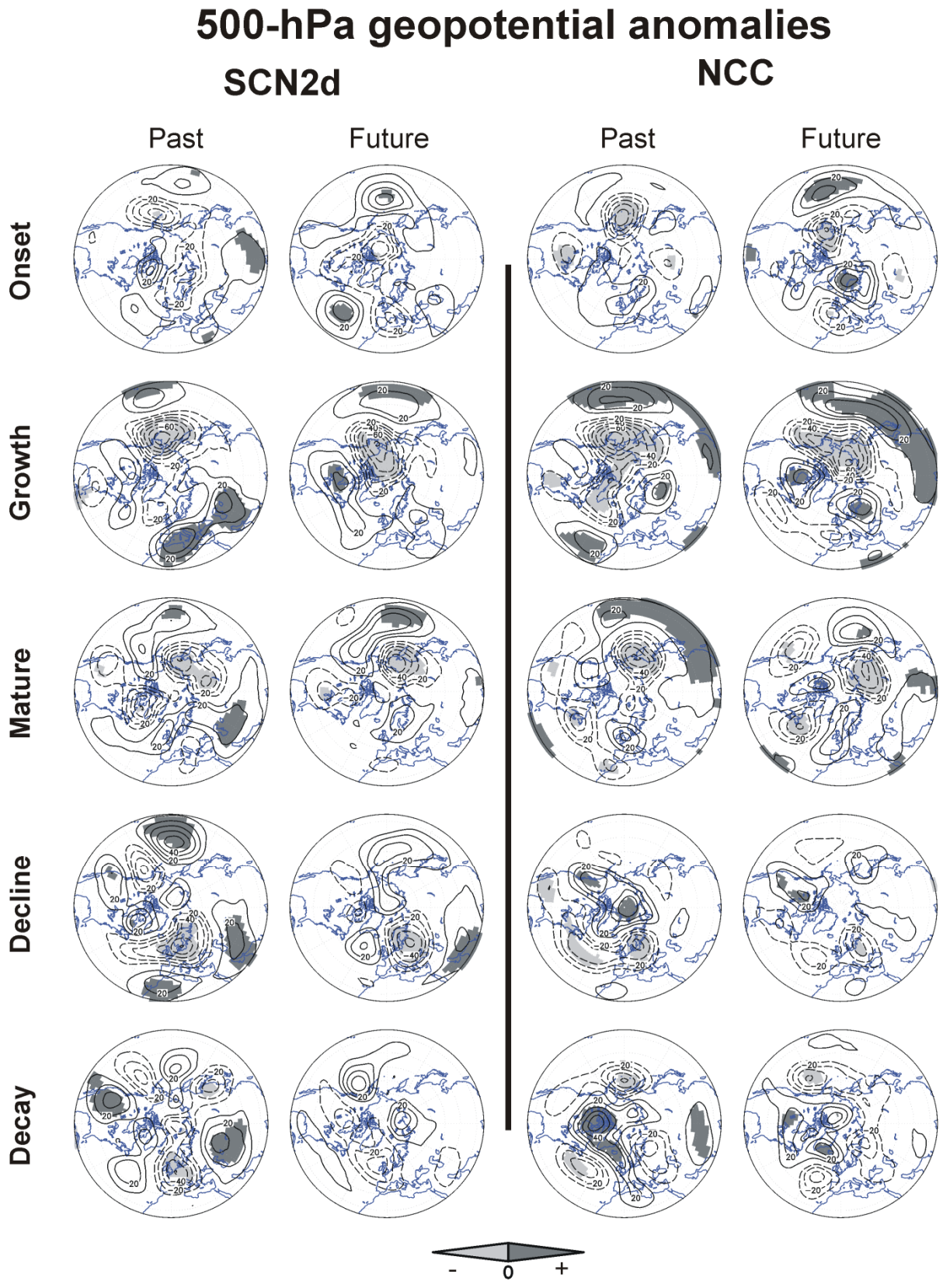

Figure V.35. As Figure V.32 but at 500 hPa.

iii. Stratosphere-troposphere coupling

The last aspect to be explored when comparing the MSWs in the past and future in both runs of EMAC-FUB (under climate change and non-climate change conditions) is the stratosphere-troposphere coupling during this stratospheric phenomenon.

As already mentioned, MSWs are one of the clearest examples of the coupling between the stratosphere and the troposphere in the Northern Hemisphere. Thus, changes in this type of events in a future climate would be likely to affect the troposphere and surface climate. In fact, variations in the coupling between the stratosphere and troposphere in chemistry-climate models or stratosphere-resolving coupled climate models in the future have been recently investigated by analyzing the Northern Annular Mode variability [Gerber et al., 2010]. However, as far as I know, the exploration of these variations in the stratosphere-troposphere coupling associated with the MSWs by a chemistry-climate model is a novelty.

Moreover, in the previous Subsection, it was clearly shown that, under climate change conditions, there is a relevant change in the synoptic evolution of the atmospheric circulation, especially at tropospheric levels. Hence, a more detailed study of possible changes due to the prescribed increasing GHG concentrations in the stratosphere-troposphere coupling following MSWs is worthy. This study is carried out in two steps. First, the downward propagation of stratospheric anomalies is examined and then, the near surface changes after MSWs are evaluated.

Downward propagation of stratospheric anomalies

Figure V.36 shows the time evolution of anomalies of zonal-mean zonal wind at 60°N ($[u]_{60N}$) in the atmospheric column prior to and after the central date of MSWs.

Consistent with the shorter duration of MSWs identified in the future under climate change conditions (*SCN2d* run), the stratospheric $[u]_{60N}$ anomalies related to this phenomenon are less persistent than in the past (Figure V.36b), even in the lower stratosphere. In fact, statistical significant differences of $[u]_{60N}$ between the future and the past are also found at tropospheric levels during 10-15 days after the central date of MSW (Figure V.36c). This might explain that the tropospheric circulation does not show the typical synoptic evolution and signatures after MSWs in the future, as mentioned above.

In contrast, under non-climate change conditions (*NCC* run), the downward propagation of the signal of MSWs in $[u]_{60N}$ anomalies does not exhibit any change in time (Figures V.36 d-e). This result highlights the relevant role of the prescribed increasing GHG concentrations in the future changes observed in the downward propagation of MSWs signal in the SCN2d simulation.

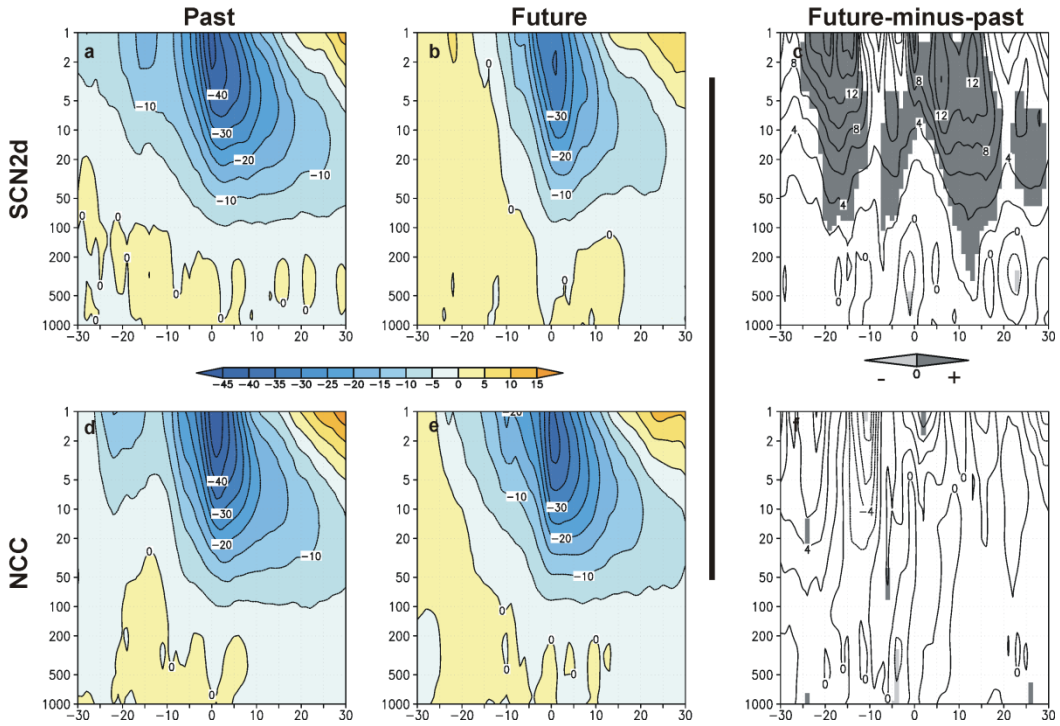

Figure V.36. Anomalies of zonal-mean zonal wind at 60°N from 30 days before until 30 days after the central date of MSW for the SCN2d and NCC runs in the past and future**.** Contour interval: 5 m s^{-1}. **Right** column**:** difference future-minus-past for each run (contour interval: 2 m s^{-1}). Grey shading shows statistically significant differences at a 95% confidence level (Student's t-test).

The responsibility of the increasing GHG concentration in the future changes identified in the downward propagation of MSWs signal is confirmed when comparing the SCN2d and NCC runs. Statistically significant differences in the $[u]_{60N}$ anomalies are found in the future between both runs, whereas they are not in the past (Figure V.37).

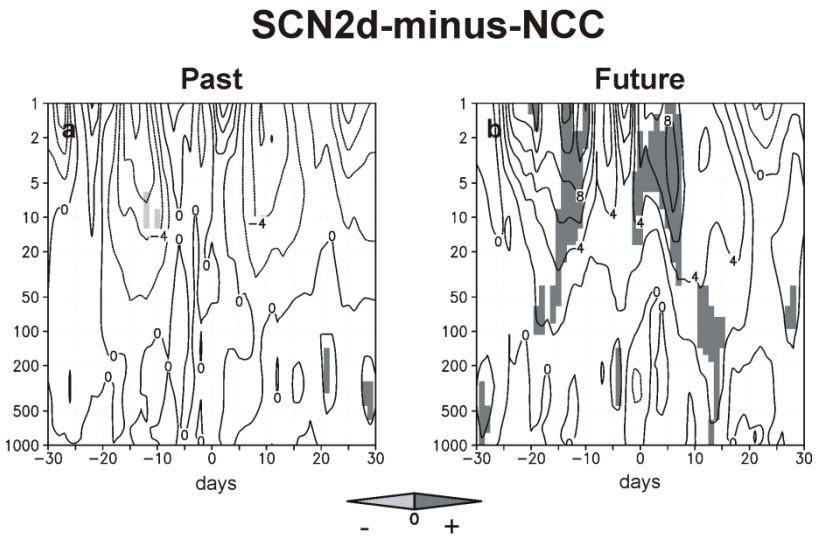

Figure V.37. SCN2d-minus-NCC runs difference composite maps of anomalies of zonal-mean zonal wind at 60°N from 30 days before until 30 days after the central date of MSW in the past and future. Shadings show statistically significant differences at a 95% confidence level (Student's t-test).

After having identified possible changes in the downward propagation associated with the increase in GHG concentrations in the future, a second question arises: does the internal variability associated with MSWs change due to increasing GHG concentrations or in contrast, does it still exist, but is it masked by the signal of the climate change? To answer this question the same analysis has been repeated but with detrended data obtained by applying Gerber et al. [2010] methodology. This method consists in calculating the anomalies as the departures from a varying climatology that accounts for slowly varying trends driven by external climate forcing (in this case, the increase in GHG concentrations), so that anomalies reflect only the internal variability. The varying trend climatology is obtained by applying first a 60-day low pass filter to daily data that regularizes them, so that the trend varies slowly throughout the year. Secondly, a 30-year low-pass filter was applied to the smoothed time series.

The results corresponding to this additional analysis, with detrended anomalies, show that the downward propagation of the MSWs signal only related to the internal variability does not change in the future in an obvious way as when including the external forcings (Figure V.38a vs Figure V.37b). In this analysis, the onset of MSWs in the SCN2d run appears again to be more abrupt in the future than in the past, but the persistence of the associated anomalies in the middle and lower stratosphere during the days following these events is, in general, comparable in both periods and runs. Thus, it might be derived that at least part of the internal variability related to MSWs is hidden by the climate change signal.

This second analysis also shows almost no changes in the downward propagation of the stratospheric anomalies in the NCC experiment, when removing possible external forcings. This is in agreement with the absence of trends in GHG concentrations in this run (Figure V.38b).

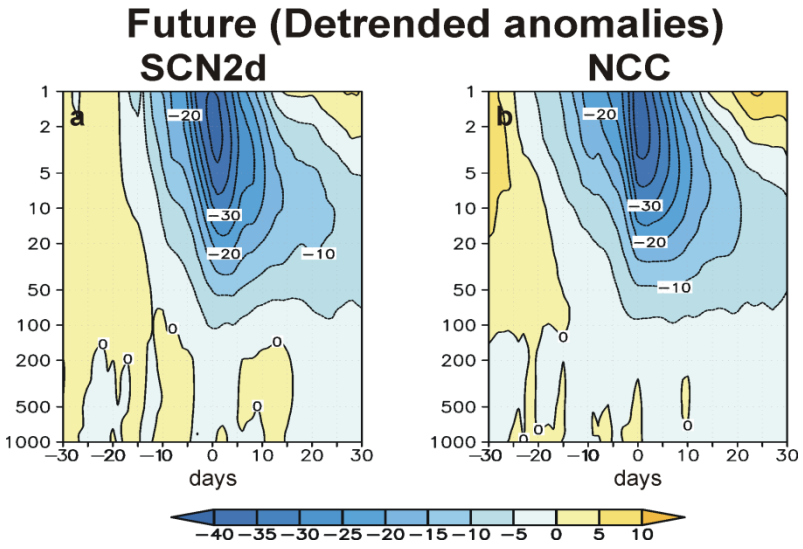

Figure V.38. Composite detrended anomalies of zonal-mean zonal wind at 60°N from 30 days before until 30 days after the central date of MSW in the future for the SCN2d and the NCC runs. Contour interval: 5 m s^{-1}.

Near surface changes following MSWs

Finally, possible **near surface changes after the occurrence of MSWs** have been evaluated. To do that, plots of composite 1000-hPa geopotential height anomalies averaged over the 60 days following MSWs for each simulation and period of study have been computed (Figure V.39). The length of the period after the central date of MSWs has been selected according to Baldwin and Dunkerton [2001], who define weak vortex "regimes" as the 60-day periods after stratospheric strong events of the 10-hPa annular mode.

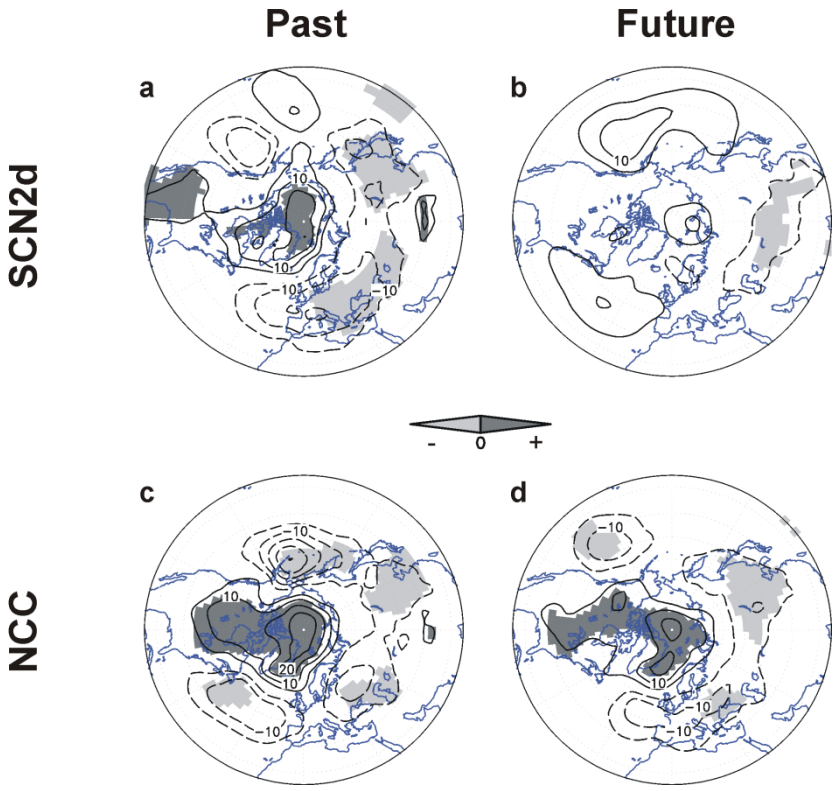

Figure V.39. Composite anomalies of 1000-hPa geopotential height averaged over 0-60 days following the onset of MSWs in the past (**left**) and the future (**right**) from the SCN2d and NCC runs. Contour interval: 5 gpm. Grey shadings correspond to statistically significant anomalies at a 95% confidence level (Student's t-test).

The Arctic Oscillation signature is present in the past in both runs (Figures V.39a and c). In contrast, in the future, whereas the NCC experiment still shows the AO signature, this pattern disappears in the SCN2d. This result agrees well with the decline of the downward propagation of MSWs signal in the future under climate change conditions, which would lead to a weaker impact on the tropospheric circulation (Figures V.36b).

On the other hand, the statistical significance of the anomalies is clearly reduced in time, particularly in the SCN2d experiment.

When applying the methodology above described to detrend data, the typical tropospheric response to MSWs is now observed in the late 21st century of the SCN2d run too (Figure V.40a). In the case of the NCC, a very similar figure to that of Figure V.39d is obtained, which is consistent with the absence of varying trends (Figure V.40b). Thus, as it happens in the downward propagation of the signal of MSWs, it can be derived that their fingerprint on the troposphere does not change in the future under climate change conditions.

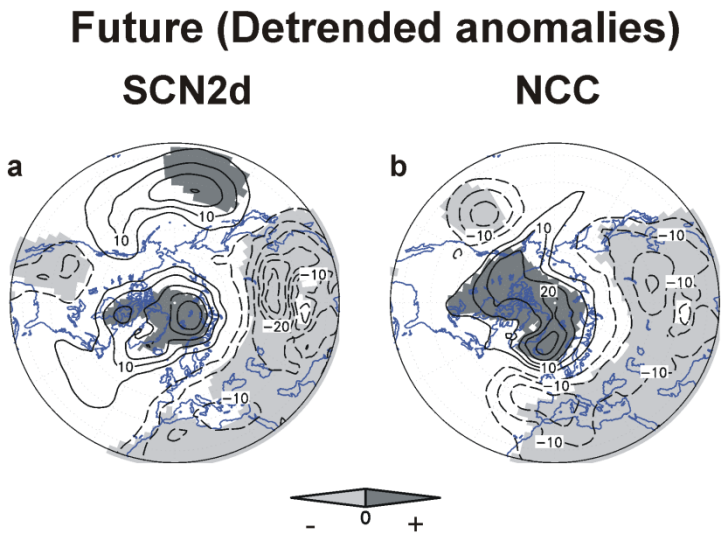

Figure V.40. Composite detrended anomalies of 1000-hPa geopotential height averaged over 0-60 days following the onset of MSWs in the future in the SCN2d **(left)** and NCC **(right)** runs. Contour interval: 5 gpm. Shadings correspond to statistically significant anomalies at a 95% confidence level (Student's t-test).

Finally, another feature to highlight is the strong negative anomalies over Asia. In order to verify if they were due to an effect of the continent, Figure V.39 was computed but for the geopotential height at 850hPa (not shown). In this new figure, the importance of these anomalies is clearly reduced, so it could be derived that the hypothesis of the continent effect is confirmed.

Final remarks

The analysis of the effects of prescribed increasing GHG concentrations on the future MSWs has derived two relevant results.

First, the main properties of these stratospheric phenomena and its associated internal variability are not affected by the climate change in the future. In fact, even the internal variability related to the stratosphere-troposphere coupling does not change, but it is only masked by the climate change signal.

Despite the mentioned unchanged properties in the mechanisms associated with MSWs in the future, a different response of the polar stratosphere to climate change between the early and mid-winter periods has been observed. In early winter, the typical radiative response of the stratosphere to an increase in GHG concentrations has been observed. In contrast, it is the dynamical mechanisms associated with the tropospheric response to the future increase in GHG concentrations (i.e. an intensification of the tropospheric wave activity) which seem to play the most important role in the variations of the polar stratospheric circulation in mid-winter. This leads to an increase in the frequency of MSWs in January and February and a cooling of the polar stratosphere, i.e., less MSWs, in the previous winter months. This result highlights the importance of separating early and mid-winter periods, when analyzing the impacts of climate change on the polar stratospheric circulation.

VI. Stratospheric Final Warmings

As indicated in Chapter II, stratospheric final warming (SFW) is one of the most important processes in the springtime stratosphere that takes place yearly in both hemispheres. It consists of an increase in the stratospheric polar temperature, which causes the breakup of the polar vortex and thus, the final transition of zonal winds from wintertime westerlies to summertime easterlies in the high latitude stratosphere [Andrews et al., 1987]. SFWs are controlled by two different kinds of processes: dynamical and radiative. When the dynamical aspects dominate SFWs, the breakup is done in a rapid way to summer conditions. In the case of radiative-controlled SFWs, a slow transition to summer circulation occurs [Labitzke and Naujokat, 2000].

Similarly to the previous chapter devoted to MSWs, SFWs are analyzed in detail considering two periods: recent past and present, and future. Depending on the period, different features are studied, taking into account the most interesting aspects in each case.

Concerning the recent past and present (Section VI.1), the study examines the interannual variability in the timing of SFWs in the Northern Hemisphere, which is very large. In particular, this part of the PhD thesis explores the possible relationship between these variations and monthly averaged changes in the troposphere. Only a few studies have recently used this approach to the analysis of the stratosphere-troposphere coupling [e.g.: Wei et al., 2007; Gimeno et al, 2007; Hardiman et al., 2011].

In the case of the future (Section VI.2), the analysis concentrates on the determination of a possible trend in the timing of SFWs due to a prescribed increase of greenhouse gas concentrations in the future. This possible effect could affect in turn the climate. Thus, the interest in the topic to be analyzed in Section VI.2 is based on the important consequences to the climate that would arise from a longer or a shorter persistence of the polar vortex.

1. Recent past and present

One of the most important characteristics of stratospheric final warmings (SFWs) in the Northern Hemisphere is the large interannual variability in their timing [e.g. Waugh and Rong, 2002], which some authors have shown to depend strongly on planetary wave activity in the previous winter [Waugh et al., 1999; Salby and Callaghan, 2007]. These variations have been shown to play a key role in the determination of changes in other relevant phenomena, such as the stratospheric circulation and mixing processes of trace gases [Waugh and Rong, 2002], or in the polar stratospheric ozone content [Shindell et al., 1998]. One important aspect associated with this variability that has not been explored in detail so far is the existence of a possible relationship between it and variations in the tropospheric fields. Some authors have very recently linked the

interannual variability in the timing of SFWs events with specific phenomena in the Northern Hemisphere, such as the number of cut-off low systems in the subsequent May and summer [Gimeno et al., 2007] or changes in the lower tropospheric circulation in early spring (February and March) [Wei et al., 2007]. However, there are still many aspects to investigate concerning the relationship between the timing of SFWs and variations in tropospheric fields in spring months.

This section includes a detailed study about the connection between the timing of SFWs and the monthly averaged changes in the tropospheric circulation in each spring month (March, April and May). The analysis has first been carried out using ERA-40 data (Section VI.1.a) and then, the results have been compared with the output of the EMAC CCMVal REF-B1 simulation, as a model validation (Section VI.1.b).

As far as I am aware, the work included in the first part of this Section differs from previous studies in four respects. First, this analysis has been done based on monthly data in contrast to most of the studies about SFWs, which are focused on daily fields surrounding the date of these events. Results from this monthly analysis could be helpful when analyzing the spring climate variability, for which monthly data are usually used. Second, the middle troposphere of the three spring months is examined, by contrast to previous monthly-based studies, which are focused only on the lower troposphere and also on late-winter (until March). Third, as a metric for tropospheric conditions, the storm track activity in addition to geopotential and zonal wind fields is explored. It should be noted that the former variable has been scarcely analyzed up to now in the SFW literature. The storm track activity provides helpful information related to the regions of the strongest baroclinic wave activity, which is known to influence regional weather, especially precipitation and winds [Pinto et al., 2007]. Finally, results from reanalysis data are compared with those from model simulation.

a. Relationship between variations in the timing of SFW and changes in the troposphere in observations

A comparative analysis of the circulation and dynamical properties in each spring month (March, April and May, denoted jointly as MAM) has been performed between two sets of years: years with a very early and very late breakup of the polar vortex. The atmospheric data used in this study have been taken from ERA-40 for the period of 1960-2000. Although ERA-40 data covers more years, it is important to highlight that the study presented here is restricted to this shorter period, so that the analyses with reanalysis and model simulation data have a common period. However, it should be mentioned that the same analysis was previously carried out for the complete period of ERA-40 [Ayarzagüena and Serrano, 2009; Appendix 4]. It should be added that the slight difference in the length of the studied period has barely modified the results.

The two groups of years with "extreme" occurrence of SFW were selected, once the dates of SFWs for the whole period were identified by using the Black et al. [2006] criterion explained in the *Methodology* chapter (Section IV.1.b). Based on the mean date of SFWs obtained for ERA-40 (15 April) and the respective standard deviation (20 days) of the 41 years of study, the years when the SFW event took place "very early" were identified as those when the SFW occurred more than one standard deviation before the mean date (hereafter "early years"; 8 cases). The years with a "very late" breakup of the polar vortex correspond to those when the SFW happened more than one standard deviation after the mean date (hereafter "late years", 8 cases) (Table VI.1).

Table VI.1. Dates of occurrence of the stratospheric final warming (SFW) events in the period of 1960-2000 according to the criterion of Black et al. [2006]. "Early years" and "late years" are marked with (E) and (L) respectively.

Day	Year	Day	Year
22 April	**1960**	22 May	**1981 (L)**
19 March	**1961 (E)**	23 April	**1982**
6 May	**1962 (L)**	21 March	**1983 (E)**
9 April	**1963**	13 March	**1984 (E)**
24 March	**1964 (E)**	4 April	**1985**
22 April	**1965**	29 April	**1986**
6 April	**1966**	8 May	**1987 (L)**
9 May	**1967 (L)**	19 April	**1988**
2 May	**1968**	15 April	**1989**
14 April	**1969**	3 June	**1990 (L)**
12 April	**1970**	5 May	**1991 (L)**
16 March	**1971 (E)**	12 April	**1992**
27 March	**1972**	14 April	**1993**
26 May	**1973 (L)**	3 April	**1994**
26 March	**1974 (E)**	26 April	**1995**
20 March	**1975 (E)**	8 April	**1996**
18 April	**1976**	3 May	**1997**
12 April	**1977**	26 March	**1998 (E)**
27 March	**1978**	6 May	**1999 (L)**
4 April	**1979**	24 April	**2000**
7 April	**1980**		

The main results derived from this analysis of the interannual variability in the timing of SFW are discussed in two parts. First, as a preliminary step, ***the differences in upward propagation of wave activity associated with this variability*** are described. Then, the second and most important part focuses on ***the stratospheric-tropospheric connection related to these variations in the dates of SFW*** by analyzing the differences in the middle-tropospheric circulation in each spring month between "early years" and "late years". The small samples of "early years" and "late years" (8 elements per each set) make the establishment of statistical significance in the differences

between both groups difficult. Thus, specific statistical tests, in particular Monte-Carlo methods, have been used to tackle this problem (see *Methodology* chapter, Section IV.4.b).

i. Dynamical study

Here, the variations in the wave activity in each spring month related to an early or late breakup of the polar vortex are presented. Only results for March and April are shown here, as due to the seasonal cycle, the wave activity and its interannual changes in May are negligible in comparison with the two previous months.

Given that the state of the mean flow is related to the upward propagation of wave activity [Charney and Drazin, 1961], it seems interesting to firstly describe the distribution of the monthly zonal-mean zonal wind, [u], along the atmospheric column in March and April for the two sets of years as well as the climatological one.

In the case of the climatology, when comparing Figures VI.1c and VI.2c, the transition from the wintertime westerly circulation (still existent in March) to the summertime easterly circulation (already apparent in the upper and middle polar stratosphere in April) can be clearly observed. This last result is consistent with the computed mean date of the SFW (15 April).

Concerning the “early years”, the polar night jet is weak in March with respect to the climatology (Figure VI.1a), consistent with the early occurrence of the SFW in that month. Consequently, in April, easterlies dominate the polar stratospheric circulation (Figure VI.2a) for this type of years. In contrast, the polar stratospheric circulation for “late years” is characterized by westerlies in both months, being in agreement with a late breakup of the polar vortex (Figure VI.1b and VI.2b).

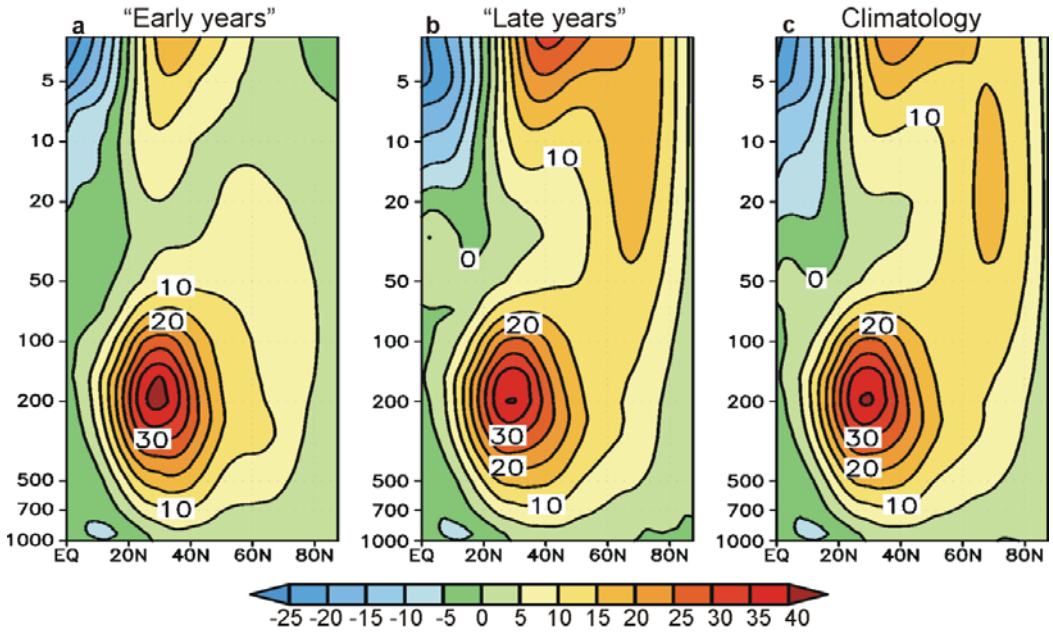

Figure VI.1. Composite cross section of the zonal-mean zonal wind in March for "early years" (8 cases), "late years" (8 cases) and the climatology (1960-2000). Contour interval is 5 m s^{-1}.

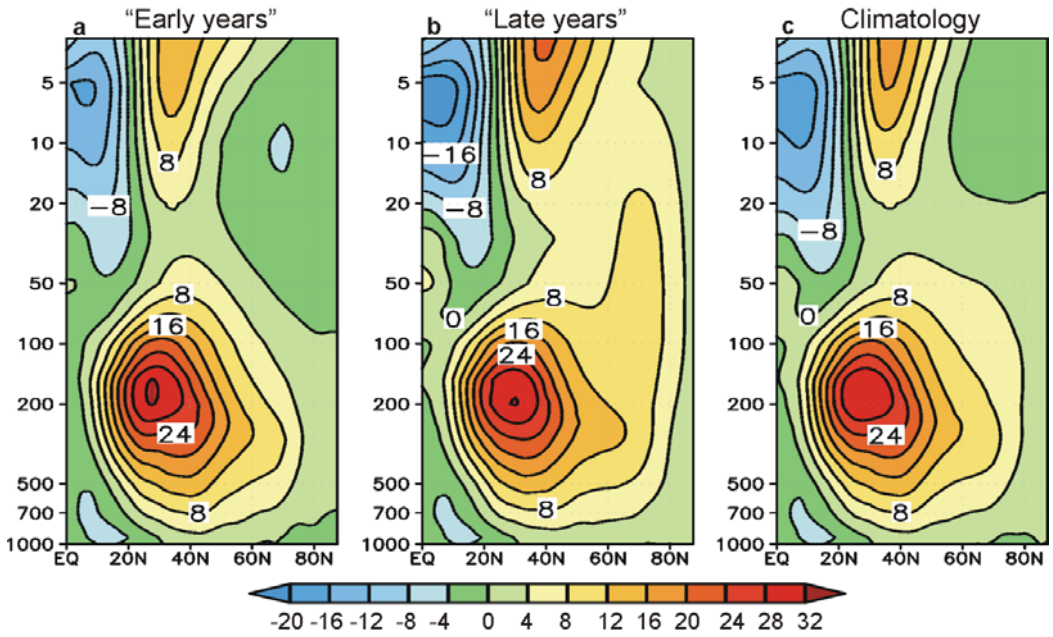

Figure VI.2. Same as Figure VI.1, but for April. Contour interval is 4 m s^{-1}.

The first aspect analyzed was the *interannual variability of stationary waves*. As seen in Figures VI.3 and VI.4, both March and April present noticeable differences in the Eliassen-Palm flux (EP flux) between the two sets of years, especially in the vertical component (F_z) and the divergence (divEP). Some of these differences in F_z and divEP are statistically significant, particularly in March (Figure VI.5). This result is particularly relevant for the analysis of the wave-mean flow interaction, as the F_z and divEP give us

information about the vertical propagation of the wave activity and its impact on the mean flow, respectively.

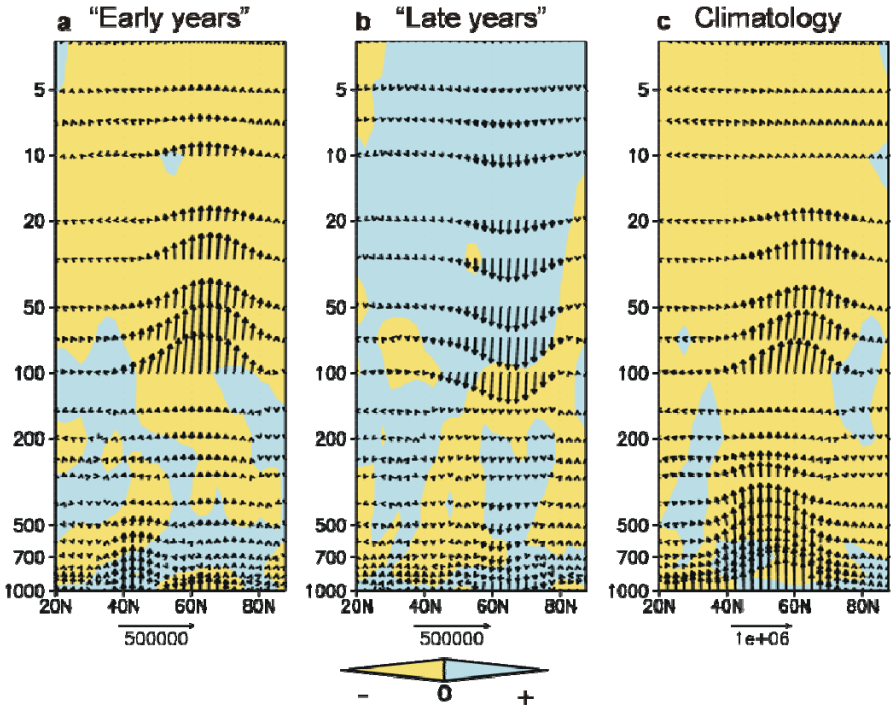

Figure VI.3. Composites of anomalous EP flux (arrows) with its divergence (shading) in March for "early years" (8 cases) and "late years" (8 cases) and climatological values (1960-2000). Arrow scale (m^3 s^{-2}) is indicated at the bottom. The meridional component of EP flux is multiplied by 0.0023 to account for the plot aspect radio. Scaling arrow at 100 hPa and higher is divided by a factor of 10 so that EP flux may be easily seen. Yellow (blue) shading shows negative (positive) values of EP flux divergence.

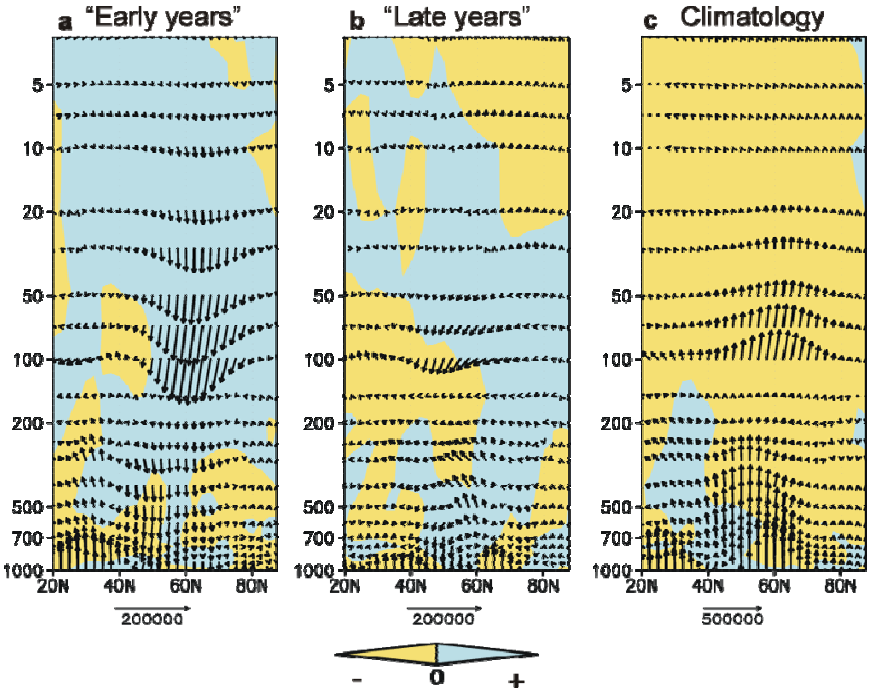

Figure VI.4. Same as Figure VI.3, but for April.

In the case of "early years", the polar vortex in March is weaker than normal (Figures VI.1a and VI.1c), which agrees well with the fact that SFW takes place in this month in this type of years and so, there will be more days than on average with easterly winds in the polar stratosphere. As part of the SFW process [Black and McDaniel, 2007], stationary waves propagate more than normal from the troposphere to the stratosphere prior to this event, which is consistent with more deceleration of the mean flow in the stratosphere (see anomalies of F_z and divEP in Figure VI.3a and compare with values of F_z and divEP in Figure VI.3c). In April, the polar vortex has already disappeared in "early years" (Figure VI.2a) and so, these conditions do not favor wave propagation into the stratosphere according to theory on upward-propagation of wave activity by Charney and Drazin [1961]. Consequently, the upward propagation of wave activity is weaker than on average, denoted by the arrows of anomalous EP flux pointing downwards in Figure VI.4a. Thus, the mean flow is less decelerated by the wave activity (indicated by the positive anomalies of divEP in Figure VI.4a).

In the case of "late years", the results are consistent with Charney-Drazin's theory as well, but it is worth highlighting some aspects. In March, stationary wave activity is strongly reduced, whereas in April the anomalies of EP flux are much less important. Thus, in March, negative F_z anomalies centered at 60°N are observed throughout the whole stratosphere, and a predominance of positive anomalies of divEP in the extratropical stratosphere (Figure VI.3b) (opposite sign from results for "early years"). In contrast to March, in April for "late years", an anomalous upward propagation in the band 55°-65°N up to the upper troposphere can be highlighted. This anomalous wave activity turns at that level towards the equator (Figure VI.4b). At the upper stratosphere, an enhancement of upward propagating wave activity between 50°-70°N is observed, which could be probably an indicator of the beginning of SFW. These results for "late years" could mean that there are relevant negative anomalies in both tropospheric and stratospheric wave activity 1-2 months before the SFW event (that is, in March). This absence of stationary wave activity can be explained by the late winter cooling conditions that characterize most of the "late years", since in 6 out of 8 cases a stratospheric warming (minor or major) was identified in February or at the beginning of March. However, important anomalies of any sign in the wave activity are not found as the time marches on.

Figure VI.5 summarizes the above results, as it shows the statistically significant differences in EP flux and its divergence between "early" and "late" years. In March, an enhancement of upward propagating wave activity is found for "early years" with respect to "late years", probably related to the triggering process of SFW in the former type of years (Figure VI.5a). This anomalous upward wave activity converges at stratospheric levels, decelerating the mean flow. In April, opposite results are observed (Figure VI.5b). However, fewer differences are found between both groups of years than in the previous month.

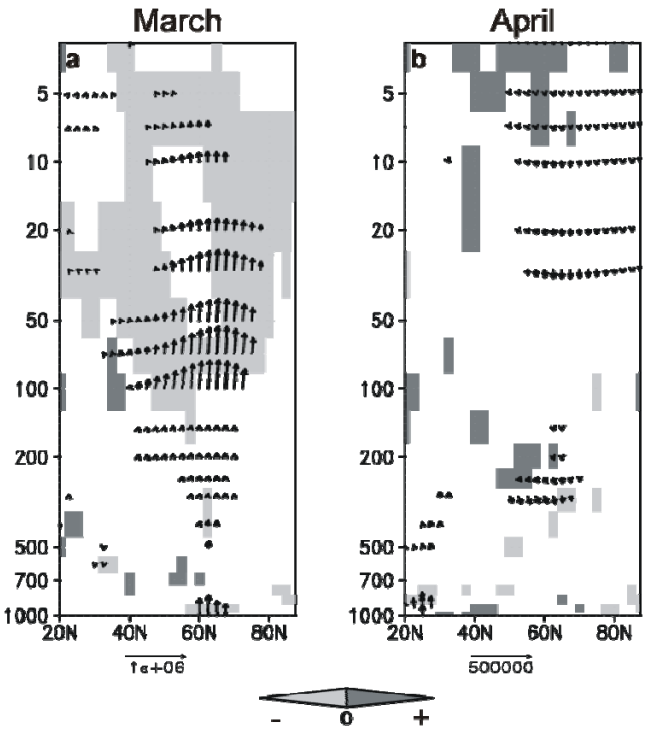

Figure VI.5. Early-minus-Late difference composites of anomalous EP flux (arrows, m^3 s^{-2}) with its divergence (shading) for March and April. Scaling arrow at 100 hPa and higher is divided by a factor of 10 so that EP flux may be easily seen. Arrows are drawn when the vertical component of the EP flux is statistically significant at a 95% confidence level. Light (dark) shadings indicate negative (positive) statistically significant differences of EP flux divergence at a 95% confidence level.

The contribution of each zonal wavenumber (k) to the differences in the upward wave propagation between "early" and "late" years has further been analyzed. In March, the zonal wavenumber-1 wave is the component that explains most of the pattern of differences in the EP flux between "early" and "late" years, shown in Figure VI.5a (see Figure VI.6a and VI.6c). Results obtained by other authors support this finding: Black and McDaniel [2007] observed anomalous upward propagation of waves with wavenumber-1 associated with SFW events (applicable to the "early years"); Limpasuvan et al. [2004] related the recovery of the polar vortex after a midwinter warming to a weakening of k=1 wave amplitude. Thus, this can explain the reduced k=1 wave activity in the "late years", since, in most of the cases, the polar vortex is under late winter cooling conditions as it has been already mentioned. However, it should be remarked that the present analysis is based on monthly averages, whereas the mentioned work was based on daily data.

In April, even though k=1 wave activity plays an important role in the upper stratosphere, the k=2 one also has a big contribution to the pattern of "early"-minus-"late" years differences (hereafter, E-minus-L) in the total stationary EP flux, particularly in the troposphere and middle stratosphere (Figures VI.6b, VI.6d and VI.5b).

The same analysis has been carried out for transient waves in "early" and "late" years. However, the areas with statistical significant differences for these waves between these two sets of years are not as large as those for stationary waves, particularly in March (not shown). The predominance of stationary waves at mid- and high-latitudes has been identified by some authors as well, although related to events of stratosphere-troposphere coupling in winter, in particular midwinter stratospheric warmings [Hartmann et al., 2000; Limpasuvan and Hartmann, 2000; Limpasuvan et al., 2004; or Haklander et al., 2007].

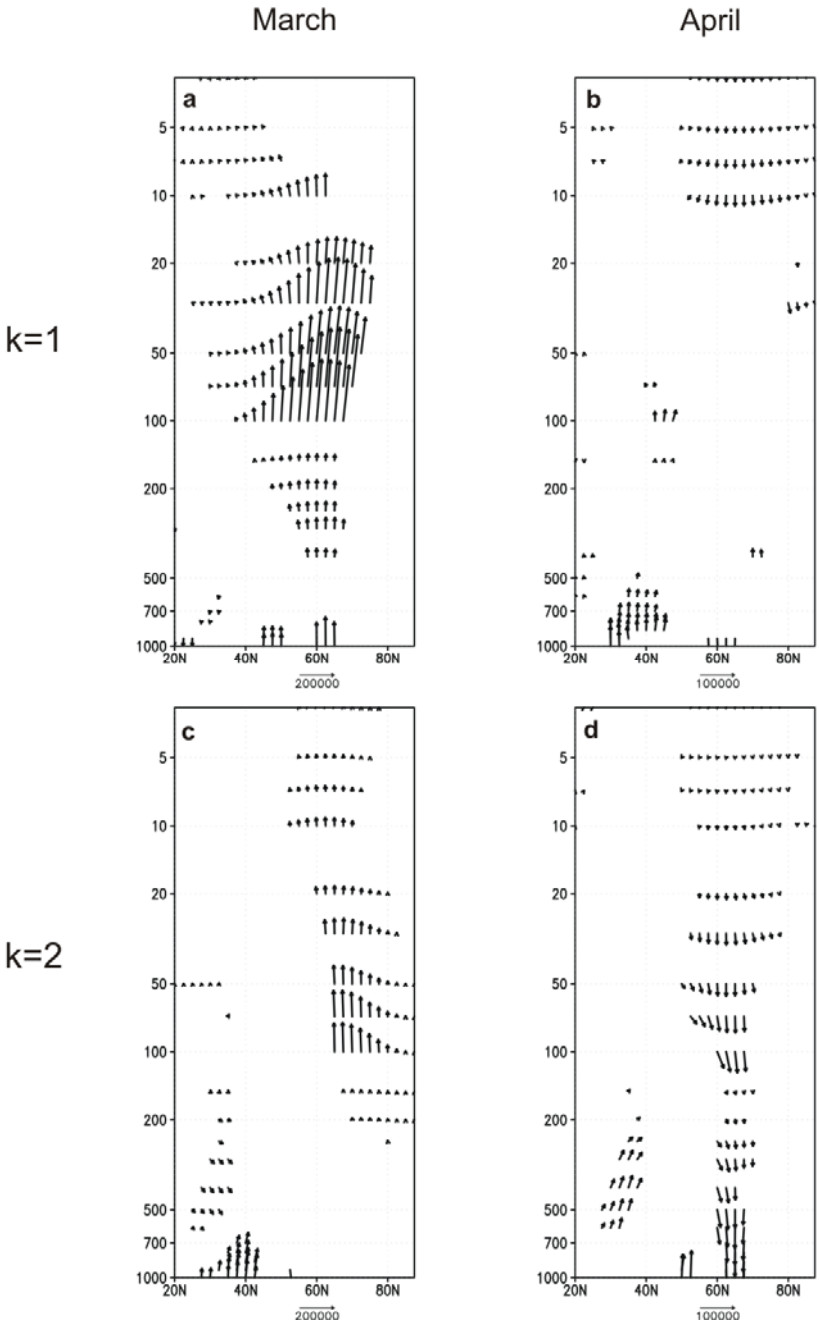

Figure VI.6. Early-minus-Late composites of EP flux ($m^3\ s^{-2}$) corresponding to March and April for the wavenumbers k=1 and k=2. Arrows are drawn when the vertical component of the EP flux is statistically significant at a 95% confidence level. Scaling arrow at 100 hPa and higher is divided by a factor of 10 so that EP flux may be easily seen.

ii. Relation between variability in the springtime stratosphere and troposphere

Figure VI.7 shows the E-minus-L differences in the cross sections of monthly zonal-mean zonal wind, [u], in March, April and May. In these plots, it can be observed that statistically significant negative differences (that is, [u] is stronger in "late" than in "early" years) shift downwards as the spring season marches on. Whereas in March they are restricted to the upper and middle stratosphere, they extend through the whole extratropical stratosphere and even reach the surface in a very narrow high latitude band (60°-70°N) in April. Although the differences of [u] in May are much smaller than in the two previous months, statistically significant values are still observed in the lower stratosphere around the 60°-70°N latitude band, which extend weakly downwards reaching 700 hPa around 60°N. Also, a small center of positive differences appears at polar latitudes (80°-90°N) in the middle troposphere in May. This latter result is quite reliable taking into account the zonal distribution of the angular momentum, despite the deficiencies in the current reanalysis data north of 80°N.

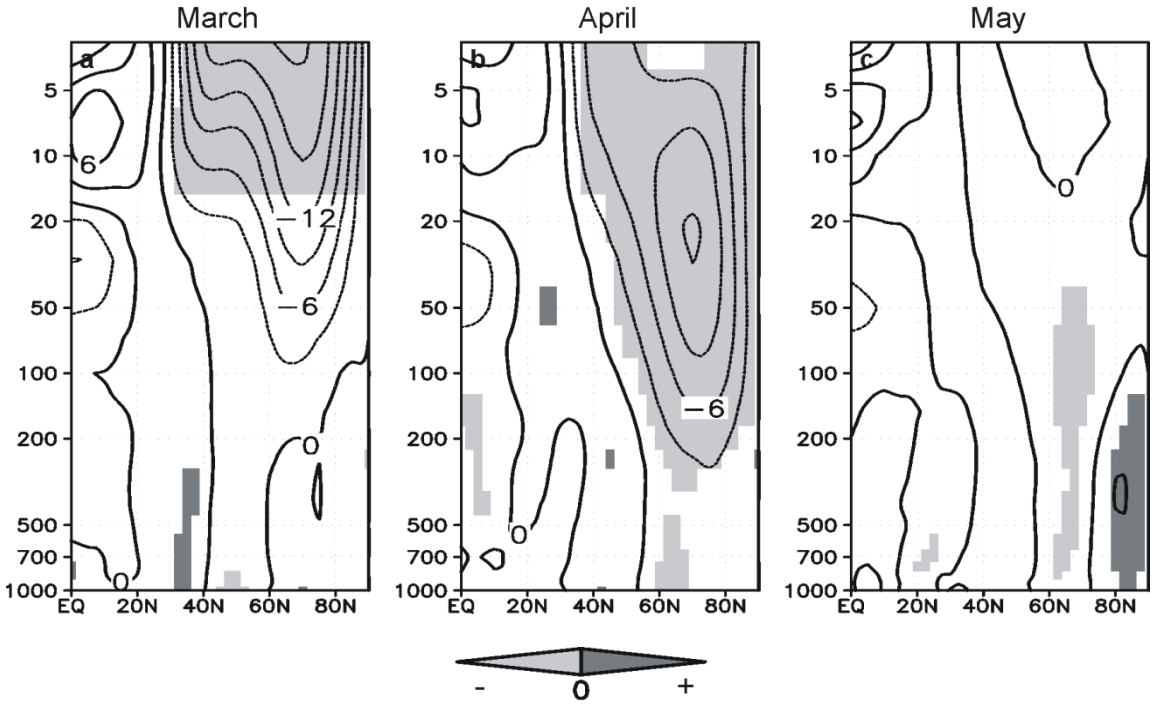

Figure VI.7. Early-minus-Late composites of the zonal-mean zonal wind for March, April and May. Contour interval is 3 m s^{-1}. Light (dark) shading corresponds to negative (positive) statistically significant differences at a 95% confidence level.

Geopotential and zonal wind in the middle troposphere

As differences in the stratosphere seem to spread downwards (according to the previous paragraph), an analysis of middle tropospheric meteorological fields was

performed. Firstly, the basic variables 500-hPa geopotential and zonal wind (hereafter Z500 and U500) in the 3-month MAM sequence have been studied. As seen in Figure VI.8, the differences in the composites of these two fields between "early" and "late" years are noticeable. The anomalies show, in general, opposite signs for each set of years in most of the Pacific area in March and in most of the Euro-Atlantic region in April (Figure VI.8). Therefore, only results for these two months are included in the discussion below.

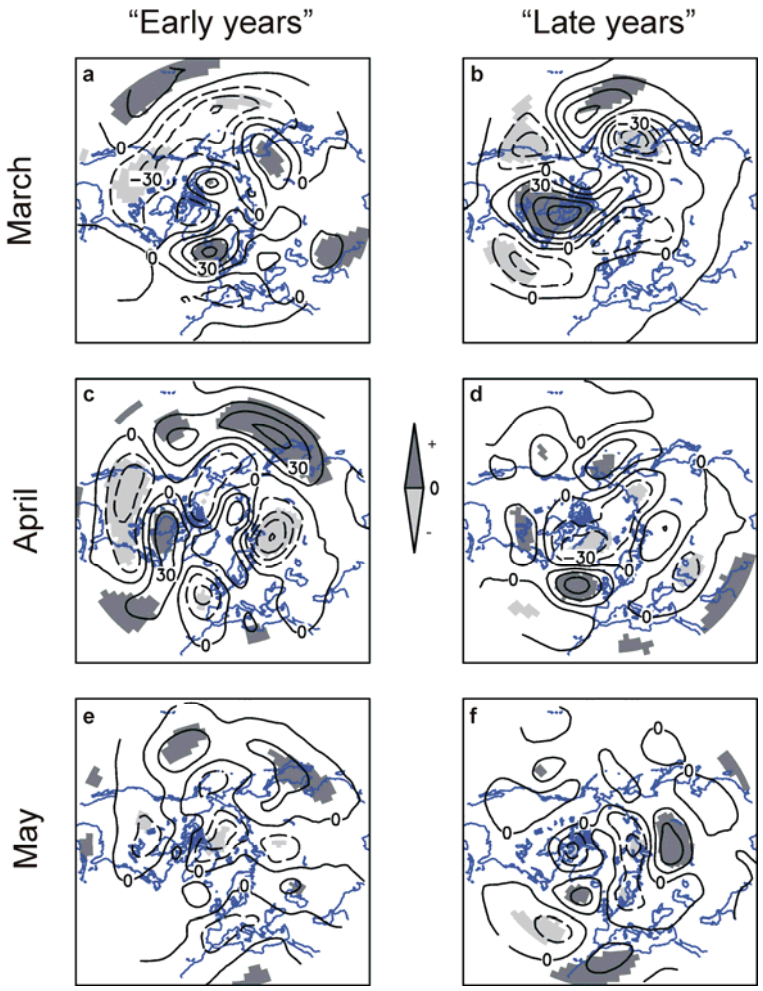

Figure VI.8. Composites of Z500 anomalies in March, April and May for "early years" (**left** column) and "late years" (**right** column). Contour interval is 15 gpm. Shaded areas correspond to statistically significant values at a 95% confidence level.

In the months of March in "late years", a quadripole of Z500 anomalies is observed at mid-latitudes, extending from the east coast of Asia to the western Atlantic, with the main antinodes located over the east coast of Asia and the Hudson Bay (Figure VI.8b). In the case of "early years", this quadripole is not present and the atmospheric pattern is composed of an important center of positive anomalies over Iceland, a band of negative anomalies from the Pacific to the east coast of America and positive anomalies over Asia (Figure VI.8a). When looking at the E-minus-L composite (Figure VI.9a), the differences between "early" and "late" years are more clearly seen along with their statistical

significance. The most extensive differences are localized over the North Pacific basin and the east coast of Asia, in good agreement with the corresponding results for U500 (Figure VI.9b).

As the phase of the Arctic Oscillation (AO) is related to the variation in the polar vortex strength [Baldwin and Dunkerton, 1999], it would be expected to identify a clear negative AO phase in "early years", due to the vortex breakdown in this month and a positive one in "late years" related to a stronger than normal polar vortex (Figure VI.1b). However, after Figure VI.8 and Table VI.2, it can be deduced that in March whereas "early years" are predominantly under negative phase of AO, "late years" do not show a clear signal. Actually, the existence of a statistical dependency between the AO phase (positive or negative) and the late/early occurrence of the SFW was checked for this month. Since the expected frequencies (under the assumption of independence between the two characters or properties) are small, this analysis was carried out by using a Fisher-Irwin exact test (explained in the *Methodology* chapter, Section IV.4.b), in which the null hypothesis H_0 is the "independence between characters". The result of applying the Fisher-Irwin test to this case of study indicates that H_0 could not be rejected with an "exact" confidence level of 50%.

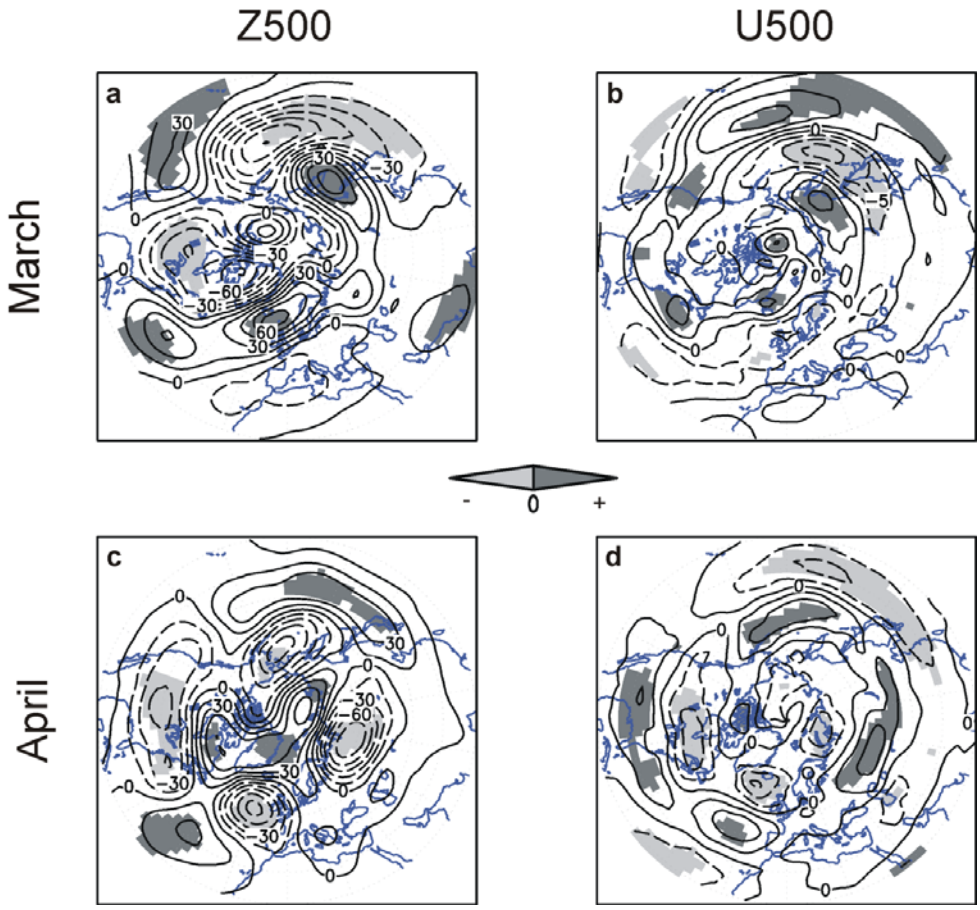

Figure VI.9. Early-minus-Late composites of (**left**) geopotential (contour interval: 15 gpm) and (**right**) zonal wind (contour interval: 2.5 m s^{-1}) at 500 hPa in March and April. Light (dark) shading corresponds to negative (positive) statistically significant values at a 95% confidence level.

Table VI.2. Contingency table displaying the number of "early years" and "late years" (in the period 1960-2000) with positive or negative AO phase in March.

MARCH	positive AO	negative AO	Total
"Early years"	2	6	**8**
"Late years"	3	5	**8**
Total	**5**	**11**	**16**

In the months of April in "late years", a dipole of Z500 anomalies is found in the North Atlantic area and is composed of negative values at high latitudes and positive anomalies west of the British Isles (Figure VI.8d). In the North Pacific region, a center of positive anomalies is localized over the Aleutian Islands. In contrast, the atmospheric pattern in "early years" is quite different from that corresponding to "late years": not only in the sign of the centers of action, but also because these centers are weaker, shifted and deformed (Figure VI.8c). The discrepancies between "early" and "late" years in Z500 in this month can also be observed in the E-minus-L composite, where more statistically significant centers are observed in the Euro-Atlantic sector than in the Pacific, in contrast to March (Figure VI.9c). This result is consistent with the corresponding E-minus-L pattern of U500 (Figure VI.9d), as the antinodes are located over the regions where the gradient of the E-minus-L differences in Z500 is at a maximum.

As for the appearance of the AO phase in the patterns of Figure VI.8c-d, the hemispheric pattern for "late years" resembles the positive AO phase (7 out of 8 "late years" according to Table VI.3), likely due to the still existing polar vortex. In contrast, "early years" does not project strongly onto a negative AO phase, probably because the strength of the AO decreases in non-winter circulation regimes. In this month, the statistical independence between AO phase and the timing of SFW could not be rejected with an "exact" confidence level of 94%. Therefore, the dependence between the AO phase and the late/early occurrence of the SFW is not statistically supported in March and April. Thus, it can be deduced that the present work cannot be seen as an analysis of the influence of stratospheric changes on the tropospheric variability only based on the AO phase like a high number of previous studies have done (e.g., Baldwin and Dunkerton, 2001). This study shows that the downward influence of SFWs should not be understood only in terms of AO phase, even though it is a phenomenon related to the strength of the polar vortex. This conclusion agrees well with Black and McDaniel [2009] that indicates that unlike major midwinter warmings, where the NAM dominates the downward propagation, SFWs are equally controlled by two different annular modes, the NAM itself and a newly identified one, called the polar annular mode. The later mode, defined for the first time by Black and McDaniel [2009], represents variability in the latitudinal position of the polar vortex and is characterized by a poleward-retracted dipole anomaly structure. In fact, some of the patterns shown in Figure VI.8 present some similarities with the polar annular mode, in particular, that corresponding to March for "early years".

Table VI.3. As Table VI.2 but for April.

APRIL	positive AO	negative AO	Total
"Early years"	3	5	**8**
"Late years"	7	1	**8**
Total	**10**	**6**	**16**

Storm-track activity

The next step of the study was to evaluate the effects of the interannual variability in the timing of SFW on the storm-track activity at 500 hPa in March, April and May and in the two high-activity areas: the North Atlantic and North Pacific sectors. The storm track activity is computed based on the standard deviation of the bandpass filtered synoptic variability of geopotential at 500 hPa (explained in the *Methodology* chapter, Section IV.2). As this variable informs about areas with the strongest baroclinic wave activity, which in turn measures the synoptic activity, this analysis appears to be an adequate way of exploring the stratosphere-troposphere connection. In addition, very few studies about SFWs have considered this variable up to now.

In the case of the North Atlantic region, Figure VI.10 shows that the most conspicuous statistically significant E-minus-L differences in storm track activity are found in April (at a 95% confidence level).

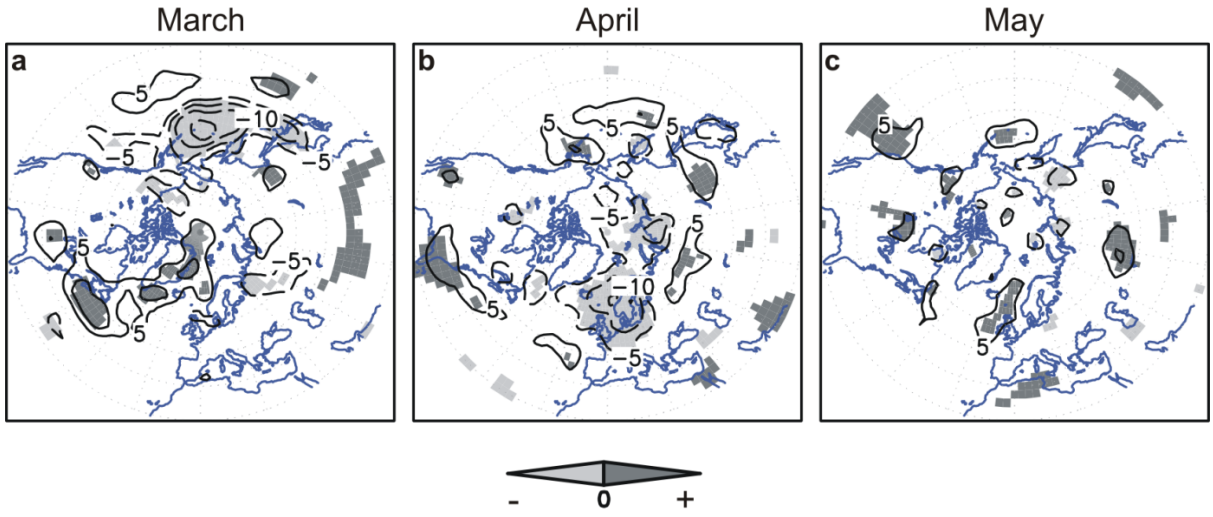

Figure VI.10. Early-minus-Late composites of storm-track activity at 500 hPa for March, April, and May. Contour interval is 5 gpm. Light (dark) shading indicates negative (positive) statistically significant difference at a 95% confidence level. Zero contours are omitted for clarity.

In order to better understand the result in the North Atlantic region, the storm-track activity in April in "early years" and "late years" is compared with the climatology

(Figure VI.11a and VI.11b vs Figure VI.11c). In "early years", a southward shift is observed in the east Atlantic along with a weakening in the whole Atlantic strip. The opposite is observed for "late years" (Figure VI.11b): the storm-track activity is stronger and located northward respect to the climatology, particularly in the East Atlantic, so that the values greater than 37.5 gpm cross the British Isles and reach Scandinavia. The importance and reliability of these differences between "early" and "late" years is supported by the statistical significance of the E-minus-L composite of the storm-track activity shown in Figure VI.10b. Statistically significant differences have been identified in one important area such as Scandinavia, the exit region of the storm tracks in the Atlantic area. Moreover, these E-minus-L differences in storm track activity are consistent with those obtained for Z500 and U500. The westerlies in "early years" ("late years") seem to be weaker (stronger) than average at high latitudes in the North Atlantic basin and stronger (weaker) at mid-latitudes, coincident with the southward (northward) shift of storm tracks.

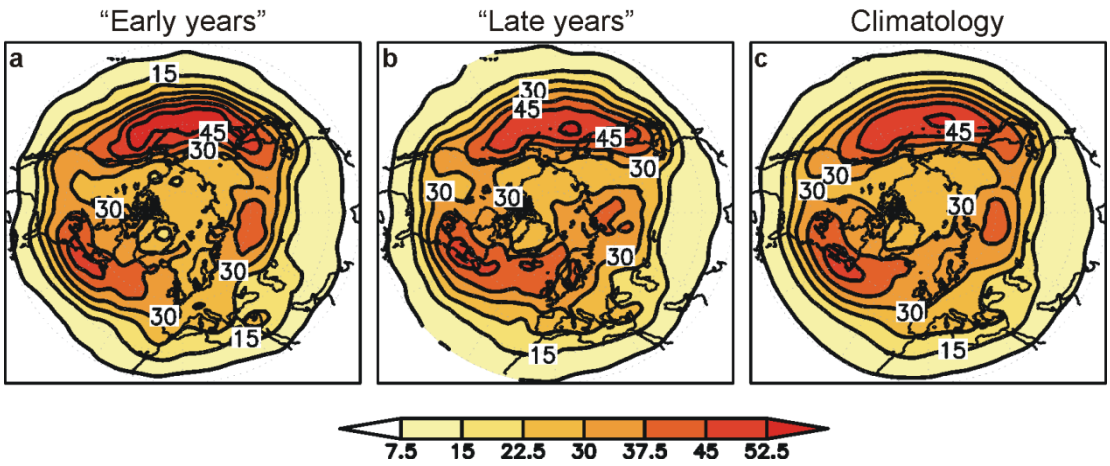

Figure VI.11. Composites of storm-track activity at 500 hPa in April for the "early years", "late years" and climatology (1960-2000). Contour interval is 7.5 gpm.

When analyzing the propagation of stationary wave activity in the troposphere by the three-dimensional Plumb flux, consistent results with those of storm track activity are obtained. Figure VI.12 shows the components of the Plumb flux at two tropospheric levels, where they attain their maximum values: the lower troposphere (700 hPa) in the case of the vertical component and the upper troposphere (300 hPa) for the horizontal component [Plumb, 1985]. In agreement with the climatology shown by Plumb [1985], two distinct major wave trains are observed: one extending from eastern Asia across the North Pacific Ocean and the other from eastern North America across the North Atlantic (Figure VI.12c). Whereas important differences between "early" and "late" years are not identified in the wave train over Asia, the wave train in the North Atlantic basin is shifted equatorward (poleward) with respect to the average in "early" ("late") years (Figure VI.12a and VI.12b). Since the same feature has been observed with the storm

track activity, this would imply that the E-minus-L differences in the stationary wave propagation described in the previous Section VI.1.a.i could be related to those found in storm track activity. In fact, model simulations have already provided evidence that planetary stationary waves play an important role in the organization and maintenance of the storm tracks [Broccoli and Manabe, 1992; Lee and Mak, 1996; Chang et al., 2002].

It may be inferred from the above results that in years when the SFW occurs late, a higher number of storms crosses Northern Europe in April. For "early years" the opposite could be concluded. This result might be, of interest for the seasonal forecasting community due to its potential connection with the predictability of precipitable water.

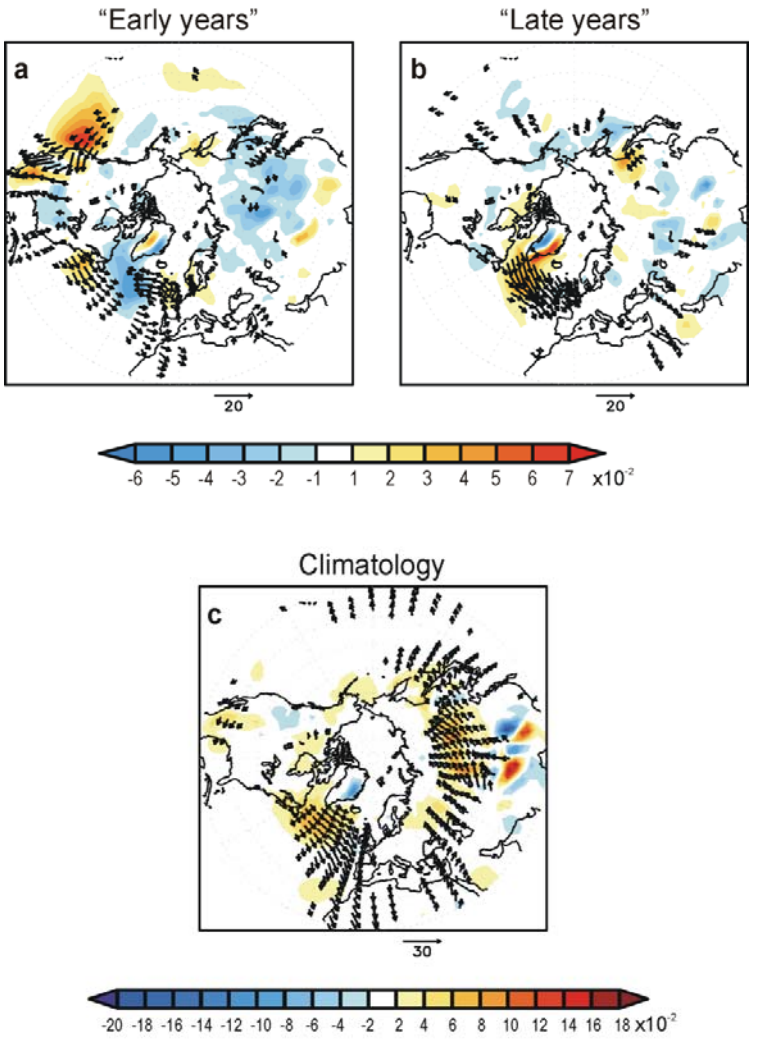

Figure VI.12. Three-dimensional Plumb flux anomalies ($m^2\ s^{-2}$) in April for "early years", and "late years" (**upper** panel), and climatological values (1960-2000) (**bottom** panel). Arrows correspond to the 300-hPa horizontal flux and shading to the 700-hPa vertical component.

As for the North Pacific sector, it is not April but March, when the statistically significant differences in the storm-track activity between "early" and "late" years are most extensive (Figure VI.10). When comparing the storm-track activity in the months

of March in “early years” and “late years” with the climatology, “early years” are characterized by a weaker-than-average storm-track activity in this area together with a southeastward shift of its maximum (Figure VI.13a vs VI.13c). In contrast, the storm-track activity in “late years” in the North Pacific region is much stronger than the climatology (Figure VI.13b vsVI.13c).

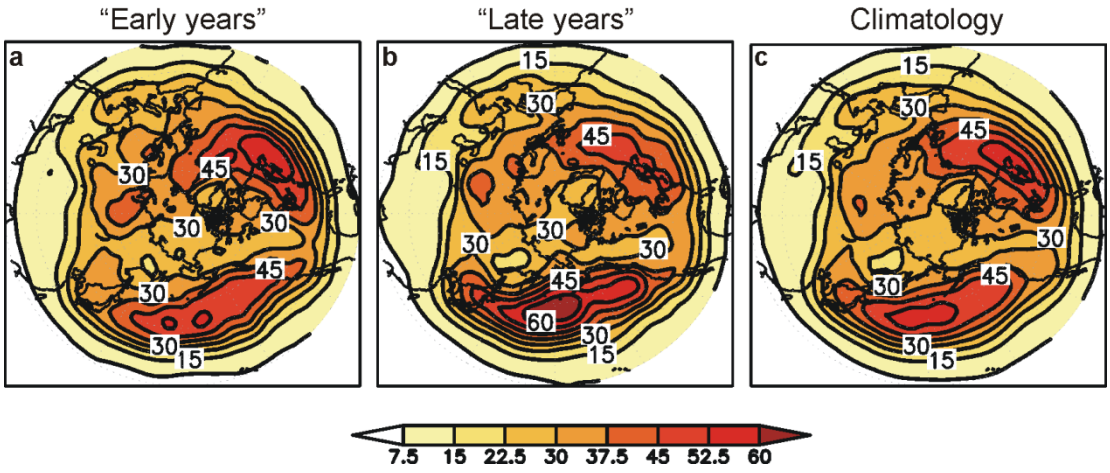

Figure VI.13. As Figure VI.11, but for March. Note that there is a 180° shift in longitude with respect to Figure VI.11.

To sum up, in case of an early breakdown of the polar vortex, the storm track activity would be weaker than on average in March (April) in the North Pacific (North Atlantic) sector. In contrast, in the case of a late SFW, the opposite could be deduced and thus, a higher number of storms would cross Northern Europe in April and the North Pacific in March.

Final remarks

The interannual variability in the timing of SFWs involves effects not only on stratospheric fields as it would be expected, but also on the upward propagation of stationary waves. Moreover, it affects the tropospheric circulation, leading to changes in the typical middle tropospheric fields (Z500 and U500) and also in the storm track activity. However, the period of the highest tropospheric response to the timing of SFWs is different in the North Pacific and North Atlantic region.

Another important remark is that the mentioned downward influence of the interannual variability of SFWs is not totally explained by the NAM, in contrast to midwinter stratospheric warmings. This might indicate that the mechanisms responsible for the troposphere-stratosphere coupling would not be exactly the same in mid- and late winter.

b. Stratospheric Final Warmings performed in a chemistry climate model simulation

After having analyzed the possible influence of the interannual variability in the timing of stratospheric final warmings (SFWs) on the boreal springtime troposphere from ERA-40 data (i.e., observations), this Section is devoted to a similar analysis from the output of the EMAC CCMVal REF-B1 simulation (hereafter EMAC REF-B1), and the subsequent comparison of results. In particular, this analysis is focused on two aspects:

- the ability of the model to reproduce the interannual variability in the timing of SFWs (Section VI.1.b.i),

- the possible relationship between this variability and changes in tropospheric fields in springtime months in the model (Section VI.1.b.ii)

The comparison of results from ERA-40 and the transient EMAC REF-B1 simulation would assess the ability to reproduce the stratosphere-troposphere coupling in spring associated with the timing of SFWs.

i. Ability of the model to simulate the interannual variability in the timing of SFWs

First, the dates of the occurrence of stratospheric final warmings were identified according to the criterion of Black et al. [2006], as done in the previous section for the ERA-40 data. The time evolution of these dates is plotted in Figure VI.14. A table with the dates is included in Appendix 3.

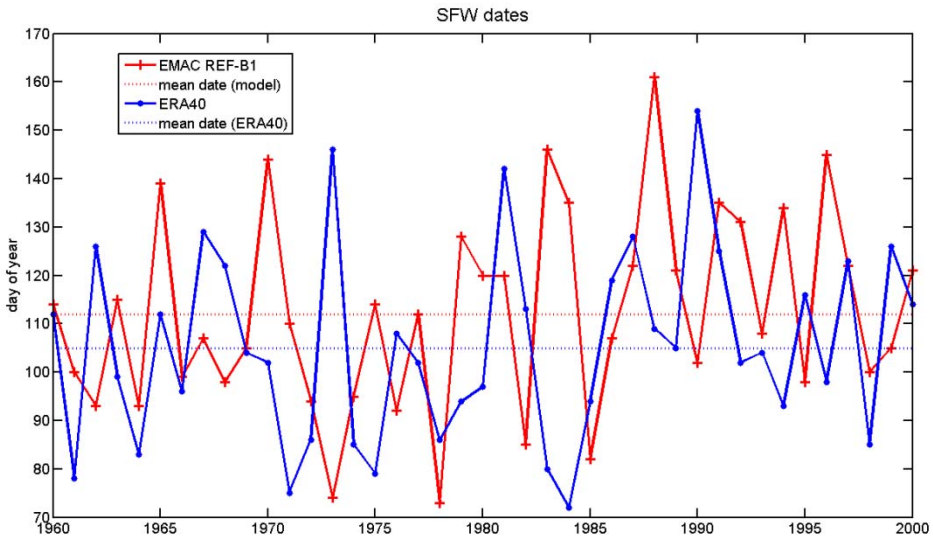

Figure VI.14. Dates of stratospheric final warmings in 1960-2000 from the EMAC REF-B1 simulation (red) and the ERA-40 reanalysis (blue).

The mean date of SFW from the model data (22 April) and the standard deviation (20 days) agree with those obtained with the ERA-40 data for the same period of time (Table VI.4). They are also consistent with those derived by Black et al. [2006] using NCEP/NCAR reanalysis. In particular, the good agreement in the standard deviation between the model and the reanalysis indicates that the model reproduces quite realistically the high interannual variability in the date of SFW.

Although a year-to-year correspondence does not exist between the model simulation and ERA-40 because of the internal model dynamics, the time evolution of the SFW dates in the model agrees in general with that in the reanalysis (Figure VI.14). In both datasets, the seventies are characterized by a bias towards early SFW, the eighties are a transition period and in the nineties, the SFWs tend to occur late in the springtime.

The distribution of SFW dates during the 41-year period in the model is similar to that in the ERA-40, too (Figure VI.15). Both distributions are platykurtic and have an asymmetry on the right of the mean value. These statistical properties are supported by a kurtosis[1] nearly zero and a Fisher asymmetry coefficient[2] higher than 0 (Table VI.4).

Table VI.4. Statistical parameters of the distribution of the frequency of the SFW dates for the EMAC REF-B1 simulation and the ERA-40 reanalysis. Period 1960-2000.

	Mean date	Standard deviation	Kurtosis coefficient	Fisher's asymmetry coefficient
Model	22 April	20 days	$3 \cdot 10^{-7}$ ($\cong 0$)	0.23
ERA-40	15 April	20 days	$1 \cdot 10^{-6}$ ($\cong 0$)	0.39

[1] The *kurtosis* is defined as the fourth standardized moment: $g_2 = \frac{m^4}{\sigma^4}$, where m^4 is the fourth moment about the mean and σ is the standard deviation. A Gaussian distribution has a kurtosis equal to 3. [Gorgas et al., 2009].

[2] The *Fisher asymmetry coefficient* is defined as the third standardized moment: $g_1 = \frac{m^3}{\sigma^3}$, where m^3 is the third moment about the mean [Gorgas et al., 2009].

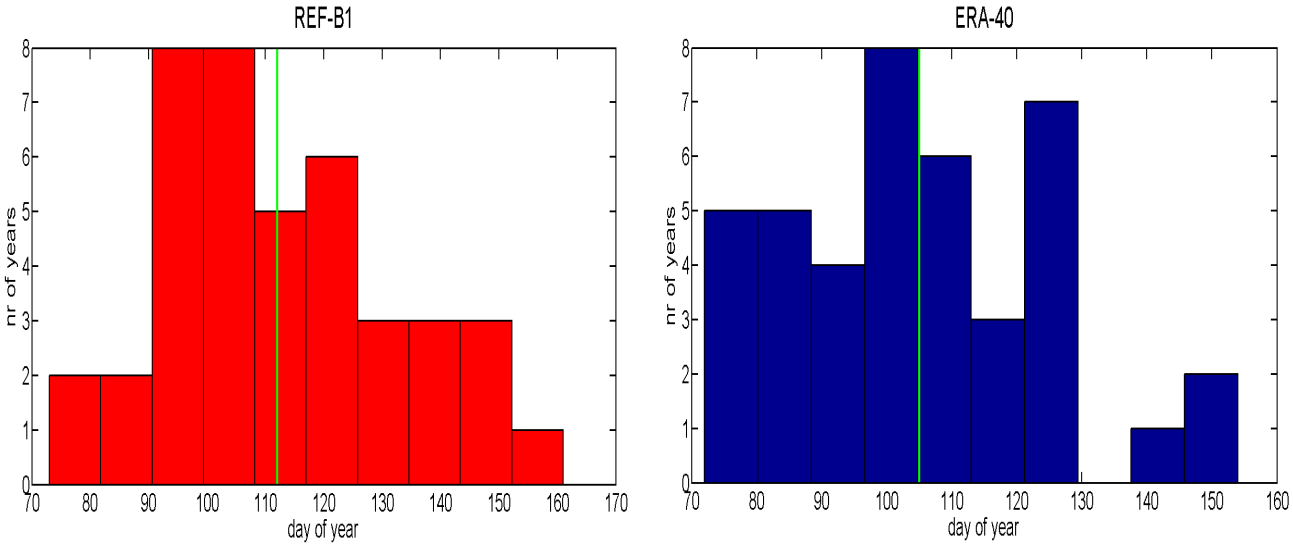

Figure VI.15. Distribution of frequency of the SFW dates during the springtime for the EMAC REF-B1 simulation (**left**) and the ERA-40 reanalysis (**right**). The green line corresponds to the mean date of the period (1960-2000).

However, despite the mentioned agreement in some SFW aspects, the model shows a delay of 7 and 6 days in the mean and median date respectively compared to the reanalysis (identified on 15 and 14 April, respectively). This discrepancy is consistent with the climatological evolution of [u] at 50 hPa (Figure VI.16) that shows a stronger modeled polar vortex than in ERA-40 from mid-January until the end of April. It also agrees well with general results from an intercomparison of Chemistry Climate Models (CCM) of the SPARC CCMVal activity [Butchart et al., 2011], which found a multimodel date of final warming significantly later than observed.

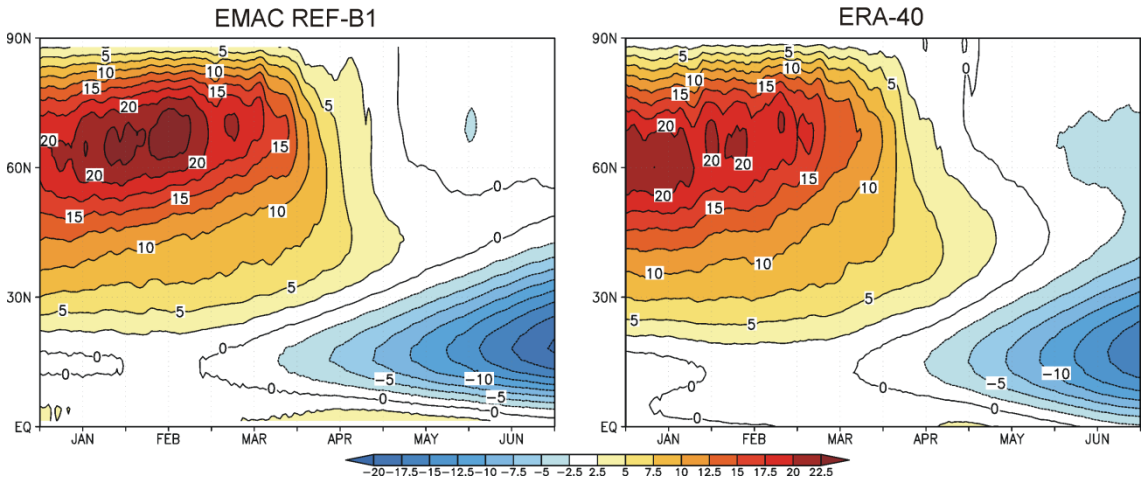

Figure VI.16. Climatology of zonal-mean zonal wind at 50 hPa for the period 1960-2000 for the EMAC REF-B1 simulation (**left**) and ERA-40 reanalysis (**right**). Contour interval: 5 m s^{-1}.

According to the previous results, the EMAC REF-B1 simulation reproduces the timing of the SFWs in the Northern Hemisphere and its interannual variability reasonably well. Hence, the output of this simulation can be used to analyze the possible relationship between this variability and tropospheric changes.

ii. Tropospheric changes associated with the timing of SFW

In order to perform a comparative analysis with the ERA-40 dataset, the EMAC years in the 1960-2000 period were grouped into two sets: "early years" (5 cases) and "late years" (8 cases) (Table App3.1 of Appendix 3). As done with the ERA-40 data, possible differences between the two groups of years in monthly fields for each spring month (March, April and May) were explored, focusing on the following aspects:

- Differences in the polar stratospheric mean flow.

- Changes in middle tropospheric fields.

For brevity, only the figures from the model simulation are included here. Respective results from ERA-40 have been shown in Section VI.1.a. However, to facilitate the visual comparison, Appendix 3 contains the figures showing results for both the model and the reanalysis.

Differences in the polar stratospheric mean flow

Figure VI.17 shows the Early-minus-Late differences in the vertical cross sections of monthly zonal-mean zonal wind, [u], in March, April and May. As it happens in ERA-40 data, the statistically significant negative differences at mid- to high latitudes shift downward and weaken as the spring season progresses, reaching tropospheric levels in April.

Despite this good agreement between the reanalysis and the model performance, some differences are seen, particularly in March. In this month, the center with the maximum difference between "early" and "late" years is found at a higher level in the reanalysis than in the model (Figure VI.7a vs Figure VI.17a). In addition, the statistically significant E-minus-L values are restricted to the upper and middle stratosphere in ERA-40, while they extend through the whole extratropical stratosphere in the EMAC simulation, because the differences in the lower stratosphere are much larger in EMAC than in ERA-40. Finally, in March, two centers of opposite sign are observed at tropospheric levels between 30°N and 50°N.

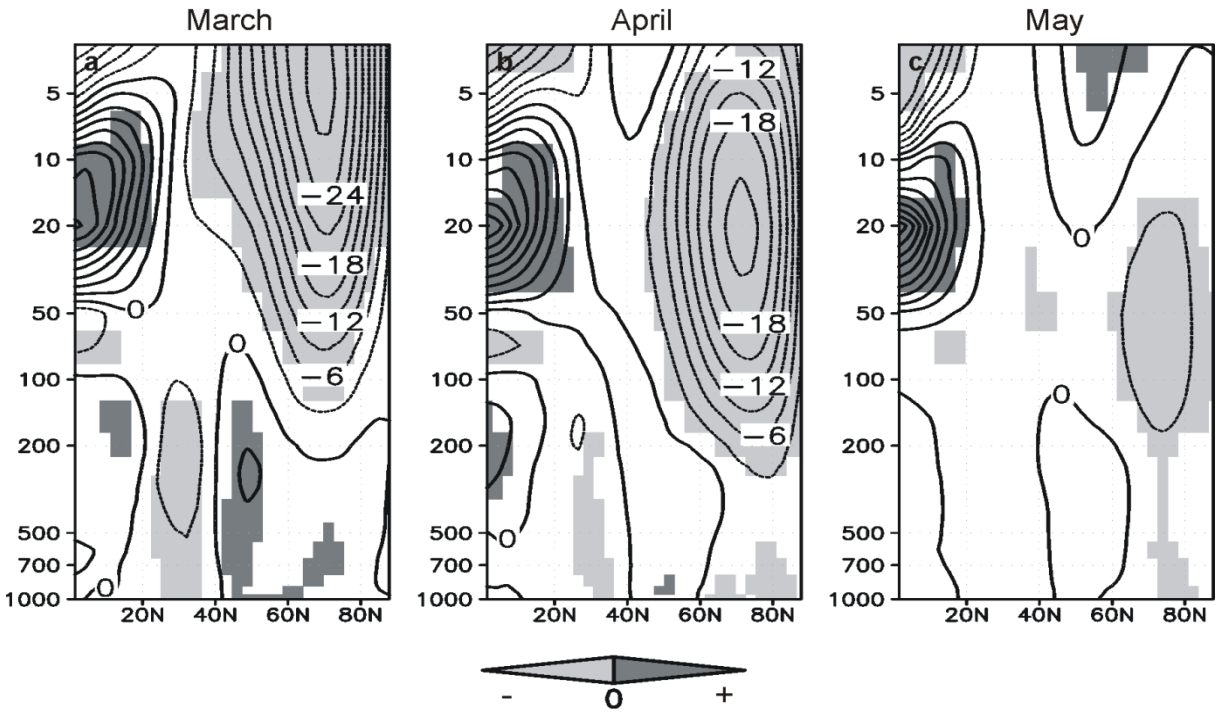

Figure VI.17. Early-minus-Late composites of the zonal-mean zonal wind for the EMAC REF-B1 simulation. Contour interval is 3 m s^{-1}. Light (dark) shading corresponds to negative (positive) statistically significant differences at a 95% confidence level. Figure VI.7 shows the same but for ERA-40.

Another point to highlight is the statistically significant vertical dipole at low latitudes found for the model simulation in the three months. There are several reasons that relate this dipole to the QBO. First, most of the "late years" show a west phase of the QBO (five out of eight) and just the opposite for the "early years" (three out of five)[3]. In addition, the pattern of [u] observed in Figure VI.17 resembles that corresponding to the west-minus-east zonal wind difference of Figure 5c of Pascoe et al. [2005] but with opposite sign. It also agrees well with the so-called *Holton-Tan effect*, even though this relationship appears to be more evident in early winter than in late winter [Holton and Tan, 1980]. Finally, the equatorial dipole seems to go downwards with time, just like the QBO signal does. In the case of the reanalysis, this aspect is not significant, although a similar but weaker structure is observed in approximately the same region. A better agreement might be expected between EMAC and ERA-40 in this aspect, as EMAC reproduces a realistic QBO, which is even in phase due to the relaxation imposed to the simulations. However, while the QBO is realistic, SFWs in EMAC occur following the internal model dynamics. Based only on the internal variability, it is thus understandable that more "early SFWs" are found in EMAC in the east phase of QBO than in ERA-40, as SFWs tend to occur earlier under QBO easterlies than under QBO westerlies [Salby and Callaghan, 2007].

[3] According to the classification of the QBO phase shown in Figure 3 of Labitzke et al. [2006]. This classification can be applied to the model simulation, because EMAC simulates the QBO.

Changes in middle tropospheric fields

Given that differences in the stratosphere between "early" and "late" years seem to spread downward, an analysis of the changes in middle tropospheric fields related to the interannual variability in the timing of SFWs has been carried out in the same way as it was done with the reanalysis data.

Geopotential and zonal wind (Z500 and U500)

The first tropospheric fields analyzed have been Z500 and U500. In this case, the discussion below focuses on the results for March and April as in Section VI.1. This is due to the fact that the analysis was finally restricted in the case of ERA-40 to March and April and moreover, "early" and "late years" in the simulation do not show important differences in Z500 in May in Figure VI.18.

The most important similarities between ERA-40 and EMAC are found in the Euro-Atlantic sector, but in most cases, the modeled results show a southeastward shift with respect to the reanalysis (Figures VI.18 and VI.19). The clearest example of this coincidence corresponds to the center of negative anomalies near the British Islands in the E-minus-L composite map of Z500 in April, which is present in both the model and the reanalysis, even if it is slightly shifted towards the European continent in the model (Figures VI.19c and VI.9c). In April, ERA-40 and the model simulation have more results in common, such as a center of negative anomalies over northern Asia and another one of positive anomalies over Japan that can be observed in both datasets, apart from that mentioned over the British islands (Figures VI.19c and VI.9c).

On the other hand, discrepancies between the model and the reanalysis are also observed in the Z500 field. First, a general disagreement is identified in the Pacific sector in the analyzed months (Figures VI.18 and VI.19 vs VI.8 and VI.9), which could be possibly related to a problem of the model to simulate some processes typical of the North Pacific region. Moreover, while April is the month when the statistically significant differences in Z500 and U500 between "early" and "late" years are most extensive in ERA-40 data, this is not the case in the model simulation (Figures VI.9 and VI.19). For the latter dataset, it is in March when the highest dissimilarities are found. This seems to be in agreement with results of Gerber et al. [2010] who show that in the NH CCMVal-2 Chemistry-Climate Models suggest the strongest coupling associated with late SSWs and early SFWs in February and March, in contrast to the observations that show the strongest connection between the troposphere and stratosphere in association with MSWs in early and mid-winter.

Concerning U500, the results are consistent with those derived from the same analysis for Z500 (e.g.: Figures VI.19c and d).

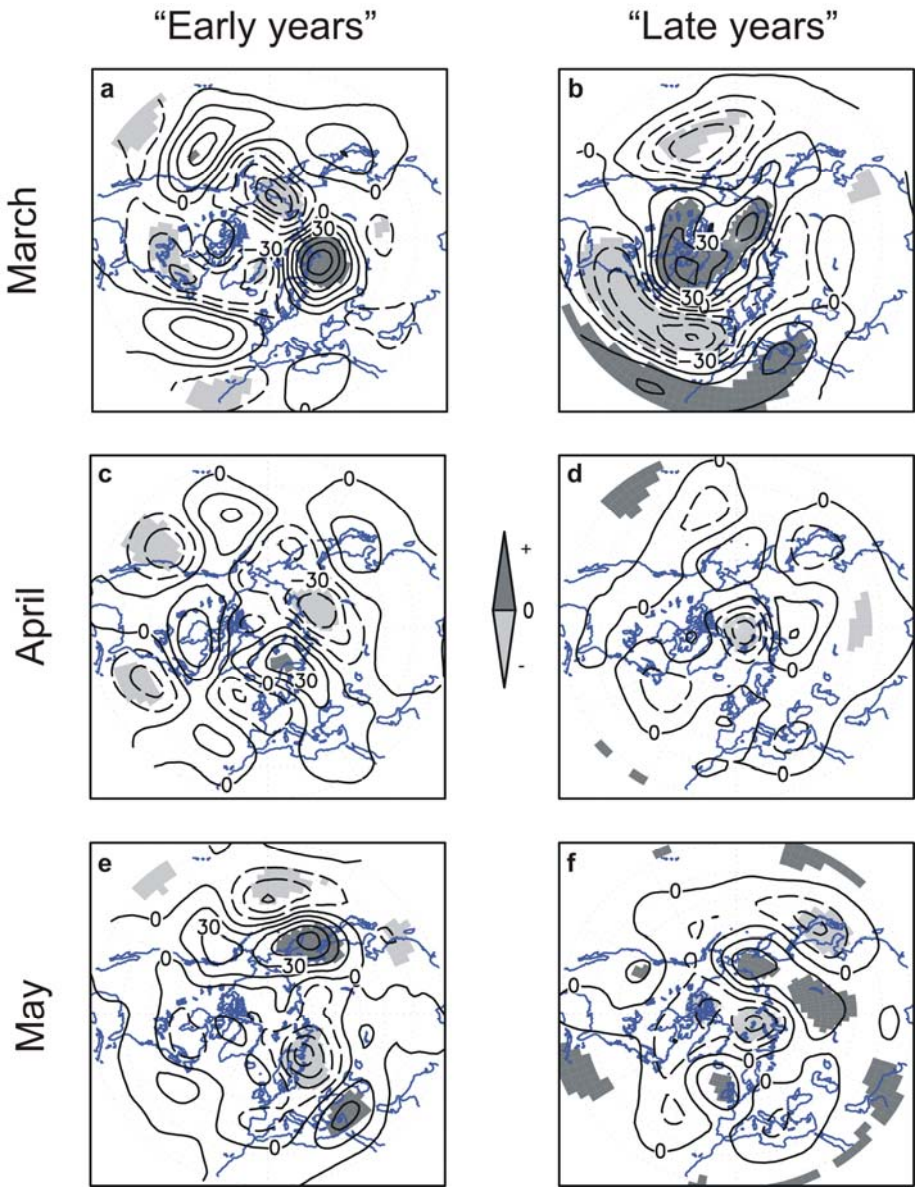

Figure VI.18. Composites of Z500 anomalies in March, April and May for "early years" "late years" for the EMAC REF-B1 simulation. Contour interval is 15 gpm. Shaded areas correspond to statistically significant values at 95%. Figure VI.8 shows the same but for ERA-40.

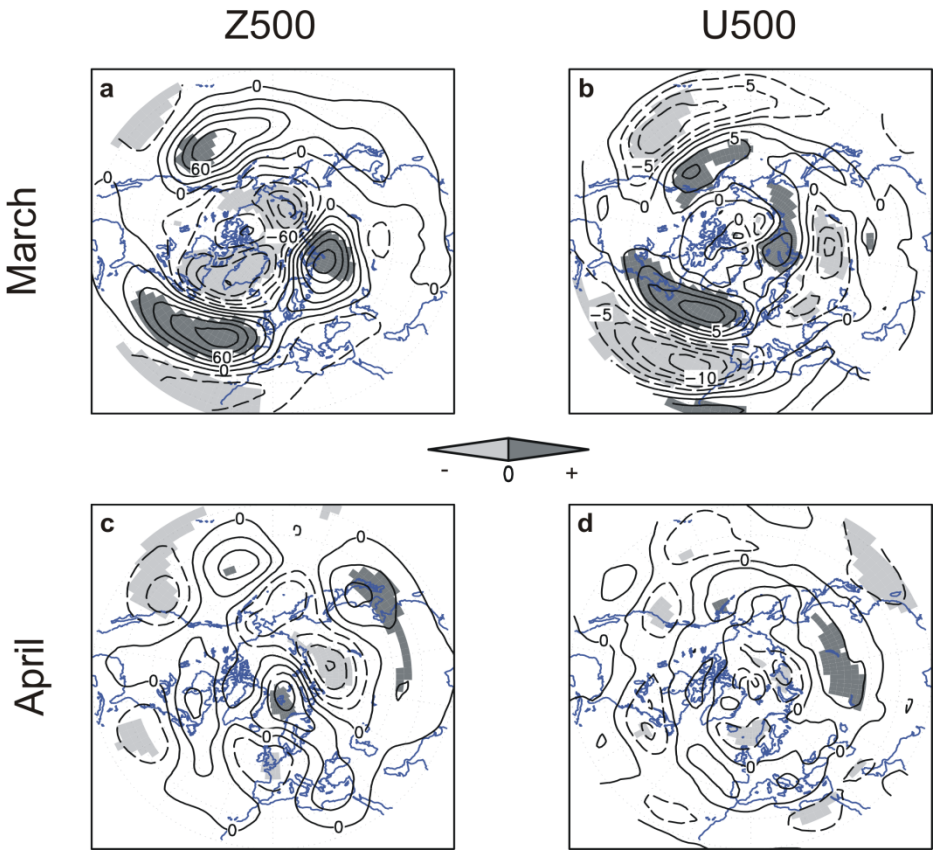

Figure VI.19. Early-minus-Late composites of (**left**) geopotential (contour interval: 15 gpm) and (**right**) zonal wind (contour interval: 2.5 m s^{-1}) at 500 hPa in March and April for the EMAC REF-B1 simulation. Light (dark) shading corresponds to negative (positive) statistically significant values at a 95% confidence level. Figure VI.9 shows the same but for ERA-40.

Storm-track activity

The analysis of the storm-track activity at 500 hPa in the two high-activity areas, i.e. North Atlantic and North Pacific [Chang et al., 2002], shows similar results as those obtained in the comparison of Z500 and U500 between ERA-40 and the model.

North Atlantic storm track

As can be seen in Figure VI.10 and VI.20, May is the month with the lowest statistical significance in the E-minus-L differences in storm-track activity in the North Atlantic sector for both the model and ERA-40 data. In the case of March, both datasets show in common statistically significant differences in the entrance region of the storm tracks (North American coast), although the statistical significance covers a more extensive region for the model results. In April the patterns of both datasets are the most similar: April in "early" ("late") years is characterized by a southward (northward) shift of the storm tracks over the North Atlantic sector compared to their monthly climatological position (Figure VI.21).

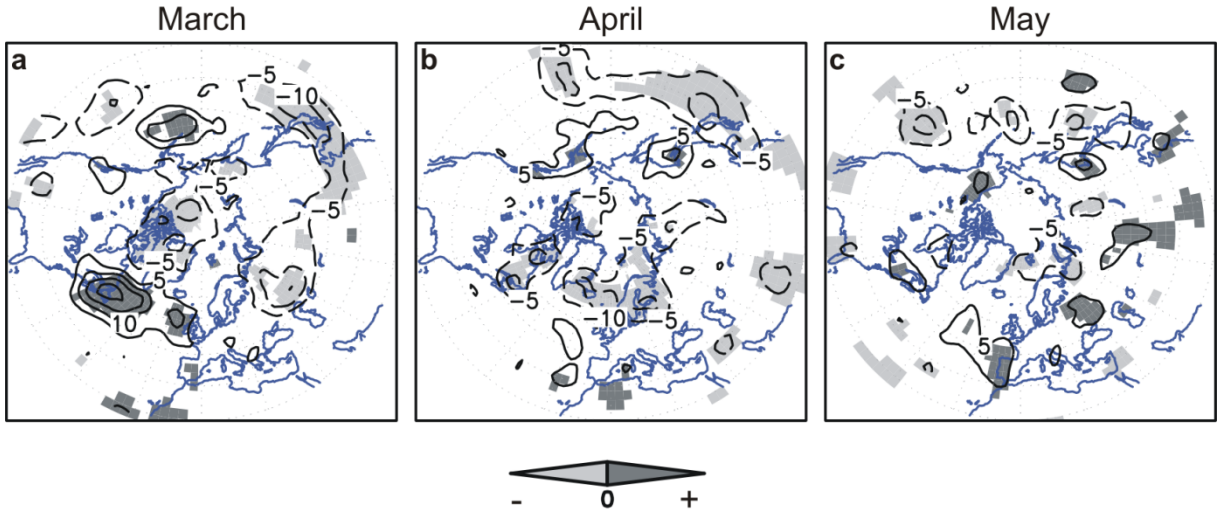

Figure VI.20. Early-minus-Late composites of storm-track activity at 500 hPa for March, April, and May for the EMAC REF-B1 simulation. Contour interval is 5 gpm. Light (dark) shading indicates negative (positive) statistically significant difference at a 95% confidence level. Zero contours are omitted for clarity. Figure VI.10 shows the same but for ERA-40.

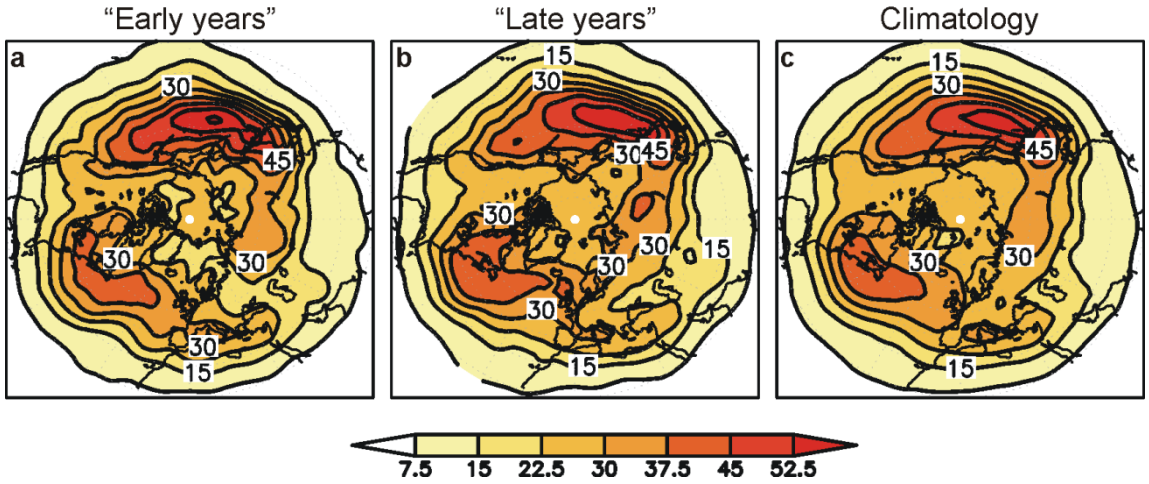

Figure VI.21. Composites of storm-track activity at 500 hPa in April for the EMAC REF-B1 simulation for "early years", "late years" and climatology. Contour interval: 7.5 gpm. Figure VI.11 shows the same but for ERA-40.

North Pacific storm track

In this sector, less agreement is found between the model and the reanalysis than in the North Atlantic basin, consistent with that observed in the Z500 field (compare Figure VI.10 vs VI.20). Thus, only similarities between both datasets are found in April, as a statistically significant center of differences over the Aleutian Islands is observed in both cases. This center can be an indication of a strengthening (weakening) and a northward (southward) shift of storm tracks associated with "early" ("late") years. Moreover, the most extensive differences between "early" and "late" years in the North Pacific region are found in March in ERA-40 and EMAC.

Nevertheless, apart from these similarities between the model and the reanalysis, important discrepancies between them have been found. For instance, in March, both datasets show opposite characteristics of the storm-track activity in the North Pacific region. Note that the modeled climatology of the storm track activity in March in the Pacific sector is different from that of the reanalysis (Figures VI.22c and VI.13c). Compared to the climatology, "early" ("late") years in the model are characterized by a northward (southward) shift of the storm tracks and just the opposite in the reanalysis data (Figure VI.22). Thus, maybe the model has some problems to reproduce some dynamical processes typical of the North Pacific region that are known to be related to the storm-track activity, such as interactions between background flow and transient eddies, baroclinic sources such as diabatic heating or barotropic effects [Chang et al., 2002].

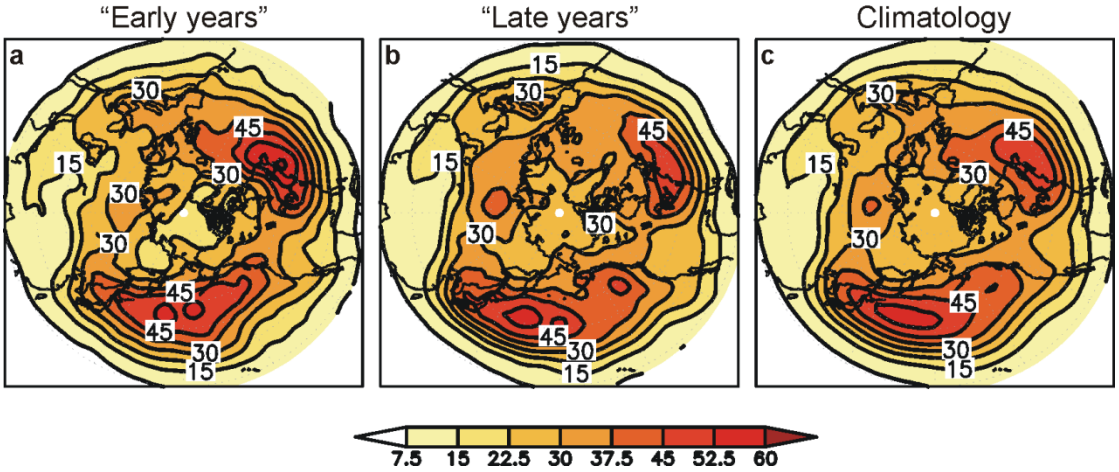

Figure VI.22. As Figure VI.21, but for March.

Final remarks

After this analysis, it can be concluded that, in spite of differences in the North Pacific region between the model and the reanalysis, an agreement between both of them has been observed in the general behavior of key aspects of the interannual variability in the timing of SFWs. Such aspects are the high variability in the date and its effects on springtime tropospheric fields. This agreement implies the validation of the EMAC REF-B1 simulation to reproduce the main results obtained in the analysis of the stratospheric final warmings in the recent past and present (issue of Section VI.1.a).

2. Stratospheric Final Warmings in a future climate: A possible trend in their timing?

Previous studies have shown a tendency of the polar vortex towards a longer persistence in the last decades due to climate change [e.g. Waugh et al., 1999; Offermann et al., 2003 and 2004; Langematz and Kunze, 2006]. Moreover, this trend has been related to relevant changes in the polar stratospheric circulation and chemistry [e.g.: Rex et al., 2004]. Thus, it seems interesting to analyze the existence of a possible trend in the timing of SFW under a changing climate in the future.

In Section VI.1.b, the ability of EMAC to simulate realistically the interannual variability in the timing of SFWs in the Northern Hemisphere has been proven for the recent past. According to this capability, the persistence of the future polar vortex is addressed in this section by comparing selected past and future periods simulated in two model simulations (1960/61-1999/2000 and 2060/61-2099/2100, respectively). The experiments are the same to those used in the study of MSWs in the future (Section V.2), i.e., SCN2d and NCC (i.e., under climate change and non-climate change conditions, respectively), both run with EMAC using the EMAC-FUB configuration.

To examine the persistence of the future polar vortex in these simulations, the dates of SFW have been identified by using the criterion of Black et al. [2006] and are shown in Table VI.5 for each period and experiment of study.

Almost no changes in the mean values are observed between the future and past periods and the two experiments. Actually, the resulting differences are not statistically significant. Concerning the standard deviations, there are also no statistical changes except for the last period, when those of the NCC and SCN2d are statistically significantly different but only at a 92.5% confidence level after a F-Fisher test. This might indicate that the interannual variability of the SFW date is different (in particular, higher) in the future. However, as the mean dates are already different for both runs in the past periods, it is not possible to derive a climate change signal from these results.

Table VI.5. Mean dates of SFW (day of year, doy) in the SCN2d and NCC simulations for the *past* (1960/61-1999/2000) and *future* (2060/61-2099/2100) periods, according to the criterion of Black et al. [2006]. The corresponding standard deviation is indicated in brackets.

	Past	Future
SCN2d	112 doy (std: 21 days)	113 doy (std: 22 days)
NCC	110 doy (std: 20 days)	110 doy (std: 17 days)

Focusing on the computed trends in the SFW date, similar slight positive values are obtained for both experiments (0.031 dy/yr in SCN2d and 0.025 dy/yr in NCC, Figure

VI.23). In addition, the corresponding Student's t-test applied confirms that these trends are not statistically different from zero, being their standard errors of the same magnitude as the trends (0.045 day/yr and 0.038 day/yr, respectively).

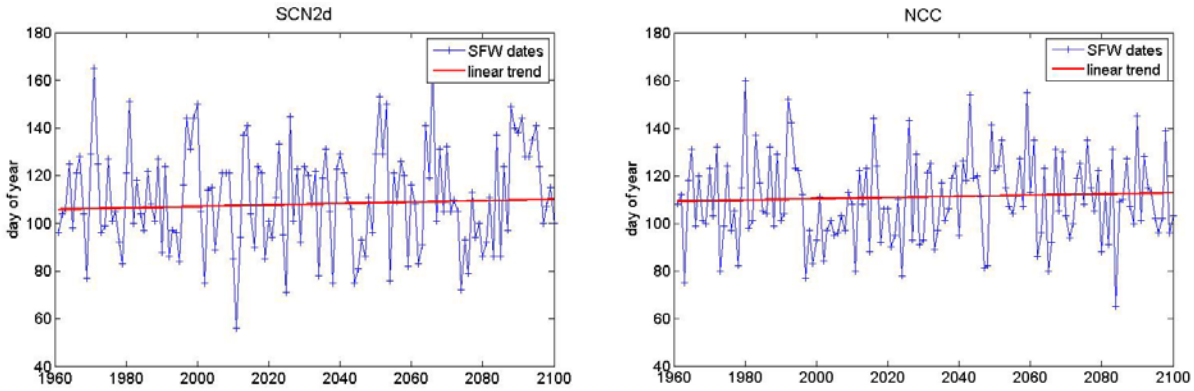

Figure VI.23. Dates of SFW in SCN2d and NCC experiments. The red line corresponds to the linear trend.

Final remarks

The above analysis leads us to conclude that no significant changes in the persistence of the polar vortex are expected due to the prescribed increase of greenhouse gas concentrations in the future. Briefly, in spite of all the consequences that the aforementioned increase has on wintertime stratospheric climate (seen in Section V.2), the seasonal transition of the polar stratospheric circulation in spring and related important features do not seem to be affected.

VII. Summary and conclusions

In this PhD thesis, an analysis of **stratospheric warmings in the Northern Hemisphere** and **their associated tropospheric-stratospheric feedbacks** has been carried out. The two most important types of stratospheric warmings of mid- and late winter (i.e., *major stratospheric warmings* and *stratospheric final warmings*, respectively) have been studied in two periods, the recent past and present (since 1960) and the future, to assess different aspects. The aim of this work has been to answer specific questions regarding stratospheric warmings that are currently under discussion or where there is no clear consensus among the scientific community.

The study has been carried out with two types of data, reanalysis data (both the European ERA-40 and the American NCEP/NCAR reanalysis) and model simulation output. The latter has been obtained from two types of models: a chemistry-climate model (EMAC, in some cases in EMAC-FUB configuration) and a coupled atmosphere-ocean general circulation model (EGMAM). In the case of the CCM simulations, they correspond to experiments that have been carried out according to the *Chemistry Climate Model Validation* (CCMVal) initiative of the WMO *Stratospheric Processes and their Role in Climate* (SPARC) project [Eyring et al., 2008]. Concerning EGMAM, it is one of the models used in the IPCC Fourth Assessment Report [2007].

The main conclusions of this study are presented here in correspondence with the specific objectives enumerated in the *Introduction* chapter (Section I.2).

Concerning **major stratospheric warmings** (MSWs), the results obtained in this study have led to the following conclusions:

Reproduction of MSWs in different types of model simulations

The ability of different types of experiments to reproduce MSWs in the past-present period and their tropospheric response has been assessed by analyzing three model simulations. The three simulations correspond to one AOGCM run under constant present-day conditions with EGMAM and two CCM experiments (a transient one and the other under present-day conditions). The comparison of model output of different types has helped to detect biases in each type. This has been very useful because previous comparative analyses have been carried out among output of models of only one kind, i.e. GCM or CCM. The results derived from this part of the PhD thesis have shown that:

- The analyzed CCM and the AOGCM can reproduce qualitatively well processes involved in MSWs. However, some aspects should be highlighted:
    - The AOGCM (EGMAM) shows a reduced interannual stratospheric variability and thus, a lower frequency of MSWs than the observed one (this latter computed from ERA-40 reanalysis). Nevertheless, once the tropospheric forcing has been sufficient to initiate the process, the

mechanism of the development of MSWs and downward propagation of their signal are well captured.

- The CCM (EMAC) presents an anomalously high stratospheric variability in early winter, which is common to models with the atmospheric ECHAM5 component. As a consequence, an extraordinarily high number of MSWs are performed in November and December that, in some cases, are unrealistic. However, processes associated with MSWs, particularly with those that take place in mid-winter, are well reproduced.

- The use of EGMAM to run a 300-yr simulation under constant present-day conditions has given evidence that long simulations in an AOGCM allow for the detection of multi-decadal climate variability in the stratosphere which has not been identified by other model simulations.

- Despite the mentioned deficiencies, EMAC and EGMAM models can be used reliably in further studies on stratosphere-troposphere coupling.

Tropospheric forcing of the stratosphere: Study of two observed Major Stratospheric Warmings

The analysis of two recent MSWs in 2009 and 2010 has helped to elucidate which trigger mechanisms are responsible for the abrupt amplification of the upward propagating wave activity prior to MSWs. Both MSWs have a very similar central date (end of January) and were preceded by a high peak of wave activity entering into the stratosphere. However, they happened under very different conditions of the external factors that influence the occurrence of MSWs (the Quasi-Biennial Oscillation, sunspot cycle or El Niño). Thus, the comparison between 2009 and 2010 MSWs has made possible to isolate the role of some processes and phenomena in triggering intense MSWs in observations [Ayarzagüena et al., 2011]. The main conclusions derived from this analysis can be summarized as follows:

- In some occasions, MSWs can originate from an extraordinarily strong forcing from tropospheric planetary waves associated with intense circulation anomalies, such as a blocking event. This was the case for the 2009 MSW. Strong anomalies associated with a deep ridge over the Pacific led to the amplification of upward wave activity and as a result, an exceptionally strong MSW happened.

- In other cases, certain combinations of phases of solar cycle, QBO and ENSO can influence the atmospheric state by modifying the vertical propagation of planetary waves into the stratosphere. In particular, the ENSO phenomenon

has revealed to be related to an enhancement of the injection of planetary wave activity into the stratosphere in January due to the amplification of stationary wavenumber-1 wave activity. In this study, the ENSO impact on climatological tropospheric waves has been shown to be the main responsible mechanism for the onset of the 2010 MSW.

Possible future changes in major stratospheric warmings

Future projections of MSWs in two transient CCM simulations have been analyzed in detail, studying aspects not yet evaluated in the literature, such as possible variations in the development of MSWs and in the downward propagation of their signal. Both transient simulations extend from recent past (1960) until 2100 and have identical model characteristics, but one of them for a climate change scenario and the other one under non-climate change conditions. The main conclusions derived from this analysis in a future climate are indicated next:

- Main properties of MSWs, such as their intensity, mean frequency per winter and the preceding wave activity do not change as a consequence of the prescribed increase of greenhouse gas (GHG) concentrations in the future (according to the A1B scenario, IPCC [2000]).

- After removing slowly varying trends driven by external forcings (in this case, the increase of GHG concentrations), the internal variability associated with MSWs (that related to the stratosphere-troposphere coupling as well) does not show significant changes in the future either.

- Although changes were not identified in the internal atmospheric variability, the typical downward propagation of the MSW signal and its tropospheric response are not clearly observed in the future. The climate change signal seems to mask the MSW fingerprint in the troposphere.

- The life cycle of future projected MSWs is also affected by the increase of GHG concentrations. The future MSWs tend to happen more abruptly and the polar vortex recovers more quickly after them.

- The separated analysis of the polar stratospheric state in early and mid-winter periods has highlighted a different response of the stratosphere to climate change in these two intraseasonal periods:

    - Radiative cooling dominates changes in early winter, leading to fewer MSWs in November and December.

    - Dynamical processes, in particular the intensification of the tropospheric wave activity due to the increase of GHG concentrations, strongly influence the variations in mid-winter polar stratospheric

circulation. As a result, an increase in the frequency of MSWs is obtained in January.

The different response of the polar stratosphere to climate change in early and mid-winter should be taken into account in following analyses of the impact of climate change in the polar stratospheric circulation. In particular, it has been highlighted the relevance of distinguishing between these two periods in contrast to most studies on this topic that did not make this distinction.

In the case of **stratospheric final warmings** (SFWs), the derived conclusions from the addressed aspects are explained next:

Study of a relationship between variations in the timing of SFWs and changes in the troposphere

The analysis of monthly tropospheric fields in springtime has shown a link between changes in the tropospheric circulation and the interannual variability of SFWs [Ayarzagüena and Serrano, 2009]. The study has been carried out with the ERA-40 dataset. The aforementioned link can be described as follows:

- Regarding dynamical aspects, relevant interannual differences in the propagation of stationary waves are found, most of them explained by variations in ultra-long ones. These differences are more important in March than in April, with opposite behavior in some areas between both months.

- A downward propagation of statistically significant differences in the monthly zonal-mean zonal wind between years with a very persistent vortex and years with a non-persistent one is observed. In April these differences reach the lowermost stratosphere and even the troposphere at high latitudes.

- The late or early occurrence of the SFW seems to have some impact on the tropospheric circulation in March and April, showing changes in storm track activity, geopotential height and zonal wind in the middle troposphere.

- Unlike in wintertime, the stratosphere-troposphere coupling in springtime associated with the timing of SFWs has been found not to be totally dominated by the Northern Annular Mode. This result has provided a new contribution in the literature with respect to previous work based on the differences in the tropospheric circulation between NAM phases [i.e.: Baldwin and Dunkerton, 2001].

Validation of CCMs to reproduce the interannual variability of SFWs in the Northern Hemisphere

A CCM has been validated, assessing its ability to reproduce the interannual variability of SFWs dates and, for the first time, their associated changes in tropospheric circulation. The validation has been achieved by the comparison of the results derived from observations with those from a transient CCM simulation that covers the same period of time (1960-2000). The comparative analysis has shown that:

- The CCM can reproduce reasonably well the high interannual variability in the timing of SFWs in the Northern Hemisphere.
- There is a general agreement between the model and observations regarding the impact of the interannual variability of SFWs in the springtime tropospheric circulation.
- However, there are some discrepancies between the model and observations in the reproduction of the link between tropospheric changes and the timing of SFWs in the North Pacific region. This was suggested to be probably related to a deficiency of the model in this region.

Stratospheric Final Warmings in a future climate: A possible trend in their timing?

The question of a possible trend of the polar vortex to persist longer in the future has been addressed by comparing selected past and future periods simulated in two transient CCM experiments, which only differ in the inclusion or not of a prescribed climate change. The conclusion from the comparative analysis has been:

- Despite the changes observed in early and mid-winter in the future stratosphere, the seasonal transition of the polar stratospheric circulation in spring does not seem to be affected by the increasing GHG concentrations prescribed in the analyzed simulations.

VIII. Outlook

Results of this PhD thesis have suggested new aspects to explore in order to continue the improvement of the knowledge of stratospheric warmings in the Northern Hemisphere. In particular:

- ✓ In this study, the influence of the oceanic variability on MSWs, in particular of the ENSO, has been proven. Thus, a further study of the impact of changes in SSTs on the polar stratospheric circulation would be interesting. For instance, the assessment of possible future variations in MSWs would require the analysis of these events in simulations performed with CCMs that also have a coupled interactive ocean such as the new EMAC-FUB simulation with coupled ocean.

- ✓ Moreover, in this PhD thesis attention has only been paid to the possible fingerprint of stratospheric warmings in the NH extratropics. Nevertheless, very recent studies have shown that MSWs might also have an effect on farther regions, showing the possible existence of an inter-hemispheric coupling during these events [Limpasuvan et al., 2011]. Thus, the analysis of changes in atmospheric circulation in the tropics and in the Southern Hemisphere would be an attractive topic for a future research.

IX. Resumen en español

1. Introducción

Si bien la mayoría de los procesos más importantes de la atmósfera se producen en la *troposfera*, que es la capa más próxima a la superficie terrestre, diversos estudios relativamente recientes han aportado evidencias observacionales de que la estratosfera influye también en las condiciones troposféricas [p.ej.: Baldwin and Dunkerton, 1999, 2001; Baldwin and Thompson, 2009].

La *troposfera*, que se extiende hasta una altura de 10 km aproximadamente, contiene alrededor del 85% de la masa total de la atmósfera. La temperatura en la troposfera presenta una distribución vertical que permite los movimientos verticales de aire, la cual es, además, completamente distinta a la de la *estratosfera*, capa inmediatamente superior, caracterizada por la estratificación estable del aire. Por todo ello, tradicionalmente se ha considerado que los procesos troposféricos eran los únicos capaces de modificar el tiempo en superficie, sin influencia de las condiciones atmosféricas en niveles superiores. Sin embargo, en los últimos 50 años esta visión ha cambiado sustancialmente, debido a la multitud de evidencias encontradas acerca del acoplamiento entre la troposfera y la estratosfera. En primer lugar, se determinó que la troposfera podía influir en el estado de la estratosfera a través de la propagación ascendente de perturbaciones de escala planetaria desde esa capa hasta la atmósfera alta bajo ciertas condiciones [Charney and Drazin, 1961]. De esta manera, se le confería a la estratosfera un papel meramente pasivo. Más tarde, diversos estudios [Baldwin and Dunkerton, 1999, 2001] aportaron pruebas observacionales sobre el hecho de que la estratosfera posee también un papel activo en la determinación del tiempo en superficie. Así, se ha observado cómo fuertes anomalías estratosféricas descendían a lo largo de la columna atmosférica hasta niveles troposféricos en una escala de semanas, con las consecuentes implicaciones en el tiempo en superficie. Todo ello ha conducido a considerar la necesidad de incluir la circulación estratosférica en las predicciones meteorológicas de más de 10 días [p. ej.: Baldwin et al., 2003; Jung and Barkmeijer, 2006], aunque quedan aún muchas dudas acerca de cómo realizar esto. De ahí, en parte, la motivación para llevar a cabo el presente estudio.

Uno de los fenómenos más prominentes de la estratosfera polar invernal son los **calentamientos estratosféricos**, los cuales poseen efectos importantes en la circulación atmosférica. En concreto, estos fenómenos consisten en un calentamiento en la estratosfera polar, que van acompañados de un descenso brusco de la intensidad del flujo estratosférico e incluso, en ocasiones, de la inversión de la circulación típica invernal en esa región (el denominado *vórtice polar estratosférico*, Figura IX. 1a) [Andrews et al., 1987]. Se distinguen distintos tipos de calentamientos estratosféricos dependiendo de su intensidad y momento de ocurrencia. En el caso de los meses centrales de invierno, los calentamientos más intensos son los llamados *calentamientos*

estratosféricos mayores (MSWs, acrónimo en inglés[1]). Estos MSWs se caracterizan por una rotura súbita del vórtice polar (Figura IX.1b) y una recuperación posterior de este último. A finales del invierno, la transición al régimen estival de temperaturas más altas y vientos del este se realiza todos los años dando lugar a los *calentamientos estratosféricos finales* (SFW, acrónimo en inglés[2]). Mientras que los SFWs ocurren cada primavera en los dos hemisferios, la casi totalidad de los MSWs observados corresponden a la estratosfera boreal debido a la diferencia a la menor actividad de ondas de Rossby en el hemisferio austral. El único MSW en el hemisferio sur, hasta la fecha, sucedió en 2002 [Roscoe et al., 2005].

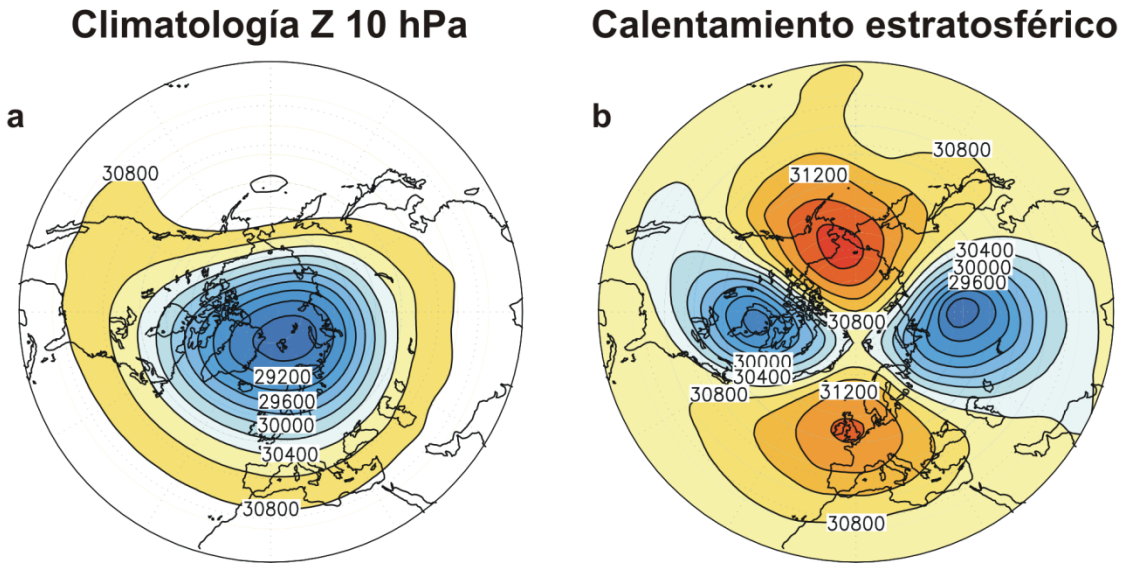

Figura IX.1. (a) Climatología de la altura del geopotencial (mgp) en 10 hPa para los meses invernales (diciembre-enero-febrero) en el periodo 1979-2010. **(b)** Mapa de la altura del geopotencial (mgp) en 10 hPa correspondiente a un calentamiento estratosférico que sucedió el 24 de enero de 2009. Intervalo de contornos: 200 mgp. Base de datos: reanálisis NCEP/NCAR.

El interés de la comunidad científica por el estudio de los fenómenos mencionados ha ido creciendo desde su descubrimiento, hecho ocurrido hace casi 60 años por Scherhag [1952]. De hecho, en los últimos años el número de trabajos dedicados a este tema ha aumentado considerablemente, sobre todo con el objetivo de poder aplicar esos conocimientos a la determinación de los posibles efectos de cambios climáticos en el futuro.

A pesar de los esfuerzos realizados hasta la fecha, existe aún mucha incertidumbre en el conocimiento de los calentamientos estratosféricos, en particular, en la comprensión de los mecanismos que los desencadenan. Aunque algunos estudios han identificado el incremento súbito de la actividad de onda que se propaga hacia arriba desde la

[1] MSW: Major Stratospheric Warming
[2] SFW: Stratospheric Final Warming

troposfera como responsable de tales eventos estratosféricos [p. ej.: Matsuno, 1971; Polvani and Waugh, 2004; Black and McDaniel, 2007], se continúan investigando cuáles pueden ser los mecanismos específicos causantes de esa amplificación abrupta de actividad de onda. Algunos autores han relacionado dicha amplificación con la aparición de patrones de la circulación troposférica, como los "bloqueos" [p. ej.: Labitzke, 1965; Martius et al., 2009; Woollings et al., 2010] o los derivados de los efectos de la cubierta de nieve sobre Eurasia [Orsolini and Kvamstø, 2009]. No obstante, se desconoce aún con certeza la naturaleza de la conexión entre estos posibles mecanismos y la ocurrencia de los calentamientos estratosféricos. Además, existen otros factores externos que añaden más incertidumbre en este tema, tales como la modulación de la circulación polar estratosférica por fenómenos como: la Oscilación Cuasi-Bienal (QBO, acrónimo en inglés[3]) [Holton and Tan, 1980], la actividad solar [p. ej.: Labitzke and van Loon, 1988] o el calentamiento anómalo de la superficie oceánica, en particular del conocido El Niño-Oscilación del Sur (ENSO, acrónimo en inglés[4]) [p. ej.: Ineson and Scaife, 2008; Cagnazzo and Manzini, 2009].

Una consecuencia de la mencionada incertidumbre es que las proyecciones de los modelos climáticos para el futuro no proporcionan un panorama común de cambio en la estratosfera. Así, mientras que algunos modelos apuntan a una intensificación y mayor persistencia de la circulación estratosférica polar de invierno en clima futuro [p.ej.: Shindell et al., 2001], otros muestran un debilitamiento de esta circulación debida a un incremento en el forzamiento futuro de onda troposférica [p.ej.: Schnadt et al., 2002; Huebener et al., 2007].

La presente tesis doctoral aborda algunos de los aspectos relativos a los calentamientos estratosféricos que actualmente muestran mayor incertidumbre o que son aún desconocidos. Por ello, desde esta perspectiva se analizan los mecanismos desencadenantes de estos fenómenos, su impacto en la circulación troposférica así como los posibles cambios en el futuro debidos a un supuesto incremento en la concentración de gases de efecto invernadero. Este análisis se realiza usando tanto datos de reanálisis como simulaciones con modelos climáticos capaces de reproducir de manera realista los procesos troposféricos y estratosféricos.

2. Objetivos

Partiendo de las consideraciones anteriores, el objetivo principal de esta tesis doctoral es el de **contribuir a mejorar el conocimiento actual** sobre **los calentamientos estratosféricos en el hemisferio norte** y, en especial, de las **interacciones estratosfera-troposfera asociadas** a estos fenómenos. Con este fin, se

[3] QBO: Quasi-Biennal Oscillation
[4] ENSO: El Niño-Southern Oscillation

han investigado detalladamente diferentes aspectos de estos eventos que, o bien no se habían investigado hasta la fecha o en los que no existe todavía consenso.

En particular, este estudio se centra en los dos tipos de calentamientos más relevantes, los **calentamientos estratosféricos mayores** y los **calentamientos estratosféricos finales**. Dicho análisis se ha realizado en dos periodos de tiempo distintos: el pasado reciente y presente (desde 1960) y el futuro. Además, se han utilizado datos de fuentes distintas: reanálisis (ERA-40 y NCEP/NCAR), considerados en cierta medida como observaciones; y salidas de simulaciones, realizadas a su vez con diferentes tipos de modelos de clima. En concreto, se han usado salidas de un modelo atmosférico con química interactiva (EMAC, ejecutado también bajo la configuración EMAC-FUB) y de un modelo atmosférico con océano acoplado (EGMAM). El primero ha sido uno de los modelos estudiados en la Iniciativa CCMVal[5] del proyecto SPARC[6] de la Organización Meteorológica Mundial [Eyring et al., 2008], y el EGMAM es uno de los modelos utilizados en el cuarto informe del IPCC[7] [2007]. Más detalles sobre las simulaciones con modelos empleadas en este trabajo están resumidos en la Tabla III.1. (Capítulo III).

En el caso de los **calentamientos estratosféricos mayores**, (MSWs) se exponen a continuación las preguntas específicas abordadas en este estudio. Se incluye también una breve descripción de cómo se ha llevado a cabo dicho análisis.

Pasado reciente y presente

- *¿En qué aspectos relacionados con los MSWs los modelos climáticos con química interactiva (CCMs, acrónimo en inglés[8]) y los modelos de circulación general de atmósfera-océano (AOGCMs, acrónimo en inglés[9]) presentan deficiencias?* (Capítulo V.1a)

  Para responder a esta pregunta, se han estudiado los MSWs identificados en tres simulaciones distintas y a continuación, se han comparado con datos de reanálisis. Dos de estas simulaciones se han realizado con un CCM, una de ellas bajo *condiciones transitorias* y la otra bajo *condiciones constantes actuales*. La tercera simulación se ha ejecutado también bajo condiciones constantes actuales, pero con un AOGCM. El análisis de las posibles diferencias en la representación de los MSWs permite determinar la importancia que tienen ciertos procesos en estos eventos estratosféricos, procesos que están descritos de manera distinta en cada modelo y/o simulación.

[5] CCMVal: Chemistry Climate Model Validation
[6] SPARC: Stratospheric Processes and their Role in Climate (www.sparc-climate.org)
[7] IPCC: Intergovernmental Panel on Climate Change (www.ipcc.ch)
[8] CCM: Chemistry Climate Model
[9] AOGCM: Atmosphere-Ocean General Circulation Model

- *¿Cuáles son los mecanismos más importantes que desencadenan una amplificación abrupta de la actividad de onda troposférica, anterior a un MSW? ¿Y cómo otros factores, que no estén directamente relacionados espacial y temporalmente con los MSWs, pueden modular este incremento repentino de actividad de onda?* (Capítulo V.1b)

  Para encontrar respuesta a estas dos preguntas, se han examinado dos MSWs recientes, que ocurrieron en 2009 y 2010. Ambos MSWs fueron precedidos por unas de las inyecciones de actividad de onda troposférica más intensas observadas hasta la actualidad (desde 1958). Además, los dos MSWs se produjeron aproximadamente en la misma fecha, finales de enero. Sin embargo, los típicos factores externos que influyen en la ocurrencia de un MSW (la Oscilación Cuasi-Bienal, el ciclo solar o El Niño) presentaron características distintas en los dos inviernos, siendo favorables en 2010 y desfavorables en 2009.

Futuro

- *¿Tendría algún efecto sobre los MSWs un incremento de los gases de efecto invernadero en el futuro?* (Capítulo V.2)

  La comparación de aspectos relevantes de los MSWs en el futuro (incluyendo los cambios troposféricos asociados a éstos) entre dos simulaciones realizadas con un CCM común ha permitido contestar a la pregunta anterior. Ambas simulaciones cubren el periodo 1960-2100, pero mientras que una de ellas incluye un cierto cambio climático prescrito, la otra no.

Con respecto a los **calentamientos estratosféricos finales** (SFWs), este estudio intenta responder a las siguientes preguntas:

Pasado reciente y presente

- *¿Existe una relación entre las variaciones en la fecha de ocurrencia de los SFWs y cambios en la troposfera?* (Capítulo VI.1a)

  Este objetivo se ha acometido analizando los cambios en campos troposféricos, promediados mensualmente, de variables atmosféricas que en cierto modo están asociadas con la variabilidad de la fecha de ocurrencia de los SFWs observados (desde 1960 a 2000).

- *¿Son capaces los CCMs de reproducir la variabilidad interanual observada de la ocurrencia de los SFWs? Si es así, ¿pueden simular dichos modelos la misma*

relación entre las fechas de ocurrencia y las anomalías de circulación troposférica que la identificada en las observaciones? (Capítulo VI.1b)

La validación de un CCM para reproducir la variabilidad interanual de la fecha de los SFWs y los cambios asociados en la circulación troposférica se ha llevado a cabo mediante la comparación de los resultados obtenidos a partir de las observaciones con aquéllos de una simulación CCM transitoria.

Futuro

- *¿Presentará una tendencia en el futuro la persistencia del vórtice polar estratosférico?* (Capítulo VI.2)

  Este aspecto es tratado mediante la comparación de periodos seleccionados del pasado y el futuro en dos simulaciones de un CCM, una de ellas bajo condiciones de un cambio climático prescrito y la otra no.

3. Conclusiones y aportaciones fundamentales de la tesis

Las principales conclusiones y aportaciones de esta tesis se exponen a continuación, separadas en los dos tipos de calentamientos estudiados.

En el caso de los **calentamientos estratosféricos mayores (MSWs)**, los resultados obtenidos en este estudio nos han llevado a concluir lo siguiente:

Reproducción de los MSWs en diferentes tipos de simulaciones con modelos de clima

De esta parte del estudio, se puede deducir que los modelos atmosféricos empleados en el estudio, tanto el modelo con química interactiva (CCMs), como el modelo con océano acoplado (AOGCMs) son capaces de reproducir cualitativamente bien los procesos involucrados en el desarrollo de los MSWs. No obstante, algunos aspectos importantes a señalar son los siguientes:

- La variabilidad interanual estratosférica del AOGCM (EGMAM) es reducida y con ello, reproduce una menor frecuencia de MSWs que las observaciones. Sin embargo, una vez que el forzamiento troposférico es lo suficientemente intenso como para iniciar el proceso, el mecanismo de desarrollo de los MSWs y la propagación descendente de la señal de éstos son semejantes al observado.

- El CCM (EMAC) presenta una variabilidad estratosférica alta en los primeros meses de invierno, lo cual es común a los modelos que poseen la misma componente atmosférica, ECHAM5. Una consecuencia de ello es que EMAC simula

un número excesivamente elevado de MSWs en noviembre y diciembre, la mayor parte de los cuales con características atípicas respecto a los MSWs reales. No obstante, los procesos asociados a los MSWs, en particular a los calentamientos que suceden en los meses centrales del inverno, están bien reproducidos por el modelo.

- El uso del EGMAM para ejecutar una simulación de 300 años, con condiciones constantes actuales, ha mostrado que simulaciones largas en un AOGCM permiten identificar la variabilidad climática multi-decadal en la estratosfera, la cual no se puede reproducir en otro tipo de simulaciones con modelos.

No obstante, es importante resaltar que, a pesar de las deficiencias mencionadas, EMAC and EGMAM pueden emplearse en estudios sobre el acoplamiento troposfera-estratosfera, tales como los acometidos en el presente trabajo, y cuyas conclusiones se exponen seguidamente.

Forzamiento troposférico de la estratosfera: Estudio de dos MSWs recientes

El análisis de dos MSWs recientes, los de 2009 y 2010, ha permitido profundizar en el estudio de los principales mecanismos que desencadenan una amplificación súbita de la actividad de onda troposférica ascendente y con ello, la ocurrencia de un MSW [Ayarzagüena et al., 2011]. Como ya se ha indicado anteriormente, estos dos MSWs presentaron características comunes, como su intensidad o la fecha de ocurrencia, pero las condiciones de los factores externos que modulan los MSWs eran completamente distintas. Las principales conclusiones que se derivan de este estudio específico han sido:

- Los MSWs se pueden originar, en algunas ocasiones, simplemente a partir de un forzamiento extraordinariamente intenso de ondas planetarias troposféricas asociado con anomalías intensas de circulación, como, por ejemplo, un bloqueo. Éste fue el caso del MSW de 2009. En esa ocasión, anomalías muy fuertes asociadas a una fuerte dorsal sobre el Pacífico condujeron a la amplificación de actividad de onda ascendente y con ello, a que se produjera un fuerte MSW.

- En otras ocasiones, ciertas configuraciones de fases del ciclo solar, QBO y ENSO pueden influir en el estado atmosférico y modificar la propagación vertical de ondas planetarias en la estratosfera. En este estudio se ha mostrado que el fenómeno ENSO está íntimamente relacionado con un incremento de la inyección de actividad de onda troposférica en enero debido a la amplificación de la actividad de ondas estacionarias con número de onda 1. Además, se ha probado que el impacto del ENSO en las ondas troposféricas climatológicas fue el principal mecanismo responsable del comienzo del MSW de 2010.

Posibles cambios en los calentamientos estratosféricos mayores del futuro

En esta parte del estudio, se han examinado con detalle las proyecciones de MSWs en el futuro obtenidas con dos simulaciones transitorias del modelo con química interactiva, EMAC. Los resultados obtenidos son de particular importancia, dado que los aspectos analizados de los MSWs, tales como los posibles cambios en su evolución y en la propagación descendente de la señal no habían sido estudiados hasta la fecha. A continuación, se enumeran las conclusiones más relevantes de este análisis.

- En primer lugar, el incremento prescrito de las concentraciones de gases de efecto invernadero (correspondiente al escenario A1B; IPCC [2000]) no ha dado lugar a variaciones estadísticamente significativas en aspectos importantes de los MSWs, tales como su intensidad, su frecuencia media por invierno y la actividad de onda que precede a su ocurrencia.

- Del mismo modo, después de eliminar las tendencias asociadas a forzamientos externos (en este caso, el incremento de concentraciones de GHG), se ha observado que la variabilidad interna relativa al acoplamiento troposfera-estratosfera asociado a los MSWs no muestra cambios importantes en el futuro.

- No obstante, aunque no se hayan identificado cambios futuros en la variabilidad interna asociada a los MSWs, la típica propagación descendente de la señal de los MSWs y la respuesta troposférica a éstos tampoco se ha observado con claridad. Por tanto, se podría afirmar que la señal asociada al cambio climático es más intensa que la variabilidad interna asociada a la ocurrencia de MSWs, de manera que la primera esconde la huella de éstos en la troposfera.

- La evolución temporal de los MSWs se ve modificada como consecuencia de los efectos sobre la estratosfera polar del incremento de la concentración de GHG en el futuro. Así, los futuros MSWs tienden a suceder de manera más abrupta y la posterior recuperación del vórtice polar se produce más rápidamente.

- La respuesta de la estratosfera polar invernal al incremento prescrito de las concentraciones de GHGs en el futuro es distinta dependiendo de los meses del invierno:

    - En los primeros meses de invierno (noviembre y diciembre), el enfriamiento radiativo domina los cambios observados en la estratosfera polar, lo cual conduce a una menor ocurrencia de MSWs en este periodo.

    - En los meses centrales de invierno (enero y febrero), los procesos dinámicos y, muy especialmente, la intensificación de la actividad de onda troposférica juegan el papel más importante en la determinación de los cambios en la circulación polar estratosférica. Como resultado, se ha obtenido para el futuro un incremento de la frecuencia de MSWs en enero.

En cuanto a los **calentamientos finales estratosféricos (SFWs)**, se detallan las principales conclusiones y aportaciones.

Estudio de una posible relación entre las variaciones en la fecha de los SFWs y cambios en la troposfera

El análisis de campos troposféricos mensuales en primavera ha mostrado que existe una conexión entre cambios en la circulación troposférica y la variabilidad interanual de los SFWs [Ayarzagüena and Serrano, 2009]. El estudio se ha llevado a cabo con datos del ERA-40. La conexión mencionada se caracteriza por las siguientes propiedades:

- En cuanto a aspectos dinámicos, se han encontrado diferencias interanuales importantes en la propagación de ondas estacionarias, en particular, en las de mayor longitud de onda. Estas diferencias son más importantes en marzo que en abril, mostrando, además, un comportamiento opuesto en algunas regiones entre ambos meses.

- Las diferencias estadísticamente significativas en la media zonal del viento zonal entre los años con un vórtice muy persistente y años con vórtice de menor persistencia se propagan hacia abajo en el tiempo. Como consecuencia, en abril tales diferencias alcanzan los niveles más bajos de la estratosfera e incluso la troposfera en latitudes altas. De este modo, la señal relativa al estado distinto de la estratosfera polar desciende a lo largo de la columna atmosférica.

- La ocurrencia temprana o tardía del SFW es capaz de influir en los campos de la troposfera media en marzo y abril, produciendo cambios en la actividad de las trayectorias de las depresiones (*storm tracks*), el geopotencial y el viento zonal.

- A diferencia de lo que sucede en invierno, el acoplamiento troposfera-estratosfera en primavera, y en particular, el asociado con la fecha de los SFWs, no se encuentra totalmente determinado por el Modo Anular del Norte (NAM, acrónimo en inglés[10]). Este resultado ha supuesto una contribución nueva en la temática con respecto a la mayoría de trabajos previos que relacionaban variaciones en la intensidad de la circulación estratosférica con cambios en la troposfera basándose únicamente en diferencias entre las fases del NAM [p.ej.: Baldwin and Dunkerton, 2001].

[10] NAM: Northern Annular Mode

Validación de CCMs para reproducir la variabilidad interanual de SFWs en el hemisferio norte

En esta parte del estudio, se ha evaluado la capacidad de un CCM (EMAC) para reproducir la variabilidad de las fechas de los SFWs y, por primera vez, para simular los cambios en la circulación troposférica asociados a dicha variabilidad. Esta validación del CCM se ha llevado a cabo mediante la comparación de los resultados obtenidos para las observaciones con aquéllos procedentes de una simulación transitoria con EMAC, cubriendo el mismo periodo de tiempo (1960-2000). Dicho análisis comparativo ha mostrado los siguientes aspectos importantes:

- El CCM es capaz de reproducir razonablemente bien la alta variabilidad interanual de los SFWs en el hemisferio norte.
- En general, la simulación del modelo y las observaciones coinciden en cuanto al impacto de la variabilidad interanual de los SFWs en la circulación troposférica de primavera.
- No obstante, se han encontrado algunas discrepancias entre el modelo y las observaciones para reproducir la conexión entre cambios troposféricos y la fecha de los SFWs, especialmente en la región del Pacífico Norte. Se ha sugerido que esto podría relacionarse con alguna deficiencia del modelo en simular ciertos procesos en esta región.

Los calentamientos finales estratosféricos en un clima futuro: ¿Poseen una posible tendencia en su fecha de ocurrencia?

La comparación de periodos seleccionados del pasado y del futuro en dos simulaciones transitorias de un CCM, con y sin condiciones de un cambio climático prescrito, ha permitido concluir lo siguiente:

- A pesar de los cambios identificados en la proyección futura de la circulación estratosférica invernal (principios y meses centrales), la transición estacional de la circulación polar estratosférica al verano no parece verse afectada por el incremento de las concentraciones de GHG prescrito en la simulación analizada.

Principales aportaciones

A continuación, se indican las aportaciones más importantes de esta tesis doctoral:

- Los resultados de la comparación de los MSWs de 2009 y 2010 han aportado nuevas evidencias de la importancia del forzamiento de onda troposférica para la generación de MSWs, además de las ya conocidas influencias externas del

ciclo solar, la QBO y el ENSO. De este modo, el presente análisis subraya la necesidad de prestar especial atención y mejorar la representación en los modelos de clima de dicho forzamiento de onda y de sus fenómenos asociados. Esto permitiría obtener una mejor representación de los MSWs y por extensión, de la variabilidad estratosférica. Una aplicación muy importante de esta mejora en la representación del forzamiento de onda troposférica tendría que ver con las proyecciones de los MSWs en el futuro, dado que ciertos estudios [e.g.: Haklander et al., 2008; Garcia and Randel, 2008] han mostrado un incremento de actividad de onda troposférica como consecuencia de un aumento de las concentraciones de gases de efecto invernadero. Finalmente, es importante indicar que dicho estudio de los MSWs en 2009 y 2010 ha dado lugar a una publicación [Ayarzagüena et al., 2011] que se adjunta en el Apéndice 4.

- En lo referente a los SFWs, a partir de datos observacionales, se han aportado evidencias de que la variabilidad interanual de la fecha de ocurrencia de estos fenómenos afecta a la circulación troposférica. Estos resultados son los mismos que los obtenidos en un estudio realizado paralelamente, pero considerando un periodo más largo de años, tal que el carácter novedoso de los mismos ha sido reconocido a través de la publicación de un artículo [Ayarzagüena and Serrano, 2009; incluido en el Apéndice 4].

- En cuanto a la capacidad de los modelos climáticos empleados (un modelo con química interactiva y otro con océano acoplado) en reproducir los MSWs, las respectivas simulaciones analizadas han proporcionado pruebas de la fiabilidad del uso de tales modelos para el estudio de la variabilidad estratosférica boreal. Asimismo, es también importante destacar que, por primera vez en la literatura, se ha comprobado si un modelo climático con química interactiva es capaz de reproducir la variabilidad interanual de los SFWs y en especial, los cambios troposféricos asociados.

- Por último, destacar que el estudio realizado sobre futuros MSWs proyectados en simulaciones con un modelo climático con química interactiva ha supuesto interesantes aportaciones. Por un lado, se han obtenido resultados concluyentes del análisis de los efectos de un cambio climático prescrito (escenario A1B del IPCC-2000) en aspectos de los MSWs no explorados hasta la fecha, como el descenso de la señal de los calentamientos estratosféricos hasta la troposfera o la evolución de éstos. Por otro lado, la identificación de una respuesta distinta al cambio climático de la estratosfera polar en los dos sub-periodos de invierno (principios frente a meses centrales) pone de manifiesto la necesidad de separar dichos sub-periodos en los estudios posteriores que se hagan en esta temática. La consideración de todo el periodo invernal conjuntamente podría llevar a la deducción de conclusiones no del todo reales.

References

Ahrens, C. D. (2000), *Meteorology Today. An Introduction to Weather, Climate, and the Environment,* Brooks/Cole, 528 pp.

Ambaum, M. H. P., B. J. Hoskins, and D. B. Stephenson (2001), Arctic Oscillation or North Atlantic Oscillation?, *J. Climate, 14,* 3495-3507.

Ambaum, M. H. P., and B. J. Hoskins (2002), The NAO troposphere-stratosphere connection, *J. Climate, 15,* 1969-1978.

Andrews, D. G., and M. E. McIntyre (1976), Planetary waves in horizontal and vertical shear: the generalized Eliassen-Palm relation and the mean zonal acceleration, *J. Atmos. Sci., 33*, 2031-2048.

Andrews, D. G., and M. E. McIntyre (1978a), Generalized Eliassen-Palm and Charney-Drazin theorems for waves on axisymmetric mean flows in compressible atmospheres, *J. Atmos. Sci., 35,* 175-185.

Andrews, D. G., and M. E. McIntyre (1978b), An exact theory for nonlinear waves on a Lagrangian-mean flow, *J. Fluid. Mech., 89,* 609-646.

Andrews, D. G., J. R. Holton, and C. B. Leovy (1987), *Middle Atmosphere Dynamics*, Academic Press, 498 pp.

Assmann, R. (1902), Über die Existenz eines wärmeren Lufstromes in der Höhe von 10 bis 15 km, *Sitzungsbericht der Königlich-Preussischen Akademie der Wissenschaften Zu Berlin, Sitzung der Physikalisch-Mathematischen Klasse Vom 1, 24,* 495-504.

Austin, J., and N. Butchart (1994), The influence of climate change and the timing of stratospheric warmings on Arctic ozone depletion, *J. Geophys. Res.*, *99*, 1127-1145.

Austin, J., D. Shindell, S. R. Beagley, C. Brühl, M. Dameris, E. Manzini, T. Nagashima, P. Newman, S. Pawson, G. Pitari, E. Rozanov, C. Schnadt, and T. G. Shepherd (2003), Uncertainties and assessments of chemistry-climate models of the stratosphere, *Atmos. Chem. Phys., 3*, 1–27.

Ayarzagüena, B., U. Langematz, and E. Serrano (2011), Tropospheric forcing of the stratosphere: A comparative study of the two different Major Stratospheric Warmings in 2009 and 2010, *J. Geophys. Res.*, *116*, D18114, doi: 10.1029/2010JD015023.

Ayarzagüena, B., and E. Serrano (2009), Monthly characterization of the tropospheric circulation over the Euro-Atlantic area in relation with the timing of Stratospheric Final Warmings, *J. Climate*, *22*, 6313-6324, doi: 10.1175/2009JCLI2913.1

Baldwin, M. P., and T. J. Dunkerton (1998), Quasi-biennial modulations of the Southern Hemisphere stratospheric polar vortex, *Geophys. Res. Lett., 25*, 3343-3346.

Baldwin, M. P., and T. J. Dunkerton (1999), Propagation of the Arctic Oscillation from the stratosphere to the troposphere, *J. Geophys. Res., 104,* 30937-30946.

Baldwin, M. P., and T. J. Dunkerton (2001), Stratospheric harbingers of anomalous weather regimes, *Science, 294,* 581-584.

Baldwin, M. P., L. J. Gray, T. J. Dunkerton, K. Hamilton, P. H. Haynes, W. J. Randel, J. R. Holton, M. J. Alexander, I. Hirota, T. Horinouchi, D. B. A. Jones, J. S. Kinnersley, C. Marquardt, K. Sato, and M. Takahashi (2001), The quasi-biennial oscillation, *Rev. Geophys., 39,* 179-229.

Baldwin, M. P., H. J. Edmon, and J. R. Holton (1985), A diagnostic study of eddy-mean flow interactions during FGGE SOP-1, *J. Atmos. Sci., 42,* 1838-1845.

Baldwin, M. P., D. B. Stephenson, D. W. J. Thompson, T. J. Dunkerton, A. J. Charlton, and A. O'Neill (2003), Stratospheric memory and skill of extended-range weather forecasts, *Science, 301,* 636-640.

Baldwin, M. P., and D. W. J. Thompson (2009), A critical comparison of stratosphere-troposphere coupling indices, *Q. J. R. Meteorol. Soc., 135,* 1661-1672, doi: 10.1002/qj.479.

Bell, C. J., L. J. Gray, and J. Kettleborough (2010), Changes in Northern Hemisphere stratospheric variability under increased CO_2 concentrations, *Q. J. R. Meteorol. Soc., 136*, 1181–1190.

Bengtsson, L., S. Hagemann, and K. I. Hodges (2004), Can climate trends be calculated from reanalysis data?, *J. Geophys. Res., 109*, D11111, doi: 10.1029/2004JD004536.

Black, R. X. (2002), Stratospheric forcing of surface climate in the Arctic Oscillation, *J. Climate, 15,* 268-277.

Black, R. X., B. A. McDaniel, and W. A. Robinson (2006), Stratosphere-troposphere coupling during spring onset, *J. Climate*, *19*, 4891-4901, doi: 10.1175/2009JCLI2730.1

Black, R. X., and B. A. McDaniel (2007), The dynamics of Northern Hemisphere stratospheric final warming events, *J. Atmos. Sci., 64*, 2932-2946, doi: 10.1175/JAS3981.1

Black, R. X., and B. A. McDaniel (2009), Submonthly polar vortex variability and stratosphere-troposphere coupling in the Arctic, *J. Climate, 22,* 5886-5901, doi: 10.1175/2009JCLI2730.1.

Braesicke, P., and J. A. Pyle (2004), Sensitivity of dynamics and ozone to different representations of SSTs in the Unified Model, *Q. J. R. Meteorol. Soc., 130,* 2033-2045.

Brewer, A. W. (1949), Evidence for a world circulation provided by the measurements of helium and water vapor distribution in the stratosphere, *Q. J. R. Meteorol. Soc., 75,* 351-363.

Brigham, E. O. (1974), *The Fast Fourier Transform*, Prentice Hall, 252 pp.

Broccoli, A. J., and S. Manabe (1992), The effects of orography on midlatitude Northern Hemisphere dry climates, *J. Climate*, *5*, 1181-1201.

Butchart, N., J. Austin, J. R. Knight, A. A. Scaife, and M. L. Gallani (2000), The response of the stratospheric climate to projected changes in the concentrations of well-mixed greenhouse gases from 1992 to 2051, *J. Climate, 13*, 2142-2159.

Butchart, N., A. J. Charlton-Perez, I. Cionni, S. C. Hardiman, K. Krüger, P. Kushner, P. Newman, S. M. Osprey, J. Perlwitz, F. Sassi, M. Sigmond, and L. Wang (2010), SPARC Report on the Evaluation of Chemistry-Climate Models, Chapter 4 Stratospheric Dynamics, In: SPARC Report on the Evaluation of Chemistry-Climate Models, V. Eyring, T. G. Shepherd, D. W. Waugh (Eds.), SPARC Report No. 5, WCRP-132, WMO/TD-No. 1526, http://www.atmosp.physics.utoronto.ca/SPARC.

Butchart, N., A. J. Charlton-Perez, I. Cionni, S. C. Hardiman, P.H. Haynes, K. Krüger, P. J. Kushner, P. A. Newman, S. M. Osprey, J. Perlwitz, M. Sigmond, L. Wang, H. Akiyoshi, J. Austin, S. Bekki, A. Baumgaertner, P. Braesicke, C. Brühl, M. Chipperfiled, M. Dameris, S. Dhomse, V. Eyring, R. Garcia, H. Garny, P. Jöckel, J.-F. Lamarque, M. Marchand, M. Michou, O. Morgenstern, T. Nakamura, S. pawson, D. Plummer, J. Pyle, E. Rozanov, J. Scinocca, T. G. Shepherd, K. Shibata, D. Smale, H. Teyssèdre, W. Tian, D. Waugh, and Y. Yamashita (2011), Multimodel climate and variability of the stratosphere, *J. Geophys. Res., 116,* D05102, doi: 10.1029/2010JD014995.

Butterworth, S. (1930), On the theory of filter amplifiers, *Experimental wireless and the wireless engineer*, *7,* 536-541.

Cagnazzo, C., and E. Manzini (2009), Impact of the stratosphere on the winter tropospheric teleconnections between ENSO and the North Atlantic and European region, *J. Climate, 22,* 1223-1238.

Castanheira, J. M., and D. Barriopedro (2010), Dynamical connection between tropospheric blockings and stratospheric polar vortex, *Geophys. Res. Lett., 37*, L13809, doi: 10.1029/2010GL043819.

Chang, E. K. M., S. Lee, and K. L. Swanson (2002), Storm track dynamics, *J. Climate, 15*, 2163-2183.

Charlton, A. J., and L. M. Polvani (2007), A new look at stratospheric sudden warmings. Part I: Climatology and modeling benchmarks, *J.* Climate, *20*, 449-469.

Charlton, A. J., L. M. Polvani, J. Perlwitz, F. Sassi, E. Manzini, K. Shibata, S. Pawson, J. E. Nielsen, and D. Rind (2007), A new look at stratospheric sudden warmings. Part II: Evaluation of numerical model simulations, *J. Climate, 20,* 470-488.

Charlton-Perez, A. J., L. M. Polvani, J. Austin, and F. Li (2008), The frequency and dynamics of stratospheric sudden warmings in the 21st century, *J. Geophys. Res., 113,* D16116, doi: 10.1029/2007JD009571.

Charney, J. G., and P. G. Drazin (1961), Propagation of planetary-scale disturbances from the lower into the upper atmosphere, *J. Geophys. Res., 66*, 83-109.

Christiansen, B. (2005), Downward propagation and statistical forecast of the near surface weather, *J. Geophys. Res., 110*, D14104, doi: 10.1029/2004JD005431.

Cohen, J., M. Barlow, P. J. Kushner, and K. Saito (2007), Stratosphere–Troposphere Coupling and Links with Eurasian Land Surface Variability, *J. Climate, 20,* 5335–5343, doi: 10.1175/2007JCLI1725.1.

Coughlin, K., and L. J. Gray (2009), A continuum of sudden stratospheric warmings, *J. Atmos. Sci., 66,* 531-540, doi: 10.1175/2008JAS2792.1.

Dobson, G. M. B. (1956), Origin and distribution of the polyatomic molecules in the atmosphere, *Proc. R. soc. London, Ser. A, 236,* 187-193.

Dunkerton, T. (1978), On the mean meridional mass motions of the stratosphere and mesosphere, *J. Atmos. Sci., 35,* 2325-2333.

Edmon, H. J., Jr., B. J. Hoskins, and M. E. McIntyre (1980), Eliassen-Palm cross sections for the troposphere, *J. Atmos. Sci., 37,* 2600-2616.

Erlebach, P., U. Langematz, and S. Pawson (1996), Simulations of stratospheric sudden warmings in the Berlin troposphere-stratosphere-mesosphere GCM, *Ann. Geophysicae, 14,* 443-463.

Eyring, V., M. P. Chipperfield, M. A. Giorgetta, D. E. Kinnison, E. Manzini, K. Matthes, P. A. Newman, S. Pawson, T. G. Shepherd, and D. W. Waugh (2008), Overview of the new CCMVal reference and sensitivity simulations in support of upcoming ozone and climate assessments and the planned SPARC CCMVal Report, *SPARC Newsletter*, *30*, 20-26.

Eyring, V., I. Cionni, G. E. Bodeker, A. J. Charlton-Perez, D. E. Kinnison, J. F. Scinocca, D. W. Waugh, H. Akiyoshi, S. Bekki, M. P. Chipperfield, M. Dameris, S. Dhomse, S. M. Frith, H. Garny, A. Gettelman, A. Kubin, U. Langematz, E. Mancini, M. Marchand, T. Nakamura, L. D. Oman, S. Pawson, G. Pitari, D. A. Plummer, E. Rozanov, T. G. Shepherd, K. Shibata, W. Tian, P. Braesicke, S. C. Hardiman, J. F. Lamarque, O. Morgenstern, J. A. Pyle, D. Smale, and Y. Yamashita (2010), Multi-model assessment of stratospheric ozone return dates and ozone recovery in CCMVal-2 models, *Atmos. Chem. Phys., 10*, 9451–9472, doi:10.5194/acp-10-9451-2010.

Fahey, D. W., and M. I. Hegglin (Coordinating Lead Authors) (2011), *Twenty questions and answers about the ozone layer: 2010 update, Scientific Assessment of Ozone Depletion: 2010,* World Meteorological Organization, Geneva, Switzerland.

Fels, S. B., J. D. Mahlman, M. D. Schwarzkopf, and R. W. Sinclair (1980), Stratospheric sensitivity to perturbations in ozone and carbon dioxide: Radiative and dynamical response, *J. Atmos. Sci., 37,* 2265-2297.

Garcia, R. R., and W. J. Randel (2008), Acceleration of the Brewer–Dobson circulation due to increases in greenhouse gases, *J. Atmos. Sci., 65,* 2731-2739, doi: 10.1175/2008JAS2712.1.

García-Herrera, R., N. Calvo, R. R. Garcia, and M. A. Giorgetta (2006), Propagation of ENSO temperature signals into the middle atmosphere: A comparison of two general circulation models and ERA-40 reanalysis data, *J. Geophys. Res., 111*, D06101, doi: 10.1029/2005JD006061.

Garfinkel, C. I., and D. L. Hartmann (2008), Different ENSO teleconnections and their effects on the stratospheric polar vortex, *J. Geophys. Res., 113*, D18114, doi: 10.1029/2008JD009920.

Garfinkel, C. I., D. L. Hartmann, and F. Sassi (2010), Tropospheric precursors of anomalous Northern Hemisphere stratospheric polar vortices, *J. Climate, 23,* 3282-3299.

Geller, M. A. (2010), Middle atmosphere research before Alan Plumb, in *The stratosphere: Dynamics, transport and chemistry, Geophys. Monogr. Ser., 190*, 5-22, doi: 10.1029/2010GM000937.

Gerber,E. P., C. Orbe, and L. M. Polvani (2009), Stratospheric influence on the tropospheric circulation revealed by idealized ensemble forecasts, *Geophys. Res. Lett., 36,* L24801, doi: 10.1029/2009GL040913.

Gerber, E. P., M. P. Baldwin, H. Akiyoshi, J. Austin, S. Bekki, P. Braesicke, N. Butchart, M. Chipperfield, M. Dameris, S. Edhomse, S. M. Firth, R. R. Garcia, H. Garny, A. Gettelman, S. C. Hardiman, O. Morgenstern, J. E. Nielsen, S. Pawson, T. Peter, D. A. Plummer, J. A. Pyle, E. Rozanov,

J. F. Scinocca, T. G. Shepherd, and D. Smale (2010), Stratosphere-troposphere coupling and annular mode variability in Chemistry-Climate models, *J. Geophys. Res., D00M06,* doi: 10.1029/2009JD013770.

Gimeno, L., R. Nieto, and R. M. Trigo (2007), Decay of the Northern Hemisphere stratospheric polar vortex and the occurrence of cut-off low systems: an exploratory study, *Meteor. Atmos. Phys., 96*, 21-28, doi: 10.1007/s00703-006-0218-3.

Giorgetta, M. A., E. Manzini, E. Röckner, M. Esch, and L. Bengtsson (2006), Climatology and forcing of the Quasi-Biennial Oscillation in the MAECHAM5 model, *J. Climate, 19,* 3882-3901.

Gorgas, J., N. Cardiel, and J. Zamorano (2009), *Estadística básica para estudiantes de ciencias*, 206 pp.

Gray, L. J. (2010), Stratospheric Equatorial Dynamics, in *The stratosphere: Dynamics, transport, and chemistry, Geophys. Monogr. Ser., 190,* 93-107, doi: 10.1029/2010GM000937.

Gray, L. J., J. Beer, M. Geller, J. D. Haigh, M. Lockwood, K. Matthes, U. Cubasch, D. Fleitmann, G. Harrison, L. Hood, J. Luterbacher, G. A. Meehl, D. Shindell, B. van Geel, and W. White (2010), Solar influences on climate*, Rev. Geophys., 48*, RG4001, doi: 10.1029/2009RG000282.

Haklander, A. J., P. C. Siegmund, and H. M. Kelder (2007), Interannual variability of the stratospheric wave driving during northern winter, *Atmos. Chem. Phys., 7,* 2575-2584.

Haklander, A. J., P. C. Siegmund, M. Sigmond, and H. M. Kelder (2008), How does the northern-winter wave driving of the Brewer-Dobson circulation increase in an enhanced-CO_2 climate simulation?, *Geophys. Res. Lett., 35*, L07702, doi: 10.1029/2007GL033054.

Harada, Y., A. Goto, H. Hasegawa, N. Fujikawa, H. Naoe, and T. Hirooka (2010), A major stratospheric sudden warming event in January 2009, *J. Atmos. Sci., 67*, 2052-2069, doi: 10.1175/2009JAS3320.1.

Hardiman, S. C., N. Butchart, A. J. Charlton-Perez, T. Shaw, H. Akiyoshi, A. J. G. Baumgaertner, S. Bekki, P. Braesicke, M. Chipperfield, M. Dameris, R. R. Garcia, M. Michou, S. Pawson, E. V Rozanov, and K. Shibata (2011), Improved predictability of the troposphere using stratospheric final warmings, *J. Geophys. Res.*, *116*, D18113, doi: 10.1029/2011JD015914.

Hartmann, D. L., C. R. Mechoso, and K. Yamazaki (1984), Observations of wave-mean flow interaction in the Southern Hemisphere, *J. Atmos. Sci., 41,* 351-362.

Hartmann, D. L., J. M. Wallace, V. Limpasuvan, D. W. J. Thompson, and J. R. Holton (2000), Can ozone depletion and global warming interact to produce rapid climate change?, *Proc. Natl. Acad. Sci. U.S A., 97,* 1412-1417.

Haynes, P. H., C. J. Marks, M. E. McIntyre, T. G. Shepherd, and K. P. Shine (1991), On the "donwnward control" of extratropical diabatic circulations by eddy-induced mean zonal forces, *J. Atmos. Sci., 48,* 651-678.

Hirooka, T., and I. Hirota (1985), Normal mode Rossby waves observed in the upper stratosphere. Part II: Second antisymmetric and symmetric modes of zonal wavenumbers 1 and 2, *J. Atmos. Sci., 42,* 536-548.

Hirooka, T., T. Ichimaru, and H. Mukougawa (2007), Predictability of stratospheric sudden warmings as inferred from ensemble forecast data: Intercomparison of 2001/02 and 2003/04 winters*, J. Meteorol. Soc. Japan, 85,* 919-925.

Hodges, J. L., Jr., and E. L. Lehmann (2004), *Basic concepts of probability and statistics*, 2nd ed., Society for industrial and applied Mathematics, 441 pp.

Holton, J.R. (1992), *An Introduction to Dynamic Meteorology,* (3rd ed.), Academic Press Inc., 511 pp

Holton, J. R., and H-C Tan (1980), The influence of the equatorial Quasi-Biennial Oscillation on the global circulation at 50 mb, *J. Atmos. Sci., 37*, 2200-2208.

Holton, J. R., and H.-C. Tan (1982), The Quasi-Biennial Oscillation in the Northern Hemisphere lower stratosphere, *J. Meteorol. Soc. Japan, 60*, 140-148.

Hu, Y., and K. K. Tung (2002), Interannual and decadal variations of planetary wave activity, stratospheric cooling, and Northern Hemisphere Annular mode, *J. Climate, 15,* 1659-1673.

Hu, Y., and K. K. Tung (2003), Possible ozone-induced long-term changes in planetary wave activity in late winter, *J. Climate, 16*, 3027-3038.

Huebener, H., U. Cubasch, U. Langematz, T. Spangehl, F. Niehörster, I. Fast and M. Kunze (2007), Ensemble climate simulations using a fully coupled ocean-troposphere-stratosphere general circulation model, *Phil. Trans. R. Soc. A, 365,* 2089-2101, doi:10.1098/rsta.2007.2078.

Hurrell, J. W. (1995), Decadal trends in the North Atlantic Oscillation region temperatures and precipitation, *Science, 269,* 676-679.

Ineson, S., and A. A. Scaife (2009), The role of the stratosphere in the European climate response to El Niño, *Nature Geosciences, 2,* 32-36*,* doi: 10.1038/NGEO381.

Itoh, H., and K-I. Harada (2003), Coupling between tropospheric and stratospheric leading modes, *J. Climate, 17,* 320-336.

IPCC (Intergovernmental Panel on Climate Change) (2000), *Special report on emissions scenarios: a special report of Working Group III of the Intergovernmental Panel on Climate Change*, 599 pp., Cambridge, University Press, Cambridge, U.K.

IPCC (Intergovernmental Panel on Climate Change) (2001), *Climate change 2001: The scientific basis. Contribution of Working Group I to the Third Assessment Report*, J. T. Houghton (Eds), Cambridge University Press, Cambridge, UK, and New York, USA, 881pp..

IPCC (Intergovernmental Panel on Climate Change) (2007), *Climate Change 2007: The Physical Science Basis: Contribution of Working Group I to the Fourth Assessment Report,* S. Solomon, D. Qin, M. Manning, Z. Chen, M. Marquis, K. B. Averyt, M. Tignor, and H. L. Miller (Eds), Cambridge University Press, Cambridge, UK, and New York, USA, 996 pp..

Jöckel, P., H. Tost, A. Pozzer, C. Brühl, J. Buchholz, L. Ganzeveld, P. Hoor, A. Kerkweg, M. G. Lawrence, R. Sander, B. Steil, G. Stilller, M. Tanarhte, J. van Aardene, and J. Lelieveld (2006), The

atmospheric chemistry general circulation model ECHAM5/MESSy1: consistent simulation of ozone from the surface to the mesosphere, *Atmos. Chem. Phys., 6,* 5067-5104.

Juckes, M. N., and A. O'Neill (1988), Early winter in the Northern Hemisphere, *Q. J. R. Meteorol. Soc, 114,* 1111-1125.

Julian, P. R., and K. B. Labitzke (1965), A study of atmospheric energetics during the January-February 1963 stratospheric warming, *J. Atmos. Sci., 22*, 597-610.

Jung, T., and J. Barkmeijer (2006), Sensitivity of the tropospheric circulation to changes in the strength of the stratospheric polar vortex*, Mon. Wea. Rev., 134*, 2191–2207, doi: 10.1175/MWR3178.1

Kalnay, E., M. Kanamitsu, R. Kistler, W. Collins, D. Deaven, L. Gandin, M. Iredell, S. Saha, G. White, J. Woollen, Y. Zhu, M. Chelliah, W. Ebisuzaki, W. Higgins, J. Janowiak, K. C. Mo, C. Ropelewski, J. Wang, A. Leetmaa, R. Reynolds, R. Jenne, and D. Joseph (1996), The NCEP/NCAR 40-year reanalysis project, *Bull. Amer. Meteorol. Soc., 77,* 437-471.

Kinoshita, T., Y. Tomikawa, and K. Sato (2010), On the three-dimensional residual mean circulation wave activity flux of the primitive equations, *J. Meteorol. Soc. of Japan, 88,* 373-394.

Kodera, K., and M. Chiba (1995), Tropospheric circulation changes associated with stratospheric sudden warmings: A case study, *J. Geophys. Res., 100,* 11055-11068.

Kodera, K., and Y. Kuroda (2002), Dynamical response to the solar cycle, *J. Geophys. Res., 107,* 4749, doi: 10.1029/2002JD002224.

Kodera, K., H. Mukougawa, and S. Itoh (2008), Tropospheric impact of reflected planetary waves from the stratosphere, *Geophys. Res. Lett., 35*, L16806, doi: 10.1029/2008GL034575.

Kolstad, E. W., and A. J. Charlton-Perez (2010), Observed and simulated precursors of stratospheric polar vortex anomalies in the Northern Hemisphere, *Clim. Dyn.,* (in press), DOI 10.1007/s00382-010-0919-7.

Kuroda, Y. (2008), Effect of stratospheric sudden warming and vortex intensification on the tropospheric climate, *J. Geophys. Res., 113,* D15110, doi: 10.1029/2007JD009550.

Labitzke, K. (1965), On the mutual relation between stratosphere and troposphere during periods of stratospheric warmings in winter, *J. Appl. Meteorol., 4,* 91-99.

Labitzke, K. (1977), Interannual variability of the winter stratosphere in the Northern Hemisphere, *Mon. Wea. Rev., 105,* 762-770.

Labitzke, K. (1981a), The amplification of height wave 1 in January 1979: a characteristic precondition for the major warming in February, *Mon. Wea. Rev., 109,* 983-989.

Labitzke, K. (1981b), Stratospheric-mesospheric midwinter disturbances: A summary of observed characteristics, *J. Geophys. Res., 86,* 9665-9678.

Labitzke, K., and M. Kunze (2005), Stratospheric temperatures over the Arctic: Comparison of three data sets, *Meteorol. Z., 14,* 65-74, doi: 10.1127/0941-2948/2005/0014-0065.

Labitzke, K., M. Kunze, and S. Brönnimann (2006), Sunspots, the QBO, and the stratosphere in the north polar region – 20 years later, *Meteorol. Z., 15*, 355-363.

Labitzke, K., and M. Kunze (2009), On the remarkable Arctic winter in 2008/09, *J. Geophys. Res*., *114*, D00I02, doi: 10.1029/2009JD012273.

Labitzke, K., and B. Naujokat (2000), The lower arctic stratosphere in winter since 1952, *SPARC Newslett., 15*, 11-14.

Labitzke, K., and H. van Loon (1988), Associations between the 11-year solar cycle, the QBO and the atmosphere, Part I: the troposphere and stratosphere in the Northern Hemisphere in winter, *J. Atmos. Terr. Phys., 50,* 197-206.

Langematz, U., and M. Kunze (2006), An update on dynamical changes in the Arctic and Antarctic stratospheric polar vortices, *Clim. Dyn., 27*, 647-660, doi: 10.1007/s00382-006-0156-2.

Lean, J., G. Rottman, J. Harder, and G. Kopp (2005), SORCE contributions to new understanding of global change and solar variability, *Solar Phys., 230,* 27-53.

Lee, W.-J., and M. Mak (1996), The role of orography in the dynamics of storm tracks, *J. Atmos. Sci., 53,* 1737-1750.

Legutke S. and R. Voss (1999), The Hamburg Atmosphere-Ocean Coupled Circulation Model ECHO-G., *Tech. Rep., 18*, DKRZ, Hamburg

Limpasuvan, V., and D. L. Hartmann (2000), Wave-maintained annular modes of climate variability, *J. Climate*, *13*, 4414-4429.

Limpasuvan, V., D. L. Hartmann, D. W. J. Thompson, K. Jeev, and Y. L. Yung (2005), Stratosphere-troposphere evolution during polar vortex intensification, *J. Geophys. Res., 110,* D24101, doi: 10.1029/2005JD006302.

Limpasuvan, V., J. H. Richter, Y. J. Orsolini, F. Stordal, and O.-K. Kvissel, (2011), The roles of planetary and gravity waves during a major stratospheric sudden warming as characterized in WACCM, *J. Atmos. Sol. Terr. Phys.,* Special issue on mesosphere-lower thermosphere, doi: 10.1016/j.jastp.2011.03.004, in press.

Limpasuvan, V., D. W. J. Thompson, and D. L. Hartmann (2004), The life cycle of the Northern Hemisphere sudden stratospheric warmings, *J. Climate*, *17*, 2584-2596.

Lindzen, R. S., and J. R. Holton (1968), A theory of the Quasi-Biennial Oscillation, *J. Atmos. Sci., 25*, 1095-1107.

Manney, G. L., M. J. Schwartz, K. Krüger, M. L. Santee, S. Pawson, J. N. Lee, W. H. Daffer, R. A. Fuller, and N. J. Livesey (2009), Aura Microwave Limb sounder observations of dynamics and transport during the record-breaking 2009 Arctic stratospheric major warming, *Geophys. Res. Lett.*, *36*, L12815, doi: 10.1029/2009GL038586.

Manzini, E., M. A. Giorgetta, M. Esch, L. Kornblueh, and E. Roeckner (2006), The influence of sea surface temperatures on the northern winter stratosphere: Ensemble simulations with the MAECHAM5 model, *J. Climate*, *19*, 3863–3881.

Manzini, E., and N. A. McFarlane (1998), The effect of varying the source spectrum of a gravity wave parameterization in a middle atmosphere general circulation model, *J. Geophys. Res., 103,* 31523–31539, doi: 10.1029/98JD02274.

Marshall, A. G., A. A. Scaife, and S. Ineson (2009), Enhanced seasonal prediction of european winter warming following volcanic eruptions, *J. Climate, 22,* 6168-6180.

Martineau, P., and S.-W. Son (2010), Quality of reanalysis data during stratospheric vortex weakening and intensification events, *Geophys. Res. Lett., 37,* L22801, doi: 10.1029/2010GL045237.

Martius, O., L. M. Polvani, and H. C. Davies (2009), Blocking precursors to stratospheric sudden warming events, *Geophys. Res. Lett., 36*, L14806, doi: 10.1029/2009GL038776.

Matsuno, T. (1971), A dynamical model of stratospheric sudden warming, *J. Atmos. Sci.*, *28*, 1479-1494.

Maycock, A. C., S. P. E. Keeley, A. J. Charlton-Perez, and F. J. Doblas-Reyes (2011), Stratospheric circulation in seasonal forecasting models: implications for seasonal prediction, *Clim. Dyn., 36,* 309–321.

McDaniel, B. A., and R. X. Black (2005), Intraseasonal dynamical evolution of the Northern Annular Mode, *J. Climate, 18,* 3820-3839.

McIntyre, M.E. (1982), How well do we understand the dynamics of stratospheric warmings?, *J. Meteorol. Soc. Japan*, *60*, 37-65.

McLandress, C., and T. G. Shepherd (2009a), Simulated anthropogenic changes in the Brewer-Dobson circulation, including its extension to high latitudes, *J. Climate, 22*, 1516-1540.

McLandress, C., and T. G. Shepherd (2009b), Impact of climate change on stratospheric sudden warmings as simulated by the Canadian Middle Atmosphere Model, *J. Climate, 22,* 5449-5463.

Mukougawa, H., H. Sakai, and T. Hirooka (2005), High sensitivity to the initial condition for the prediction of stratospheric sudden warming, *Geophys. Res. Lett., 32,* L17806, doi: 10.1029/2005GL022909.

Nakagawa, E. I., and K. Yamazaki (2006), What kind of stratospheric sudden warming propagates to the troposphere?, *Geophys. Res. Lett., 33,* L04801, doi: 10.1029/2005GL024784.

Nakamura, H., and M. Honda (2002), Interannual seesaw between the Aleutian and Icelandic lows. Part III: Its influence upon the stratospheric variability*, J. Meteorol. Soc. Japan, 80*, 1051-1067.

Nash, E. R., P. A. Newman, J. E. Rosenfield, and M. R. Schoeberl (1996), An objective determination of the polar vortex using Ertel's potential vorticity, *J. Geophys. Res., 101,* 9471-9478.

Naujokat, B. (1986), An update of the observed quasi-biennial oscillation of the stratospheric winds over the tropics, *J. Atmos. Sci., 43,* 1873-1877.

Naujokat, B., K. Krüger, K. Matthes, J. Hoffmann, M. Kunze, and K. Labitzke (2002), The early major waming in December 2001 – exceptional?, *Geophys. Res. Lett., 29,* doi: 10.1029/2002GL015316.

Newman, P. A., and E. R. Nash (2009), The extreme major stratospheric sudden warming of January 2009, paper presented at 15th Conference on Middle Atmosphere, American Meteorological Society, Stowe, USA.

Newman, P. A. (2010), Chemistry and dynamics of the Antarctic ozone hole, in *The stratosphere: Dynamics, transport, and chemistry, Geophys. Monogr. Ser., 190,* 157-171, doi: 10.1029/2010GM000937.

Nishii, K., and H. Nakamura (2004), Tropospheric influence on the diminished Antarctic ozone hole in September 2002, *Geophys. Res. Lett., 31*, L16103, doi: 10.1029/2004GL019532.

Nishii, K., H. Nakamura, and T. Miyasaka (2009), Modulations in the planetary wave field induced by upward-propagating Rossby wave packets prior to stratospheric sudden warming events: A case-study, *Q. J. R. Meteorol. Soc.*, *135*, 39-52, doi: 10.1002/qj.359.

Nishii, K., H., Nakamura, and Y. J. Orsolini (2010), Cooling of the wintertime Arctic stratosphere induced by the western Pacific teleconnection pattern, *Geophys. Res. Lett.*, *37*, doi: 10.129/2010GL043551.

Nissen, K. M., K. Matthes, U. Langematz, and B. Mayer (2007), Towards a better representation of the solar cycle in general circulation models, *Atmos. Chem. Phys., 7*, 5391–5400.

Offermann, D., M. Donner, P. Knieling, K. Hamilton, A. Menzel, B. Naujokat, and P. Winkler (2003), Indications of long-term changes in middle atmosphere transports. *Adv. Space Res., 32*, 1675-1684.

Offermann, D., M. Donner, P. Knieling, and B. Naujokat (2004), Middle atmosphere temperature changes and the duration of summer, *J. Atmos. Solar. Terr. Phys., 66,* 437-450.

Orsolini, Y. J., and N. G. Kvamstø (2009), Role of Eurasian snow cover in wintertime circulation: decadal simulations forced with satellite observations, *J. Geophys. Res., 114*, D19108, doi: 10.1029/2009jd012253.

Pascoe, C. L., L. J. Gray, S. A. Crooks, M. N. Juckes, and M. P. Baldwin (2005), The Quasi-Biennial Oscillation: Analysis using ERA-40 data, *J. Geophys. Res., 110*, D08105, doi: 10.1029/2004JD004941.

Pascoe, C. L., L. J. Gray and A. A. Scaife (2006), A GCM study of the influence of equatorial winds on the timing of sudden stratospheric warmings, *Geophys. Res. Lett.,* 33, L06825, doi:10.1029/2005GL024715.

Peixoto, J. P., and A. H. Oort (1992), *Physics of Climate*, Springer-Verlag, 520 pp.

Perlwitz, J., and N. Harnik (2003), Observational evidence of a stratospheric influence on the troposphere by planetary wave reflection, *J. Climate, 16*, 3011–3026.

Pinto, J. G., M. Reyers, and U. Ulbrich (2011), The variable link between PNA and NAO in observations and in multi-century CGCM simulations, *Clim. Dyn., 36,* 337-354, doi:10.1007/s00382-010-0770-x

Pinto, J. G., U. Ulbrich, G. C. Leckebusch, T. Spangehl, M. Reyers, and S. Zacharias (2007), Changes in storm track and cyclone activity in three SRES ensemble experiments with the ECHAM5/MPI-OM1 GCM. *Clim. Dyn., 29,* 195-210, doi: 10.1007/s00382-007-0230-4.

Pitman, E. J. G. (1937), Significance tests which may be applied to samples from any populations. *J. R. Statist. Soc., Suppl. 4,* 119-130.

Plumb, R. A. (1984), The Quasi-Biennial Oscillation, in *Dynamics of the Middle Atmosphere,* edited by J. R. Holton and T. Matsuno, pp. 217-251, Terra Sci., Tokyo.

Plumb, R. A. (1985), On the three-dimensional propagation of stationary waves, *J. Atmos. Sci., 42*, 217-229.

Plumb, R. A. (2010), Planetary waves and the extratropical winter stratosphere, in *The stratosphere: Dynamics, transport, and chemistry, Geophys. Monogr. Ser., 190,* 23-41, doi: 10.1029/2010GM000937.

Polvani, L. M., and D. W. Waugh (2004), Upward wave activity flux as a precursor to extreme stratospheric events and subsequent anomalous surface weather regimes, *J. Climate, 17,* 3548-3554.

Preisendorfer, R. W., and T. P. Barnett (1983), Numerical model-reality intercomparison tests using small-sample statistics, *J. Atmos. Sci., 40*, 1884-1896.

Proakis, J. G., and D. G. Manolakis (2003), *Tratamiento digital de señales, 3ª edición,* Prentice Hall, Madrid.

Quiroz, R. S. (1977), The tropospheric-stratospheric polar vortex breakdown of January 1977, *Geophys. Res. Lett., 4*, 151-154.

Quiroz, R. S. (1986), The association of stratospheric warmings with tropospheric blocking, *J. Geophys. Res., 91*, 5277-5285.

Randel, W. J., K. P. Shine, J. Austin, J. Barnett, C. Claud, N. P. Gillet, P. Keckhut, U. Langematz, R. Lin, C. Long, C. Mears, A. Miller, J. Nash, D. J. Seidel, D W. J. Thompson, F. Wu, and S. Yoden (2009), An update of observed stratospheric temperature trends, *J. Geophys. Res., 114,* D02107, doi:10.1029/2008JD010421.

Rex, M., R. J. Salawitch, P. von der Gathen, N. R. P. Harris, M. P. Chipperfield, and B. Naujokat (2004), Arctic ozone loss and climate change, *Geophys. Res. Lett., 31*, L04116, doi: 10.1029/2003GL018844.

Rico, T., B. Ayarzagüena, and E. Serrano (2008), Diferencias entre los reanálisis ERA40 y NCEP/NCAR en la variabilidad estratosférica de la temperatura y del viento zonal, *Proceedings of XXX Jornadas Científicas de la Asociación Meteorológica Española. Agua y Cambio Climático. IX Encuentro Hispano-Luso de Meteorología and XII Congreso Latinoamericano e Ibérico de Meteorología,* ISBN: 978-84-612-9981-2.

Rind, D., R. Suozzo, N. Balachandran, and M. Prather (1990), Climate change and the middle atmosphere. Part I: The doubled CO_2 climate, *J. Atmos. Sci., 47*, 475-494.

Röckner, E., K. Arpe, L. Bengtsson, M. Chrisoph, M. Claussen, L. Dümenil, M. Esch, M. Giorgetta, U. Schlese, and U. Schulzweida (1996), The atmospheric general circulation model ECHAM-4:Model description and simulation of present-day climate. *Max-Planck-Institut für Meteorologie, Report No. 218,* Hamburg, 90 pp.

Röckner, E., R. Brokopf, M. Esch, M. Giorgetta, S. Hagemann, L. Kornblüh, E. Manzini, U. Schlese, and U. Schulzweida (2006), Sensitivity of simulated climate to horizontal and vertical resolution in the ECHAM5 atmosphere model, *J. Climate, 19,* 3771-3791.

Rogers, J.C., and M. McHugh (2002), On the separability of the North Atlantic Oscillation and Arctic Oscillation, *Clim. Dyn., 19*, 599-608.

Roscoe, H. K., J. D. Shanklin, and S. R. Colwell (2005), Has the Antarctic vortex split before 2002?, *J. Atmos. Sci., 62,* 581-588.

Salby, M. L., and P. F. Callaghan (2007), Influence of planetary wave activity on the stratospheric final warming and spring ozone, *J. Geophys. Res.*, *112*, D20111, doi: 10.1029/2006JD007536.

Sander, R., A. Kerkweg, P. Jöckel, and J. Lelieveld (2005), Technical note: The new comprenhensive atmospheric chemistry module MECCA, *Atmos. Chem. Phys., 5,* 445-450.

Santer, B. D., T. M. L. Wigley, A. J. Simmons, P. W. Kållberg, G. A. Kelly, S. M. Uppala, C. Ammann, J. S. Boyle, W. Brüggemann, C. Doutriaux, M. Fiorino, C. Mears, G. A. Meehl, R. Sausen, K. E. Taylor, W. M. Washington, M. F. Wehner, and F. J. Wentz (2004), Identification of anthropogenic climate change using second-generation reanalysis, *J. Geophys. Res., 109,* D21104, doi: 10.1029/2004JD005075.

Scaife, A. A., N. Butchart, C. D. Warner, D. Stainforth, W. Norton, and J. Austin (2000), Realistic Quasi-Biennial Oscillations in a simulation of the global climate, *Geophys., Res., Lett., 27,* 3481-3484.

Scaife, A. A., J. R. Knight, G. K. Vallis, and C. K. Folland (2005), A stratospheric influence on the winter NAO and North Atlantic surface climate, *Geophys. Res. Lett.*, *32,* L18715, doi:10.1029/2005GL023226.

Scaife, A. A., T. Spangehl, D. R. Fereday, U. Cubasch, U. Langematz, H. Akiyoshi, S. Bekki, P. Braesicke, N. Butchart, M. P. Chipperfield, A. Gettelman, S. C. Hardiman, M. Michou, E. Rozanov, and T. G. Shepherd (2011), Climate change projections and stratosphere–troposphere interaction, *Clim. Dyn*., doi:10.1007/s00382-011-1080-7.

Scherhag, R. (1952), Die explosionartigen Stratosphärenerwärmungen des Spätwinters 1951/52, *Ber. Dtsch. Wetterdienst. U. S. Zone, 38,* 51-63.

Schimanke, S., J. Körper, T. Spangehl, and U. Cubasch (2011), Multi−decadal variability of sudden stratospheric warmings in an AOGCM, *Geophys. Res. Lett.*, *38*, L01801, doi: 10.1029/2010GL045756.

Schnadt, C., M. Dameris, M. Ponater, R. Hein, V. Grewe, and B. Steil (2002), Interaction of atmospheric chemistry and climate and its impact on stratospheric ozone, *Clim. Dyn., 18*, 507-517.

Schultz, M., et al. (2007), Emission data sets and methodologies for estimating emissions (http://retro.enes.org/reports/D1-6_final.pdf), Reanalysis of the tropospheric chemical composition over the past 40 years, A long-term global modeling study of tropospheric chemistry funded under 5th EU framework program, EU-Contract No. EVK2-CT-2002-00170.

Shaw, T. A., J. Perlwitz, and N. Harnik (2010), Downward wave coupling between the stratosphere and troposphere: The importance of meridional wave guiding and comparison with zonal-mean coupling, *J. Climate, 23,* 6365-6381, doi: 10.1175/2010JCLI3804.1.

Shiogama, H., and H. Mukougawa (2005), Influence of ENSO on stratosphere-troposphere coupling during stratospheric sudden warming events, *SOLA, 1*, 125-128, doi: 10.2151/sola.2005-033.

Shindell, D., D. Rind, and P. Lonergan (1998) Increased polar stratospheric ozone losses and delayed eventual recovery owing to increasing greenhouse-gas concentrations, *Nature*, *392*, 589-592.

Shindell, D.T., G.A. Schmidt, L. Miller, and D. Rind (2001), Northern Hemisphere winter climate response to greenhouse gas, ozone, solar, and volcanic forcing, *J. Geophys. Res.*, 106, 7193-7210.

Sigmond, M., P.C. Siegmund, E. Manzini, and H. Kelder (2004), A simulation of the separate climate effects of middle-atmospheric and tropospheric CO_2 doubling, *J. Climate, 17,* 2352-2367.

Simmons, A. (2004), Representation of the stratosphere in ECMWF operations and ERA-40, *Proceedings of ECMWF/SPARC Workshop on modelling and assimilation for the stratosphere and tropopause.*

Spangehl, T., U. Cubasch, C. C. Raible, S. Schimanke, J. Körper, and D. Hofer (2010), Transient climate simulations from the Maunder Minimum to present day: Role of the stratosphere, *J. Geophys. Res.*, *115*, D00I10, doi: 10.1029/2009JD012358.

SPARC (2006), SPARC Assessment of Stratospheric Aerosol Properties (ASAP), Tech. Rep. WMO-TD No. 1295, WCRP Series Report No. 124, SPARC Report No. 4, Berrieres le Buisson Cedex.

Taguchi, M., and D. L. Hartmann (2006), Increased occurrence of stratospheric sudden warmings during El Niño as simulated by WACCM, *J. Climate, 19*, 324-332.

Takaya, K., and H. Nakamura (1997), A formulation of a wave-activity flux for stationary Rossby waves on a zonally varying basic flow, *Geophys. Res. Lett., 24*, 2985-2988.

Takaya, K., and H. Nakamura (2001), A formulation of a phase-independent wave activity flux for stationary and migratory quasigeostrophic eddies on a zonally varying basic flow, *J. Atmos. Sci., 58*, 608-627.

Teisserenc de Bort, M. L. (1902), Variations de la température de l'air libre dans la zone comprise entre 8 km et 13 km d'altitude, *C. R. Hebd. Séances Acad. Sci., 24*, 987-989.

Thompson, D. W. J., and J. M. Wallace (1998), The Arctic Oscillation signature in the wintertime geopotential height and temperature fields, *Geophys. Res. Lett., 25,* 1297-1300.

Thompson, D. W. J., and J. M. Wallace (2000), Annular modes in the extratropical circulation. Part I: Month-to-month variability, *J. Climate, 13,* 1000-1016.

Thompson, D. W. J., and J. M. Wallace (2001), Regional climate impacts of the Northern Hemisphere annular mode, *Science, 293*, 85-89.

Thompson, D. W. J., M. P. Baldwin, and J. M. Wallace (2002), Stratospheric connection to Northern Hemisphere wintertime weather: Implications for prediction, *J. Climate, 15,* 1421-1428.

Tomikawa, Y. (2010), Persistence of easterly wind during major stratospheric sudden warmings, *J. Climate, 23*, 5258-5267.

Trenberth, K. E., D. P. Stepaniak, J. W. Hurrell, and M. Fiorino (2001), Quality of reanalyses in the tropics*, J. Climate, 14*, 1499-1510.

Tyrlis, E., and B. J. Hoskins (2008), Aspects of Northern Hemisphere atmospheric blocking climatology, *J. Atmos. Sci*., *65*, 1638-1652, doi:10.1175/JAS2337.1.

Ulbrich, U., J.G. Pinto, H. Kupfer, G.C. Leckebusch, T. Spangehl, and M. Reyers (2008), Changing Northern Hemisphere storm tracks in an ensemble of IPCC climate change simulations. *J. Climate*, *21*, 1669-1679, doi: 10.1175/2007JCLI1992.1.

Uppala, S. M., P. W. Kållberg, A. J. Simmons, U. Andrae, V. da Costa Bechtold, M. Fiorino, J. K. Gibson, J. Haseler, A. Hernandez, G. A. Kelly, X. Li, K. Onogi, S. Saarinen, N. Sokka, R. P. Allan, E. Andersson, K. Arpe, M. A. Balmaseda, A. C. M. Beljaars, L. van de Berg, J. Bidlot, N. Bormann, S. Caires, F. Chevallier, A. Dethof, M. Dragosavac, M. Fisher, M. Fuentes, S. Hagemann, E. Hólm, B. J. Hoskins, L. Isaksen, P.A.E.M. Janssen, R. Jenne, A. P. McNally, J.-F. Mahfouf, J.-J. Morcrette, N. A. Rayner, R. W. Saunders, P. Simon, A. Sterl, K. E. Trenberth, A. Untch, D. Vasiljevic, P. Viterbo, and J. Woollen (2005), The ERA-40 Reanalysis, *Q. J. R. Meteorol. Soc., 131,* 2961-3012, doi: 10.1256/qj.04.176.

van Loon, H., and K. Labitzke (1987), The Southern Oscillation. Part V: The anomalies in the lower stratosphere of the Northern Hemisphere in winter and a comparison with the Quasi-Biennial Oscillation, *Mon. Wea. Rev., 115*, 357-369.

van Loon, H., and K. Labitzke (2000), The influence of the 11-year solar cycle on the stratosphere below 30 km: a review, *Space Science Reviews, 94*, 259-278.

von Storch, H., and F. W. Zwiers (2001), *Statistical analysis in climate research*, Cambridge University Press, 484 pp.

Walker, G. T., and E. W. Bliss (1932), World weather V. *Mem. Roy. Meteor. Soc., 4***,** 53–84.

Wallace, J. M., 2000: North Atlantic Oscillation/annular mode: Two paradigms—one phenomenon, *Q. J. R. Meteorol. Soc., 126***,** 791–805.

Waugh, D. W. (1997), Elliptical diagnostics of stratospheric polar vortices, *Q. J. R. Meteorol. Soc., 123,* 1725-1748.

Waugh, D. W., and L. M. Polvani (2010), Stratospheric polar vortices, in *The stratosphere: Dynamics, transport and chemistry, Geophys. Monogr. Ser, 190*, 43-57, doi: 10.1029/2010GM000937.

Waugh, D. W., W. J. Randel, S. Pawson, P. A. Newman, and E. R. Nash (1999), Persistence of the lower stratospheric polar vortices, *J. Geophys. Res.*, *104*, 27191–27201.

Waugh, D. W., and P.-P. Rong (2002), Interannual variability in the decay of lower stratospheric Arctic vortices, *J. Meteorol. Soc. Japan, 80,* 997-1012.

Wei, K., W. Chen, and R. H. Huang (2007), Dynamical diagnosis of the breakup of the stratospheric polar vortex in the Northern Hemisphere, *Sci. China Ser. D-Earth Sci., 50*, 1369-1379.

Whipple, F. J. W. (1923), The high temperature of the upper atmosphere as an explanation of zones of audibility, *Nature, 111,* 87.

Wilks, D. S. (1995), *Statistical methods in the atmospheric sciences,* Academic Press, 467 pp.

Winter, B., and M. Bourqui (2010), Wave forcing in the stratosphere under doubled-CO_2 conditions in a 100-year coupled chemistry-climate model study, *J. Geophys. Res., 115,* D12126, doi: 10.1029/2009JD012777.

Woollings, T., A. Charlton-Perez, S. Inerson, A. G. Marshall and G. Masato (2010), Associations between stratospheric variability and tropospheric blocking, *J. Geophys. Res., 115,* D06108, doi: 10.1029/2009JD012742.

World Meteorological Organization (WMO)/United Nations Environment Programme (UNEP) (2007), Scientific Assessment of Ozone Depletion: 2006, World Meteorological Organization, *Global Ozone Research and Monitoring Project, Report No. 50*, Geneva, Switzerland.

Yamazaki, K. (1987), Observations of the stratospheric final warmings in the two hemispheres, *J. Meteorol. Soc. Japan, 65,* 51-66.

Yoden, S., T. Yamaga, S. Pawson, and U. Langematz (1999), A composite analysis of the stratospheric sudden warmings simulated in a perpetual January integration of the Berlin TSM GCM, *J. Meteorol. Soc. Japan, 77*, 431–445.

Appendixes

Appendix 1: Primitive equations in log-pressure coordinates on the sphere

Primitive equations are derived from equations (A1.1), which describe the motions of a compressible gas surrounding an approximately spherical, rotating planet (the Earth).

$$\text{Momentum eq.:} \quad \frac{\mathrm{D}\mathbf{v}}{\mathrm{D}t}+\frac{1}{\rho}\nabla\mathbf{p}+2\boldsymbol{\Omega}\times\mathbf{v}=\mathbf{g}+\mathbf{F}_{\mathbf{f}}$$

$$\text{Energy eq.:} \quad c_p\frac{\mathrm{D}T}{\mathrm{D}t}-\frac{1}{\rho}\frac{\mathrm{D}\mathbf{p}}{\mathrm{D}t}=Q \qquad \text{(A1.1)}$$

$$\text{Continuity mass eq.:} \quad \frac{\partial\rho}{\partial t}+\nabla\left(\rho\,\mathbf{v}\right)=0$$

where **v** is the 3-dimensional velocity (u,v,w), ρ is the air density, **p** is the atmospheric pressure, **Ω** is the Earth's rotation rate, **g** is the gravity acceleration, $\mathbf{F_f}$ corresponds to friction or other nonconservative mechanical forcing, c_p is the specific heat capacity at constant pressure and Q is the diabatic heating term [Holton, 1992].

i. General

Equations (A1.1) can be rewritten in a more simple form by applying some approximations and simplifications related to the orders of magnitude of the various terms. For instance, scale analysis shows that the Coriolis force associated with the horizontal component of the earth's rotation vector can be neglected, the distance from some atmospheric point to the center of the earth can be replaced by a mean radius (hereafter denoted, *a*) and the vertical component of the vertical momentum can be replaced by the hydrostatic equation: $\frac{1}{\rho}\frac{\partial p}{\partial z}+g=0$.

After the above mentioned approximations, the resultant equations are denoted *primitive equations.* The expressions of these primitive equations using the spherical coordinates in the horizontal (λ, φ) and the log pressure coordinate, z, (derived from the hydrostatic relation: $z=-H\ln\left(p/1000\,\mathrm{hPa}\right)$) are the following:

Momentum eq.:
$$\frac{\mathrm{D}u}{\mathrm{D}t}-\left(f+\frac{u\tan\varphi}{a}\right)v+\frac{1}{a\cos\varphi}\frac{\partial\Phi}{\partial\lambda}=F_{f_\lambda}$$
$$\frac{\mathrm{D}v}{\mathrm{D}t}+\left(f+\frac{u\tan\varphi}{a}\right)u+\frac{1}{a}\frac{\partial\Phi}{\partial\varphi}=F_{f_\varphi}$$
$$\frac{\partial\Phi}{\partial z}-\frac{RT}{H}=0 \qquad \text{(A1.2)}$$
Energy eq.:
$$\frac{\mathrm{D}T}{\mathrm{D}t}+\frac{R}{c_p}\frac{Tw}{H}=\frac{Q}{c_p}$$
Continuity mass eq.:
$$\frac{1}{a\cos\varphi}\frac{\partial u}{\partial\lambda}+\frac{1}{a\cos\varphi}\frac{\partial(v\cos\varphi)}{\partial\varphi}+\frac{1}{\rho}\frac{\partial(\rho w)}{\partial z}=0$$

where f is the Coriolis parameter (=2 Ω sinϕ), Φ is the geopotential, R is the gas constant and H is the scale height (7 km for the middle atmosphere).

ii. Quasi-geostrophic flow (extratropical approximation)

Although the primitive equations of equations (A1.2) have been already obtained from a simplification of the general equations, they are still complicated and difficult to resolve as they describe a very wide type of processes. Hence, more approximations can be done in order to get simpler expressions that focus on the phenomena issues of this PhD thesis, i. e. larger-scale, slower motions that take place in the extratropical regions. These approximations are the following [Andrews et al., 1987]:

- *Geometrical simplification,* which consists of these two following steps:
  - Replace spherical coordinates (λ, φ) by eastward and northward Cartesian ones (x, y).
  - Restrict the flow domain to some neighborhood of the latitude φ_0, so that (x, y) correspond to the eastward distance and northward distance from some origin (λ_0, φ_0) and the Coriolis parameter, f, can be rewritten as: $f = f_0 + \beta y$, with $\beta = 2\,\Omega\, a^{-1}\cos\varphi_0$. This is called the *beta-effect*.
- *Geostrophic approximation* (for large-scale, low-frequency and extratropical flows)*:*
  - Due to the flow features, the horizontal accelerations, Du/Dt and Dv/Dt, and the nonconservative terms (F_f) are neglected and f is made equal to f_0. Thus, the horizontal flow is balanced by the horizontal gradients of pressure and so, it satisfies equation (A1.3). It is called *geostrophic wind* $|\boldsymbol{v_g}|$ (u_g, v_g) :

$$u_g = -\frac{1}{f_0 \rho}\frac{\partial p}{\partial y} \quad v_g = \frac{1}{f_0 \rho}\frac{\partial p}{\partial x} \tag{A1.3}$$

- Combining these expressions with the hydrostatic relationship, the thermal wind expression (eq. (A1.4)) is obtained, which relates the vertical shear of the horizontal wind to the temperature meridional gradient.

$$u_T = \frac{\partial u_g}{\partial z} = -\frac{R}{f H}\frac{\partial T}{\partial y} \quad v_g = \frac{\partial v_g}{\partial z} = \frac{R}{f H}\frac{\partial T}{\partial x} \tag{A1.4}$$

- *Quasi-geostrophic approximation:* Under these conditions, the actual flow is very close to the geostrophic one, so that its deviations from the latter, called ageostrophic velocities ($\mathbf{v_a}$ = (u-u_g, v-v_g, w)), are small in comparison with $\mathbf{v_g}$. This approximation is very useful to investigate the time development of the geostrophic flow and most of the analysis of the middle atmosphere research is based on it.

The final set of the primitive equations describing the quasi-geostrophic flow is the following:

$$\begin{aligned}
&\text{Horizontal momentum eqs.:} && D_g u_g - f_0 v_a - \beta y v_g = F_{f_x} \\
& && D_g v_g + f_0 u_a + \beta y u_g = F_{f_y} \\
&\text{Mass continuity eq.:} && \frac{\partial u_a}{\partial x} + \frac{\partial v_a}{\partial y} + \frac{1}{\rho_0}\frac{\partial(\rho_0 w_a)}{\partial z} = 0 \\
&\text{Energy eq.:} && D_g \theta_e + w_a \frac{\partial \theta_0}{\partial z} = Q
\end{aligned} \tag{A1.5}$$

where $D_g \equiv \frac{\partial}{\partial t} + u_g \frac{\partial}{\partial x} + v_g \frac{\partial}{\partial y}$ is the time derivative following the geostrophic wind, θ is the potential temperature $\left(\theta = T\left(\frac{p_0}{p}\right)^{R/c_p}\right)$ and θ_e corresponds to the departure from the reference potential temperature, $\theta_0(z)$.

Appendix 2: Acronyms and abbreviations

AO: Arctic Oscillation

AOGCM: Atmosphere-Ocean General Circulation Model

CCM: Chemistry Climate Model

CCMVal: Chemistry Climate Model Validation

CFC: ChloroFluoroCarbon

CW: Canadian Warming

DJF: December, January and February

ECMWF: European Centre for Medium-Range Weather Forecasts

EGMAM: ECHO-G with Middle Atmosphere Model

EMAC: ECHAM Atmospheric Chemistry Model

EP flux: Eliassen-Palm flux

ERA: ECMWF Re-Analysis

FUB: Freie Universität Berlin

GCM: General Circulation Model

GHG: Greenhouse Gas

IPCC: Intergovernmental Panel on Climate Change

JJA: June, July and August

MAM: March, April and May

MPI: Max Planck Institute

MPI-OM: Max-Planck-Institute Ocean Model

MSW: Major Stratospheric Warming

NAM: Northern Annular Mode

NAO: North Atlantic Oscillation

NCEP/NCAR: National Centers for Environmental Prediction/National Center for Atmospheric Research

NH: Northern Hemisphere

NOAA: National Oceanic and Atmospheric Administration

ODS: Ozone Depletion Substances

PNJ: Polar Night Jet

PSC: Polar Stratospheric Cloud

QBO: Quasi-Biennial Oscillation

SAD: Surface Area Densities

SAO: Semi-Annual Oscillation

SFW: Stratospheric Final Warming

SH: Southern Hemisphere

SIC: Sea Ice Concentration

SON: September, October and November

SPARC: Stratospheric Processes and their Role in Climate

SST: Sea Surface Temperature

SSW: Stratospheric Sudden Warming

WMO: World Meteorological Organization

WN: Wave-Number

Appendix 3: Additional information of Chapter VI

Dates of SFWs in EMAC REF-B1

Table App3.1. Dates of occurrence of the stratospheric final warming (SFW) events in the period of 1960-2000 according to the criterion of Black et al. [2006] for the EMAC REF-B1 simulation. "Early years" and "late years" are marked with (E) and (L) respectively.

Day	Year	Day	Year
23 April	**1960**	30 April	**1981**
10 April	**1961**	26 March	**1982 (E)**
3 April	**1962**	26 May	**1983 (L)**
25 April	**1963**	14 May	**1984 (L)**
2 April	**1964**	23 March	**1985 (E)**
19 May	**1965 (L)**	17 April	**1986**
9 April	**1966**	2 May	**1987**
17 April	**1967**	9 June	**1988 (L)**
7 April	**1968**	1 May	**1989**
15 April	**1969**	12 April	**1990**
24 May	**1970 (L)**	15 May	**1991 (L)**
20 April	**1971**	10 May	**1992**
3 April	**1972**	18 April	**1993**
15 March	**1973 (E)**	14 May	**1994 (L)**
5 April	**1974**	8 April	**1995**
24 April	**1975**	24 May	**1996 (L)**
1 April	**1976 (E)**	2 May	**1997**
22 April	**1977**	10 April	**1998**
14 March	**1978 (E)**	15 April	**1999**
8 May	**1979**	30 April	**2000**
29 April	**1980**		

Comparative figures relative to changes in atmospheric fields associated with the timing of SFW

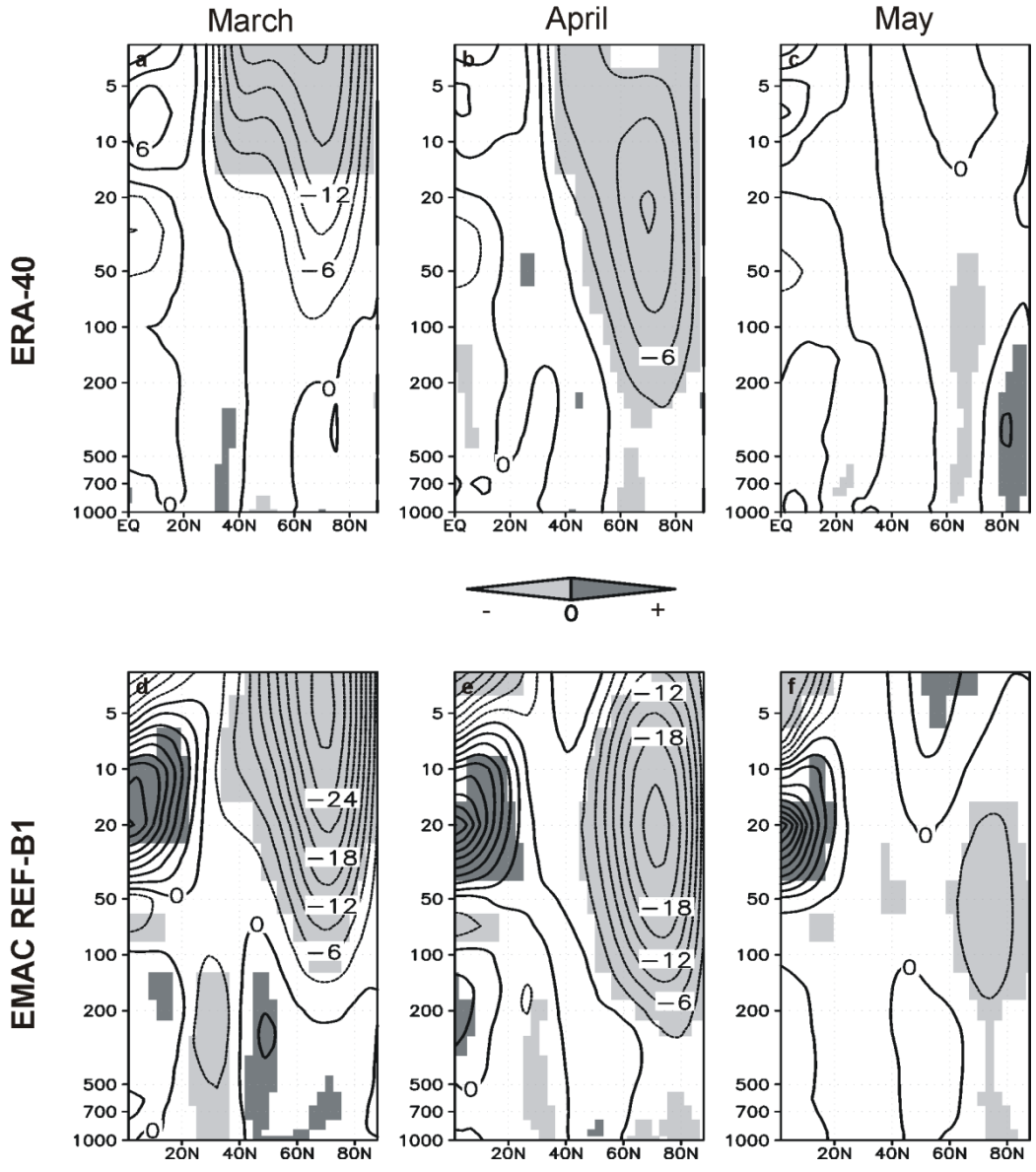

Figure App3.1. E-minus-L composites of the zonal-mean zonal wind for ERA-40 (upper panel) and the EMAC REF-B1 simulation (bottom panel). Contour interval is 3 m s^{-1}. Light (dark) shading corresponds to negative (positive) statistically significant differences at a 95% confidence level.

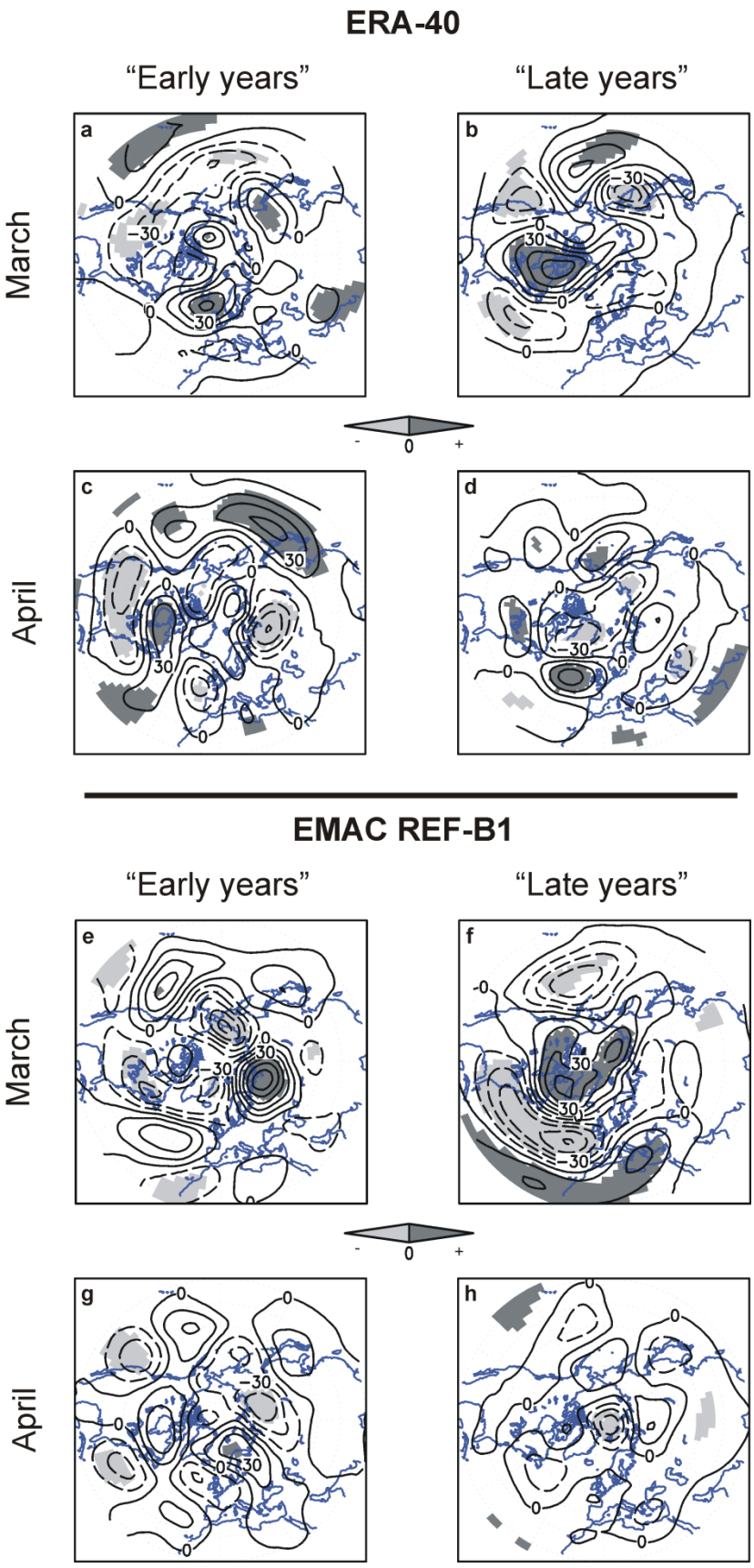

Figure App3.2. Composites of Z500 anomalies in March and April for ERA-40 (upper panel) and the EMAC REF-B1 simulation (bottom panel). Contour interval is 15 gpm. Shaded areas correspond to statistically significant values at a 95% confidence level.

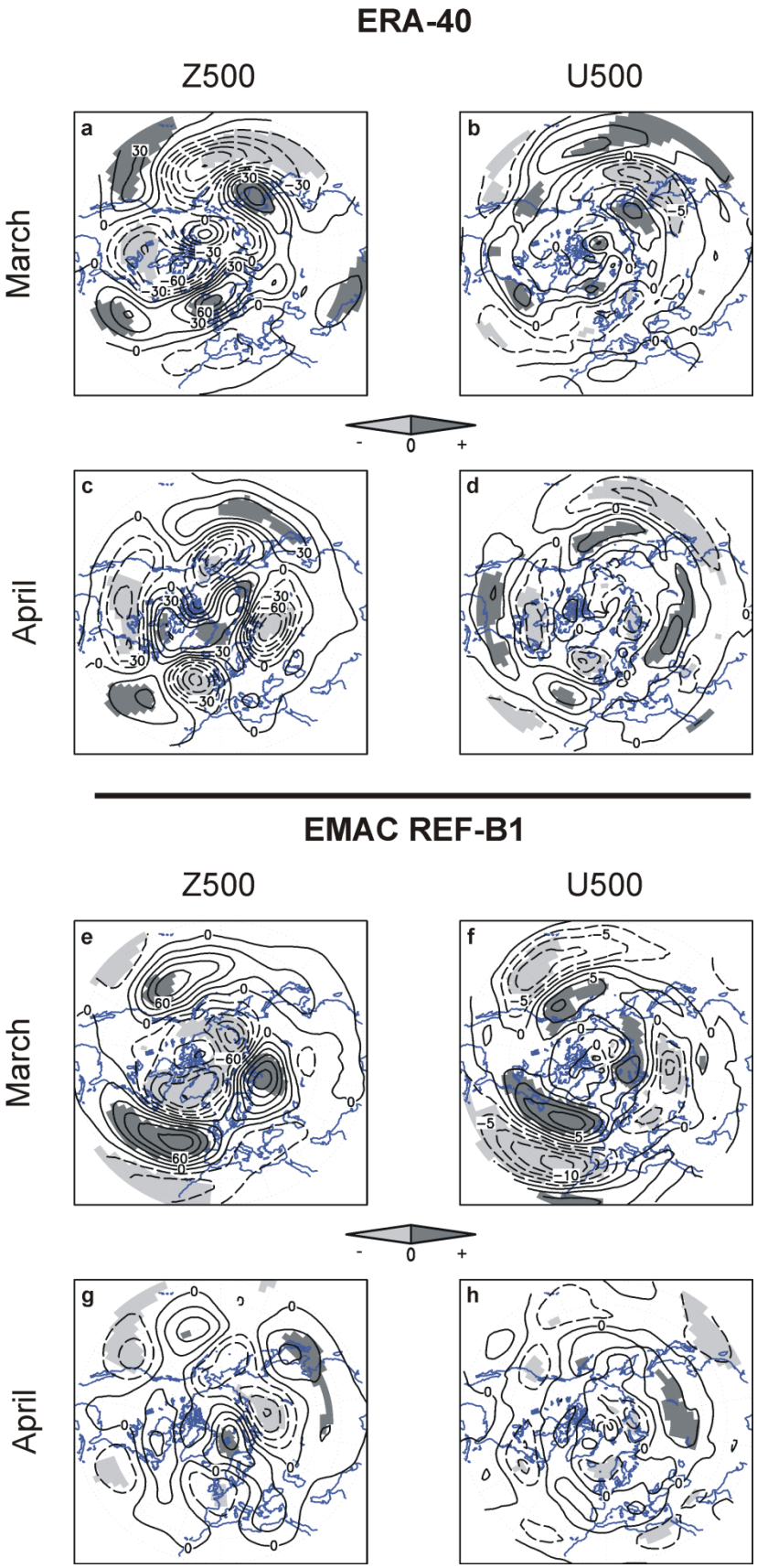

Figure App3.3. E-minus-L composites of (left) geopotential (gpm) and (right) zonal wind (m s^{-1}) at 500 hPa in March and April for ERA-40 (upper panel) and the EMAC REF-B1 simulation (bottom panel). Light (dark) shading corresponds to negative (positive) statistically significant values at a 95% confidence level.

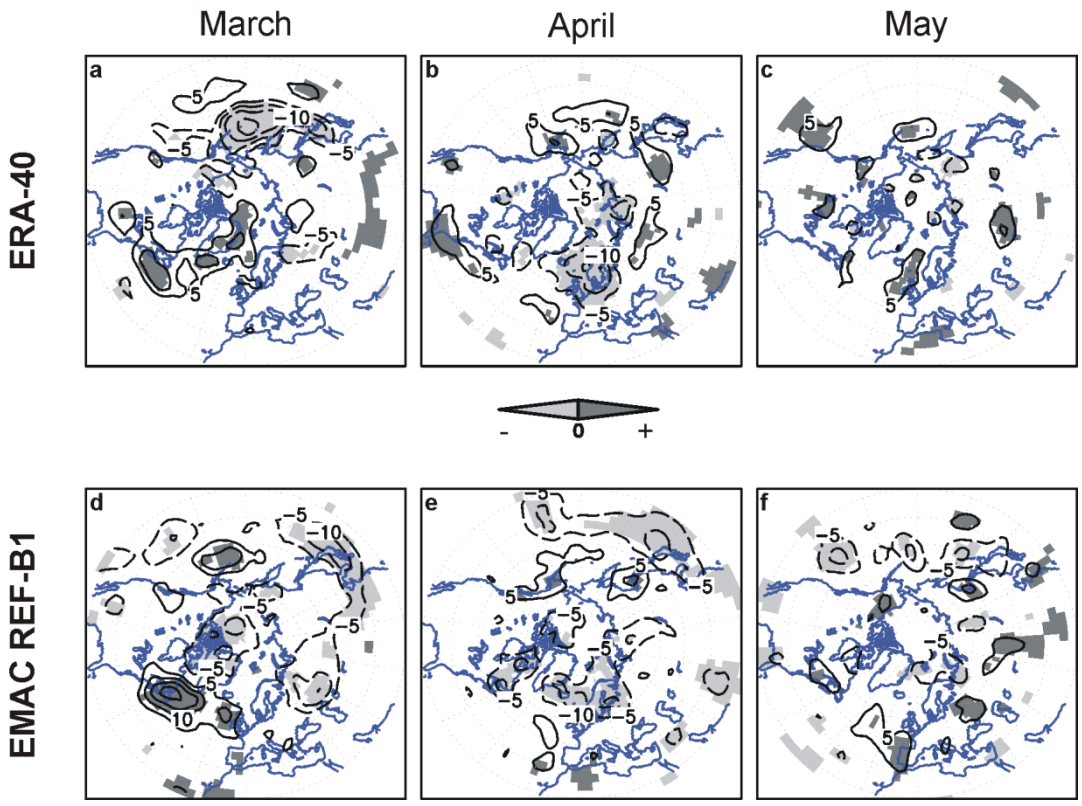

Figure App3.4. E-minus-L composites of storm track activity at 500 hPa for ERA-40 (upper panel) and the EMAC REF-B1 simulation (bottom panel). Contour interval is 5 gpm. Light (dark) shading indicates negative (positive) statistically significant difference at a 95% confidence level. Zero contours are omitted for clarity.

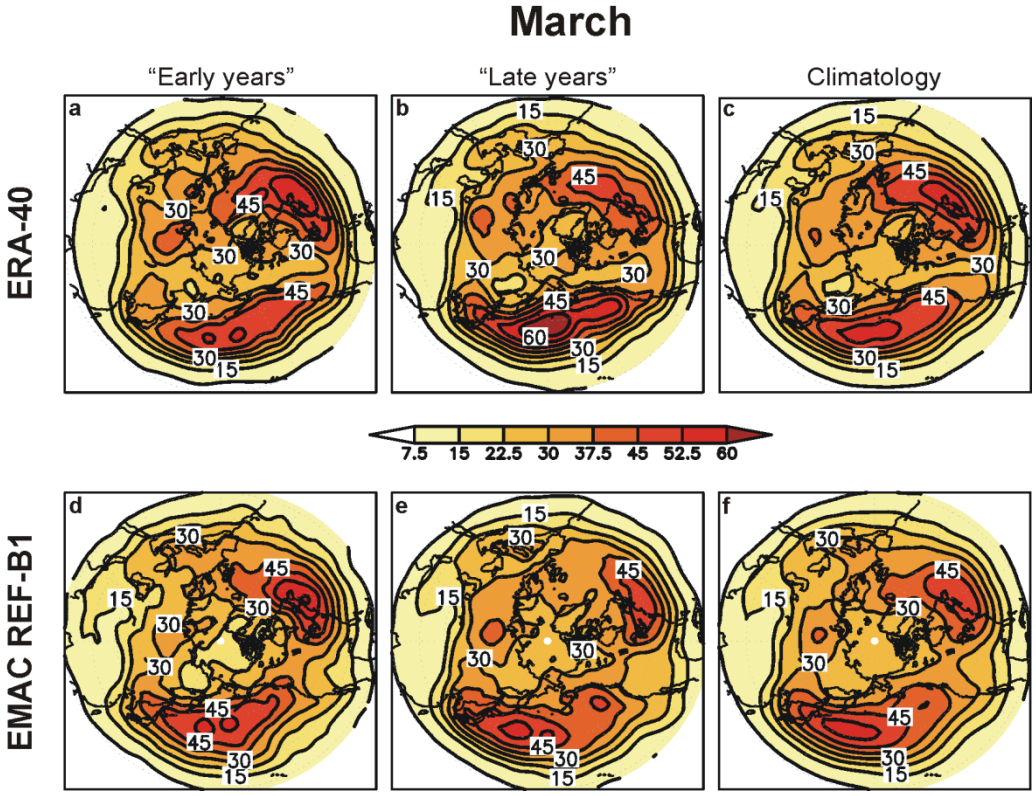

Figure App3.5. Composites of storm-track activity at 500 hPa in March for ERA-40 (upper panel) and the EMAC REF-B1 simulation (bottom panel). Contour interval is 7.5 gpm.

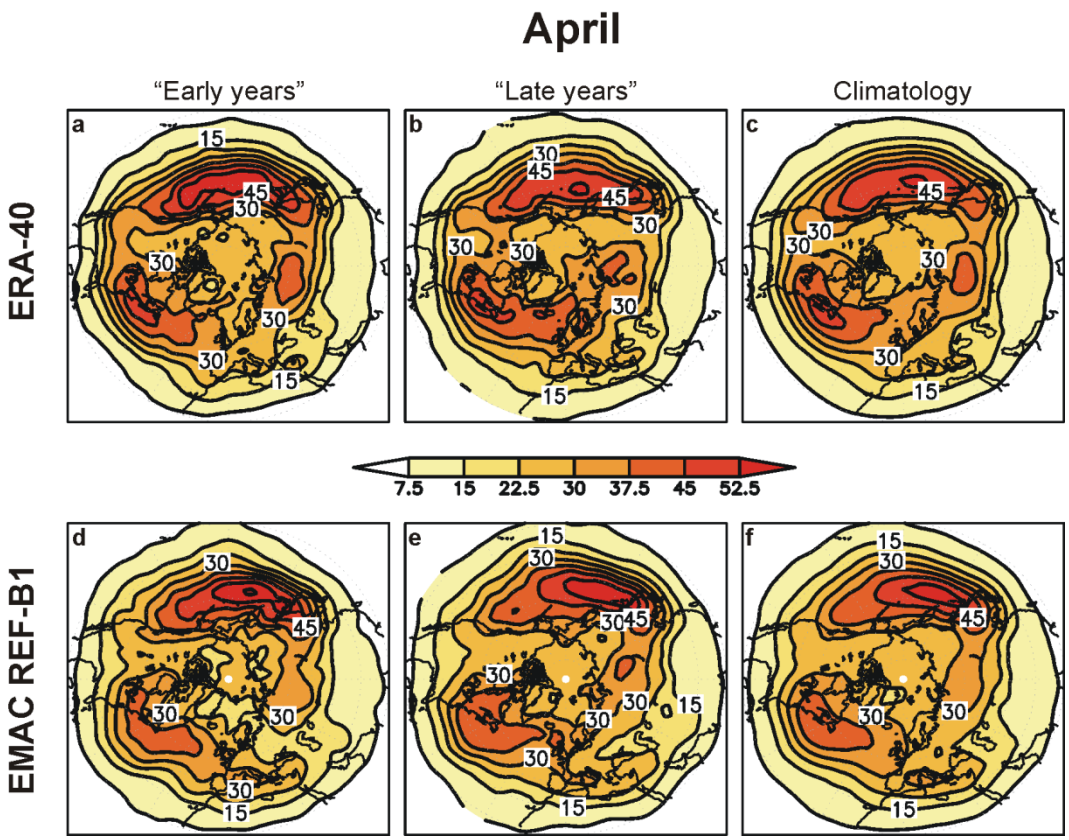

Figure App3.6. As Figure App3.5, but for April. Note that there is a 180º shift in longitude with respect to Figure App3.5.

Appendix 4: Associated publications

1. Ayarzagüena, B, and E. Serrano (2009), Monthly characterization of the tropospheric circulation over the Euro-Atlantic area in relation with the timing of Stratospheric Final Warmings, *J. Climate*, *22*, 6313-6324, doi: 10.1175/2009JCLI2913.1.
http://journals.ametsoc.org/doi/abs/10.1175/2009JCLI2913.1

2. Ayarzagüena, B., U. Langematz, and E. Serrano (2011), Tropospheric forcing of the stratosphere: A comparative study of the two different Major Stratospheric Warmings in 2009 and 2010, *J. Geophys. Res.*, *116*, D18114, doi: 10.1029/2010JD015023.

http://www.agu.org/pubs/crossref/2011/2010JD015023.shtml